REBURNING RENEWABLE BIOMASS FOR EMISSIONS CONTROL AND ASH DEPOSITION EFFECTS IN POWER GENERATION

A Dissertation

by

HYUK JIN OH

Submitted to the Office of Graduate Studies of
Texas A&M University
in partial fulfillment of the requirements for the degree of

DOCTOR OF PHILOSOPHY

August 2008

Major Subject: Mechanical Engineering

REBURNING RENEWABLE BIOMASS FOR EMISSIONS CONTROL AND ASH DEPOSITION EFFECTS IN POWER GENERATION

A Dissertation

by

HYUK JIN OH

Submitted to the Office of Graduate Studies of
Texas A&M University
in partial fulfillment of the requirements for the degree of

DOCTOR OF PHILOSOPHY

Approved by:

Co-Chairs of Committee,	Kalyan Annamalai
	Jerald Caton
Committee Members,	Sai Lau
	Adonios Karpetis
Head of Department,	Dennis O' Neal

August 2008

Major Subject: Mechanical Engineering

ABSTRACT

Reburning Renewable Biomass for Emissions Control and Ash Deposition Effects in Power Generation. (August 2008)

Hyuk Jin Oh, B.S., Chonbuk National University;

M.S., Texas A&M University

Co-Chairs of Advisory Committee: Dr. Kalyan Annamalai
Dr. Jerald Caton

Cattle biomass (CB) has been proposed as a renewable, supplementary fuel for co-firing and reburning. Reburning coal with CB has the potential to reduce NO_x and Hg emissions from coal fired systems. The present research focuses on three areas of combustion: 1) Biomass reburning experiments are conducted to determine the optimum operating conditions for the NO_x reduction using blends of coal and CB as reburn fuels. 2) Since CB contains higher ash contents compared to coals, the fouling behavior is also investigated under the transient and short-time operation. 3) Finally CB contains higher Cl compared to coals, which oxidizes Hg to $HgCl_2$. To understand the Hg oxidation behavior, a fundamental study of Hg oxidation in coal combustion is conducted using a plug flow reactor (PFR).

The main parameters investigated are types of the reburn fuel, reburn equivalence ratios (ER_{RBZ}), O_2 concentrations in the reburn gas, injection angles of the reburn fuel, cross-sectional geometries of the reburn nozzles, symmetric and asymmetric reburn injections, reburn heat inputs, baseline NO_x concentrations, and presence and absence of the heat exchangers (HEX). The results of reburning show that CB is a very effective fuel in NO_x reduction, and the extent of NO_x reduction is strongly dependent to the ER_{RBZ}. The optimum conditions of the boiler operation for biomass reburning are as follows: ER_{RBZ} = 1.1, 45° upward circular reburn nozzles,

12.5% O_2 in the reburn gas, symmetric injection, and presence of HEXs. To make an effective reburn process, the baseline NO_x concentrations must be higher than 230 g/GJ (0.5 lb/mmBTU) and the reburn heat input higher than 20%.

The results of ash fouling show the presence of ash in the hotter region of the furnace seems to promote heat radiation thus augmenting the heat transfer to the HEX. The growth of the layer of ash depositions over longer periods typically lowers overall heat transfer coefficients.

The addition of HCl to Hg containing gases in the PFR significantly increases Hg oxidations. The addition of NO inhibited the overall reaction and shifted the reaction temperature higher while the addition of O_2 promoted Hg oxidations and lowered the reaction temperature. For heterogeneous cases, the use of the VWT catalyst promotes the reduction of Hg^0 and shifted the reaction temperatures lower than those for homogeneous cases.

DEDICATION

To my lovely wife, son and daughter

For their endless support and understanding

And

To my parents

For their loving guidance to pursue my dreams

ACKNOWLEDGEMENTS

I would like to express my deep appreciation to my adviser, Dr. Kalyan Annamalai, for the opportunity to join this outstanding research group and work on the hot and exciting project. Without his academic and economical supports, this work would never have been completed.

I would like to give special thanks to my co-adviser, Dr. Jerald A. Caton who has advised me for my Master's degree, for backing me up during a long period of my Master and Ph.D. degrees.

Special thanks to my other committee members, Dr. Sai Lau and Dr. Adonios Karpetis, for their help, interest, and support on my research.

Thanks also go to all of the graduate students who have worked with me in Coal and Biomass Energy Laboratory, in particular, Nicholas Carlin, Gerardo Gordillo, Benjamin Lawrence, Paul Goughnor, Uday Arcot V, and Pat Gomez. It was precious time and fun to discuss and chat with them, and it gave me so much energy.

Finally, I would like to express my gratitude to my family and parents. Their endless love and support have been the foundation of my life and the cozy shelter of my sprit.

This research was supported in part by Texas Commission on Environmental Quality (TCEQ) and Department of Energy (DOE - Pittsburgh Energy Technology Center and Golden Field Office). However, any findings, conclusions, or recommendations expressed herein are those of the author and do not necessarily reflect the opinions or views of TCEQ and DOE.

NOMENCLATURE

AB	Agricultural Biomass
AFT	Ash Fusion Temperature
AGR	Advance Gas Reburning
As Rec.	As Received
ASTM	American Society for Testing and Materials
B/A	Basic/Acidic Oxides
BF	Burnt Fraction
BTU	British Thermal Unit
CAAA	Clean Air Act Amendments
CB	Cattle Biomass or Cattle Manure
CBEL	Coal and Biomass Energy Laboratory
CEMS	Continuous Emission Monitoring System
CFB	Circulating Fluidized Bed
Cl	Chlorin
CVAAS	Cold-Vapor Atomic Absorption Spectrometry
CVAFS	Cold-Vapor Atomic Fluorescence Spectrometry
DAF	Dry Ash Free
DB	Dairy Biomass
DOE-EIA	Department Of Energy - Energy Information Administration
DOE-NETL	Department Of Energy - National Energy Technology Laboratory
E3 Lab	Engines, Emissions, and Energy Research Laboratory
EPA	Environmental Protection Agency

ER or ϕ	Equivalence Ratio
ESP	Electrostatic Precipitator
FB	Feedlot Biomass
FC	Finished Compost
FixC	Fixed Carbon
FF	Fabric Filter
FGD	Flue Gas Desulphurization
FGR	Flue Gas Recirculation
GPM	Gallon per Minute
HADB	High Ash Dairy Biomass
HAFB	High Ash Feedlot Biomass
HAPCFB	High Ash Partially Composted Feedlot Biomass
HC	Hydrocarbon
HEX	Heat Exchanger
Hg	Mercury
Hg^0	Elemental Mercury
Hg^{2+}	Oxidized Form of Mercury
Hg_p	Particle-Bound Mercury
Hg^T	Total Mercury
HHV	High Heating Value
IC	Internal Combustion
I.D.	Inner Diameter
LADB	Low Ash Dairy Biomass
LAFB	Low Ash Feedlot Biomass

LAPCFB	Low Ash Partially Composted Feedlot Biomass
LASS	Low Ash Separated Solid
LASSDB	Low Ash Partially Composted Separated Solid Dairy Biomass
LB	Poultry Litter Biomass
LHV	Low Heating Value
LMTD	Log Mean Temperature Difference
LNB	Low-NO_x Burner
LOI	Loss on Ignition
MFC	Mass Flow Controller
MMF	Mineral Matter Free
MSW	Municipal Solid Waste
N	Nitrogen
NG	Natural Gas
NDIR	Nondispersive Infrared Sensor
NO_x	Nitrogen Oxides
O.D.	Outer Diameter
OFA	Overfire Air
OH	Ontario Hydro
OHTC or *U*	Overall Heat Transfer Coefficient
PC	Partially Composted
PFR	Plug Flow Reactor
PM	Particulate Matter
PM-SDA	Particulate Matter Spray Dryer Absorber
RBZ	Reburn Zone

RM	Raw Manure
RT	Residence Time
SATP	Standard Ambient Temperature and Pressure
SCCM	Standard Cubic Centimeter per Minute
SCFH	Standard Cubic Feet per Hour
SCR	Selective Catalytic Reduction
SDA	Spray Dryer Absorber
SLPM	Standard Liters per Minute
SMD or d_{32}	Sauter Mean Diameter
SNCR	Selective Non-Catalytic Reduction
SR or λ	Stoichiometric Ratio
SRI	Southern Research Institute
TAMU	Texas A&M University
TGA	Thermogravimetric Analysis
TXLC	Texas Lignite Coal
UV	Ultraviolet
VCM	Volatile Combustible Matter
VM	Volatile Matter
VWT	Vanadium-Tungsten-Titanium or V_2O_5-WO_3/TiO_2
WFGD	Wet Flue Gas Desulfurization
WYC	Wyoming Subbituminous Coal

TABLE OF CONTENTS

Page

Page

Page

LIST OF FIGURES

FIGURE Page

FIGURE Page

FIGURE Page

FIGURE Page

FIGURE Page

FIGURE Page

LIST OF TABLES

TABLE Page

1. INTRODUCTION

This section presents the, causes of NO_x and mercury (Hg) emissions, problems caused by them, and the current studies to reduce NO_x and Hg emissions from power generation utilities using fossil fuels. Ash fouling which is one of the main problems in fossil fuel fired utilities is also introduced. Combustion of biomass fuels and their effects on both gaseous emissions and fouling problems are introduced. Finally the outline of the dissertation is given.

1.1 NO_x Emissions and Reductions

Nitrogen oxides (NO_x) is identified as byproducts of combustion in air, and the term used to describe primarily NO and NO_2. NO_x emissions causing environmental problems and human health concerns are generated from transportation (i.e. onroad and nonroad engines), electric utilities and other industrial sources. The environmental problems are acid rain, poor water quality, photochemical smog formation, global warming, and ground-level ozone formation. The human health effects by exposures to NO_x are respiratory illness and pulmonary problems. The major sources of anthropogenic NO_x emissions caused by human activities are mobile sources and stationary (or fuel combustion) sources. Though emissions from mobile sources have decreased 15% over the past 20 years, 12% increment has been reported for heavy duty vehicles equipped diesel engines over the past 10 years [1]. Since 1983 the steady increment of NO_x emissions has also been reported for nonroad vehicles such as aircraft, locomotives and construction equipment [1]. NO_x emissions from these two sources make up 93% of the total NO_x emissions in 2002 [1]. Environmental Protection Agency (EPA) is developing new standards for these heavy duty and nonroad vehicles.

This dissertation follows the style of *Combustion and Flame.*

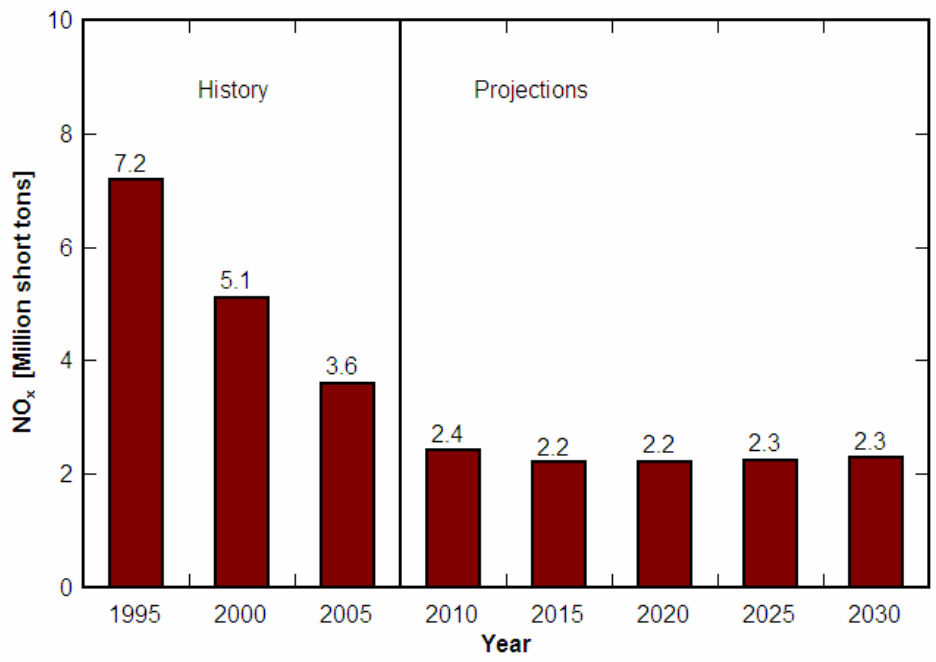

Figure 1.1. National NO_x emissions from the electric coal-fired utilities [4].

Electric power utilities in the US consume 80% of the one billion tons of coal produced annually [2]. Coal will continue to be a dominant fuel used in the generation of electricity, thus new technologies of NO_x emission controls must be developed to meet the stringent standard. Emission controls for fossil fuel combustion sources particularly coal-fired electric utility power generators have been regulated by Clean Air Act Amendments (CAAA). Phase I of the program started January 1, 1996 and has achieved the NO_x reduction of 400,000 tons per year in the US. These reductions were achieved by the installation of low-NO_x burner (LNB) on dry-bottom wall-fired and tangentially fired boilers [1, 3]. Phase II which began in the year 2000 established lower emission limit for the boilers in Phase I program, and established NO_x emission limit for cell-burner, cyclone, wet-bottom wall-fired boilers, and other types of coal-fired boilers [1, 3]. Due to EPA regulations, NO_x emissions are projected to decrease from 3.6 million short tons in 2005 to 2.3 million short tons in 2030 as shown in figure 1.1. Phase II program will result in the

additional NO_x reduction of 820,000 tons per year [3]. Figure 1.2 shows the geographic distribution of NO_x emission based on the tonnage per square mile for each county in 2001. The eastern half produces heavier NO_x emission than the other half of the country probably due to the density of industrial plants.

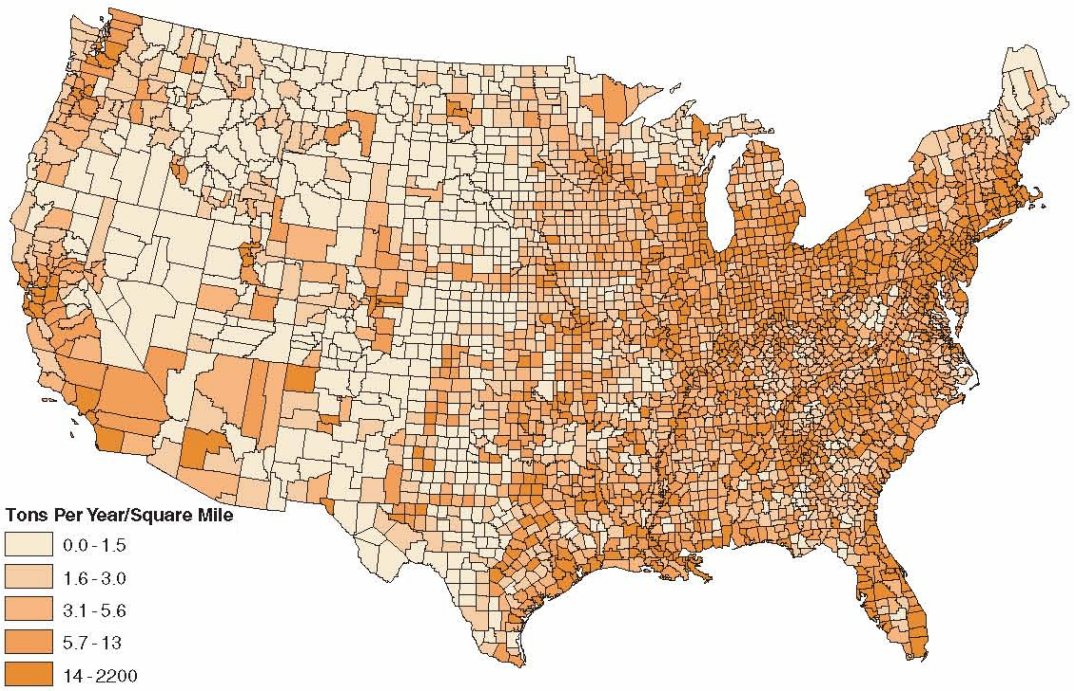

Figure 1.2. Geographic distributions of NO_x emissions for each county in 2001 [1].

NO_x control techniques are classified into two categories: pre-combustion controls and post-combustion controls. Pre-combustion controls reduce NO_x formation during the combustion process, while post-combustion controls reduce NO_x after it has been formed. Pre-combustion controls includes 1) low-NO_x burners (LNBs), overfire air (OFA), flue gas recirculation (FGR), reburn process, and operational modifications such as changing equivalence ratio (ER or ϕ) for power plants and 2) spark timing and compression ratio for internal combustion (IC) engines.

Post-combustion controls include selective catalytic reduction (SCR) and selective non-catalytic reduction (SNCR). The prevalent applications of NO_x control are a combination of the existed technologies such as LNB with reburning or reburning with OFA. Each technology will be reviewed later.

1.2 Hg Emissions and Oxidations

Mercury (Hg) emission could be traced to natural and anthropogenic sources. Natural sources of Hg emissions are volcanoes, geologic deposits, and volatilization from the ocean. Anthropogenic sources of Hg emissions are mainly combustion facilities such as electric utility power plants. Mercury emitted to the environment settles on agricultural lands, lakes, and oceans. Some of the absorbed Hg are converted into the most toxic form, methylmercury (CH_3Hg), and enter the food chain. Health problems caused by Hg include memory loss, nerve system failure, skin rashes, muscle weakness, etc. In the 1990s, mercury was identified as a serious air pollutant by the U.S. EPA. Figure 1.3 presents an atmospheric mercury cycle on soil. Both elemental mercury (Hg^0) and oxidized mercury (Hg^{2+}), mainly mercuric chloride ($HgCl_2$), are emitted from coal combustion sources and waste incinerators. Dry deposition is defined as the settlement of Hg on soil and is more likely to remove particulate forms of mercury from the environment. Wet deposition is defined as the removal of Hg via rain and other types of precipitation and is most efficient at removing oxidized forms of mercury in the air [5]. Elemental mercury is removed by dry deposition and wet deposition after oxidation by other pollutants (O_3, H_2O_2, Cl_2, and H_2O) in the air. Mercuric chloride can be partially converted to Hg^0 through reverse reactions.

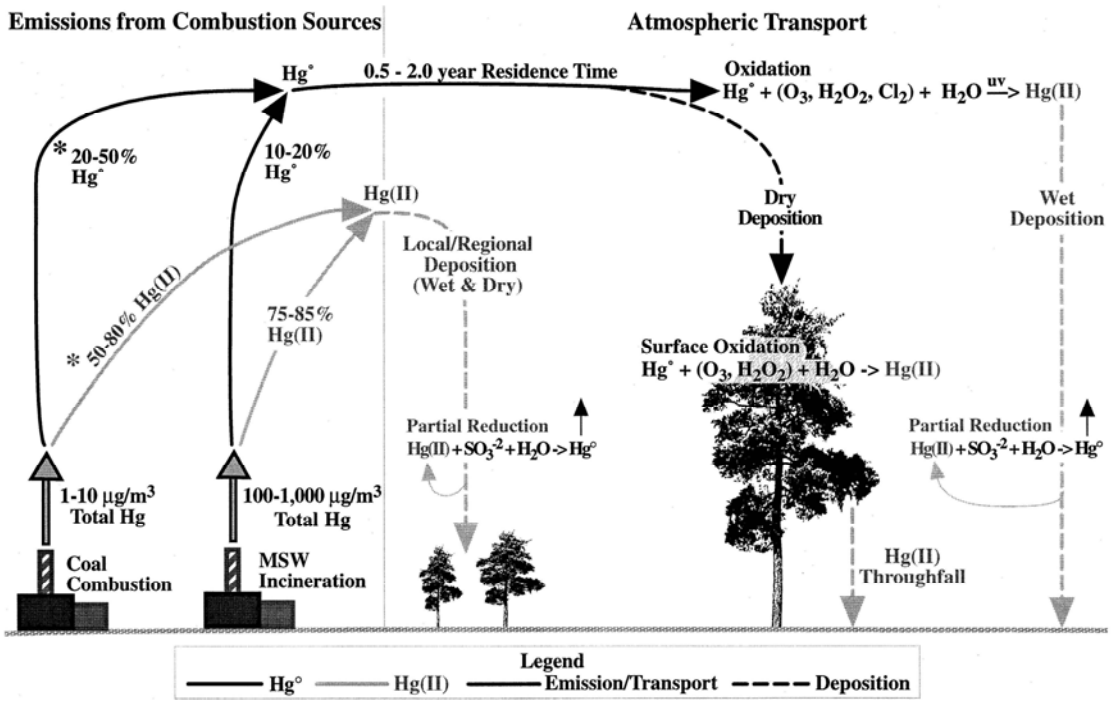

Figure 1.3. Atmospheric mercury (Hg) cycles on soil [6].

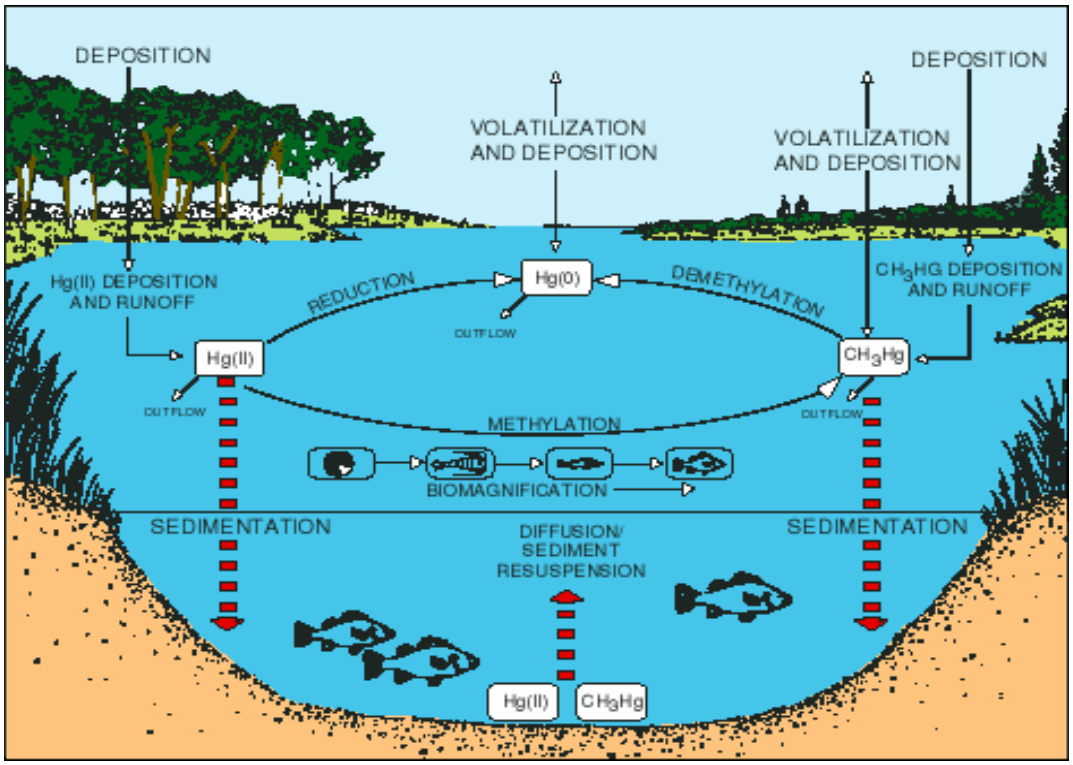

Figure 1.4. Aquatic mercury (Hg) cycles under water [7].

Figure 1.4 shows an aquatic mercury cycle under water. Mercury deposition to the aquatic ecosystems is primarily caused by the rainfall. oxidized mercury (Hg^{2+}) is the major component deposited in water though some mercury can be released back to the atmosphere by volatilization. Methylmercury produced by the conversion of mercury is consumed partially by wildlife under water, enters the food chain and then cause problems for human health.

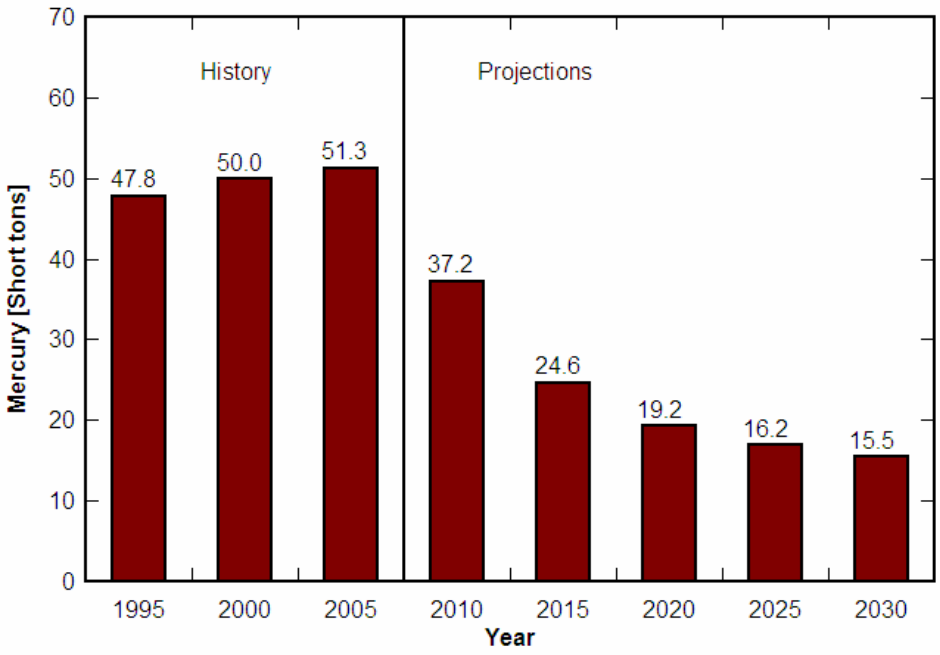

Figure 1.5. National Hg emissions from the electricity generations [4].

Coal-fired electric utilities are the largest source of mercury emissions in the US. The EPA reported 48 tons out of 158 tons of Hg were released from coal-fired combustion sources, 28 tons were released from industrial and commercial boilers, 30 tons were released from municipal waste combustors, and the rest were from medical waste, manufacturing, and natural sources in 1997 [8, 9]. Figure 1.5 shows national Hg emissions from the electric coal-fired utilities. The Hg emissions are projected to decrease from 51.3 short tons in 2005 to 15.5 short tons in 2030, and

more stringent regulations have been proposed by several eastern States [4]. The five power plants in Texas were ranked in the top ten facilities which contributed to the largest amounts of Hg emission.

Mercury in coal is vaporized as elemental forms at high temperatures in boilers, yielding vapor concentrations in the range of 1 to 20 ng/m^3 [10]. Most coals typically contain 0.08 to 0.22 μg of mercury per g of coal while bituminous coals contain 160 μg of chlorine per g of coal [9]. The mercury content is not a function of the coal rank (0.18 ppm for anthracite, 0.08 – 0.2 ppm for bituminous, 0.08 – 0.19 for subbituminous, and 0.13 – 0.22 for lignite) but is inversely proportional to the chlorine (Cl) content in coals. Typically, bituminous coals contain high Cl contents, and subbituminous and lignite coals contain low Cl contents.

Mercury is typically released into air in three forms: elemental mercury (Hg^0), particle-bound mercury (Hg_p) and oxidized mercury (Hg^{2+}). Particle-bound mercury is easily captured by electrostatic precipitators (ESP) and fabric filters (FF), and Hg^{2+} is water soluble and likely to be absorbed by the fly ash from fuel combustion. However, elemental mercury is insoluble and difficult to capture. Therefore, the technology for the conversion of Hg^0 into an oxidized form plays an important role in reducing Hg emissions. In solid fuel combustion systems, the elemental form of mercury is released at the high temperature, and reacts with gaseous O_2, HCl, Cl_2, and NO_x in the combustor to produce oxidized forms such as $HgCl_2$ or HgO [11]. The gaseous forms of oxidized Hg are captured on residual ash particles or fly ash particles.

1.3 Alternative Fuel, Co-firing and Reburn Processes

There is growing intent in alternate fuels due to concerns with the production of greenhouse gas and the rising cost of fuels used in power generation. Some well known alternative fuels are biomass, biodiesel, biogas, bioalcohol, and vegetable oil. Most alternative fuels serve as sources

of renewable energy. The renewable fuels are being extensively experimented either as co-fired fuels [12 – 26] or as reburn fuels [3, 23, 27 – 43]. Co-firing is defined as the firing of two dissimilar fuels in the boiler. In the mixed method of the co-firing technique, the alternate fuel is mixed with coal before the coal feeder, and the blend is fired in existing pulverized coal-fired boiler burners. In the reburn process of the co-firing technique, an additional fuel usually natural gas (NG) is injected downstream of coal-fired boiler burners and burn under fuel-rich conditions in order to reduce NO_x generated by coal burners. Then OFA is introduced beyond the reburn zone (see figure 1.6) in order to complete combustion. A conventional, vertically upward-fired coal-fired burner in reburn technology with OFA is presented in figure 1.6 [3]. In this dissertation, emphasis is given to the reburn process of the co-firing technique.

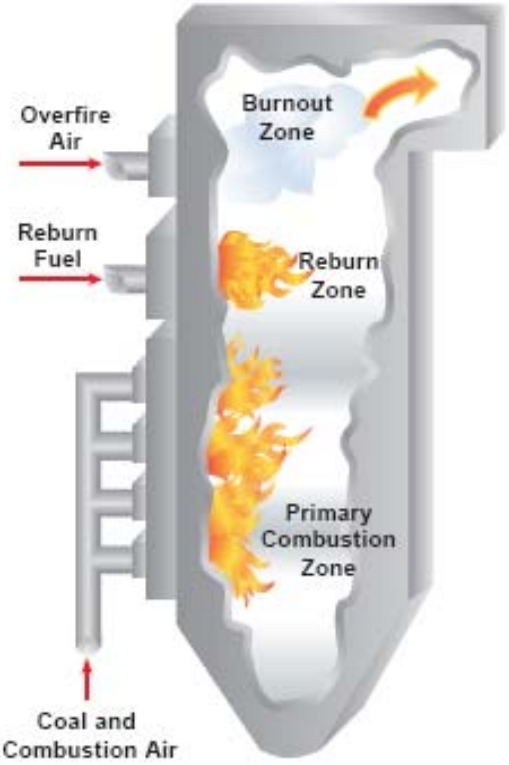

Figure 1.6. A schematic of a conventional, vertically upward coal-fired burner in reburning with OFA [3].

Due to the high cost of NG ($6 to $7 per mmBTU reported in 2007), alternate fuels (e.g., biomass) and coals ($1.5 to $2 per mmBTU) are used as reburn fuels [44, 45]. As alternate fuels, biomass fuels have attracted a lot of attention in recent years due to growing energy needs and shrinking fossil fuel supplies. Animal wastes such as cattle, chicken and pig manure have been proposed as co-fried fuels in coal-fired boiler facilities. Cattle manure (termed as cattle biomass, CB) as a reburn fuel in a small scale coal-fired boiler was first tested in Coal and Biomass Energy Laboratory (CBEL) at Texas A&M University (TAMU) [27]. The results revealed about an 80% reduction in NO_x emissions, and the process has resulted in an US Patent # 6,973,883 issued to Annamalai and Sweeten [46]. Extensive research in CBEL at TAMU has been done in the area of CB combustion as a technology to reduce coal consumption, reduce fuel costs, lower emissions, and dispose of biomass [2, 12, 13, 15, 22, 25, 27, 41, 47, 48, 49, 50]. It was found that co-firing 10% agricultural biomass (AB) with coal reduced NO_x emissions by about 10% since N is low in AB, but the CO emissions increased [12]. This new technology has the potential to reduce NO_x emissions in coal-fired boilers located near cattle feedlots and also relieves the cattle industry of the waste material.

1.4 Ash Fouling

Since the massive usage of subbituminous coals in the 1980s, the ash fouling problems for heat exchangers (HEXs) in utility boilers have increased even at low temperatures due to high level of calcium in the subbituminous coals [51]. Fouling is defined as any kind of inorganic deposits accumulated on HEXs during the combustion. The low heat transfer rate caused by the ash depositions in lignite utility boilers reduces the boiler efficiency. Cattle biomass (i.e., cattle feedlot biomass, FB) contains higher amounts of ash than coals, thus the use of CB as a co-fired or reburn fuel will generate more ash in the boiler resulting in more ash deposition on HEXs and

hence increase corrosion, slagging, and fouling problems. The primary purpose of the boiler is to transfer heat from hot flue gases to the cold water/steam circulated through HEXs. Hence heat transfer rate is affected. The reduction of heat rates caused by build up is used to study the ash fouling characteristic. Annamalai et al. used a 150 kW (500,000 BTU/h) pilot plant facility located at Department of Energy - National Energy Technology Laboratory (DOE-NETL) facility in Pittsburgh in order to study the ash fouling behavior of coal and FB blends in co-firing conditions [25]. It is reported that ash deposition causes heat transfer rate to decrease with time due to ash buildup, and this deposition is more severe for blends of coal and high ash FB than for pure coal. The extent of combustion and fouling depend on the type of FB and the amount of ash. Thus, ash fouling potential must be evaluated when this fuel is used for co-firing or reburning. Fouling using fiber cane and sugar cane bagasse has been evaluated in co-firing pilot- and full-scale experiments, and the composition and microstructure of ash deposits were analyzed [14]. Compact ash deposits of high density were produced by the coal combustion while low density and high porous structure deposits were produced by the pure biomass combustion. It was found that high levels of potassium and sulfur were the key factors to produce higher density of fouling.

Small ash particles tend to stick to the surface of the HEX while large ash particles impact. Sodium sulfate (Na_2SO_4) is one of the important compounds of ash particles which cause sticky behavior at low temperatures while glassy silicate-based components are responsible to make ash particles sticky at high temperatures [51, 52]. The ash fouling can cause 60% decrease of the heat transfer [53]. It was also suggested that the velocity of the flue gas and the fluid in the HEX affect the ash fouling behavior. The optimum velocity of the flue gas to destroy ash layers built on the HEX was investigated and the minimum velocity of the flue gas for avoiding particulate fouling was determined [54].

Fouling problems increase the operating cost of electric utility power plants. Self-cleaning systems are required to increase the boiler performance (e.g., soot blower) and the heat transfer efficiency and to decrease the operation cost and corrosion conditions of HEXs.

1.5 Outline

The dissertation is divided into 9 sections and organized in the following format.

Section 2 presents literature reviews on the formation and destruction mechanisms of NO_x and Hg. The reduction technologies and their effectiveness are presented with particular emphasis on the reburn technology using coal and biomass as reburn fuels. The formation and removal of ash fouling are also briefly reviewed.

In **Section 3**, objectives and detailed tasks are presented.

The description of experimental facilities is presented in **Section 4**: the reburn boiler facilities for studies of NO_x reduction and fouling and the plug flow reactor (PFR) facilities for studies of Hg oxidation. Experimental methods, procedures, and cases are described. The operating conditions of the facilities before the actual tests are also presented.

All methodologies used to analyze the results are described in **Section 5**. The fuel analysis includes proximate analysis, ultimate analysis, fuel particle size analysis, and ash analysis. In order to compare the results, the emission and HEX analyses are presented. The fuel nitrogen conversion efficiencies and the ash formation analyses for the combustion performances are also described. In order to ensure the accuracy of the results, the uncertainty and repeatability analyses are presented.

Section 6 presents the results and discussion of NO_x reduction during the biomass reburning using a bench-scale boiler. The variables studied include: reburn fuels, reburn equivalence ratios

(ER_{RBZ} or ϕ_{RBZ}), reburn heat inputs, non-vitiated/vitiated reburn gases, heat exchangers (HEXs), reburn injection configurations, and baseline NO_x concentrations.

Section 7 presents and discusses the results of the fouling behavior during the biomass reburning under the transient and short-time operations.

The **Section 8** covers the Hg emissions from the bench-scale reburn boiler as well as the results of the fundamental study for Hg oxidation or reduction using a PFR under homogeneous and heterogeneous oxidation conditions.

Finally, **Section 9** summarizes the conclusions drawn from the current work and presents recommendations for the further research.

2. LITERATURE REVIEW OF NO_x AND MERCURY FORMATIONS AND DESTRUCTIONS IN POWER GENERATION

Literature is reviewed on combustion process of coal and biomass fuels, the formation and destruction mechanisms of NO_x and Hg, the currently available reduction technologies, the effectiveness of the various technologies, and ash fouling problems in coal-fired power plants using coal and biomass as reburn fuels. Further, brief summaries of previous and current studies of reburning and Hg reduction are presented.

2.1 Coal and Biomass Combustion

2.1.1 Biomass as a Renewable Energy Source

Biomass typically refers to plant derived material which can be used as fuel and is used to describe waste products and dedicated energy crops [15]. More generally biomass includes animal wastes, dedicated energy crops, forest products, and industrial wastes. The animal wastes which are led with agricultural rations include cattle manure, pig waste and poultry litter. The dedicated energy crops include sorghum, sugar cane, corn husks, and wheat chaff. The forest products are materials mainly from logging residues. The industrial wastes include municipal waste, sewage sludge, garbage, and landfill gas. The use of biomass for combustion benefits to utilities and environments since blending biomass and coal can reduce net emissions of CO_2 and SO_2. Biomass is a CO_2 neutral fuel due to the majority of CO_2 released during combustion can be traced from plants and is reabsorbed by plants. Thus, net CO_2 released is near zero. Dutch utilities realized more than 3 million tons of CO_2 per year can be reduced by the substitution of coal with biomass [16]. Most agricultural biomass fuels have very little or no sulfur, thus SO_2

emissions can also be reduced by biomass combustion. Biomass can be used for direct co-firing and indirect co-firing. In the direct co-firing system, pre-processed biomass is directly fed to the boiler. In the indirect co-firing system, biomass is gasified, and its syngas is fed to the boiler. Many studies have been done in the part on coal and biomass combustion as a technology for reducing emissions of air pollutants, expenses of fuels and consumptions of coal and biomass. Some biomass fuels used in co-firing or reburning studies are: cattle manure [12, 22, 39, 41], sewage sludge [17, 40, 55], sawdust [18, 40], municipal solid waste [56], straw [19, 20], and wood [21, 34, 36, 57].

The average cattle feedlot may hold over 10,000 head of cattle, and it is estimated that there are over 10 million cattle in feedlots in the US at any given time [58]. The Texas Panhandle region (the largest region of cattle feeding in Texas) produces about 7.2 million fed cattle, and the amounts of animal wastes have doubled since 1978 [13]. If not carefully disposed of the cattle feedlot biomass (FB) may lead to water and air pollution problems. Heavy rains wash manure off the feedlot surface into local water streams, or nearby sources of drinking water. Stored manure emits pollutant gases and creates an odor, dust, and fly problems, particularly in a long term stockpile. Limited amounts of manure can be applied safely and economically to farm land as a fertilizer. Solving the disposal problem of manure is to use it as an energy source to generate electrical power. Cattle manure (termed as cattle biomass, CB) can be used as a renewable energy source to generate electrical power. The combustion application of CB has achieved only limited success due to its high moisture, low heating value, high sulfur, high nitrogen, and high ash [59]. The high moisture and ash contents of CB result in flame stability problems in direct combustion.

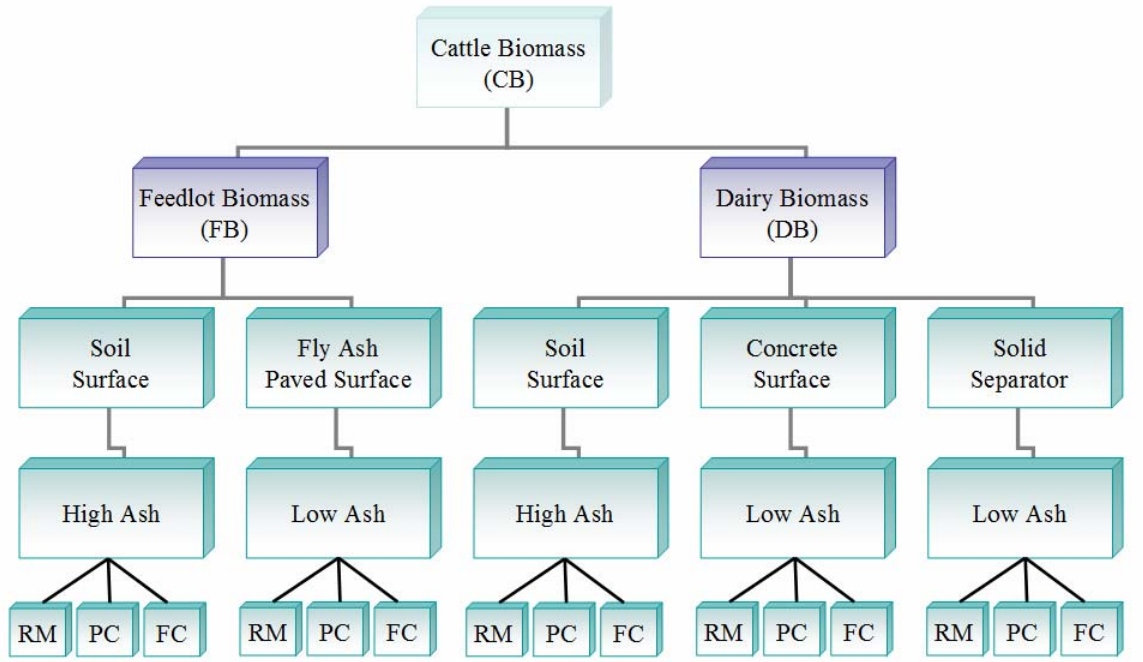

Figure 2.1. Classifications of cattle biomass (CB).

Two types of CB, feedlot biomass (FB) and dairy biomass (DB) can be used for reburn and co-firing processes to reduce gaseous emissions. The classification of CB is presented in figure 2.1. CB is classified by which surface it is collected from. For FB, manure is removed from two types of feedpen surfaces. Manure collected on soil surfaces contains high amounts of ash and is termed high ash FB (HAFB) while one collected on fly ash paved surfaces contains low ash content and is termed as low ash FB (LAFB). For DB from dairy farms, manure collected on soil surfaces contains high amounts of ash and is termed high ash DB (HADB) while one collected on concrete surfaces contains low ash content and is termed as low ash DB (LADB). Sometimes, solid is separated from water flushed manure by a solid separator, which contains low ash, and it termed as low ash separated solid (LASS). Processes of the collection, storage, and disposal of CB are described elsewhere [59]. CB is also characterized by the composting process. Samples prior to composting are termed as raw manure (RM), and samples taken after about 45 days of

composting involving successive wetting and turning cycles are termed partially composted (PC) [47]. Samples taken after about 120 days of composting (involving continuing wetting and turning cycles) are termed finished compost (FC). The composting process increases the quality of CB for use as a fertilizer and an energy source by increasing the homogeneity. The action of aerobic bacteria in CB raises the temperature (exothermic process), and the properties of CB are changed [59]. Amounts of nitrogen and moisture in CB are reduced, and nitrogen is converted to a non-volatile form during the composting process. Samples are typically analyzed for the following parameters: proximate, ultimate, BTU, ash elemental analysis, chlorine, phosphorus, and metals in ash. Like coals, CB has fixed carbon (FixC), volatile matter (VM), moisture, and ash. The major elements include C, H, O, N, and S. Pyrolysis, ignition, and fuel characteristics of CB are described elsewhere [60].

2.1.2 Process of Coal and Biomass Combustion

Coals are classified into four major categories called “ranks” based on heating value, VM content, FixC content, and agglomerating behavior, and each rank is subdivided into groups based on decreasing heating value and FixC and increasing VM [9]. The coal ranks are explained from the highest to the lowest. Anthracite coals are the highest rank class of nonagglomerating coals containing FixC > 86% and VM < 14% on a dry, mineral-matter-free (MMF) basis. This coal rank is subdivided into meta-anthracite, anthracite and semi-anthracite coals. Bituminous coals contain FixC < 86% and 14% VM on a dry, MMF basis, and a heating value > 10,500 BTU/lb on a moist, MMF basis. They are subdivided into low-volatile bituminous, medium-volatile bituminous, high-volatile bituminous A, B, and C. Subbituminous coals (nonagglomerating coals) have a heating value between 8,300 and 11,500 BTU/lb on a moist, MMF basis. This coal rank is subdivided into subbituminous A (10,500 to 11,500 BTU/lb),

subbituminous B (9,500 to 10,500 BTU/lb) and subbituminous C (8,300 to 9,500 BTU/lb). Lignite coals are the lowest coal rank having heating value < 8,300 BTU/lb on a moist, MMF basis and subdivided into lignite A (6,300 to 8,300 BTU/lb) and lignite B (< 6,300 BTU/lb). According to Department of Energy (DOE) Energy Information Administration (EIA), the demonstrated reserve base of coal in the US approximately 508 billion tons: 2% is anthracite, 53% is bituminous, 36% is subbituminous, and 9% is lignite [61].

Coals contain approximately 1 – 2% nitrogen (N), which is called fuel-N, and the amounts of fuel-N depend on the rank of the coal. Unlike coals, fuel-N content in biomass can vary widely: wood, straw, sawdust, and corn residue contain less than 1%, FB contains 3 – 4%, poultry litter biomass contains 1 – 5%, and meat and bone meal contain 9 – 11% on a dry ash free (DAF) basis [13, 16]. Fuel-N is released to the gas phase during coal and biomass combustion and could either finally form NO in fuel-lean combustion and N_2 in fuel-rich combustion. Also, fuel-N released from coal and biomass could be in the form of HCN and/or NH_3 depending on the coal rank and biomass type. Fuel-N release is coupled with the release rate of volatiles [62]. It is found that low rank coals with high volatile contents (e.g., Texas lignite) release high amounts of NH_3 while high rank coals with low volatile contents (e.g., anthracite) release high amounts of HCN [63]. It was also found that NO emissions decrease with an increase of the VM amounts in the fuels [64]. The release rate of fuel-N is closely related to processes of devolatilization, volatile combustion and char combustion. Though the fuel-N plays a fundamental role in the formation and reduction of NO_x; to the author's knowledge, there are very little systematic studies on the characterization of fuel-N in coal and biomass.

The physical process occurring during heating, ignition and combustion of isolated particles is presented in figure 2.2. When a fuel particle enters the combustion chamber, thermal effects of radiation energy from other particles and furnace walls and convection from hot gases propagate

into the particle. When the particle temperature reaches pyrolysis level, thermal decomposition occurs and the particle starts releasing volatiles. This process is called devolatilization and it relies on the heating rate. Lighter VM contained in the coal is released rapidly at lower temperatures, and heavier volatiles are released at a slower rate at higher temperatures [65]. The amount of fuel-N released depends on the devolatilization characteristics [66]. The release rate of fuel-N is assumed to be approximately proportional to the rate of the fuel weight loss. If nitrogen is released in a fuel-lean combustion, enough oxygen is available to oxidize fuel-N to NO and thus significant NO formation takes place. In contrast, under the fuel-rich environment, fuel-N from the coal may be released as HCN, NH_3 and N_2; but N_2 may combine with hydrocarbon (HC) fragments to form more HCN. After the ignition, the combustion continues until all volatiles are consumed, and then the char combustion occurs by the remaining carbon in fuels. The main composition of the last stage of thecombustion is ash.

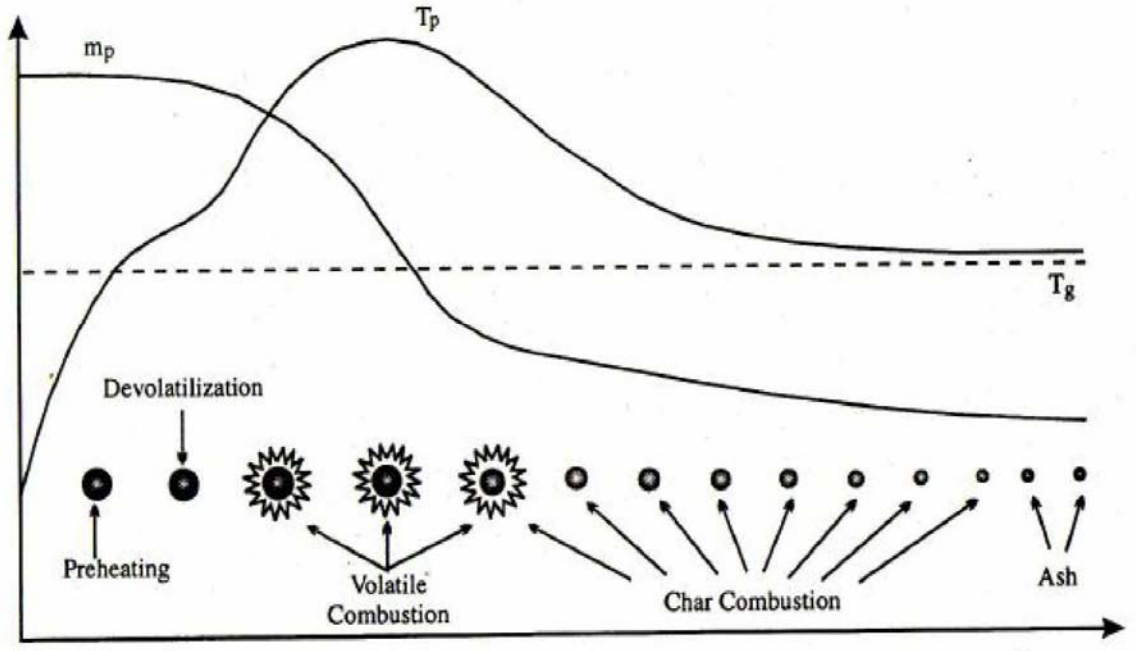

Figure 2.2. Physical processes in ignition and combustion of isolated particles [67].

2.2 Emissions in Coal-fired Power Plants

2.2.1 NO_x Formations

Nitrogen oxides (NO_x) form during the coal and biomass combustion of hydrocarbons in air depending on many parameters such as the type of fuels, the amount of oxygen available and the temperature of the flame. Though NO_x formation during coal combustion has been well established, NO_x formation during biomass combustion is still not well understood. The chemical and physical principals of NO_x formation during coal combustion should also apply to biomass combustion. The formation of NO_x in coal combustions mainly occurs through three reaction mechanisms: thermal NO_x (Zeldovich mechanism), prompt NO_x (Fenimore mechanism) and fuel NO_x [68].

A) Thermal NO_x. The most significant NO_x formation is by the thermal NO_x mechanism. The reactions occurring at elevated temperatures higher than 2400°F (1600 K) during combustion processes generate both nitrogen and oxygen atoms by dissociation of the respective molecules which subsequently lead to the formation of NO [68, 69]. The three main reactions of the Zeldovich mechanism are described below [69]:

$$O + N_2 = N + NO \quad (2.1)$$

$$N + O_2 = O + NO \quad (2.2)$$

$$N + OH = H + NO \quad (2.3)$$

NO is formed in both the flame front and the postflame gases [69]. The reaction (2.3) mainly takes place in a near stoichiometric and a very rich mixture gas. Although the formation rate of thermal NO_x is slow compared to combustion reactions, thermal NO_x contributes the largest

portion to the total NO_x formed during coal combustion [70]. For most coal-fired units, thermal NO_x contributes 25% of the total NO_x emission [3]. The quantity of NO_x formed depends on residence time, local stoichiometric composition (equivalence ratio), turbulence, and especially, reaction temperature.

B) Prompt NO_x. The prompt NO_x is formed directly at the flame front in fuel rich environments and provides less than 10% of overall NO_x emission [69, 71]. The hydrocarbon fragments such as C, C_2, CH and CH_2 react with the atmosphere nitrogen and their subsequent combination to produce nitrogen species such as CN, HCN, H_2CN and NH [72]. These nitrogen species react with oxygen to form NO_x. The reaction mechanisms are [72]:

$$CH + N_2 = HCN + N \quad (2.4)$$

$$N + O_2 = NO + O \quad (2.5)$$

$$HCN + OH = CN + N_2O \quad (2.6)$$

$$CN + O_2 = NO + CO \quad (2.7)$$

C) Fuel NO_x. For the fuel NO_x reaction mechanism, the reaction occurs in the combustion process from chemically/bound nitrogen in fuels [73]. The mechanism of fuel NO_x formation is presented in figure 2.3. This nitrogen evolves from the fuel in the form of HCN, NH_3 and NH_2, and then these compounds oxidize to produce NO_x strongly depending on the local stoichiometric conditions. Fuel NO_x is mainly formed in fuel lean combustions. For most coal-fired units, fuel NO_x contributes 75% of the total NO_x emission [3].

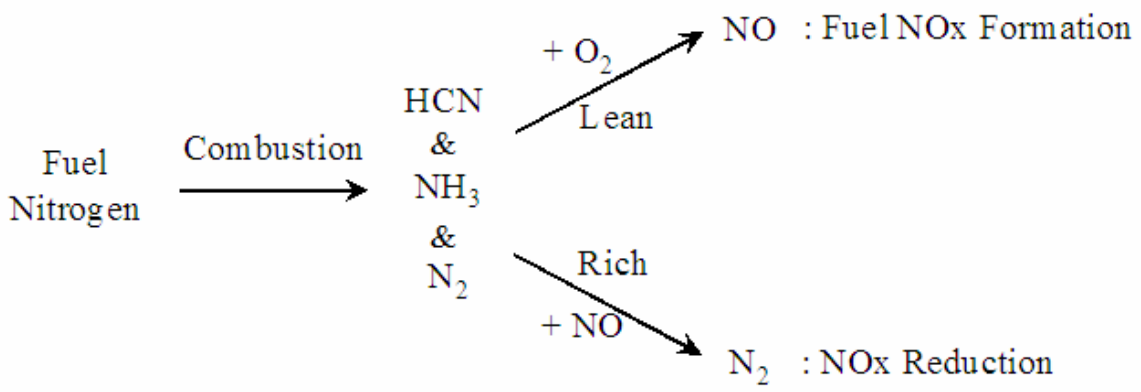

Figure 2.3. NO_x formation and reduction paths by fuel-N depending on the stoichiometry.

2.2.2 Hg Speciation and Measurements

Mercury (Hg) forms in the flue gas from coal-fired electric utility plants are typically classified into three forms: elemental form (Hg^0), oxidized form (Hg^{2+}) and particle-bound form (Hg_p). Mercury speciation generally depends on coal properties, combustion conditions, flue gas composition, fly ash composition, and temperatures. Figure 2.4 shows the production paths of Hg speciation. Mercury in coals is completely vaporized as elemental form at high temperatures during combustion. The vaporized elemental form is released into the atmosphere as Hg^0 by the direct emission, Hg^{2+} by the catalytic oxidation and $HgCl_2$ by the chlorination. Fly ash formed during the combustion absorbs some gaseous Hg forms to produce particle-bound forms. The oxidized forms of Hg include gaseous mercury chloride ($HgCl_2$), mercury oxide (HgO) and mercury sulfate ($HgSO_4$) [9]. The majority of the oxidized form formed in the flue gas in coal-fired electric utility boilers is believed to be $HgCl_2$. Some of the Hg oxidation reactions within the gas phase of a combustor are reported as chemical reactions from (2.8) to (2.19) [11, 74]. The most important species for Hg oxidation in the post-combustion process is the chlorine-containing species such as HCl and Cl_2. The reaction of Hg with atomic Cl is very fast when compared to the other forms of chlorine species.

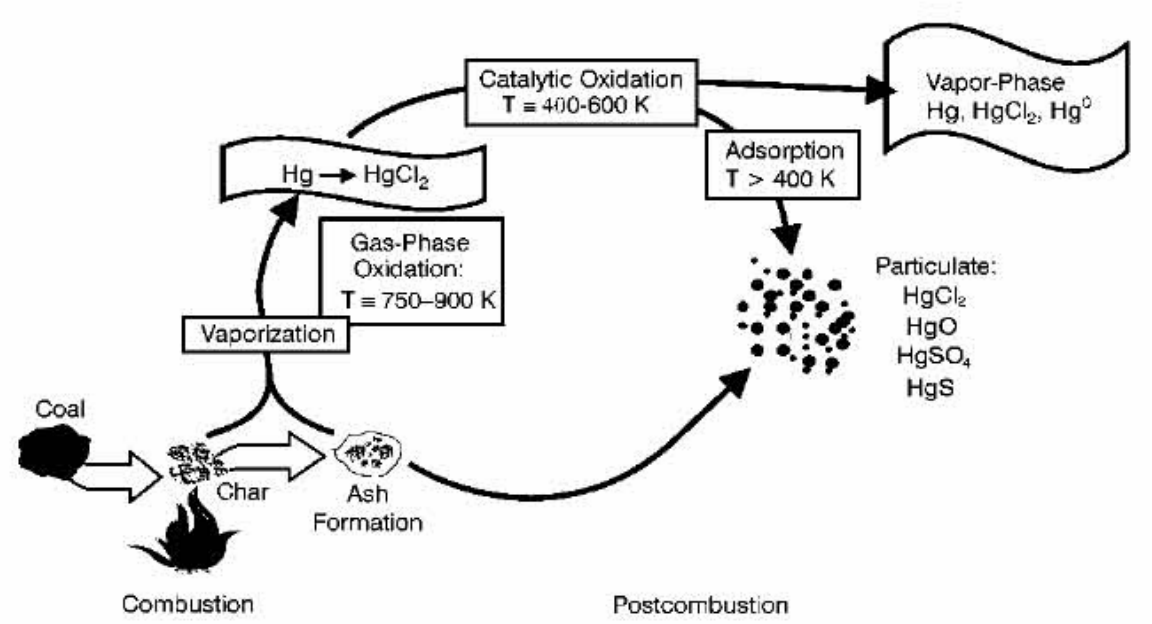

Figure 2.4. Production paths of Hg speciation [75].

$$2Hg^0 + 4HCl + O_2 \rightarrow 2HgCl_2 + 2H_2O \quad (2.8)$$

$$Hg^0 + Cl_2 \rightarrow HgCl_2 \quad (2.9)$$

$$Hg^0 + Cl \rightarrow HgCl \quad (2.10)$$

$$HgCl + Cl \rightarrow HgCl_2 \quad (2.11)$$

$$Hg^0 + HCl \rightarrow HgCl + H \quad (2.12)$$

$$Hg^0 + HOCl \rightarrow HgCl + OH \quad (2.13)$$

$$HgCl + HCl \rightarrow HgCl_2 + H \quad (2.14)$$

$$Hg^0 + O_3 \rightarrow HgO + O_2 \quad (2.15)$$

$$2Hg^0 + O_2 \rightarrow 2HgO \quad (2.16)$$

$$Hg^0 + N_2O \rightarrow HgO + N_2 \quad (2.17)$$

$$Hg^0 + NO_2 \rightarrow HgO + NO \quad (2.18)$$

$$Hg^0 + NO \rightarrow HgO \quad (2.19)$$

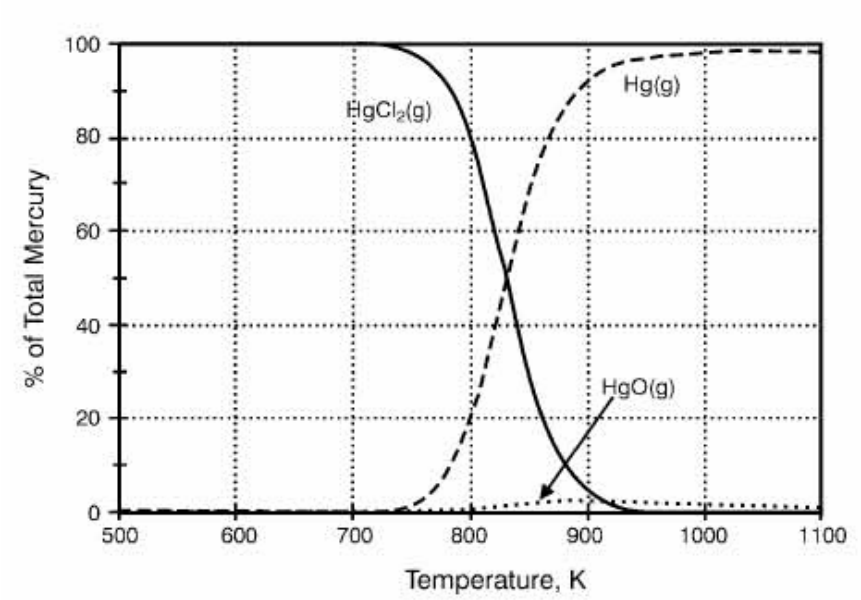

Figure 2.5. Predicted distributions of Hg species for Pittsburgh coals at equilibrium, as function of temperature [10, 75].

Figure 2.5 presents the predicted distribution of Hg species using Pittsburgh coals at equilibrium as a function of temperature. All the mercury seems to exist as $HgCl_2$ below 450ºC (725 K), and above 700ºC (975 K) is 99% gaseous Hg^0 and 1% gaseous HgO. The proportion of $HgCl_2$ and Hg^0 at temperatures between 450 and 700ºC depends on the chlorine (Cl) concentration in coals. It seemed that the heterogeneous reactions were also important for Hg oxidation at low temperatures. Thermodynamical estimation showed that all of Hg presented in the flue gas over 800°C was in elemental form [76]. It was suggested that homogeneous oxidation of Hg^0 to Hg^{2+} occurs between 400 and 700ºC by chemical equilibrium calculations [9]. It was reported that the conversion of $HgCl_2$ to Hg^0 which was called a back reaction, was

achieved 100% over 650°C, and Hg oxidation by HCl probably occurred in the cooling area between the furnace exit and the measurement port [77]. There are, however, results in apparent contradiction to the equilibrium results. In tests of pilot- and full-scale coal-fired boilers the complete Hg oxidation did not take place as predicted by the equilibrium calculations [78]. Models employed the simple equilibrium approach did not adequately predict the results of the multi-components gas stream containing sulfates [10]. Many experimental results suggests that Hg oxidation occurs above temperatures at which equilibrium would predict only Hg^0 should exist [79, 80]. Hg^0 still exists in a flue gas at temperatures even lower than 450°C [8].

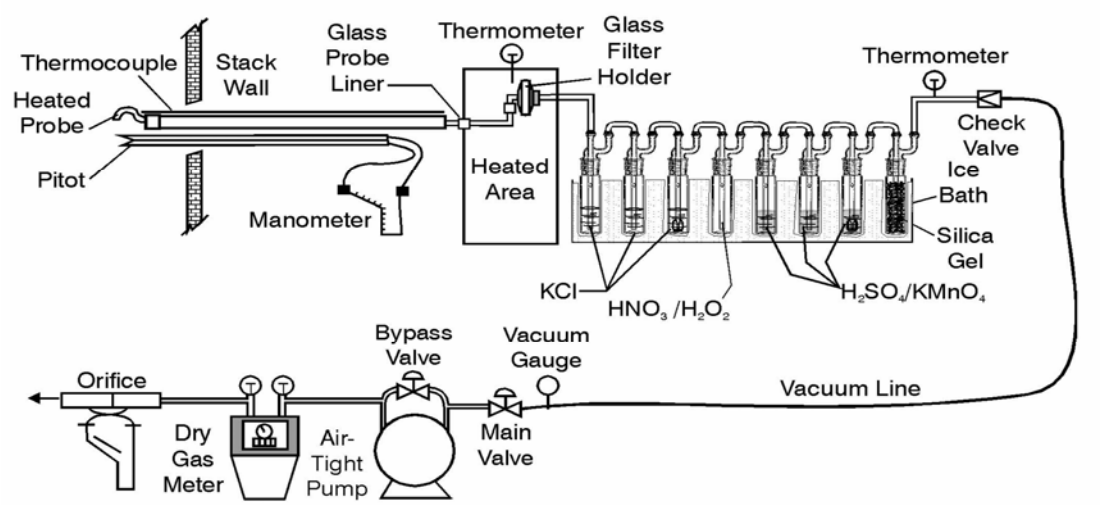

Figure 2.6. The Ontario Hydro (OH) method for Hg measurement in the flue gas form coal-fired electric utility plants on an online basis [9].

Elemental Hg can be directly measured by laser instruments, but almost all systems hardly measure oxidized form directly. To estimate the oxidized mercury, the Ontario Hydro (OH) method as shown in figure 2.6 has been commonly adopted. The OH method attempts to measure all Hg forms in the flue gas form coal-fired electric utility plants on an online basis. In principle, a nozzle and probe are operated isokinetically, a filter collects particulate matter (PM)

and chemical solutions in impingers capture gaseous mercury. A strong oxidizing solution like potassium permanganate ($KMnO_4$) captures the oxidized mercury while Hg^0 passes through the solution. The description of other methods such as the EPA Method 29, 101A and 101B, Tris-Buffer Method and MESA Method are available in Reference [9].

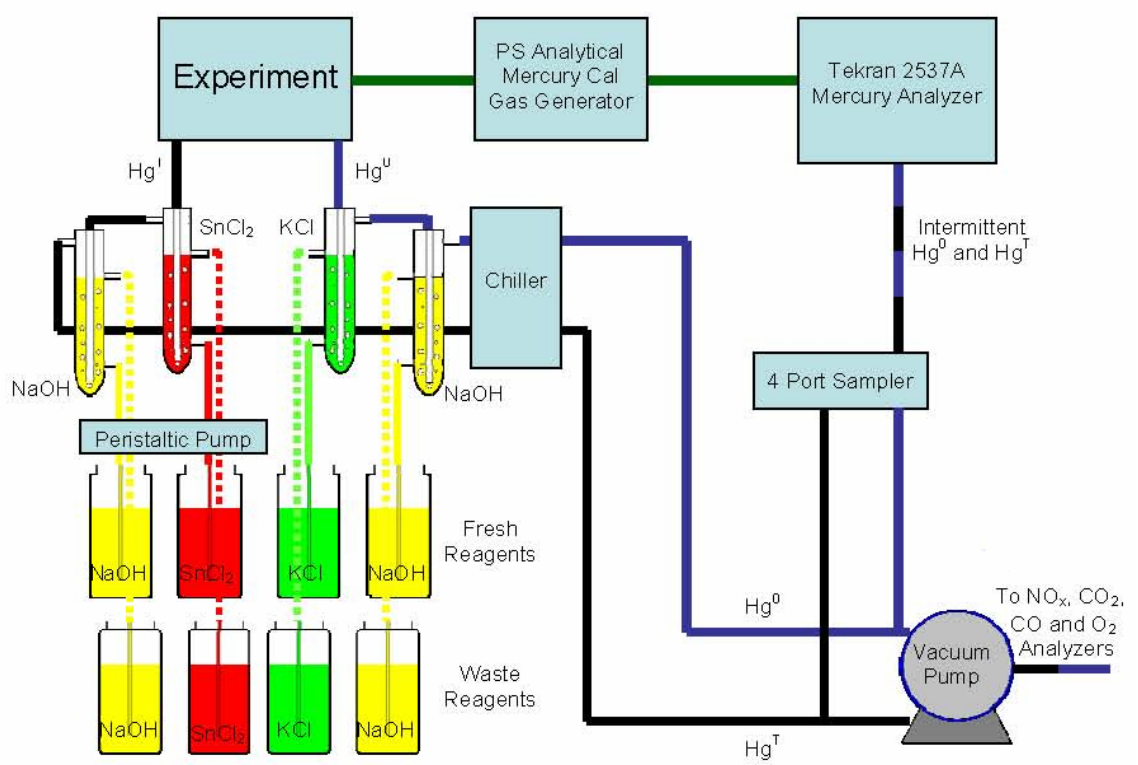

Figure 2.7. A Hg measurement method designed by Southern Research Institute (SRI) [81].

A method designed by Southern Research Institute (SRI) which is a modified method of OH method is presented in figure 2.7. In principle, two chemical solutions, KCl (potassium chloride) and NaOH (sodium hydroxide) solutions, are used for the measurements of Hg^0 and another two chemical solutions, $SnCl_2$ (stannous chloride) and NaOH (sodium hydroxide) solutions, are used for the measurements of total mercury (Hg^T). The KCl absorbs the oxidized mercury presented

in the gas stream and the $SnCl_2$ acts as a reducing agent to reduce Hg^{2+} to Hg^0. The chemical reaction between $SnCl_2$ and $HgCl_2$ is presented as Eq. (2.20). NaOH helps in absorbing SO_2 and other acidic gases, and a chiller removes water vapor. Thus the interference by SO_2 and water vapor is prevented in measuring Hg with a system based on the absorption of ultraviolet (UV) light inside the measurement system. The fresh solutions are continuously provided from each large reservoir, and the dirty solutions are stored in each waste reservoir. The concentration of oxidized mercury is represented by the measurement difference between Hg^T and Hg^0.

$$SnCl_2 + HgCl_2 \rightarrow SnCl_4 + Hg \tag{2.20}$$

Another Hg measurement method is using a continuous emission monitoring system (CEMS) which is capable of providing a real-time measurement over long time periods while Ontario Hydro (OH) method is typically used for the short-term measurement. CEMS is the integrated equipment for the determination of a gas or particulate matter (PM) concentration or emission rate using pollutant analyzers and a conversion equation, graph, or computer program to produce results in units of the applicable emission limitation or standard [82]. The use of Hg CEMS in the United States has been limited to research applications, especially the Hg measurement from the coal-fired combustion [9]. The prevalent Hg CEMS employ cold-vapor atomic absorption spectrometry (CVAAS) or cold-vapor atomic fluorescence spectrometry (CVAFS) as a detection technology. Though the accepted techniques such as OH method and Hg CEMS have been demonstrated good performances on Hg measurements, they are limited to certain applications. Therefore, developments of other technologies or the improvement of the existing technologies are still required in the field of Hg measurements.

2.3 Control Technologies of NO_x Emission

Techniques of the NO_x emission control are classified into two categories: pre-combustion controls and post-combustion controls. Pre-combustion controls reduce NO_x formation during the combustion process, while post-combustion controls reduce NO_x after it has been formed. Pre-combustion controls include low-NO_x burners (LNBs), overfire air (OFA), flue gas recirculation (FGR), operational modifications such as changing equivalence ratio (ER), reburn process, and co-firing process. Post-combustion controls include selective catalytic reduction (SCR) and selective noncatalytic reduction (SNCR). The prevalent applications in combination using the existed techniques are LNB with reburning and reburning with OFA. Each technology is discussed as the following.

2.3.1 Pre-Combustion Technology

A) Low-NO_x Burners (LNBs). LNBs delay the complete mixing of fuel and air to reduce oxygen in the primary combustion zone. Rich combustion causes the decrease of the flame temperature, residence time at peak temperatures, and hence the NO_x reduction. The lower flame temperature is achieved by premixing the fuel with deficient air so that there is no high temperature front in the flame. The combustion is staged so that not all of the heat is released in the same area thus lowering the high temperature of this zone. The concentration of unburned carbon is increased due to the rich combustion. The effectiveness of a LNB depends on several factors such as the properties of coals, amounts of volatiles in coals and the size of the furnace. LNBs along with OFA are typically chosen over secondary NO_x controllers in coal-fired power plants. They have been implemented in approximately 75% of all power plants in US. The NO_x reduction rates by using a LNB range from 40 to 70% [83].

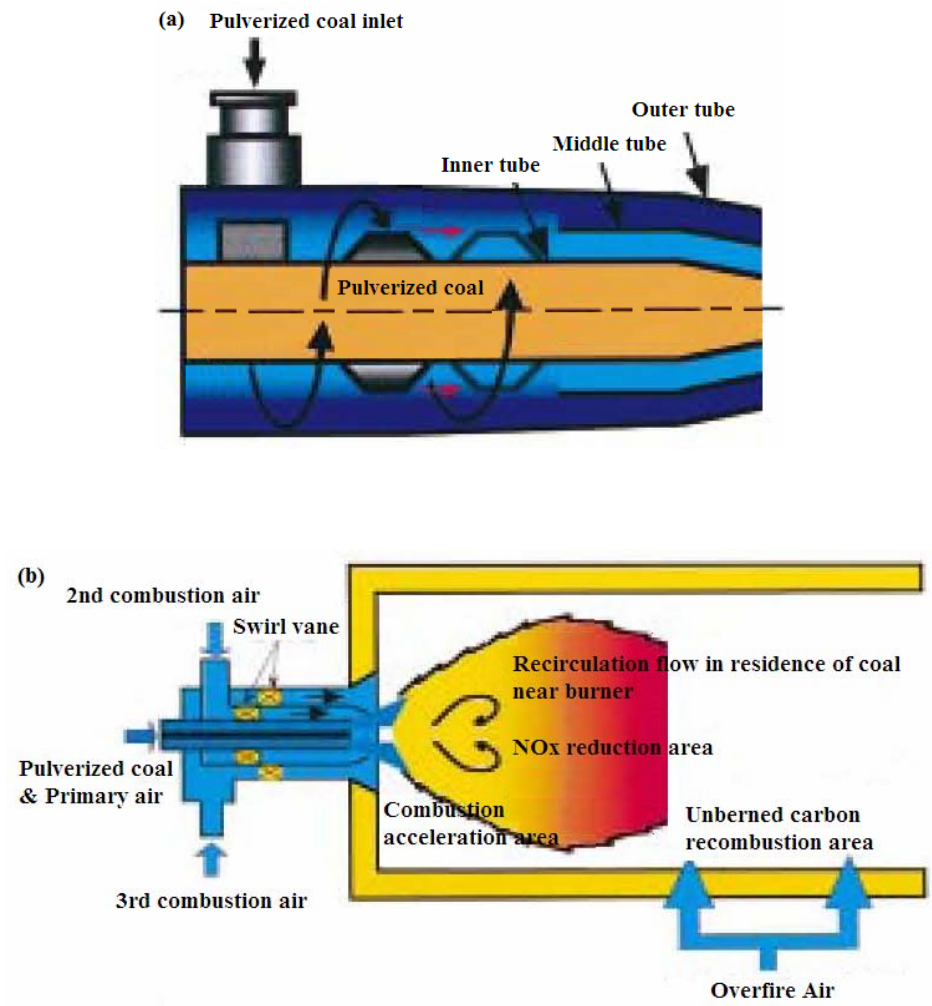

Figure 2.8. (a) Structure of the LNB and (b) Concept of the LNB with OFA [84].

A wide-range pulverized coal LNBs as shown in figure 2.8 was built to reduce NO_x emission and unburned carbon concentration in fly ash, and it could maintain stable combustion at a load of 20% [84]. The pulverized coal was fired with a small amount of air at the burner outlet, and then an oxygen deficient zone was quickly generated at the downstream region. The OFA was injected from several locations instead of one as with conventional methods. The burner was used for bench-and large-scale tests. The results showed that 30% NO_x reduction less than 3% unburned carbon concentration in fly ash.

(B) Overfire Air (OFA). The technology requires the introduction of combustion air to be separated into primary and secondary combustion regions to achieve complete burnout and to encourage the formation of N_2 rather than NO_x. OFA is typically used in conjunction with LNBs or reburn process. It is typically 20% of the total air flow with an overall excess air level of 15 – 25% [3].

(C) Flue Gas Recirculation (FGR). In this technique, a part of the flue gas is re-circulated to the furnace. It lowers flame temperature and reduces the oxygen concentration in the furnace to reduce NO_x formation. Though the heat content of the re-circulated flue gas contributes to heat recovery, too much FGR lowers the combustion performance and too little FGR increase NO_x emissions.

(D) Operational Modifications. The technique is changing certain boiler operational parameters to create conditions in the furnace to reduce NO_x formation [3]. It includes changing equivalence ratio (ER), stoichiometric ratio (SR), burners-out-of-service, low excess air, and biased firing. The ER is typically defined as the ratio of the fuel-to-air ratio to the stoichiometric fuel-to-air ratio which is an inverse value of the SR.

(E) Reburning. The reburn process which is the technology used in the current study has been introduced in the early 1970's. As shown in figure 1.6, the basic reburn technology uses two separated combustion regions: a primary combustion region where the primary fuel is fired, and a reburn combustion region where the additional fuel is fired. In the primary combustion region, coal or natural gas (NG) is fired under normal to low excess air conditions (or SR = 1.1) at between 1200 and 1500ºC and generates 70 to 90% of the total heat. Due to less amounts of

the fuel, the level of the NO_x is formed about 10% less than the NO_x formation in the case with 100% heat input. In the reburn combustion region using conventional fuels (e.g., NG and coals), reburn fuel molecules break down to hydrocarbon (HC) fragments which react atmospheric nitrogen to produce HCN and NH_3. These HCN and NH_3 react with NO_x in the slightly rich combustion to produce N_2. The optimal SR in the reburn combustion region is 0.85 to 0.95 (or ER = 1.05 to 1.18) [3] and the typical temperature is between 1200 and 1400ºC. The reburn fuel produces 10 to 30% of the total heat, while biomass co-firing in coal-fired units is typically limited to 5% of the heat input. OFA is typically used in the downstream of the reburn zone to create a burnout zone with SR = 1.15 at between 900 and 1300ºC for complete combustion. NG, coal and fuel oil reburn applications are in operation. Recently the US DOE has performed NO_x reductions in coal-fired boilers by the reburn technology to evaluate its performance and economics: coal reburning for cyclone boiler NO_x control, gas reburning and low-NO_x burners on a wall-fired boiler, and micronized coal reburning [3]. The effective parameters on the reburn process are temperature, mixing, residence time, fuel type, and reburn stoichiometry. NO_x reduction increases with low temperature, high degree of mixing, longer residence time, high nitrogen fuel, and low oxygen concentration.

NO_x reduction in reburning with OFA using a down-fired pilot-scale (300 kW) combustion facility was examined for the effect of metal-containing compounds [28]. The schematic of the pilot-scale combustor is shown in figure 2.9. NG was used as the main fuel and the reburn fuel. Metal-containing compounds such as sodium carbonate, potassium carbonate, calcium acetate, and fly ash were injected with the main fuel or the reburn fuel. It resulted in the reduction of SO_2 and NO_x while CO increased, and the co-injection with the main fuel had more effect than with the reburn fuel. In the modeling results, the increase in NO_x reduction in the reburn area was because of the slow oxidation of the reburn fuel in the presence of sodium.

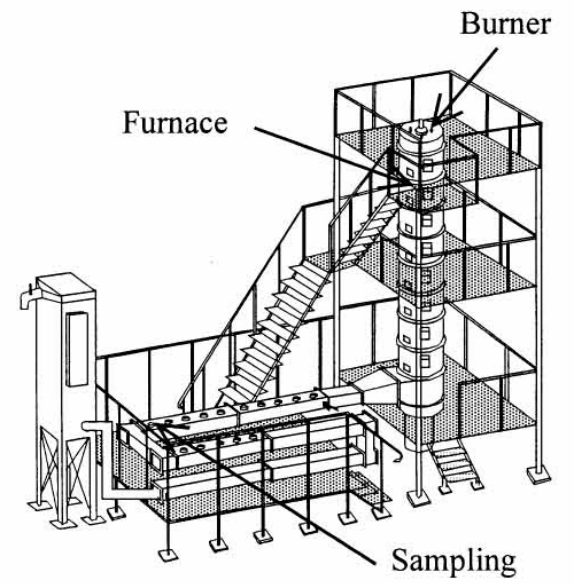

Figure 2.9. A schematic of the down-fired pilot-scale (300 kW) combustion facility [28].

There are numerous studies on the reburn technology in the literature [3, 22, 23, 27 – 43, 57, 85, 86]. In Table 2.1, recently reburn studies are listed in chronicle order, and the important test variables and results are summarized. The overview of the literatures indicates the NO_x reduction efficiency depends on the operating conditions of the reburn process. It strongly depends on the primary stoichiometric ratio (SR_1 or λ_1) and the reburn stoichiometric ratio (SR_2 or λ_2), the reburn fuel type, and the particle size of the reburn fuel. Reburn temperature, oxygen concentration (i.e. FGR), heat input, baseline NO_x concentration, mixing time, and residence time are also important variables to control NO_x emissions. Some of the results indicate that biomass including cattle manure and wood showed higher potentials in NO_x reduction than coals. The addition of promoters such as alkali compounds, fly ash and catalysts increases NO_x reduction efficiencies. The use of the pyrolysis gas from the biomass gasification as a reburn fuel is another way to dispose biomass with high NO_x reduction. Advance gas reburning (AGR) by injecting N-agent, typically NH_3 or urea, is one of the effective methods on NO_x control.

Table 2.1. Summary of reburn experiments.

Ref.	Boiler Capacity	Reburn Fuel (Heat Input)	Fuel Particle Size (Reburn Temp.)	Reburn SR (Main SR)	Residence Time	Max. NO_x Reduction (Baseline NO_x)	Conclusion
[57] 1995	38 kW + OFA	Wood (10%)	100% < 1680 μm (1700 K)	0.85 - 1.05 (1.15)	0.4 s	60% (200 - 500 ppm)	Wood was used effectively as a reburn fuel in a pulverized coal-fired furnace.
[29] 1996	300 MW + OFA & FGR	NG, oil & coal (15 - 20%)	80% < 44 μm (1800 K)	0.9	NA	65% (600 ppm)	A multifuel reburn system was installed and successfully reduced NO_x emissions.
[30] 1996	Electric furnace + OFA	CH_4, synthetic gas & pyrolysis gas of coal	Gas (1300 - 1700 K)	0.65 - 1.15 (0.65-1.15)	1.2 - 3 s	88% (NA)	Pyrolysis gas was shown to be effective as a reburn fuel, and the longer residence time, the lower NO_x emission.
[31] 1997	105 MW + OFA & AGR	NG (10 - 20%)	Gas (1200 - 1400 K)	0.9	NA	70% (0.62 lb/mmBTU)	Advance gas reburning (AGR) by the injection of N-agent with NG significantly improved NO_x reduction as well as the stack CO emissions.
[32] 1997	200 kW + OFA & AGR	Bituminous coals (10 - 35%)	75% < 63 μm (1600 K)	0.83 - 1.0 (1.0 - 1.18)	0.12 - 0.84 s	65% (600 ppm)	The extent of NO_x reduction was strongly dependent on the reburn SR, and the optimum residence time in the reburn zone was found to be 0.45 s.
[33] 1998	17 kW & 0.9 MW	NG (7 - 25%)	Gas (800 - 1100 K)	1.2 (1.2 - 1.3)	NA	60% (250 - 2600 ppm)	The fuel-lean reburning tested using laboratory and pilot scale boilers was found to be an effective way to control NO_x.
[34] 1998	265 MW + OFA	Wood (15%)	80% < 800 μm (1900 K)	< 0.9 (1.05)	0.3 - 1.2 s	60% (~ 1300 ppm)	Wood was successfully used as a reburn fuel on NO_x reduction using a cyclone fired boiler.

Table 2.1. Continued.

Ref.	Boiler Capacity	Reburn Fuel (Heat Input)	Fuel Particle Size (Reburn Temp.)	Reburn SR (Main SR)	Residence Time	Max. NO_x Reduction (Baseline NO_x)	Conclusion
[35] 1999	300 kW + OFA & AGR	Biomass, coals, CRDF, & orimulsion (10 - 20%)	70% < 75 μm (1700 K)	0.88 - 0.99 (1.1)	0.4 - 0.7 s	91% (AGR) (200 - 1300 ppm)	Advanced gas reburning (AGR) by the addition of N-agent with promoters greatly increased NO_x reduction.
[36] 2000	300 kW + OFA	Wood, waste, walnut shell, & NG (10 - 25%)	55% < 75 μm (1700 K)	0.84 - 0.99 (1.1)	0.82 s	72% (400 - 900 ppm)	NO reductions by walnut shell were as high as results by NG. (NG > walnut shell > furniture waste > willow wood).
[28] 2001	300 kW + OFA	NG (5 - 25%)	Gas (1700 K)	0.83 - 1.05 (1.1)	0.82 s	66% (600 ppm)	Reburning with alkali compounds was effective in the control of NO_x emissions.
[37] 2002	35 kW	Switchgrass & alfalfa (4 - 23%)	75% < 1000 μm (1600 K)	1.05 - 1.4	0.81 s	70% (500 ppm)	Reburning was tested using an overall fuel-lean boiler. High N-containing fuel was used successfully as a reburn fuel.
[22] 2003	30 kW	FB & LB (30%)	70 - 90% < 75 μm (1500 K)	0.91 - 1.0 (1.05)	1 s	80% (600 ppm)	Feedlot biomass (FB) and litter biomass (LB) were successfully used for co-firing, reburning and gasification processes.
[38] 2004	Kinetic model	NG & CH_4 (10 - 30%)	Gas (900 - 1450 K)	0.51 - 0.99	0.12 s	80% (850 - 920 ppm)	Modeling results were similar to experimental results. Injecting NH_3 into a reburn system improved NO reduction.
[23] 2004	600 kW + OFA	Syngas (5 - 23%)	Gas (1000 - 1500 K)	0.95 - 1.3 (1.1 - 1.4)	1.6 s	46% (460 ppm)	Syngas used in reburning was effective on NO_x reduction though it contained low hydrocarbon content.

Table 2.1. Continued.

Ref.	Boiler Capacity	Reburn Fuel (Heat Input)	Fuel Particle Size (Reburn Temp.)	Reburn SR (Main SR)	Residence Time	Max. NO_x Reduction (Baseline NO_x)	Conclusion
[39] 2004	30 kW	CB, coals, & coal:CB blends (30%)	50 - 70% < 100 μm (1500 K)	0.83 - 1.0 (1.05)	0.4 - 0.9 s	62% (600 ppm)	Cattle biomass (CB) resulted in higher NO_x reduction than coal, and circular jet/flat spray reburn nozzles were tested.
[86] 2005	80 kW + OFA	Carboxylic salts with C_3H_8 (9 - 20%)	NA (1400 K)	0.86 - 1.03 (1.05)	NA	80% (NA)	Addition of carboxylic salts to propane as a reburn fuel improved the reburn process.
[40] 2005	30 kW + OFA	Pyrolysis gas of sewage sludge, sawdust, etc. (40%)	Gas (1600 K)	0.75 - 1.15 (1.15)	2 s	89% (1000 - 1200 mg/m^3)	Pyrolysis gas from biomass using as a reburn fuel contributed high NO_x reduction and the net CO_2 reduction.
[41] 2006	30 kW	CB, coals, & coal:CB blends (30%)	60 - 90% < 150 μm (1500 K)	0.87 - 1.0 (1.05)	0.6 - 0.7 s	95% (400 ppm)	Cattle biomass (CB) was used as a reburn fuel successfully. NO_x reduction was significant in fuel-rich conditions.
[42] 2007	Laminar flow reactor	Synthetic gas (CH_4 + C_2H_6)	Gas (900 - 1500 K)	0.6 – 2.0	> 0.8 s	50% (850 ppm)	Fuel mixing was effective for reburning due to the change in local stoichiometry and residence time.
[43] 2007	1 MW + LNB & OFA	Coals (15 - 25%)	Micronized D_{median}: 11 - 54 μm (1600 K)	0.85 - 0.95 (1.05)	NA	80% (775 - 820 ppm)	Micronized fuels resulted in little increase in NO_x reduction in a tangential fired boiler. The optimum position of the reburn nozzle was tested.

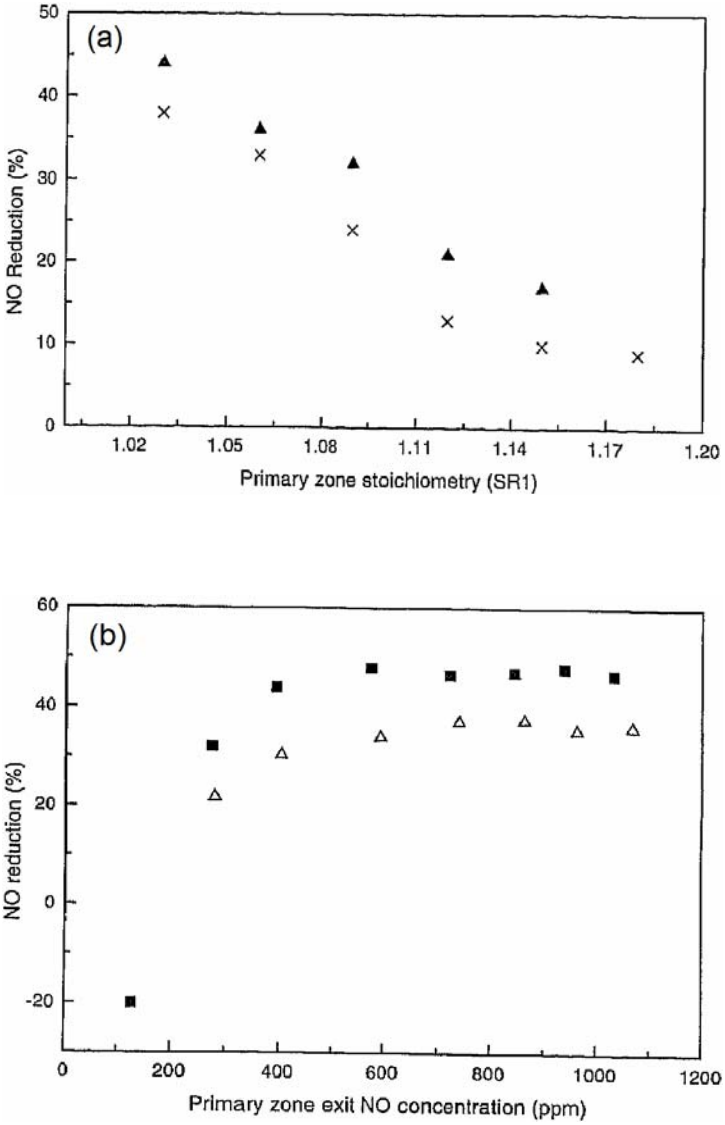

Figure 2.10. NO_x reductions using bituminous coals as a function of (a) Primary stoichiometric ratio in the conditions of $\lambda_2 = 0.92 - 1.04$ and (b) Baseline NO_x concentration in the conditions of $\lambda_1 = 1.01 - 1.03$ and $\lambda_2 = 0.94$ [32].

Several bituminous coals were tested for reburning using a 0.2MW pilot-scale furnace over a wide range of operation parameters, and the effects of SR_1 are presented in figure 2.10 (a). The NO_x reductions decreased with an increase in SR_1 due to the high O_2 concentration. This effect is similar to the effect of reburn stoichiometric ratio (SR_2). In figure 2.10 (b), High NO_x reductions

were found with the baseline NO_x concentrations higher than 300 ppm while about 20% of the NO_x formation was observed with the baseline NO_x of 117 ppm. The results also showed the NO_x reductions remained constant beyond the baseline NO_x of 600 ppm. It indicated the reburn technology was very effective for the systems with high NO_x reductions. When the oxygen concentration in the carrier gas of the reburn fuel decreased from 21% to 12%, NO_x reductions increased.

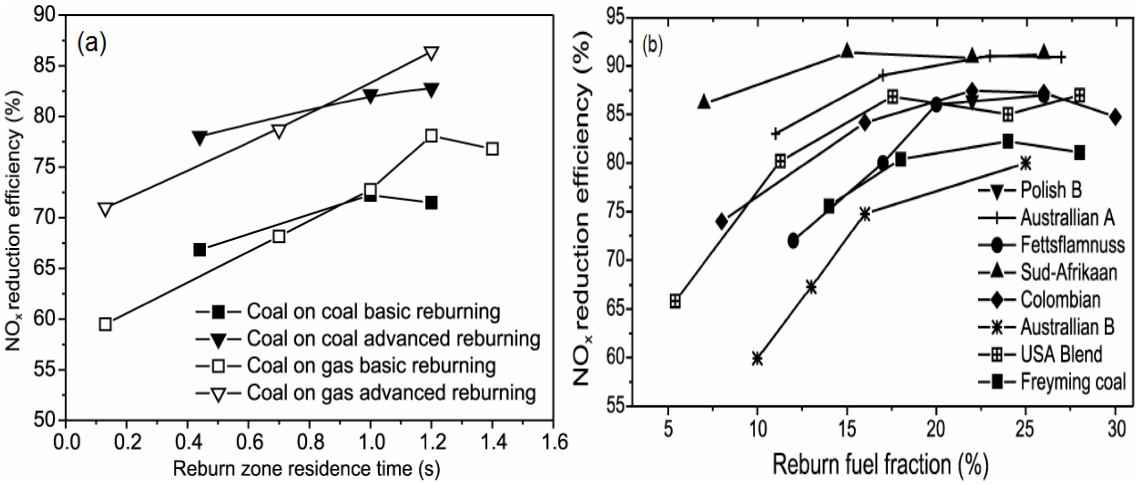

Figure 2.11. (a) Effects of the residence time in the conditions of baseline NO_x = 770 ppm, λ_1 = 1.05, and reburn fuel fraction = 22% at 3% O_2 and (b) Effect of the reburn fuel fraction in the conditions of AGR-lean combustion, λ_1 = 1.05, and residence time = 1.2 s [85].

In figure 2.11, effects of the residence time in the reburn zone and the fraction of the reburn fuel are presented using several coals as reburn fuels for conventional and AGR operations in a bench-scale down-fired combustor. The use of AGR achieved about 85% NO_x reduction and 10% higher than the results of the conventional operation. The NO_x reduction improved about 5% for the conventional operation and about 14% for the AGR operation with increasing reburn residence time. The improvements were comparable between the coal on coal case and the coal on gas case. The primary fuel was coal for the coal on coal case and NG for the coal on gas case.

The reburn fuel fraction was varied from 7 to 28% in the conditions of AGR, λ_1 = 1.05, and residence time = 1.2 s. The NO_x reductions increased with an increase of the reburn fuel fraction in AGR-lean combustion as shown in figure 2.11 (b), and some results showed it decreased with an increase of the reburn fuel fraction in AGR-rich combustion. It indicated AGR was less effective with higher reburn fuel fraction.

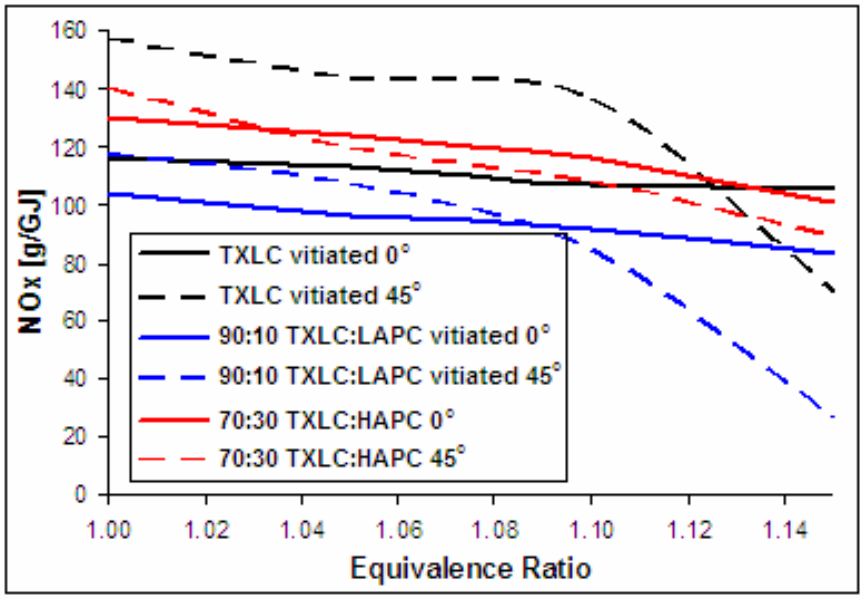

Figure 2.12. NO_x emissions for pure coals and coal:CB blends as a function of the equivalence ratio in the reburn zone [41].

Cattle biomass has been proposed to use in coal-fired boiler facilities and were experimented as reburn fuel using a bench-scale (30 kW) boiler facility [27]. The reburn process has resulted in an US Patent # 6,973,883 [46]. In a previous study, the results of cattle biomass (CB, termed as feedlot biomass, FB) as a reburn fuel shown in figure 2.12 indicated that 90 – 95% NO_x reduction was achieved using a bench-scale boiler [41]. The effects of equivalence ratios (ER or ϕ), fuel injection angles (0° and 45°), blending proportions (pure fuels, 90:10 and 70:30 blends

on a mass basis), and oxygen concentrations (vitiated: 12.5% O_2 & non-vitiated: 20.9% O_2) were tested with FB as a reburn fuel. The equivalence ratio (ER) is defined as the inverse value of the stoichiometric ratio (SR) which boiler industries prefer to use (SR = 1 / ER). The performance was compared with those of Texas Lignite coal (TXLC) as standard reburn fuels. The results are presented in figure 2.12. With increased equivalence ratio, the oxygen in the combustion zone is depleted quickly. Low levels of oxygen slow down the NO_x formation and allow the NO_x reduction to be dominant in the combustion zone. The significant influence on NO_x reduction is shown with an increase in ER. To simulate the flue gas recirculation (FGR), nitrogen gas with the reburn air was used and it was called the vitiation,. In the vitiation condition, higher NO_x reduction was achieved. The 45° injection of the reburn fuel showed the significant increase of NO_x reduction compared to the 0° injection. The 45° upward injection caused the increase of mixing time, residence time and gas temperature in the boiler.

The effects of reburn fuels such as wood, pulverized coal and NG on NO_x reduction as a function of the SR of the reburn zone are shown in figure 2.13, and the results of wood were slightly better than those of NG and coal. It was reported that the use of the flue gas recirculation (FGR) system to feed the wood particles increased the potential of the reburn process. The use of wood as a reburn fuel in a cyclone-fired boiler also resulted in the good control of NO_x emissions [34]. The co-firing results of 20% wood and 80% coal by mass showed a strong potential for the reduction of the greenhouse gas emissions [21]. It was reported that wood chips could be economically hauled up to 60 miles to an energy facility. However, it is difficult to maintain the peat power production since the relative low heating value (LHV) of wood chips. It was recommended that wood not be fired during a winter time because of the difficulty of the firing of the frozen wood. Wood is also an effective renewable fuel for both reburning and co-firing.

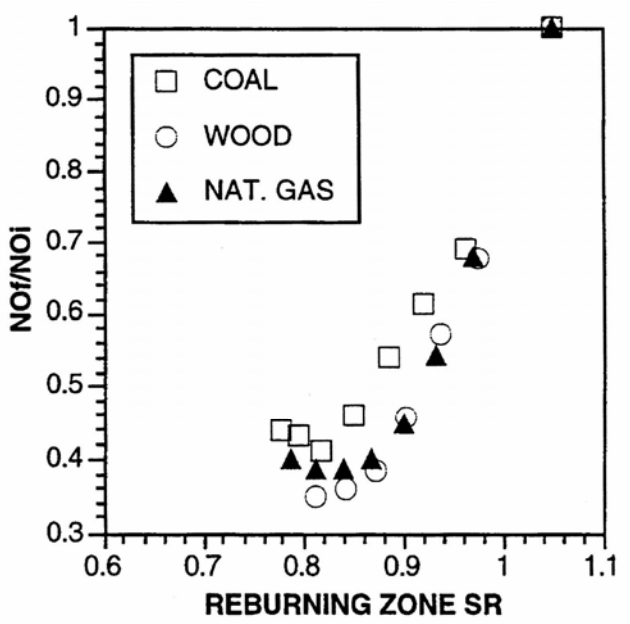

Figure 2.13. NO_x reductions as a function of stoichiometric ratio (SR) in the reburn zone using various reburn fuels [34].

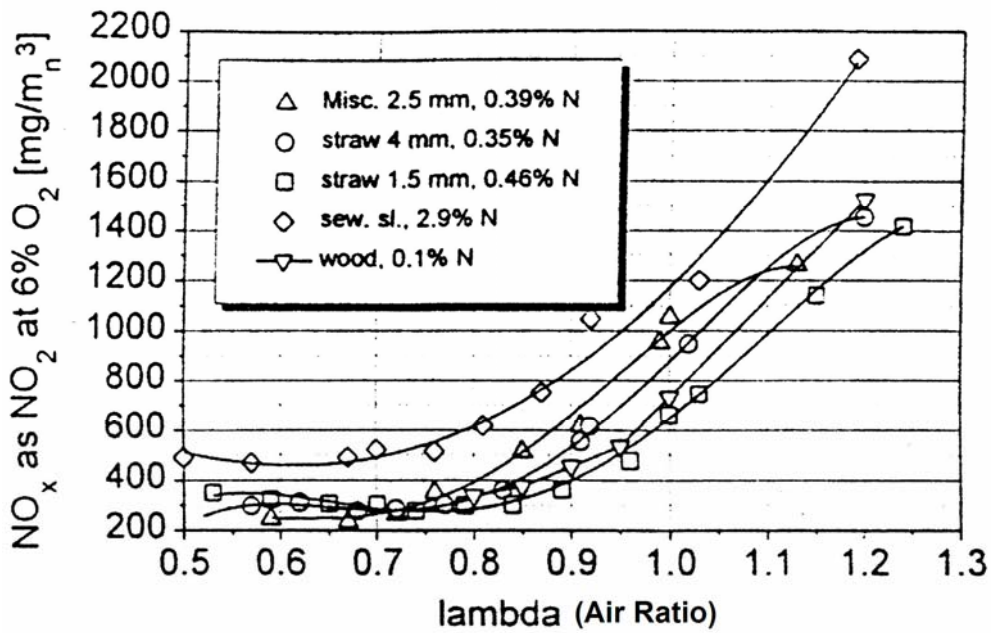

Figure 2.14. NO_x emissions for air-staging with different kinds of biomass (lambda = SR) [17].

Sewage sludge was examined for the effect of co-combustion of biomass on NO_x emission in pulverized fuel furnaces [17]. A semi-industrial pulverized-coal boiler was designed as a vertical cylinder with a top-fired burner and produced a thermal output of 0.5 MW. They found that the burner design and operation mode have a great influence on the NO_x emissions. The use of the biomass reduced NO_x emission when air staging and reburning were used. About 300 mg/m^3 or less NO_x emissions were obtained with 6% oxygen concentration. Figure 2.14 shows the effect of various reburn fuels on NO_x emissions. Biomass reburning was tested using wood, straw, Miscanthus, and sewage sludge. With the decrease of SR (or lambda) in the reburn zone, NO_x emissions decreased. SO_2 emissions rose since the sludge contained the higher level of sulfur than that in coals used.

(F) Co-firing. Among the co-firing studies in biomass combustion [12 – 26], a co-firing with CB was proposed where CB was ground, mixed with coal, and then fired in existing pulverized coal-fired boiler burner facilities [12]. The test was performed with using bench- and large-scale boiler burner facilities. The cattle feedlot biomass (FB) has approximately half the heating value of coal, twice the VM of coal, and four times the N content of coal on heat basis. The results are presented in figure 2.15. NO_x production by the fuel blend near the fuel nozzle was higher than the NO_x for coal; however, the exhaust emission of NO_x was lower in the fuel blend than in the coal. Figure 2.15 (b) shows that NO_x formation is increased with an increase of the O_2 concentration in the reburn zone. The results revealed that the blend reduced NO_x emissions, increased CO emissions and burned more completely than 100% coal in the boiler. The reduction of NO_x is attributed to the high VM and N content. This new co-firing technology has the potential to reduce NO_x emissions in coal fired boilers located near cattle feedlots and also relieves the cattle industry of the waste material.

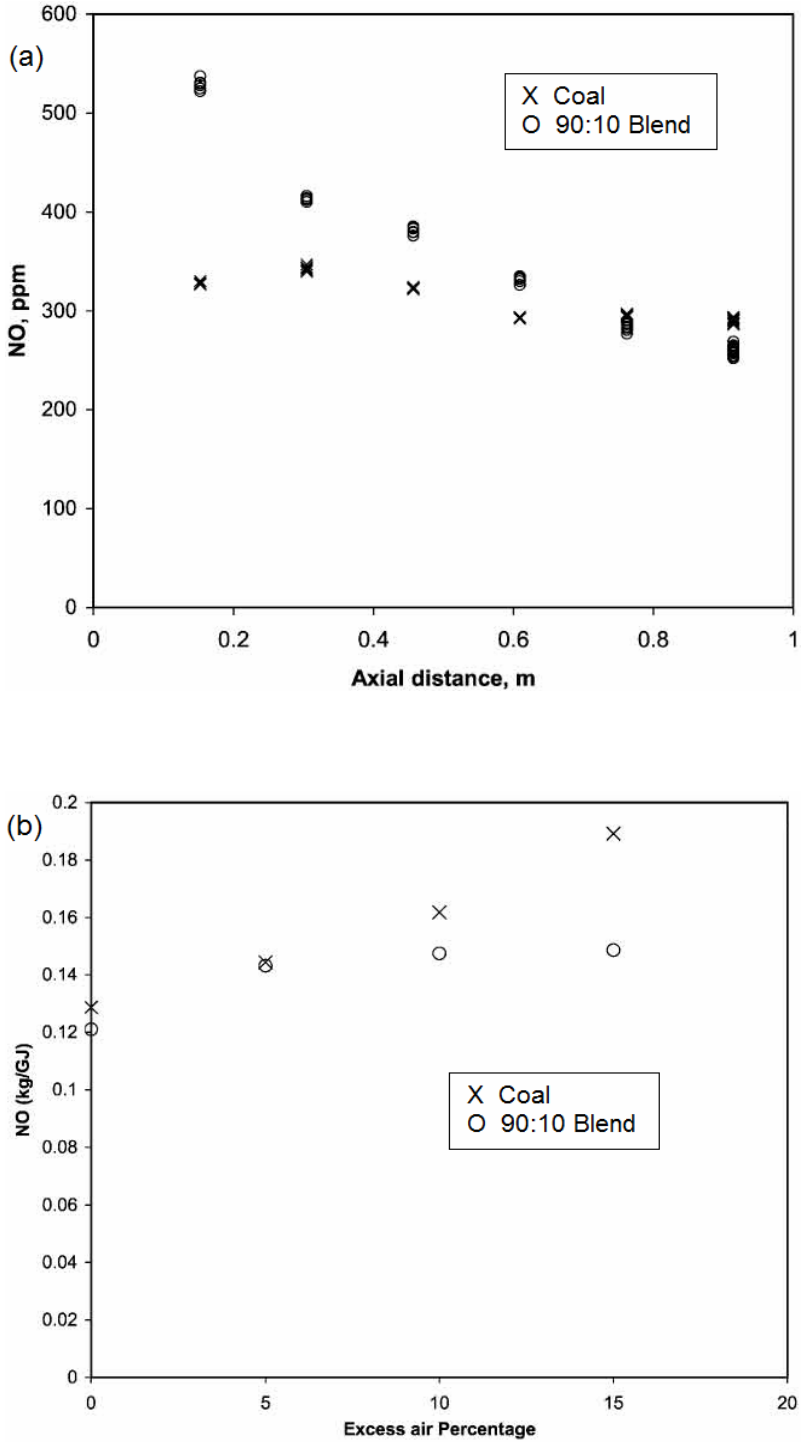

Figure 2.15. (a) NO_x emissions as a function of the axial distance from the fuel nozzle and (b) NO_x emissions as a function of the excess air in the reburn zone [12].

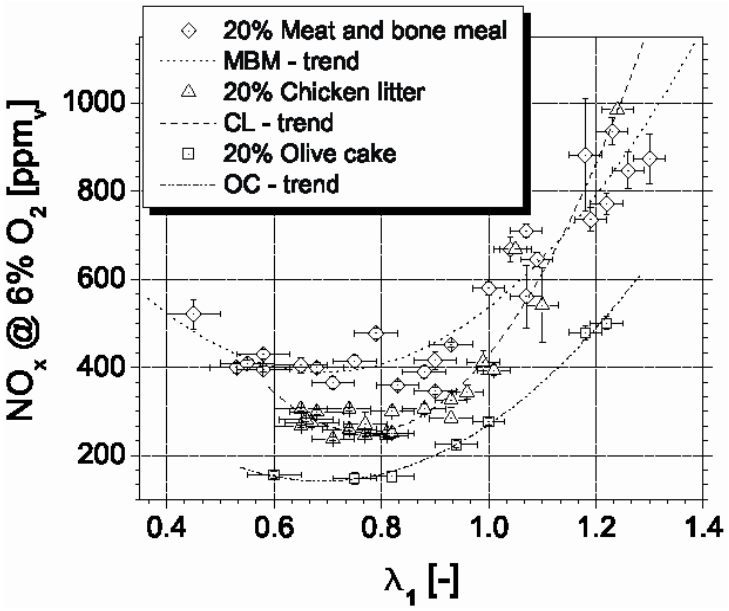

Figure 2.16. Effects of primary stoichiometric ratios (λ_1) and fuels on NO_x emissions [16].

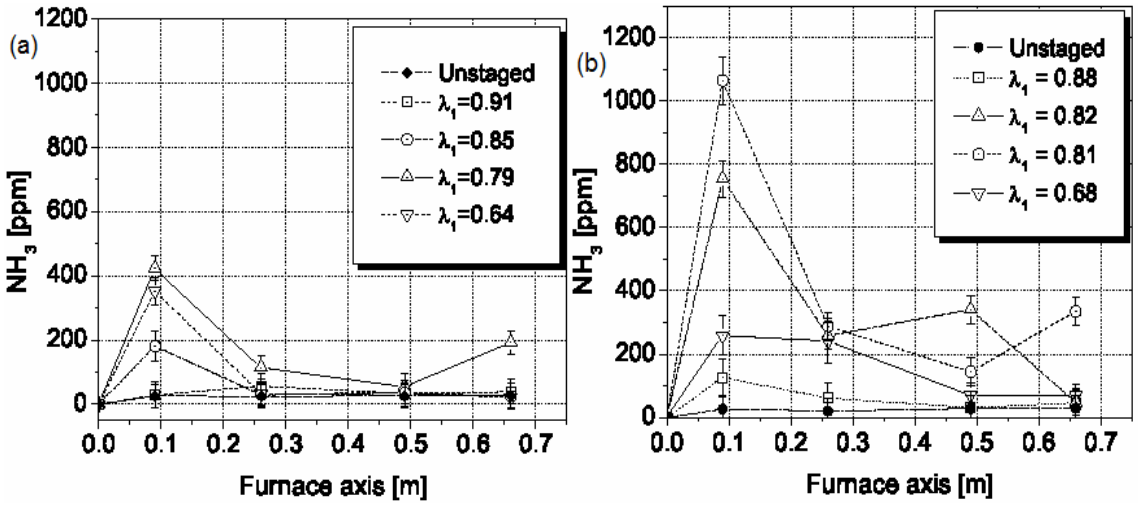

Figure 2.17. Productions of NH_3 as a function of the primary stoichiometric ratio and the furnace axis: (a) 100% coal combustion and (b) 80:20 coal:LB co-firing [16].

The effects of several co-firing fuels and the primary stoichiometric ratio (SR_1 or λ_1) on NO_x emissions were presented in figure 2.16. The fuels blended 20% biomass and 80% bituminous coal on a thermal basis. The poultry litter biomass (LB) co-firing presented the highest NO_x

reduction. The optimal range of SR_1 was found to be between 0.7 and 0.9. In fuel-lean combustion, NO_x emissions increased due to high concentrations of O_2 which reacted with N_2 to form NO while in very fuel-rich combustion ($\lambda_1 < 0.7$), high productions of NH_3 and HCN were oxidized to NO in the burnout zone. Figure 2.17 presented the production of NH_3 along with the furnace axis for both coal and biomass co-firing. The highest production of NH_3 was observed at $\lambda_1 = 0.79$ for the coal and $\lambda_1 = 0.81$ for the coal:LB blend. Results in figures 2.16 and 2.17 indicated higher concentrations of NH_3 increased NO_x reductions.

Pine sawdust which contained 50 – 65% moisture on an as received basis was investigated for co-firing using a tangentially-fired pulverized-coal boiler [18]. The boiler facility was equipped with roller coal mills, modern LNBs, OFA, electrostatic precipitators (ESPs) and flue gas desulphurization (FGD) plants. During the tests, sawdust proportions of 2.5 – 8% (from the fuel input) were examined. NO_x level and unburned carbon in the fly ash increased when both coal and sawdust were simultaneously pulverized by the coal mills and fed into the boiler. The increase of NO_x and unburned carbon was attributed to larger coal particles sizes and the moisture in the wood causing a delay in the ignition of the coal and biomass. For the long-term use, the separated grinding and feeding systems for coal and biomass is recommended.

The use of straw and residual wood with coal in an existing power plant (509 MW) in Germany was significantly lowered NO_x and SO_2 emissions [19]. The addition of 10% straw by mass reduced the emissions of NO_x and SO_2 by approximately 46% and 80%, respectively. The results of the residual wood showed lower environmental impacts than those of straw, which found 66% NO_x reduction and 95% SO_2 reduction for the residual wood. These measurements were taken after desulphurization and denitrofication treatments were performed. Because of the high chlorine content in straw, the HCl emissions were high, and it could affect another chemical reaction such as Hg oxidation.

2.3.2 Post-Combustion Technology

(A) Selective Catalytic Reduction (SCR). This technology uses a catalyst in the downstream of the furnace along with a reducing agent, usually NH_3, to remove NO_x to N_2 in the exhaust gas. The catalyst promotes reactions between NO_x and ammonia to form nitrogen and water. Since NO is the primary component of NO_x emitted from combustion sources, the reactions (2.21) and (2.22) are the overall main reactions which occur during the SCR process with NH_3 [87]. NO_x reductions as high as 90% are achievable. Any ammonia emission is called ammonia slip.

$$4NH_3 + 6NO \rightarrow 5N_2 + 6H_2O \quad (2.21)$$

$$4NH_3 + 4NO + O_2 \rightarrow 4N_2 + 6H_2O \quad (2.22)$$

(B) Selective Non-Catalytic Reduction (SNCR). The SNCR process uses only a reducing agent (ammonia or urea) without catalysts. The reducing agent reacts with NO_x to form nitrogen and water. The SNCR process has lower NO_x removal efficiency at relatively higher operating temperatures. The capital cost of the SNCR process is lower than the SCR process due to the high cost of catalysts. NH_3 slip (reducing the effective NO removal) occurs more in SNCR than in SCR.

2.4 Hg Emission and Oxidation

2.4.1 Control Technologies for Hg Emission

Several techniques can be used to capture or remove mercury from coal-fired power plants; electrostatic precipitators (ESP), fabric filters (FF), particle scrubbers, and mechanical collectors. For the nationwide distribution of existing PM emission controls used for coal-fired electric utility boilers in 1999, ESP is the predominant control device (82.9%) [88]. Fabric filters are used on about 13.6% of the coal-fired boilers, particle scrubbers are used for 2%, mechanical collectors are used for 0.4%, and control device in combination is used for 1.1%.

Some fly ashes have an important role in Hg oxidations [9, 89, 90]. Fly ashes from bituminous coals showed high Hg oxidations than fly ashes from subbituminous coals and lignite, and the oxidation rate depends on the composition of the fly ash, especially the iron content, and the constituents of the flue gas, especially HCl or NO_x [9]. Also gaseous forms of both Hg^0 and Hg^{2+} are adsorbed onto the unburned carbon in fly ash to produce particle-bound form (Hg_p), and the particle-bound forms are collected by ESP or FF in the downstream of the system. Thus the coal-fired electric utility boilers equipped with ESP or FF can achieve high efficiency of Hg oxidation or Hg capture. Electrostatic precipitators operate by attaching electrically charged particles on to oppositely charged metal plates while FF operates by collecting fly ash through porous fabric materials.

To ensure the high efficiency of Hg_p capture, many coal-fired boilers can be equipped the PM control device such as ESP or FF with a wet flue gas desulfurization (WFGD) scrubber or a particulate matter spray dryer absorber (PM-SDA) system. In the WFGD system, gaseous forms of Hg^{2+} are absorbed in the liquid slurry and react with dissolved sulfides in the flue gas to form mercuric sulfide (HgS) which is precipitated as sludge. In the SDA system, the principle is the same as the WFGD system except using a fine mist of lime slurry instead of the aqueous slurry.

Gaseous mercury can be also removed and captured from the gas stream by the sorbent injection (SI) into the exhaust stream. The surface area of the sorbent is the most common characteristic properties to capture mercury. Removal of mercury is increased with an increase of the pore surface area of the highly porous sorbent [9]. Many studies have been focused on carbon and calcium-based sorbents which is not a low-cost product. New classes of Hg sorbents are required to improve the removal efficiency and to reduce the operating cost.

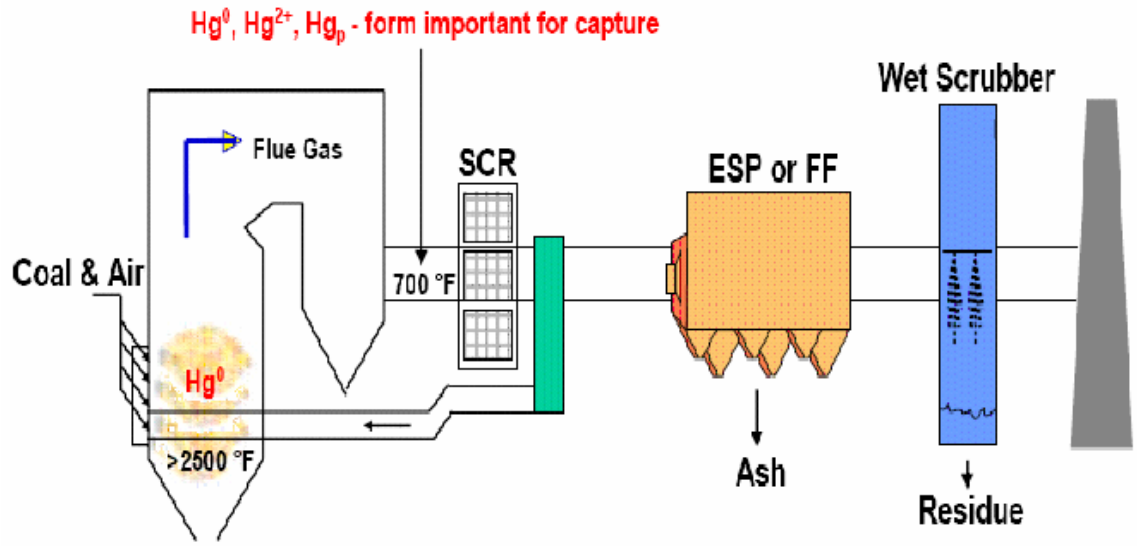

Figure 2.18. A schematic of an electric utility boiler facility equipped with SCR, ESP (or FF) and wet scrubber systems [91].

Some recent studies suggest that the operation of selective catalytic reduction (SCR) promoted the formation of oxidized mercury forms in coal combustion flue gases [75, 92, 93]. Figure 2.18 shows an existing boiler facility equipped with SCR, ESP, FF, or wet scrubber to enhance Hg capture. Catalysts such as V_2O_5 and TiO_2 could promote the formation of oxidized mercury [93, 94, 95]. The effect of the SCR operation appeared to be dependent on the coal properties, the reaction temperature, NH_3 concentration and SCR catalyst type, size and age [93,

96, 97]. Activated carbon injection is very promising technology in the municipal waste combustor industry and is capable of removing more than 90% of Hg in a certain condition [75, 98]. Carbon or calcium content in fly ash can also increase the Hg oxidation [9, 98]. Bituminous coals which include high chlorine (Cl) content showed significant promotion while subbituminous coals which include low chlorine showed poor Hg oxidation.

Another possible method to reduce Hg emission without using the additional post-combustion emission controls is that reducing the amount of Hg in the coal by the coal cleaning process before it is shipped to an electric utility power plant. The coal cleaning is defined as a series of processes given to coals to lower SO_2 emissions from the utility boiler [9]. The conventional physical coal cleaning includes size reduction, size screening and gravity separation.

2.4.2 Hg Emission from Boiler Facilities

Capturing of Hg^{2+} and Hg_p is somewhat easier since Hg^{2+} is water soluble and likely to be absorbed by the fly ash and Hg_p is captured by ESP and FF. Therefore, the conversion of Hg^0 to an oxidized form is a key for reducing Hg emissions. Entrained-flow reactors have been used to determine the conversion of Hg^0 to Hg^{2+} [9, 99 – 101]. It is known that the temperature and some of flue gas components such as HCl, Cl, Cl_2, SO_2, SO_3, O_2, O_3, NO, NO_2, and H_2O have significant effect on Hg formations. In Table 2.2, numerous studies on Hg oxidation, reduction and capture using boiler facilities are listed in chronicle order [24, 99, 100, 102 – 105], and the experimental conditions, important findings and results are presented. The temperature of the sampling gas was below 750 K. The literatures indicate that most of chlorine in coals are converted into HCl, thus firing high-chlorine fuels reduces Hg emissions. The use of fly ash, catalysts and active carbon increases mercury captures and oxidations.

Table 2.2. Summary of Hg studies using boilers.

Ref.	System	Fuel Type	Temperature Range	Residence Time	Max. Total Hg emission	Conclusion
[102] 2000	1.0 MW & 500 MW boilers + CVAA	UK coals (Thoresby, Welbeck, etc.)	420 - 720 K (sampling gas)	NA	11.7 μg/m^3	About 80% of vapor Hg presented in oxidized forms, and the Hg retention linearly increased with an increase of the carbon content in dust.
[105] 2000	16.1 kW NG furnace + CAVV + EPA Method 29	NG with Hg^0 & HCl injections (Hg^0 = 53 - 1390 μg/Nm^3)	1125 - 1345 K (furnace) 300 - 400 K (sampling gas)	1.4 s	13.25 μg/Nm^3	No Hg oxidation was occurred in the absence of HCl. About 75% oxidation was found in the presence of 638 ppm HCl at 1345 K.
[99] 2004	700 MW stream turbine + SCR & scrubber	Bituminous and Kentucky coals	1020 K & 430 K (sampling gas)	NA	13.53 μg/m^3	For both field and lab tests, Hg in the flue gas was well measured by a UV spectrometer. About 90% of the Hg^T was found to be oxidized forms.
[100] 2004	160 kW PC fired boiler + entrained flow reactor	Subbituminous Belle Ayr coal	1310 - 1780 K (boiler) 420 - 670 K (reactor) 520 K (sampling gas)	3 s (boiler) 0 - 7 s (reactor)	11.7 μg/Nm^3 (boiler) 10.36 μg/Nm^3 (reactor)	The most significant Hg transformations occurred at 420 K. About 30% of the Hg^T oxidized at temperatures higher than 400°C.
[103] 2005	100 MW PC boiler + OH method + SCEM & ESP	Kentucky and Illinois coals	430 - 640 K (sampling gas)	NA	29.78 μg/Nm^3	Chlorine in coals promoted Hg oxidations while large amounts of sulfur inhibited. About 65 - 80% of the Hg^T was oxidized.
[24] 2007	50 kW entrained flow PF combustor (ash < 500 μm) + FTIR & CVAA	Bituminous coal, wood, chicken manure, & olive residue	1270 - 1570 K (combustor) 370 - 400 K (sampling gas)	2.2 - 2.6 s	4.7 μg/m^3	Higher amount of chicken manure containing high Cl caused higher Hg oxidation, but calcium might react with Cl to suppress Hg oxidation.
[104] 2007	30 kW PC fired boiler + CVAA & Wet chemistry	Dairy biomass, Texas lignite coal & Wyoming coal	1300 - 1400 K (combustor) 300 - 350 K (sampling gas)	0.6 - 0.7 s	3.1 μg/m^3	The increase in the blending portion of biomass increased Hg oxidation. About 75% Hg oxidation was found in co-firing 80% coal and 20% DB.

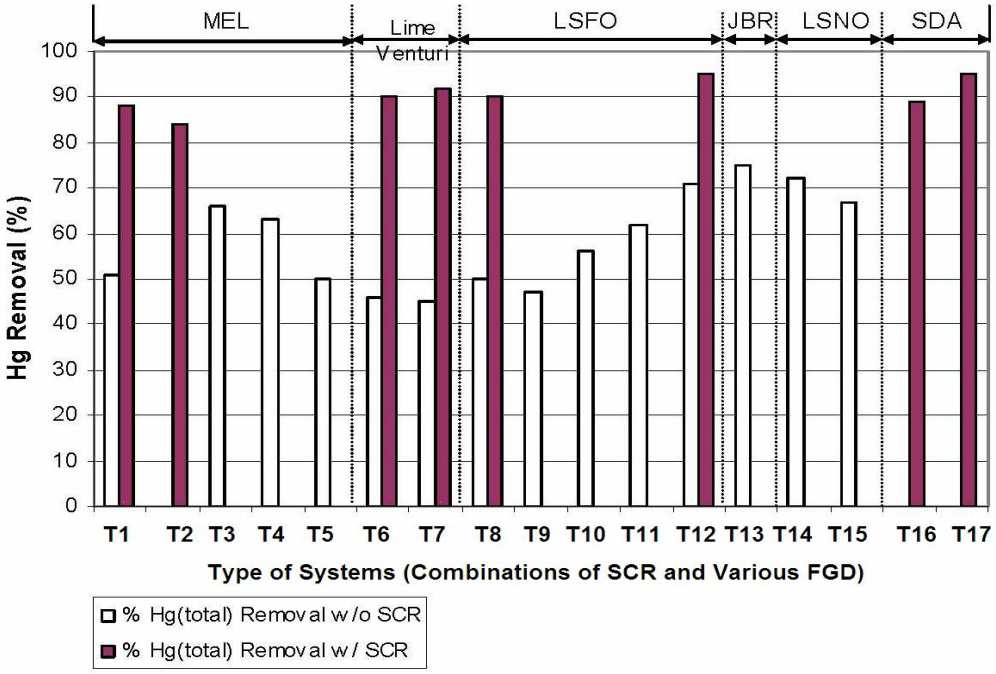

Figure 2.19. Hg removals in the presence and absence of a SCR system [97].

Figure 2.19 shows Hg removals in the presence and absence of a SCR system with various wet flue gas desulfurization (WFGD) systems. It is clear that the use of the SCR system increased the Hg removals, and the combination of the SCR and WFGD systems yielded the Hg removal nearly 90%. It is also reported that firing bituminous coals is more effective with using the SCR system than firing subbituminous or lignite coals. The effect of the SCR operation appeared to be dependent on the coal properties, the reaction temperature, NH_3 concentration and SCR catalyst type, size and age [93, 67]. However, the limitations of using the SCR technology still exist; high capital costs, high operation costs, high pressure drop, ammonia slip, and catalyst poisoning.

The measurement of total, elemental and oxidized Hg in the flue gas from a coal-fired boiler at 750°C of the thermal converter temperature was performed, and its results are presented in figure 2.20 [99]. Initially, 0.8 ppb Hg^0 was detected in the carrier gas of the mixture of water

vapor and N_2 gas. The Hg^0 concentration was increased to 1.4 ppb by adding $HgCl_2$, which indicated as Hg^T. About 20% conversion of the Hg^T was measured by adding certain amounts of SO_2, NO_2, HCl, O_2, CO_2, and NO.

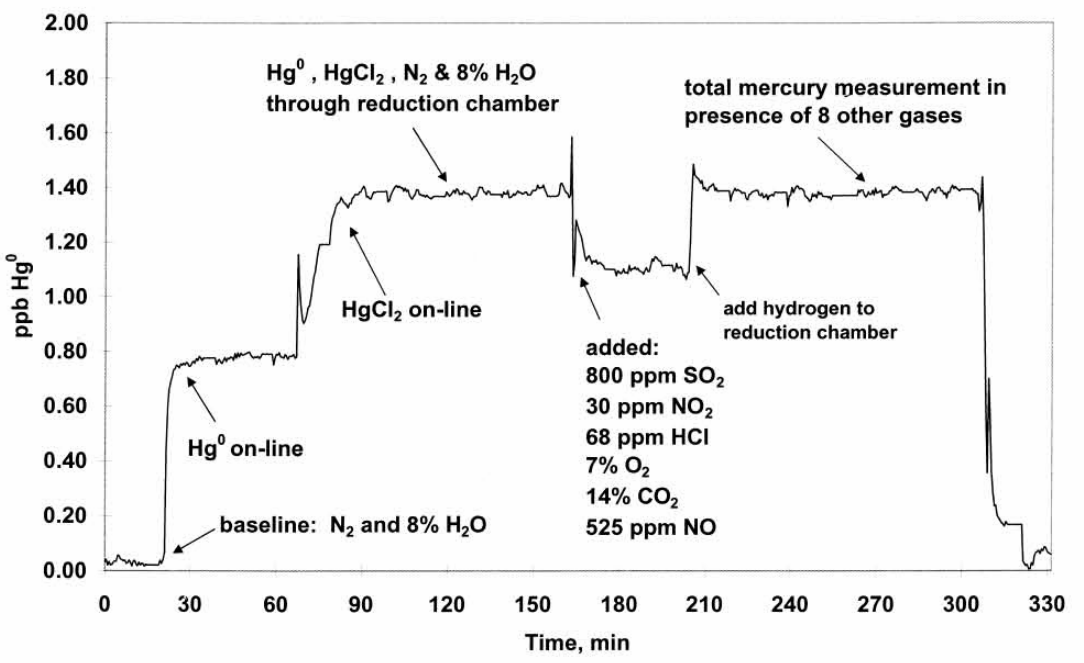

Figure 2.20. Emissions of Hg^T and Hg^0 in the flue gas of a coal-fired boiler [99].

In a previous study during biomass and coals combustion, mercury species were measured in a bench-scale boiler facility using blends of biomass and coals as reburn fuels [41]. The primary fuel (NG) and several reburn fuels such as TXLC, Wyoming coal (WYC) and blends of TXLC and FB were examined. Since FB contains high chlorine content, high oxidation of Hg^0 during combustion was expected. To measure Hg^T and Hg^0, a modification method of the Ontario Hydro (OH) method was applied with chemical solutions (KCl, $SnCl_2$ and NaOH). The oxidized mercury was determined by the difference of Hg^T and Hg^0. The mercury content in reburn fuels are 0.17 *mg* per 1 *kg* of TXLC, 0.14 *mg* per 1 *kg* of WYC and 0.06 *mg* per 1 *kg* of LAPCFB on

an as received basis. Measurement results are presented in figures 2.21 to 2.23 which is plotted based on data in Table 6.3 of the Reference [41]. The tests were performed in the presence and absence of 400 ppm NO_x in the boiler. Figure 2.21 presents the measurements of Hg^T, figure 2.22 shows the levels of elemental forms, and figure 2.23 shows the concentrations of oxidized forms. Note that emissions of all Hg forms are greater for WYC than TXLC, and the results of fuel blends are in the middle. It is because feed rates of reburn fuels were different based on the same amount of heat produced. The Hg^T and Hg^0 are least observed when the equivalence ratio (ER_{RBZ}) in the reburn combustion region is 1.05. Table 2.3 shows the proportion of oxidized mercury in the Hg^T. Since the high chlorine content in LAPCFB, the productions of the oxidized mercury are higher for fuel blends than other reburn fuels. It was also noted that the presence of NO_x probably reduced the Hg^0 due to the reaction (2.23).

$$Hg + NO \rightarrow HgO + \frac{1}{2}N_2 \tag{2.23}$$

Table 2.3. Proportion of oxidized Hg in the Hg^T [41].

ER_{RBZ}	Without NO_x			With 400 ppm NO_x		
	WYC	TXLC	80:20 WYC:LAPCFB	WYC	TXLC	80:20 WYC:LAPCFB
0.95	33.3%	37.5%	57.9%	72%	66.7%	68.8%
1	21.9%	25%	36.8%	50%	37.5%	52.9%
1.05	37.5%	42.9%	50%	70.6%	71.4%	64.7%
1.1	30.3%	20%	-	73.9%	22.2%	62.5%

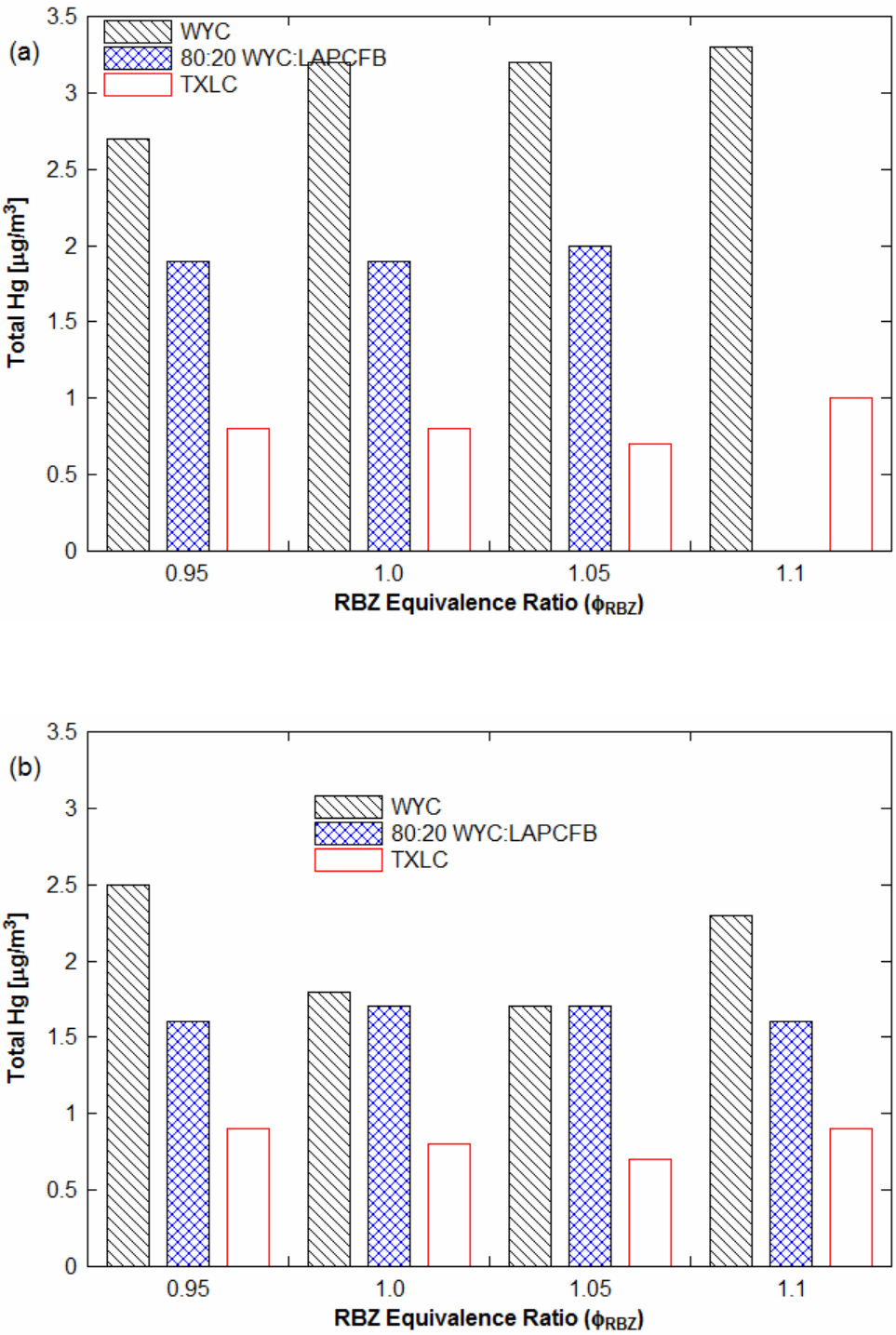

Figure 2.21. Measurements of total Hg (plotted based on data in Table 6.3 of the Reference [41]): (a) Total Hg without NO_x and (b) Total Hg with 400 ppm NO_x.

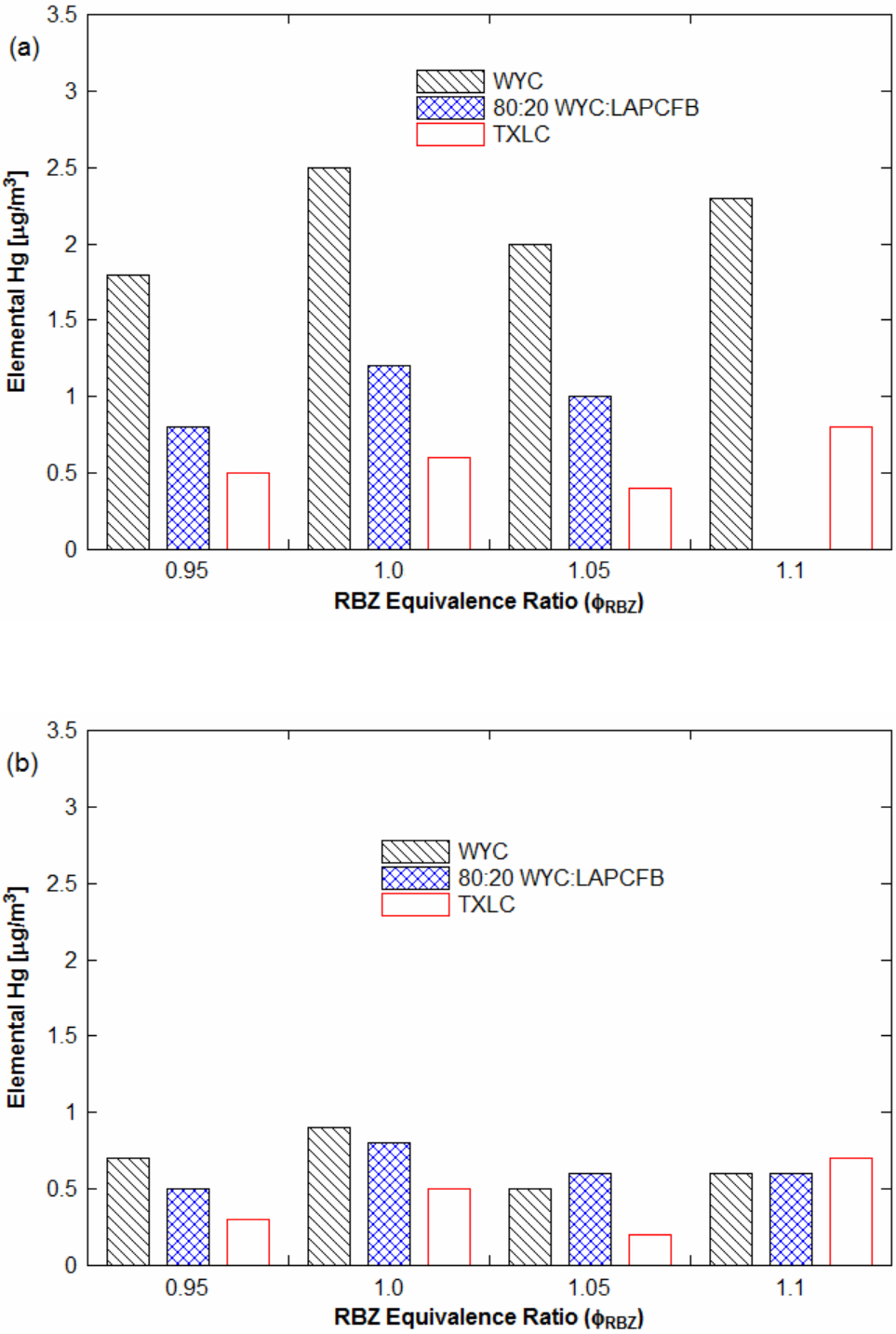

Figure 2.22. Measurements of elemental Hg (plotted based on data in Table 6.3 of the Reference [41]): (a) Hg^0 without NO_x and (b) Hg^0 with 400 ppm NO_x.

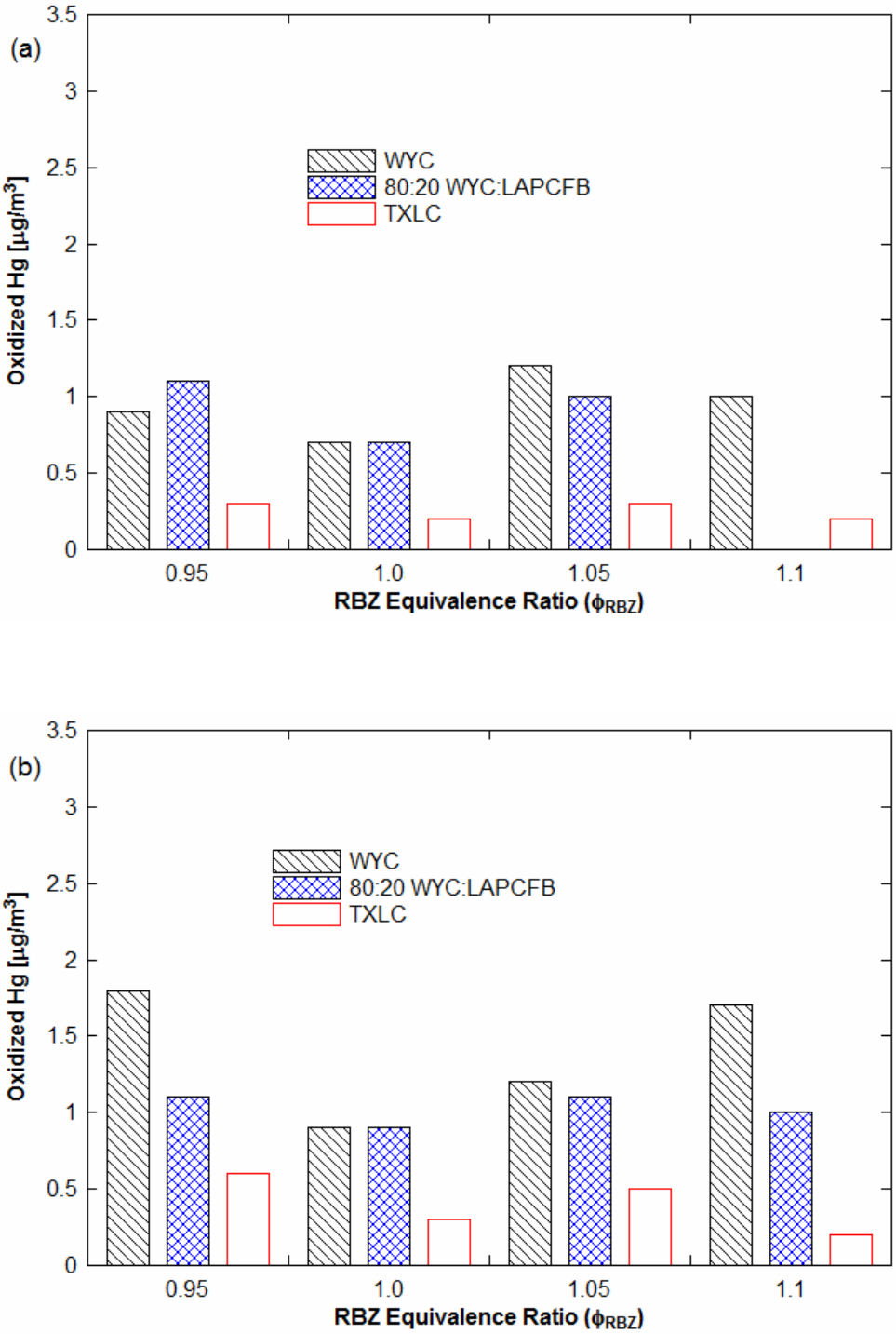

Figure 2.23. Measurements of oxidized Hg (plotted based on data in Table 6.3 of the Reference [41]): (a) Oxidized Hg without NO_x and (b) Oxidized Hg with 400 ppm NO_x.

Mercury oxidation from a operating of a down-fired furnace (16.1 kW) between 860 and 1170ºC was examined [79], and the data was compared with similar results from other literatures. Figure 2.24 presents comparison results of Hg oxidation using data from literatures in the neighborhood of 900ºC. The results show Hg oxidation apparently occurs at temperatures around 900ºC. It is in apparent contradiction to the equilibrium results that Hg oxidation takes place between 450 and 700ºC. The gas compositions are HCl, H_2O, CO_2, N_2, and O_2 in the case tested by Sliger et al. [79], simulated flue gases in the case tested by Widmer et al. [106], HCl and O_2 in the case tested by Hall et al. [80]. The effect of gas compositions is significant on Hg oxidation. It is suggested that the elementary reaction Hg and HCl is hindered by a very high energy barrier and unlikely to be important under practical conditions. The global oxidation of Hg by HCl requires high temperatures to be activated.

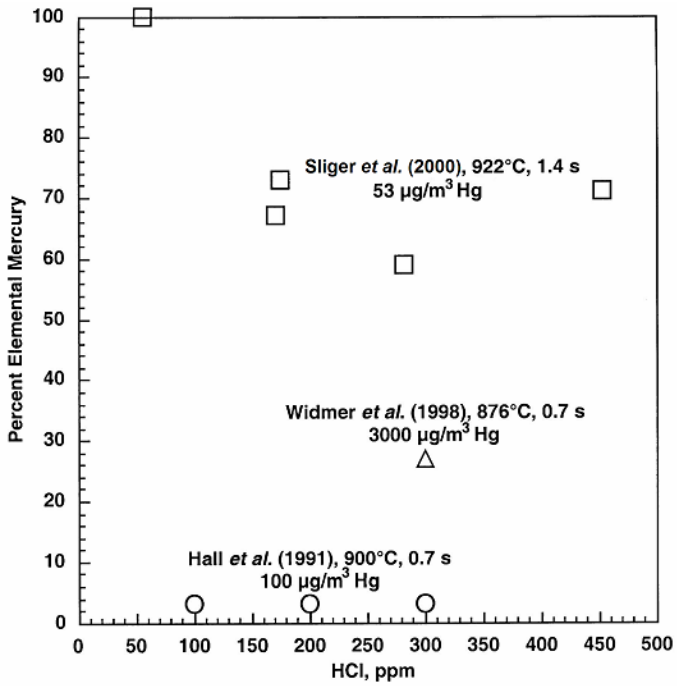

Figure 2.24. Comparison results of Hg oxidation using data from literatures at about 900ºC [79].

2.4.3 Hg Oxidation in Flow Reactors

Flow reactors have been also extensively tested on Hg oxidation and capture with chlorine compounds [8, 77, 80, 81, 89, 92, 94, 106 – 112], and their results are summarized in chronicle order in Table 2.4. The literatures indicate that chlorine species such as HCl and Cl_2 are very effective to oxidize Hg^0 while sulfur and moisture inhibit Hg oxidation. The use of fly ash, catalysts and active carbon increases mercury captures and oxidations.

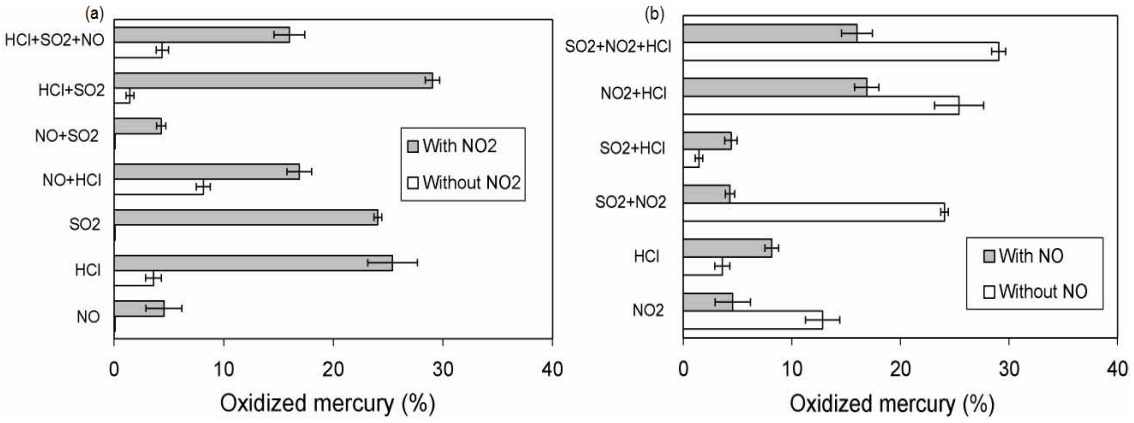

Figure 2.25. Heterogeneous Hg oxidations using Blacksville fly ash at 180°C: (a) Effect of NO_2 and (b) Effect of NO [89].

Heterogeneous interactions between fly ash and Hg in a simulated flue gas were studied to identify the role of fly ash on Hg oxidation, the effect of HCl and SO_2 on Hg oxidation, and the individual impact of NO and NO_2 in the presence of fly ash [89]. The baseline blend consisted of CO, CO_2, O_2, and balance N_2. It was reported that HCl, SO_2 and NO_2 promoted Hg oxidation while NO inhibited Hg oxidation between 120 and 180°C, and the results of NO_2 and NO are presented in figure 2.25. The result of the presence of fly ash was also found critical on Hg oxidation. Though the addition of fly ash had critical effects on Hg oxidation, the flue gas composition was the most important factor, especially NO_2 and HCl.

Table 2.4. Summary of Hg studies using flow reactors.

Ref.	System	Chlorine Species	Gas Composition	Temperature Range	Residence Time	Max. Hg Oxidation	Conclusion
[80] 1991	Flow reactor + CVAA + 17 kW propane fired flue gas generator	HCl & Cl_2	O_2, NO, NO_2, NH_3, SO_2, & H_2S	300 - 1170 K	1.5 s	90%	Hg reacted with Cl_2, HCl, NO_2, and O_2. Hg could be oxidized by a number of different routes during combustion.
[77] 1995	Flow reactor + CVAA	HCl	O_2, N_2, SO_2 with soda lime	> 925 K	NA	100% backward reaction	Conversions of $HgCl_2$ to Hg^0 were tested. All of pure $HgCl_2$ were converted into Hg^0 over 925 K in the presence of HCl and O_2.
[107] 1998	Flow reactor	HCl	O_2, CO_2, & N_2	750 - 1030 K	0.97 - 1.22 s	88%	For high temperatures, Hg oxidation increased with an increase in concentrations of HCl and Cl.
[106] 1998	Flow reactor + EPA method 29	HCl	O_2, CO_2, H_2O, & N_2	700 - 1150 K	0.7 - 1.16 s	95%	High Hg conversion resulted in high temperatures and the longer residence time by the preheating of the gas mixture.
[108] 2002	Photoreactor with an UV beam	HCl	O_2, CO, CO_2, SO_2, SO_3, N_2, H_2O, & NO_x	300 - 450 K	2 s	72%	Photochemical oxidation of Hg with 253.7 nm radiation was a potential means of Hg removal from flue gases.
[92] 2002	Flow reactor + catalyst	HCl	O_2, CO_2, SO_2, H_2O, NO_x, & N_2	470 - 670 K	SV: 1,000 - 10,000 h^{-1}	98%	Some of titanium-vanadium-based catalysts were capable of oxidizing Hg^0 in flue gas.
[109] 2002	Entrained flow reactor + activated carbon	HCl	O_2, NO_x, N_2, SO_2, & H_2O	370 - 470 K	3 - 4 s	90%	Hg removals in the presence of the active carbon in a fixed-bed reactor were achieved over 80%.

Table 2.4. Continued.

Ref.	System	Chlorine Species	Gas Composition	Temperature Range	Residence Time	Max. Hg Oxidation	Conclusion
[110] 2002	Flow reactor + TiO_2 + UV beam	HCl & CH_2Cl_2	Dry air, Ar, & TiO_2 precursor	300 - 460 K	NA	98%	Hg oxidation/capture by HCl and TiO_2 particles was significantly increased. Interactions between HCl and TiO_2 particles catalytically generated Cl_2.
[89] 2003	Flow reactor + coal fly ash (> 10 μm) + CVAA	HCl	O_2, CO, CO_2, NO, SO_2, N_2, NO_2, & H_2O	450 K	NA	30%	Potential catalytic effects of fly ash on Hg oxidation at low temperatures were tested. NO inhibited Hg oxidation while SO_2 and NO_2 promoted it.
[94] 2004	Flow reactor + SCR	HCl	O_2, CO_2, NO, SO_2, H_2O, NH_3, & N_2	< 620 K	Space velocity: $2600h^{-1}$	97%	HCl was important for providing the source of Cl and titanium-vanadium catalysts promoted the Hg oxidation.
[111] 2004	Flow reactor + coal fly ash (< 50 μm)	HCl & Cl_2	H_2, CO, NH_3, HCN, H_2S, H_2O, COS, & Ar	520 - 1020 K	NA	95%	The ash characteristics had a significant impact on Hg speciation. Interactions between fly ash and flue gas promoted Hg oxidation rates.
[81] 2005	Flow reactor + Natural gas burner (1000 BTU/h)	Cl_2	Combustion gas	< 1000 K	0.8 - 3.0 s	98%	About 70% of the Hg^T was oxidized by injection Cl_2 and Hg^0 into the burner. Higher quenching rates resulted in higher Hg conversions.
[112] 2005	Flow reactor + fly ash + UV beam	HCl	N_2, O_2, CO_2, H_2O, & SO_2	> 700 K 525 K (ash)	0.6 s	90%	Transition metal oxides, CuO and Fe_2O_3, in ash exhibited significant catalytic activity in Hg oxidation in the presence of HCl.
[8] 2006	Flow reactor + SCEM	Cl_2	N_2, O_2, CO, CO_2, H_2O, SO_2, & NO	450 - 820 K	6 s	92%	The addition of H_2O, SO_2, and NO inhibited the homogeneous Hg oxidation by Cl_2.

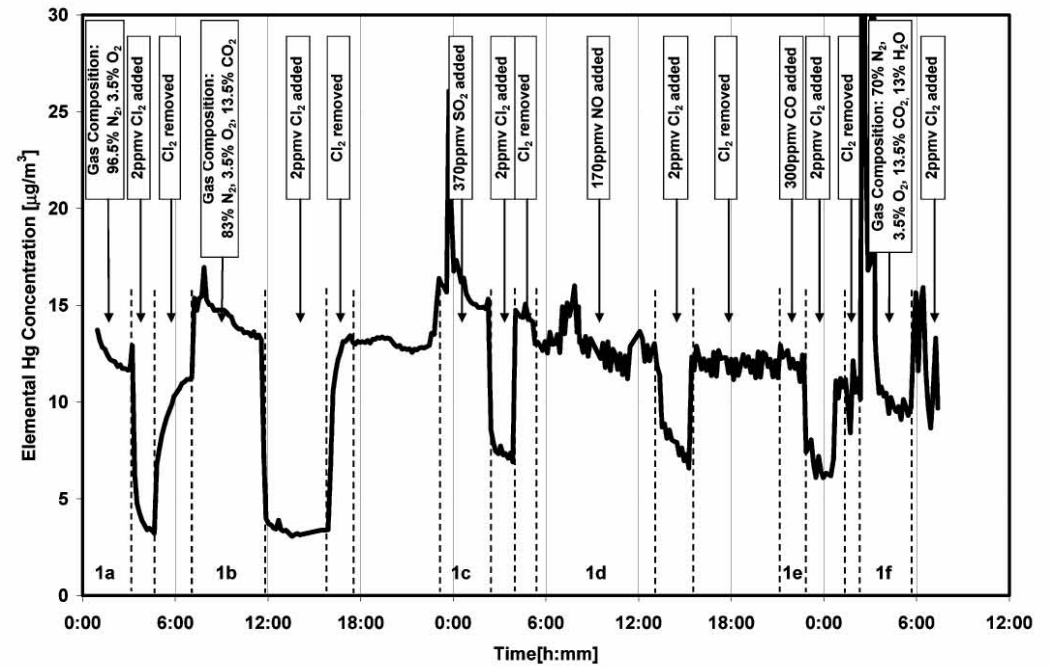

Figure 2.26. Homogeneous Hg oxidations in the simulated flue gas consisted of N_2, O_2, CO_2, H_2O, SO_2, NO, CO, and Cl_2 [8].

Results of homogeneous Hg oxidation in the simulated flue gas consisted of N_2, O_2, CO_2, H_2O, SO_2, NO, CO, and Cl_2 at temperatures between 180 and 550°C are presented in figure 2.26 [8]. The baseline case was the Hg measurement in certain amounts of N_2 and O_2 mixtures. Various components of CO_2, SO_2, NO, CO, and H_2O were added into the gas steam with and without Cl_2. It was found that H_2O, SO_2 and NO inhibited homogeneous Hg oxidation by Cl_2, and the presence of H_2O increased inhibitory effect of SO_2 and NO. The presence of CO_2 and CO did not have a significant effect on Hg oxidation. Two new reaction paths were suggested based on results of SO_2 and NO shown as chemical reactions (2.24) and (2.25).

$$SO_2 + Cl_2 \rightarrow SO_2Cl_2 \tag{2.24}$$

$$2NO + Cl_2 \rightarrow 2NOCl \tag{2.25}$$

Reaction mechanisms of homogeneous Hg oxidation by HCl as a primary chlorine-containing species in the system were investigated [74]. It was found that O_2 weakly promoted homogeneous Hg oxidation, while H_2O strongly inhibited Hg oxidation between 300 and 1000°C. It was also concluded NO could promote or inhibit Hg oxidation depending on its concentration at 922°C.

It was found that increasing HCl concentrations resulted in increased Hg oxidations, and the addition of SO_2 resulted in decreased Hg oxidation above 755°C [9]. It was found that 7% Hg oxidation with 50 ppmv HCl and increased to 27% Hg oxidation with 200 ppmv HCl while 15% Hg oxidation with 200 ppmv HCl and 500 ppmv SO_2 was measured. The addition of H_2O also decreased Hg oxidation. 10% Hg oxidation with 200 ppmv HCl, 500 ppmv SO_2 and some H_2O was reported.

A previous DOE-NETL project evaluated various catalysts in small, fixed sand-bed reactors to demonstrate the long-term effectiveness of those catalysts on the oxidation of Hg^0 [93]. Four catalysts were tested; a commercial palladium catalyst, commercial titanium-vanadium catalyst, tire-derived activated carbon, and active fly ash. It resulted in 68% Hg oxidation by the titanium-vanadium catalyst and 92% Hg oxidation by the palladium catalyst during the initial tests, indicating significant increase in the Hg oxidation; however, the extent of the Hg oxidation decreased with time. After 60 days in operation, the Hg oxidation decreased 92 to 60% for the palladium catalyst and 68% to 30% for the titanium-vanadium catalyst. Not only the age of the catalysts is typically concerned for the decrease of the Hg oxidation, but also a buildup of fly ash in the boiler caused the oxidation drop in these cases since the Hg oxidation was restored after the cleaning process.

2.5 Ash Fouling Problems in Coal-Fired Power Plants

2.5.1 Classification of Ash Fouling

The production of fouling differs from industry to industry and depends on many experimental parameters; velocity of the gas stream, flue gas compositions, temperatures of the flue gas, the geometry and material of heat exchangers (HEXs), and temperatures of the HEXs. Mechanisms of the fouling creation are classified into five types; sedimentation fouling, inverse solubility fouling, chemical reaction fouling, corrosion product fouling, and combined mechanisms [113]. Sedimentation fouling is produced by mineral contents in the cooling water, and the velocity of the gas stream is one of the key parameters to produce it on the surface of HEXs. Inverse solubility fouling is created by the crystallization of salts in natural water, especially calcium sulfates. Chemical reactions of the flue gas are the major cause to make solid phase depositions such as coke on the surface of the HEXs. The ash deposition is a type of the chemical reaction fouling. Corrosion of the metal surface of HEXs may occur during the combustion to produce fouling. The cleaning process of the corrosion product fouling may deteriorate the corrosion of the facility and break the surfaces of the facility and the HEXs. However, most of the fouling process in power generations typically occurs in combination of four mechanisms mentioned above.

Ash buildup is typically divided into two mechanisms: solidified slag deposition and powdered ash deposition. The compositions of the ash deposition depend on the temperature of the flue gas in the operating boiler. The solidified slag deposition is formed when the flue gas temperature is between 1470 and 1920ºF (about 800 and 1050ºC); contains high content of Fe_2O_3 and sulfates and low content of SiO_2 and Al_2O_3. The powdered ash deposition occurs when the temperature of the fuel gas is below 1470ºF (800ºC), and contains more than 50% SiO_2 and over 20% Al_2O_3 [53]. The rates of the ash buildup depend on many factors including the flue gas

velocity, the ash composition, the ash particle size, and the flow speed in the HEX. The effect of the flow speed in a HEX on the ash deposition was studied elsewhere [53]. The effects of ash composition and ash particle size on the growth of ash deposition focusing on sodium sulfate were investigated [52]. Unlike the ash buildup in the system during coal combustion, fly ash and bottom ash are easy to be removed. Fly ash which consists of light particles is reused as mixing with concrete depending on the ash composition. Bottom ash mainly consists of heavier particles and is typically buried in lakes.

In our previous study by Annamalai et al. [25] the fouling studies under co-firing conditions for blends of coal and high ash FB (42.7% ash as received) were conducted using a Department of Energy – National Energy Technology Laboratory (DOE-NETL) 150 kW (500,000 BTU/h) pilot plant facility. It was reported that ash deposition causes greater decrease in heat transfer rate due to ash buildup when blending coal and high ash FB than for pure coal under similar heat input and operating conditions.

The mineral analysis of ash for the reburn fuels tested were found to be very important since the mineral composition of the ash affected the deposition rate, fusion and melting points, corrosion rate, and erosion rate of the HEXs. Higher alkaline oxide contents (CaO, MgO, Na_2O, and K_2O) resulted in a higher probability of fouling due to faster growing oxide layers on HEX surfaces [114].

2.5.2 Removal Techniques of Ash Fouling

Fouling is a common problem associated with the electric utility power plants burning coals. Some periodic processes to remove fouling are strongly required to be installed. For other exterior cleaning methods, soot blowing, scraping, sand blasting, hydro-blasting, and rotary brushing can be applied for mechanical fouling removals [115]. Water, air or steam can be used

as media in sootblowers to remove deposits from the HEX surfaces. A high velocity water jet system is very common to clean interior and exterior HEXs. Like some fouling is produced in chemical reactions, a chemical cleaning technique can be applied on the fouling removal. For example, carbonate deposits can be removed by chlorination. No disassembly of HEXs and other equipments are necessary, but it may shorten the life of the HEXs.

For the interior cleaning techniques, a ball or brush is used to pass through HEXs to remove corrosion products. In the techniques, the ball can be recirculated by the fluid in HEXs, and the brush can be moved forward and backward by the reversible cooling water system. The feature using an oversized sponge rubber ball is utilized at Amertap System, and the feature using a plastic brush is utilized at M.A.N. System [113].

3. RESEARCH OBJECTIVES

In this section, purposes of the current research and contributions of this study on areas of fossil fuel combustion and emission control are discussed. Detailed works to achieve the current study successfully are described.

The overall objective of the current study is to develop thermo-chemical energy conversion technologies for cattle wastes or cattle biomass (CB) which includes feedlot biomass (FB) and dairy biomass (DB) as fuels. The proposed facility for the current energy conversion studies is a bench-scale (30 kW or 100,000 BTU/h) Boiler Burner Research Facility at Coal and Biomass Energy Laboratory (CBEL) of Mechanical Engineering, Texas A&M University (TAMU). The facility can either be operated as coal and biomass co-fired facility or as reburn facility for NO_x and Hg reduction studies. The overall objective has the following sub-objectives: 1) Determine the optimum operating condition of coal-fired boilers for the maximum NO_x reduction, 2) Evaluate the ash fouling potential on the surface of heat exchangers (HEXs) during the reburn studies and 3) Conduct a fundamental study of homogeneous and heterogeneous Hg oxidation during coal combustion in order to understand the effect of CB fuels on Hg reduction. The tasks performed to accomplish the overall objectives and sub-objectives are summarized as follows:

1. Characterize thermo-physical and chemical properties of reburn fuels by the analysis of samples for FB, DB, Texas lignite coal (TXLC), and Wyoming subbituminous coal (WYC), and then determine the properties of blend fuels on a mass basis for blends of FB:TXLC, blends of DB:TXLC, and blends of FB:DB.

2. Estimate the operating conditions in the primary and reburn combustion regions. They include flow rates of primary and reburn fuels, flow rates of primary and reburn air, flow rates of NH_3 and N_2, concentrations of O_2 in the exhaust gas, and equivalence ratios (ER) in primary and reburn combustion regions, etc.
3. Calculate the minimum amounts of NH_3 and reburn fuels required to achieve the best NO_x reduction.
4. Investigate the followings on NO_x reduction:
   (i) Effects of reburn fuels (FB, DB and coals)
   (ii) Effects of fuel blending (coal:DB, coal:FB and DB:FB)
   (iii) Effects of reburn equivalence ratios (ER_{RBZ} or ϕ_{RBZ} = 0.95 to 1.10)
   (iv) Effects of reburn heat inputs (20 to 30%)
   (v) Effects of oxygen concentrations (12.5 and 20.9%) in the reburn gas
   (vi) Effects of reburn injection parameters:
      (a) Injection configurations (0° lateral and 45° upward) of the reburn fuel
      (b) Cross-sections (circle and oval) of reburn nozzles
      (c) Symmetric and asymmetric configurations
   (vii) Effects of baseline NO_x concentrations (125 to 630 ppm) generated by the NH_3 injection in the primary combustion region
   (viii) Effects of the presence and absence of HEXs. (Air and water are used as the coolants in three single-pass HEXs.)
5. Develop a diagnosis method of ash fouling behavior in transient boiler operations and conduct the fouling tests to determine overall heat transfer coefficients (OHTCs) using the log mean temperature difference (LMTD) method.

6. Determine combustor performance as measured by burnt fractions (BF) or combustible losses, extent of NO_x reduction and flue gas analyses (CO, CO_2, SO_2, and C_xH_y).
7. Conduct bench-scale tests to investigate homogeneous and heterogeneous Hg oxidations using a plug flow reactor (PFR) and study effects of the followings on Hg oxidation or reduction:
   (i) Effects of various gas species (HCl, NO, O_2, and N_2) and their reactions
   (ii) Effects of temperatures (25 – 1200ºC)
   (iii) Effects of residence times
   (iv) Effects of a vanadium-tungsten-titanium (V_2O_5-WO_3/TiO_2 or VWT) catalyst

The current study can lead to 1) development of the reburn technology with CB as reburn fuels for NO_x reduction, 2) ash fouling behavior under transient and short-time boiler operations and 3) a fundamental understanding of Hg oxidation chemistry with gaseous species and the impact of catalyst on Hg reduction.

4. EXPERIMENTAL TECHNIQUES

This section presents the details of the reburn boiler burner facility in Coal and Biomass Energy Laboratory (CBEL) and the plug flow reactor (PFR) facility in Engines, Emissions, and Energy Research Laboratory (E3 Lab) at Texas A&M University (TAMU). Experimental methods, procedures, and parametric cases are described. Methods for determining operating conditions of the facilities are presented.

4.1 Reburn for NO_x Reduction and Ash Fouling

4.1.1 Experimental Facilities

A schematic of the reburn boiler burner facility in CBEL at TAMU is presented in figure 4.1 (a). The diagram shows all of the major components of the reburn facility: primary burner, solid fuel feeder and hopper with a venturi eductor, gas components, air pre-heater, temperature acquisition system, emission analyzer, HEXs, exhaust system with water spray, and ash port. Figure 4.1 (b) shows the side view of the boiler burner indicating the primary combustion zone, the reburn zone, the post-reburn region, and reburn nozzles. The facility is used to conduct both biomass reburning on NO_x reduction and ash fouling experiments during reburning. It is a bench-scale 30 kW (100,000 BTU/h) boiler burner which can be fired with coals, CB, and blends of coal and CB as reburn fuels. The boiler burner consists of a 6 in (15.24 cm) diameter, 72 in (182.88 cm) long vertically down-fired combustor. The combustor is made with a steel frame containing a 2 in layer of insulation and a 2 in section of refractory.

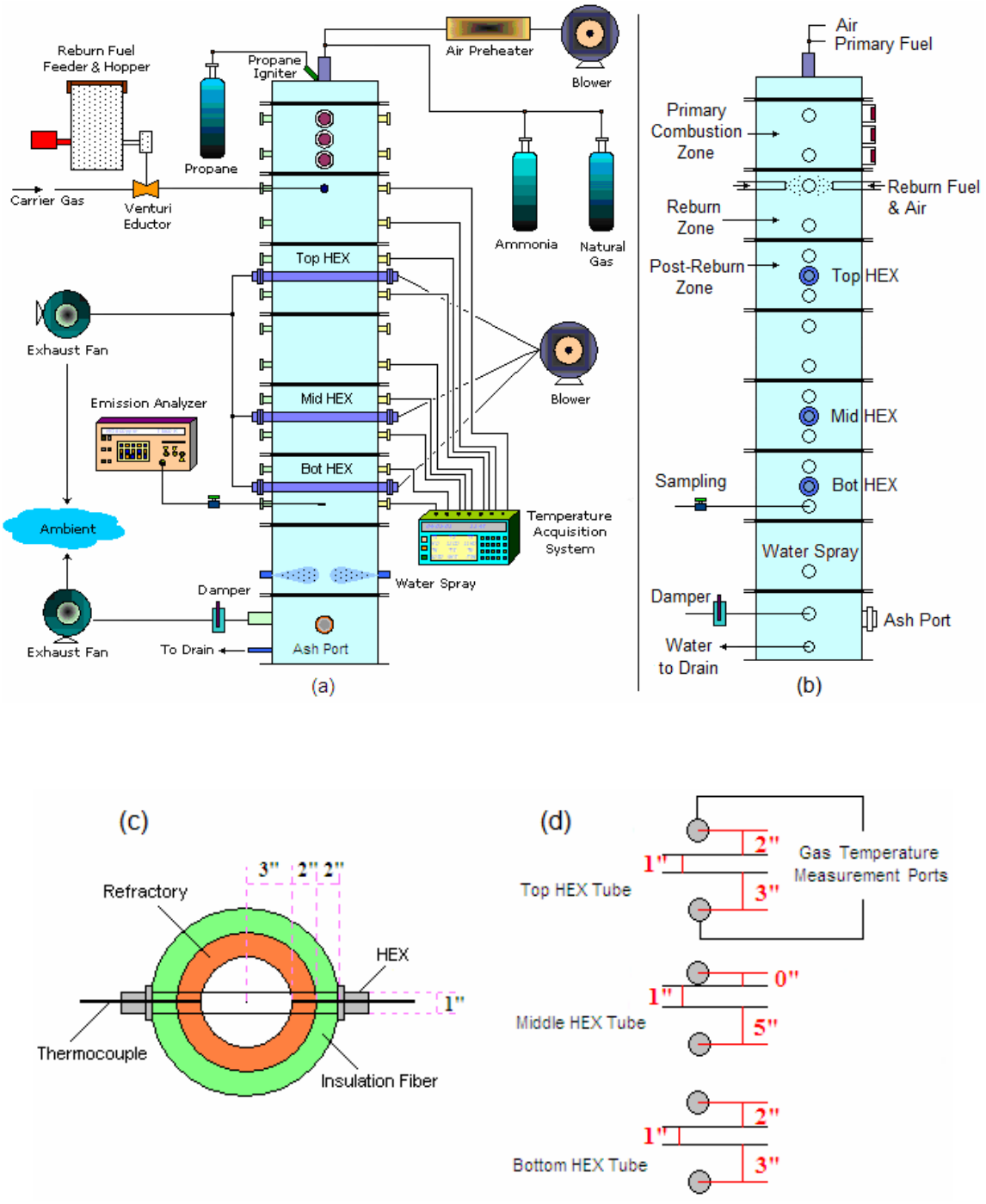

Figure 4.1. A schematic of the experimental setup for reburning: (a) Front view of the small-scale down-fired boiler burner facility, (b) Side view of the boiler burner, (c) Cross-section of the furnace, and (d) Distance between HEXs and temperature measurement ports.

The primary air is supplied using an air blower and is preheated to about 120ºC using a pre-heater. The air is mixed with NG and the premixed gas flows into the primary burner. A propane torch is used to ignite the flame of premixed gas, and it preheats the furnace. Along the walls of the boiler burner are temperature measurement ports at spaced intervals 6 in (15.24 cm) below the reburn zone (RBZ). The gas stream is cooled down by the jet water in the quenching area at the bottom of the furnace. The exhaust gas vents out through an exhaust system. In conventional operational mode, the primary fuel (natural gas) and air are injected from the top into the primary combustion zone in order to generate 70% of the total heat (21 kW or 70,000 BTU/h). The reburn fuel (coal:FB mixtures) and air (about 20% of total air) are injected laterally into the reburn zone in order to produce 30% of the total heat (9 kW or 30,000 BTU/h).

Three single-pass HEXs were fabricated and mounted in the boiler. The dimensions of the HEXs are 2.7 cm (1.06 in) O.D., 2.1 cm (0.83 in) I.D. and 15.24 cm (6 in) long. Three HEXs whose surfaces are clean and dry are laid perpendicular to the downward flow of the hot flue gas stream. The HEXs are located below the reburn zone between 31 and 46 cm (or 12 and 18 in), between 92 and 107 cm (or 36 and 42 in), and between 122 and 137 cm (or 48 and 54 in), respectively. The temperatures of the cold fluid at the inlet and exit of the HEXs and the gas temperatures at top and bottom surfaces of the HEXs are monitored. Typically, the temperatures of the hot gas stream around the HEXs increase from about 430 to 1150ºC (800 to 2100ºF) depending on the location. The cross-section of the furnace with the HEX is presented in figure 4.1 (c). The inlet and exit temperatures of the HEXs are measured 3 inches from the reactor center, at the inner surface of the refractory. The locations of temperature measurement ports above and below HEXs are illustrated in figure 4.1 (d). In the past, the usage of water has led to difficulties in measuring the temperature difference accurately, particularly in a small scale reactor facility; hence air is first used as the HEX cold fluid, and the air flow is typically set to

20 SCFH (standard cubic feet per hour) or 9.44 SLPM (standard liters per minutes) based on standard ambient temperature and pressure (SATP). After slight modification, water as the cold fluids in HEXs could also be used. The water flow is typically set to 1.1 GPM (gallon per minutes). Ash samples are collected from four different places for several cases to analyze the boiler performance, where are each surface of the HEXs and the ash port at the bottom of the furnace. The ash port is filled with water during the operation, and the ash sample collected from the ash port is called the bottom ash.

4.1.2 Experimental Procedures

1. The experiment began with preheating the primary air to 120ºC, and then injecting it into the reactor with the primary fuel (NG). The flame was ignited by a propane torch.
2. The furnace operates at a relatively low temperature, and NH_3 is supplied to generate NO_x was generated with ammonia (NH_3). The NH_3 was injected with the primary fuel and was converted to NO_x during combustion. It is important to maintain a fuel-lean condition (typically $\phi = 0.95$) for the primary combustion zone for the conversion of all NH_3 to NO_x.
3. The temperatures along the reactor axis were then monitored.
4. For ash fouling studies, the cold fluid flowed into HEXs. Thermocouple probes were kept at the center of each HEX.
5. After the temperature stabilization in the burner, the reburn fuel and carrier gas (air) were injected. The temperature of the reburn zone may be near the steady state; however, the temperatures near HEXs may not achieve the steady state.
6. The instantaneous temperatures of the cold fluid and the hot flue gas stream were monitored.
7. After the reburn temperature reached the steady state condition, the electrochemical sensor-based gas analyzer was used to determine concentrations of NO_x, O_2, CO, CO_2, SO_2, and

combustibles (C_xH_y) at the measurement ports (at 137 cm or 54 in below the reburn nozzles). Electrochemical sensors were used to measure 0 – 25% O_2, 0 – 8000 ppm CO, 0 – 4000 ppm NO_x, 0 – 100 ppm NO_2, and 0 – 4000 ppm SO_2. Nondispersive infrared sensors (NDIR) were used to measure 0 – 15% CO, 0 – 20000 ppm C_xH_y and 0 – 15% CO_2.

8. The duration of reburn tests was limited to 3 to 4 hours due to safety concerns. An entire single experiment, including the boiler preheating, the reburn combustion and the boiler cooling, lasted 9 to 10 hours.
9. Once the experiments were completed, the reburn fuel was shut off followed by NG. After the furnace completely cooled down, the HEXs were detached from the boiler, and ash samples were scraped off from the HEX surfaces and collected from the ash port for the analysis.

4.1.3 Operating Conditions

The bench-scale reburn boiler facility in CBEL at TAMU generates 30 kW (100,000 BTU/h) heat. Using the gross or higher heating value (HHV) of each reburn fuel, the flow rates of primary and reburn fuels required for the primary and reburn zones are calculated. With the ultimate and proximate analyses of the reburn and primary fuels including the heating value, the requirements of the primary fuel ($CH_hN_nO_oS_s$) and air (15% humidity) are calculated with the addition of NH_3 using Eq. (4.1). The operating conditions of the primary combustion zone are always the same and listed in Table 4.1. The primary fuel used is NG (mainly CH_4) with 40835 kJ/m^3 of HHV. The HHV was found to be 37050 kJ/m^3 by the overall empirical chemical formula. The conditions of the primary combustion zone are maintained the same for each experiment. Equation (4.1) allows the control of NO_x emissions with the flow of NH_3. The baseline NO_x concentration created by the combustion of NH_3 in the primary combustion zone

before the injection of the reburn fuel and air is 420 – 440 ppm. For the NH_3 reaction, it is important to maintain a fuel-lean combustion or these NH_3 probably be slip.

$$CH_hN_nO_oS_s + \frac{(1+h/4+s-o/2)}{\phi}(O_2 + A\cdot H_2O + B\cdot N_2) + bNH_3 \rightarrow cCO_2 + dH_2O + eNO + fO_2 + gN_2 \quad (4.1)$$

Table 4.1. Operating conditions of the primary combustion zone.

Primary fuel	Natural gas (NG)
Fuel flow rate	30.1 SLPM (63.9 SCFH)
Heat input	21 kW or 70,000 BTU/h
Proportion of heat input	70%
Equivalence ratio, ER_{PRI}	0.95
Air flow rate	320.3 SLPM (678.7 SCFH)
NH_3 injection	0.12 SLPM (0.265 SCFH)
Baseline NO_x emission	420 – 440 ppm

Table 4.2. Operating conditions of the reburn zone for the base case.

Reburn fuel	TXLC
Fuel flow rate (depending on the reburn fuel)	36.9 g/min (4.88 lb/hr)
Heat input	9 kW or 30,000 BTU/h
Proportion of heat input	30%
Equivalence ratio, ER_{RBZ}	0.95 – 1.1
Air flow rate (depending on the reburn fuel)	115 – 136 SLPM (244 – 288 SCFH)
O_2 % or Vitiation	20.9% or No
HEX	No
Injection Configurations	Angle: Lateral (0°) Cross-section: Circular nozzles Direction: Symmetric

With the ultimate and proximate analyses of the reburn fuels, a chemical formula ($CH_hN_nO_oS_s$) can be derived, and the requirements of the reburn fuel and air are then calculated with Eq. (4.2). The humidity of air was assumed 15%. The operating condition of the base case is listed in Table 4.2. The reburn fuel of the base case is TXLC. The equivalence ratio (ER) is typically defined as the ratio of the fuel-to-air ratio to the stoichiometric fuel-to-air ratio which is an inverse value of the stoichiometric ratio (SR). In real power plants, the ER_{PRZ} in the primary combustion zone is typically maintained less than 1.0, and the ER_{RBZ} in the reburn zone is generally kept greater than 1.0. For current studies, ER_{PRZ} is maintained at 0.95 to generate 70% of the total heat (21 kW or 70,000 BTU/h) in the primary zone, and ER_{RBZ} is varied from 0.95 to 1.10 to generate 30% of the total heat (9 kW or 30,000 BTU/h) in the reburn zone. Equation (4.2) assumes that there is no C_xH_y and $C_{(s)}$ and provides an estimate for the levels of CO and SO_2 in the exhaust. The CO estimate may be a little higher than measured values since some unburned carbon is in the form of hydrocarbons. The estimate for SO_2 may also be high since some sulfur reacts to form SO_3, and some is left in the ash. These estimates will function as a guideline to ensure that the measured results are reasonable.

$$CH_hN_nO_oS_s + a(O_2 + A\cdot H_2O + B\cdot N_2) \rightarrow bCO_2 + cCO + dH_2O + eSO_2 + fO_2 + gN_2 \quad (4.2)$$

where $A = 0.0234$, $B = 3.785$, $a = \dfrac{(1+h/4+s-o/2)}{\phi}$, $b = 1-c$, $d = \left(\dfrac{h}{2} + A\dfrac{(1+h/4+s-o/2)}{\phi}\right)$,

$e = s$, $f = \left(1+\dfrac{h}{4}+s-\dfrac{o}{2}\right)\left(\dfrac{1}{\phi}-1\right)$, and $g = \left(\dfrac{B}{\phi}\left(1+\dfrac{h}{4}+s-\dfrac{o}{2}\right)+\dfrac{n}{2}\right)$.

If $\phi \le 1$, *then* $c = 0$, and $\phi > 1$, *then* $c = \left(o + 2\dfrac{(1+h/4+s-o/2)}{\phi} - 2b - \dfrac{h}{2} - 2s\right)$.

Table 4.3. Experimental cases for the current studies with the baseline NO_x of 420 – 440 ppm.

Reburn Fuel	Vitiation	ER_{RBZ}	HEXs	Reburn Heat Input	Injection Angle	Cross-Section of Nozzles
LAPCFB	No	0.95 – 1.10	Yes & No	20 – 30%	0°	Circle
HAPCFB	No	0.95 – 1.10	Yes	30%	0°	Circle
LASSDB	Yes & No	0.95 – 1.10	Yes & No	20 – 30%	0° & 45° Asymmetric	Circle
TXLC	Yes & No	0.95 – 1.10	Yes & No	30%	0° & 45°	Circle
WYC	No	0.95 – 1.10	Yes	30%	0°	Circle
90:10 TXLC:LAPCFB	No	0.95 – 1.10	Yes	30%	0°	Circle
90:10 TXLC:HAPCFB	No	0.95 – 1.10	Yes	30%	0°	Circle
90:10 TXLC:LASSDB	Yes & No	0.95 – 1.10	Yes & No	30%	0° & 45°	Circle & Oval
80:20 TXLC:LASSDB	Yes & No	0.95 – 1.10	Yes & No	30%	0° & 45°	Circle & Oval
70:30 TXLC:LAPCFB	No	0.95 – 1.10	Yes	30%	0°	Circle
70:30 TXLC:HAPCFB	No	0.95 – 1.10	Yes	30%	0°	Circle
70:30 LASSDB:LAPCFB	No	0.95 – 1.10	No	30%	0°	Circle
30:70 LASSDB:LAPCFB	No	0.95 – 1.10	No	30%	0°	Circle

4.1.4 Experimental Cases

Table 4.3 lists the experimental cases for the current studies. Various reburn fuels and equivalence ratios are studied. Non-vitiation (20.9% O_2 in pure air) and vitiation (12.5% O_2 in pure air) are tested. The conditions with and without HEXs are tested. Various heat inputs (20 to 30% by reburn fuels) are examined for the pure LAPCFB and LASSDB cases. As shown in figure 4.2, various reburn injection configurations are also examined such as lateral (0°) & 45°

upward injections, circle & oval cross-section reburn nozzles, and symmetric and asymmetric reburn injections. For the oval injection, the longer diameter of the nozzles is normal to the furnace axis. A few cases are selected to vary the baseline NO_x concentration. The base case uses the non-vitiated reburn air (20.9% O_2) without HEXs, 30% reburn heat input, 0° injection with circular nozzles in the symmetric configuration.

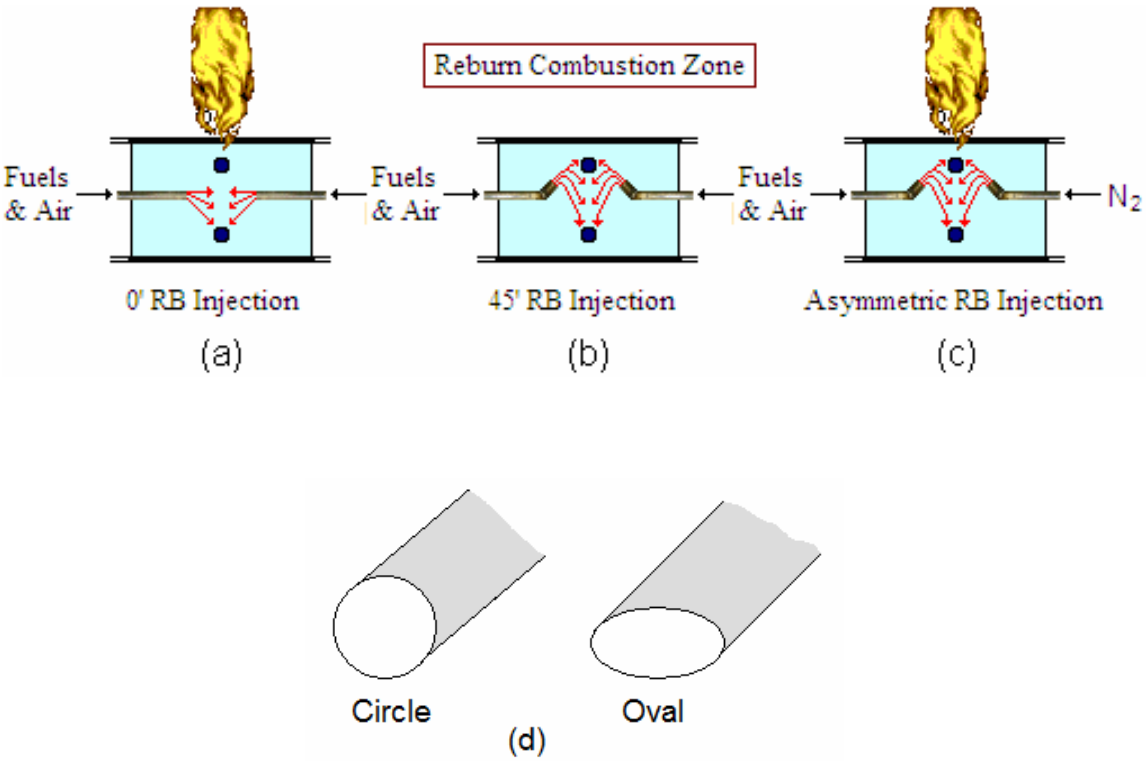

Figure 4.2. Injection configurations of reburn fuels: (a) Symmetric lateral (0°) injection, (b) Symmetric 45° upward injections, (c) Asymmetric 45° upward injection, and (d) Circle and oval shapes of the reburn nozzles.

4.2 Plug Flow Reactor (PFR) Studies for Hg Oxidation

4.2.1 Experimental Facilities

The plug flow reactor (PFR) facility in Engines, Emissions, and Energy Research Laboratory (E3 Lab) at Texas A&M University (TAMU) shown in figure 4.3 is composed of four major systems: (1) sources of simulated flue gas, (2) a mercury generation system, (3) an electrical heating furnace (or flow reactor), and (4) a mercury measuring system. Each of these systems is described in the following sub-sections.

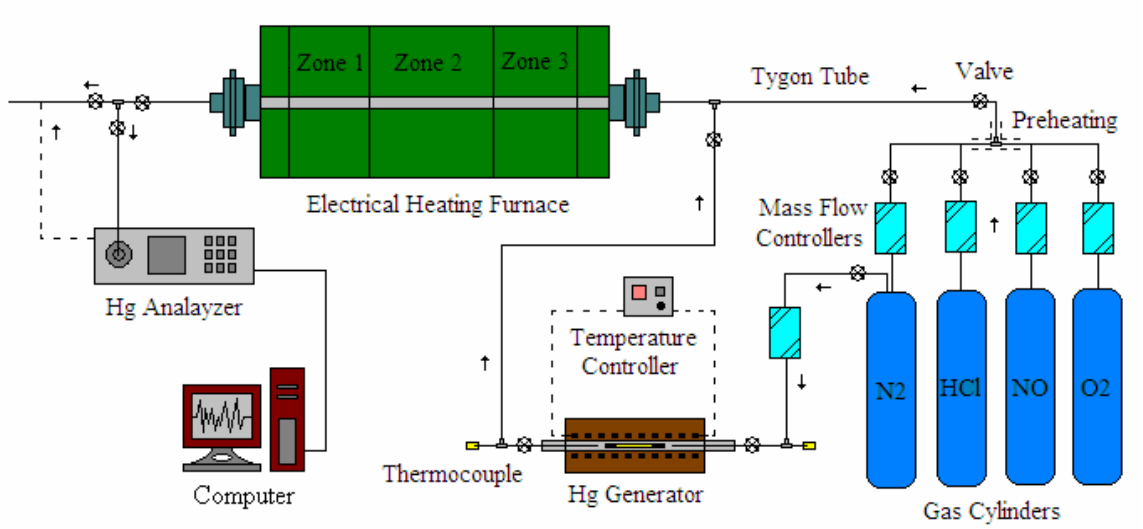

Figure 4.3. A schematic of the flow reactor facility used for Hg oxidation experiments.

A) Sources of Simulated Flue Gas. The unit includes gas cylinders and mass flow controllers (MFCs). The volume fraction (or mole fraction) of each gas species in the standard gas cylinders were 0.047% HCl, 1.98% NO and 50.2% O_2 with N_2 balance at the standard temperature (25°C) and the ambient pressure (1 atm). The balance nitrogen was an ultra high purity N_2 with a purity of 99.99%. The pressure of the simulated gas stream in the system was near atmospheric pressure. After passing through the MFCs, gas species were preheated to about

50 – 60ºC and well-mixed. The simulated gas stream (the mixtures of HCl, NO and O_2 with balance N_2) entered into a long quartz-tube inside the electrical heating furnace. For flowing elemental mercury (Hg^0), pure N_2 was used as the carrier gas for Hg^0, which entered into a short quartz-tube inside the mercury generation system.

B) Mercury (Hg) Generation System. The mercury generator contained a certified permeation tube of Hg^0 (VICI Metronics, Inc.). The permeation tube of Hg^0 (length = 73 mm) was placed in the short quartz-tube (O.D. = 20 mm, I.D. = 16 mm and L = 510 mm) in the mercury generator. The total emission rate of Hg^0 was about 1750 ng/min ± 35 ng/min (or ± 2%) at 100ºC. Flexible electric heating tapes were wrapped around the short quartz-tube. The quartz-tube was covered by insulation, and sealed into an aluminum box. A temperature controller was used to keep the temperature inside the quartz-tube constant. The temperature of the Hg^0 carrier gas (or pure N_2) was measured at each end of the permeation tube. The mercury vapor from the Hg generator was mixed with the main gas stream before the entrance to the electrical heating furnace. The total flow rate of the simulated flue gas was 1100 SCCM (standard cubic centimeter per minute at 25°C and 1 atm). The temperature of the Hg^0 carrier gas in the quartz-tube often increased or decreased 0.2 or 0.3ºC from one measurement to the next measurement. However, this temperature change between two consecutive measurements had a minor effect on the Hg^0 concentration. Most of the ending temperatures of the carrier gas were 1.0ºC higher than the beginning temperatures after the three-hour experiment. Also, the initial concentration of Hg^0 in N_2 showed no change up to 1200°C.

C) Plug Flow Reactor (PFR). The simulated gas mixture flowing through the reactor was heated to reach the desired temperatures by a three-zone furnace which has an electronic control

unit. The initial heating zone (Zone 1) and the final heating zone (Zone 3) are 150 mm long and the center zone (Zone 2) is 300 mm long. The electrical energy in the furnace is transferred to a reactor (Inconel 600 steel, I.D. = 25.4 mm and L = 1060 mm) for the entire length of the furnace. The long quartz-tube (O.D. = 12 mm, I.D. = 6 mm and L = 1220 mm) is located in the center of the reactor and supported by clamps and clamps holders. The reactor temperature of each heating area could be increased up to a maximum of 1200ºC. The gas temperature was eventually equal to the furnace temperature. The temperature at the furnace exit was typically below 500ºC. After the gases exit the furnace, they are rapidly cooled to near the ambient temperature, and the temperature at the entrance to the mercury analyzer is about 25ºC. The area between the furnace exit and the analyzer entrance is called the cooling area in the system.

D) Catalyst. For the heterogeneous Hg reduction or capture, a vanadium-tungsten-titanium (V_2O_5-WO_3/TiO_2 or VWT) honeycomb monolithic catalyst is placed in the middle of Zone 2 in the PFR. The VWT catalyst has specific gravity of 1.8, specific surface area of 1015 m^2/m^3, pH of 5, and the cell size of (1/3) cm × (1/3) cm. Its operating temperature is lower than 430ºC. Space velocity is defined as the ratio of the total gas flow rate to the catalyst volume, expressed in per hour. At a constant gas flow rate, space velocity is inversely proportional to the catalyst volume such that increasing catalyst volume corresponds to decreasing space velocity. More details are explained elsewhere [116].

E) Mercury Measuring System. The concentrations of Hg^0 were measured by mercury vapor monitor (Mercury Instruments VM-3000) near the ambient temperature. The system was capable of continuous monitoring Hg^0 in gases like air, nitrogen and argon below the gas temperature of 65ºC. A membrane pump inside VM-3000 provided a flow rate of 500 *ml/min*,

and the measurement range was selected up to 1000 μg/m^3. The gas stream enters an optical cell where ultra violet light of wavelength 253.7 nm passes through and light absorption takes place depending on the concentration of the mercury present. The absorption of light at this wavelength is a direct indication of mercury concentrations in the flue gas stream which is displayed instantaneously at the screen and is recorded at the workstation computer. The analyzed gas stream is then vented out with the rest of the total flue gas.

4.2.2 Experiment Procedures

Initially, the total flow rate of 1100 SCCM (which included balance N_2 of 900 SCCM and Hg^0 carrier N_2 of 200 SCCM) flowed into the system at ambient temperature (about 25ºC). The main gas stream (900 SCCM) was preheated to about 60ºC. A certain amount of Hg^0 from the mercury generator mixed with the main gas stream. The initial or baseline concentration of Hg^0 was between 61 and 63 ppb at the reactor temperature of about 25ºC for the homogeneous cases. The baseline Hg^0 concentration was defined as the Hg^0 concentration in the 1100 SCCM pure N_2 at 700ºC (unless otherwise stated). The extent of Hg oxidation is defined as the ratio of the removed Hg^0 concentration to the supplied Hg^0 concentration. The removed concentration is obtained by the difference of the supplied and measured concentrations. When gas components were added to the main gas stream, the amount of balance N_2 was adjusted to keep the total flow rate constant. The amount of the mercury carrier gas was fixed at all times. Measurements were taken after the concentration of Hg^0 stabilized. The stabilization of Hg^0 concentrations is considered as the fluctuation of the concentration can be ± 5 μg/m^3 (about ± 1% of the initial Hg^0 concentration) over 5 minutes. After measurements were recorded, the temperatures of the reactor were then increased. The temperatures increased up to 1200ºC for the homogeneous cases, and increased up to 400ºC for the heterogeneous cases with the VWT catalyst. To ensure

that the permeation rate of Hg^0 from the mercury generator did not change during the experiment, the temperature of the mercury generator was monitored, and the concentrations of Hg^0 at the initial and final stages with 1100 SCCM of pure N_2 at 700ºC for all experiments were measured. Some experiments were repeated at least twice.

Table 4.4. Experiment cases for the mixtures of HCl, NO and O_2 in balance N_2.

Phase	Test	Gas Composition	VWT Catalyst	Temperature Range	Residence Time at 700ºC
Homogeneous	Case *I*	NO	No	700 – 1200ºC	0.16 *s*
	Case *II*	O_2	No	700 – 1200ºC	0.16 *s*
	Case *III*	NO + O_2	No	700 – 1200ºC	0.16 *s*
	Case *IV*	HCl	No	25 – 1200ºC	0.16 *s* & 0.26 *s*
	Case *V*	HCl + NO	No	25 – 1200ºC	0.16 *s*
	Case *VI*	HCl + O_2	No	25 – 1200ºC	0.16 *s* & 0.25 *s*
	Case *VII*	HCl + NO + O_2	No	25 – 1200ºC	0.16 *s* & 0.25 *s*
Hetero-geneous	Case *VIII*	HCl	Yes	25 – 400ºC	0.25 *s*
	Case *IX*	HCl + O_2	Yes	25 – 400ºC	0.25 *s*
	Case *X*	HCl + NO + O_2	Yes	25 – 400ºC	0.25 *s*

4.2.3 Experimental Cases

To investigate the effects of gas composition on homogeneous and heterogeneous Hg oxidations, several gas compositions consisting of mixtures of HCl, NO and O_2 in balance N_2 were tested, and they are listed in Table 4.4. These gas compositions included a single gas component (HCl, NO and O_2), two-gas components (NO + O_2, HCl + O_2 and HCl + NO), and three-gas components (HCl + NO + O_2). The ranges of the reactor temperature were between 25 and 1200ºC and 700 and 1200ºC. For the heterogeneous Hg reduction, a vanadium-tungsten-

titanium (V_2O_5-WO_3/TiO_2 or VWT) catalyst was placed in the middle of Zone 2 in the PFR. Three cases from the homogeneous cases were selected for the heterogeneous tests, and the space velocity used in experiments was 70000 h^{-1}. The temperature range was much lower than that of the homogeneous cases. The baseline concentration of Hg^0 for heterogeneous cases was about 50 μg/m^3 (or 6 ppb) due to a small piece of the VWT catalyst was used. The conversion factor between [ppb] and [μg/m^3] was calculated using the ideal gas law with 1 atm and 25ºC.

In figure 4.4, the temperature distributions of the flue gas in the flow reactor were presented resulting from activating heating zones 2 & 3 and activating all three heating zones with the total flow rate of 1100 SCCM. The measured temperatures were a little higher at the center area and were a little lower at both ends than the set temperature of the reactor. Both the heated length and the temperature are important for determining the residence time (RT), and it is expressed in Eq. (4.3). Residence times were calculated at temperature of 700ºC as 0.16 *s* for the cases activating heating zones 2 & 3 and 0.25 *s* activating all three heating zones. The use of a total flow rate of 700 SCCM at 700ºC resulted in the residence time of 0.26 *s*.

$$RT = \frac{AL}{\dot{V}} \frac{T_{amb}}{T} \tag{4.3}$$

where A is a cross-section area of the quartz-tube, L is a heating length, $\dot{V}$ is a volume flow rate, T_{amb} is a ambient temperature, and T is a reactor temperature measured.

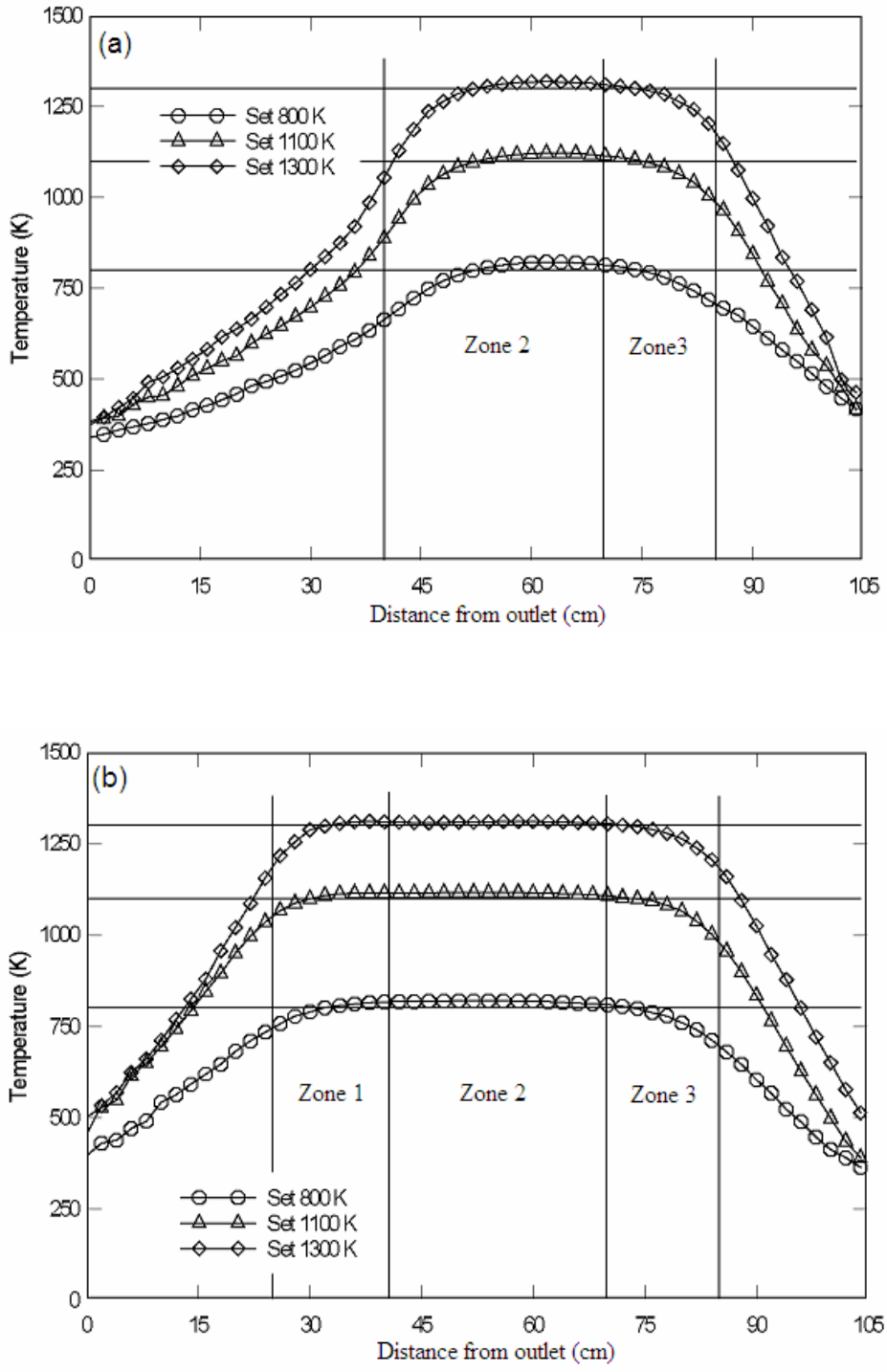

Figure 4.4. Temperature distributions of the simulated gas in the flow reactor: (a) Activating heating zones 2 & 3 and (b) Activating all three heating zones [116].

5. METHODOLOGY FOR RESULT ANALYSIS

In order to present and discuss the results, all methodologies used to obtain the results and analyses used in deriving other results are described in this section. The fuel analysis includes the proximate analysis, ultimate analysis, the fuel particle size analysis, and ash analysis. The fuel-N analysis for the fuel, conversion efficiencies and the ash formation analysis for the combustion performances are also described. In order to establish limits of accuracy of results, uncertainty and repeatability analyses are presented.

5.1 Fuel Analysis

5.1.1 Primary Fuels

Natural gas (NG) is used as the primary fuel, and its gas compositions are shown in figure 5.1. The compositions of NG consisted of 94.3% methane (CH_4), 1.7% carbon dioxide (CO_2), 2.4% ethane (C_2H_6), 0.7% nitrogen (N_2), 0.5% propane (C_3H_8) and trace amounts of several other gases. Its overall empirical chemical formula is $CH_{3.87}N_{0.0068}O_{0.033}$ with a higher heating value (HHV) of 37050 kJ/m^3. For all calculations performed in the current research, the NG composition was assumed to be pure CH_4 with a heating value of 36340 kJ/m^3 indicating that actual value is about 2% higher in heating value. These changes have negligible effect on the conditions of the primary and reburn combustion such as ER_{PRZ} and ER_{RBZ}, flow rates of the primary and reburn air, flow rates of the primary and reburn fuels, and flow rate of NH_3. It is important to maintain slightly fuel-lean combustion in the main burner to burn NG completely. The compositions of NG used during the fouling experiments were different from the NG compositions as shown in figure 5.1. The compositions of NG used in ash fouling consisted of

94.5% CH_4, 1.7% CO_2, 2.3% C_2H_6, 0.5% N_2, and 0.6% C_3H_8. Its chemical formula is $CH_{3.84}N_{0.0086}O_{0.032}$ with a heating value of 37055 kJ/m^3.

Gas Analysis Report

(August 19, 2007)

Analysis id: 93006400 Test Number: 361454

Source Information

Operator	Texas A & M University
Source	Texas A&m Power Plant(ireland Dr)
County	Brazos
State	Tx
Freq	Daily

Field Data

Date Sampled from to 08/10/2007

Static Pressure (psia)	253
Diff Pressure (inches)	0
Flowing Temp (deg. f.)	91
Water Vapor (lbs/mmcf)	2
Hydrogen Sulfide (ppm)	0
Sampled by	BOND
Field BTU @ 14.65D	1022
Field Rel Den (R)	0.592

Analysis Results

Constituent	MOL %	Gal/MCF
Helium	0.00	
Carbon Dioxide	1.69	
Oxygen	0.00	
Nitrogen	0.69	
Methane	94.32	
Ethane	2.40	0.64
Propane	0.49	0.13
Isobutane	0.10	0.03
N-Butane	0.12	0.04
Isopentane	0.05	0.02
N-Pentane	0.03	0.01
Hexanes+	0.11	0.05
Hydrogen Sulfide	0.00	
Totals	100.00	0.92

Laboratory Data

Calculated BTU @ 14.65 Dry	1022.513
Calculated BTU @ 14.65 Saturated	1004.62
Relative Density(real)	0.5983
Total Inerts	
Interchange Factor	1306
Date Reported	08/19/2007

Composite Contract Quality Requirements

	Minimum	Maximum
BTU	950	1100
Relative Density		0
Interchange	0	0
Water Vapor(lbl/mmcf)		7
Carbon Dioxide(%)		2
Oxygen(%)		0.05
Nitrogen(%)		
CO2+N2		
Total Inerts(%)		4
Hydrogen Sulfide(gr/ccf)		0.25
Hydrocarbon Dew Pt(F)		40

Remarks

Approved by DC

Figure 5.1. Gas compositions of NG used during the reburn experiments.

5.1.2 Reburn Fuels

Various samples of reburn fuels are such as High Ash Partially Composted Feedlot Biomass (HAPCFB) composted manure collected with more amounts of soil, Low Ash Partially Composted Feedlot Biomass (LAPCFB) composted manure collected with less soil or specially paved feedlots, Low Ash Partially Composted Separated Solid Dairy Biomass (LASSDB) which solids separated from water flushed dairy manure, Texas Lignite Coal (TXLC), and Wyoming Subbituminous Coal (WYC) were collected from feedlots in Amarillo, Texas and analyzed for the proximate and ultimate analyses on an as received (as rec.) and dry basis. Three samples of

each fuel were analyzed and the average values are listed in Tables 5.1 and 5.2. The reburn fuel of the base case is TXLC, and its mixtures with FB or DB are used to compare the results. The FB and DB will be more generally called as cattle biomass (CB). The tested reburn fuels are pure coals, pure CB and blends of coal:CB on a mass basis. LAPCFB and LASSDB mainly used in the current study contain about 2.5 times more fuel-N contents than coals on a dry basis, and their samples are presented in figure 5.2.

Table 5.1 Proximate analysis for reburn fuels.

Proximate (%)	HAPCFB		LAPCFB		LASSDB		TXLC		WYC	
	As Rec.	Dry	As Rec.	Dry	As Rec.	Dry	As Rec.	Dry	As Rec.	Dry
Moisture	17.00	0	19.64	0	25.26	0	38.34	0	32.88	0
Ash	53.85	64.88	16.50	20.53	14.93	19.97	11.46	18.59	5.64	8.40
Volatile Matter	25.79	31.07	52.33	65.11	46.86	62.70	24.79	40.20	28.49	42.45
Fixed Carbon	3.36	4.05	11.54	14.36	12.95	17.33	25.41	41.21	32.99	49.15
HHV, kJ/kg (BTU/lb)	5207 (2240)	6247 (2685)	13267 (5705)	16507 (7095)	12844 (5522)	17182 (7387)	14289 (6145)	23172 (9960)	18196 (7823)	27114 (11655)

Table 5.2 Ultimate analysis for reburn fuels.

Ultimate (%)	HAPCFB		LAPCFB		LASSDB		TXLC		WYC	
	As Rec.	Dry	As Rec.	Dry	As Rec.	Dry	As Rec.	Dry	As Rec.	Dry
Carbon, C	14.92	17.97	33.79	42.05	35.20	47.09	37.18	60.30	46.52	69.32
Hydrogen, H	1.39	1.68	3.65	4.55	3.12	4.17	2.12	3.44	2.73	4.06
Nitrogen, N	1.13	1.36	1.97	2.45	1.93	2.58	0.68	1.11	0.66	0.98
Oxygen, O	11.40	13.73	23.94	29.78	19.15	25.62	9.61	15.58	11.29	16.83
Sulfur, S	0.31	0.38	0.51	0.64	0.43	0.57	0.61	0.98	0.27	0.41

Figure 5.2. Fuel samples used in CB reburning: (a) LAPCFB, (b) LASSDB and (c) TXLC.

Estimated values of fuel properties based on the proximate and ultimate analyses and the operating conditions are listed in Table 5.3 including the overall empirical chemical formula and the ash loadings [kg/GJ] of the reburn fuels. Even though mass based ash content of LAPCFB is about three times that of WYC as shown in Table 5.1, the ash content on a heat basis in Table 5.3 is almost four times that of WYC due to the lower heat value of LAPCFB. The pure HAPCFB has the highest ash loading and only limited tests have been conducted due to safety concerns. Even though the HHV of as received fuels range from 5207 to 18196 kJ/kg, the HHV in kJ per kg of stoichiometric air is approximately same for coals and CB as shown from 3055 to 3425 kJ/kg which implies that the oxygen consumption will be same when same thermal output

is maintained; i.e. the same air flow rate is maintained when switching the fuels and the fuel flow is adjusted until similar O_2% in exhaust is maintained when operated under slightly fuel-lean conditions.

Table 5.3 Fuel properties for reburn fuels on an as received basis.

	HAPCFB	LAPCFB	LASSDB	TXLC	WYC
HHV, kJ/kg (BTU/lb)	5207 (2240)	13267 (5705)	12844 (5520)	14289 (6145)	18196 (7823)
HHV in kJ per kg Stoich Air, (BTU/lb)	3055 (1315)	3235 (1390)	3425 (1475)	3115 (1340)	3150 (1355)
HHV in kJ per kg Stoich O_2, (BTU/lb)	13285 (5710)	14065 (6045)	14845 (6380)	13540 (5820)	13690 (5885)
DAF HHV, kJ/kg (BTU/lb)	17865 (7680)	20775 (8930)	21474 (9232)	28465 (12240)	29600 (12725)
Ash Loading, kg/GJ	103.42	12.44	11.62	8.02	3.10
Chemical Formula	$CH_{1.11}N_{0.065}O_{0.57}S_{0.008}$	$CH_{1.28}N_{0.05}O_{0.53}S_{0.006}$	$CH_{1.06}N_{0.05}O_{0.41}S_{0.005}$	$CH_{0.68}N_{0.02}O_{0.19}S_{0.006}$	$CH_{0.7}N_{0.01}O_{0.18}S_{0.002}$

5.1.3 Ash Fusion Temperature (AFT)

The mineral analysis of ash for the reburn fuels tested are very important since the mineral composition of the ash affects the deposition rate, fusion and melting points, corrosion rate, and erosion rate of heat exchangers (HEXs). The mineral analysis is presented in Table 5.4. Higher alkaline oxide contents (CaO, MgO, Na_2O, and K_2O) result in a higher probability of fouling due to faster growing oxide layers on HEX surfaces [25, 114]. LAPCFB and LASSDB have high alkaline contents probably due to the collection of CB from fly ash paved feedlots or concrete surfaces. The ash fusion temperature depends upon the ratio of basic oxides to acidic oxides, B/A, and it is represented as Eq. (5.1) [26]. The ratios of basic oxides to acidic oxides (B/A) are summarized in Table 5.4. The higher the amounts of basic oxides, the lower the ash fusion temperature (AFT).

Table 5.4 Ash analysis.

Compositions	HAPCFB	LAPCFB	LASSDB	TXLC	WYC	Melting (°C)
Silicon, SiO_2	65.55	20.78	31.36	48.72	31.73	1713
Aluminum, Al_2O_3	11.2	4.94	2.89	16.04	17.27	2040
Titanium, TiO_2	0.52	0.22	0.20	0.85	1.35	1830
Iron, Fe_2O_3	2.99	1.71	1.62	7.44	4.61	1565
Calcium, CaO	7.47	21	26.40	11.70	22.20	2299
Magnesium, MgO	2.29	7.54	7.47	1.93	5.62	2800
Sodium, Na_2O	1.38	5.26	2.28	0.29	1.43	1132
Potassium, K_2O	4.66	14.6	6.90	0.61	0.67	763
Phosphorus, P_2O_5	2.43	13.77	6.01	0.1	0.8	300
Sulfur, SO_3	1.3	4.47	4.72	10.80	10.40	17
Chlorine, Cl	0.41	5.07	0.92	< 0.01	< 0.01	-101
Carbon dioxide, CO_2	0.51	0.59	9.49	0.08	0.37	-57
Basic/Acidic oxides, B/A	0.27	2.46	1.47	0.34	0.7	-

Note: Values given in percent mass. Ash was calcined at 600°C (1100°F) prior to analysis

$$\frac{B}{A} = \frac{Fe_2O_3 + CaO + MgO + Na_2O + K_2O + P_2O_5}{SiO_2 + Al_2O_3 + TiO_2} \tag{5.1}$$

The ash fusion temperatures (AFTs) of reburn fuels are presented for both reducing and oxidizing atmospheres in Table 5.5. The values of AFTs are HAPCFB > TXLC and LASSDB > LAPCFB > WYC in the reduction condition while they are HAPCFB > TXLC > LASSDB > WYC > LAPCFB in the oxidizing condition. In Table 5.4, the values of basic/acidic oxides (B/A) is LAPCFB > LASSDB > WYC > TXLC > HAPCFB. Therefore, the AFT results of the

oxidizing condition show a good agreement with the results that the higher B/A causes the lower AFT. However, the previous results using a DOE-NETL pilot-scale facility indicated the ash layer deposited by FB combustion were more difficult to remove than the ash layer deposited by coal combustion [25]. Their result seems to indicate that the amounts of ash in reburn fuels influence the "fouling behavior" more than the basic ash fusion characteristics. Thicker the ash layer, hotter is the outer surface ash temperature and more is "sticking" tendency.

Table 5.5. Ash fusion behavior for reburn fuels.

Properties	HAPCFB	LAPCFB	LASSDB	TXLC	WYC
-- Reducing atmosphere --					
Initial deformation temperature, IDT, ºF (ºC)	2177 (1190)	2126 (1165)	2153 (1178)	2111 (1155)	2112 (1156)
Softening temperature, ST, ºF (ºC)	2222 (1220)	2143 (1170)	2169 (1187)	2150 (1175)	2124 (1162)
Hemispherical temperature, HT, ºF (ºC)	2286 (1250)	2148 (1175)	2175 (1191)	2181 (1195)	2130 (1166)
Flow temperature, FT, ºF (ºC)	2380 (1305)	2156 (1180)	2181 (1194)	2190 (1200)	2140 (1171)
-- Oxidizing atmosphere --					
Initial deformation temperature, IDT, ºF (ºC)	2202 (1205)	2124 (1160)	2190 (1199)	2238 (1225)	2184 (1196)
Softening temperature, ST, ºF (ºC)	2253 (1235)	2186 (1200)	2198 (1203)	2256 (1235)	2190 (1199)
Hemispherical temperature, HT, ºF (ºC)	2315 (1270)	2146 (1175)	2201 (1205)	2276 (1245)	2197 (1203)
Flow temperature, FT, ºF (ºC)	2400 (1315)	2154 (1180)	2206 (1208)	2310 (1265)	2210 (1210)

5.1.4 Size Distribution of Fuel Particles

The size analysis of fuel particles is very important because of its significant effect on scale of heating, release of volatiles and subsequent reduction of O_2 due to oxidation and hence their effects on NO_x emissions. In general, solid fuels used in utility boilers are about 70% of solid fuels having the particle size less than 75 μm (or 200-mesh screen) [117]. The Rosin Rammler distribution is widely used to describe the particle size of pulverized solid fuels [48]. The tested fuels were as fine as one could get with present available grinders. First, fuel samples of HAPCFB, LAPCFB, TXLC, and WYC were analyzed for the FB reburning. Second, fuel samples of LASSDB, LAPCFB and TXLC were analyzed for the DB reburning, Fuel samples were selected and analyzed in two different time-lines for the FB and DB reburn experiments. Results between the same fuels in two different time-lines were observed, and they were somewhat different, but relatively similar.

The distribution of particle sizes for the FB reburn experiments as presented in figure 5.3 showed that particles smaller than 75 μm were 78% for HAPCFB, 43% for LAPCFB, 38% for WYC, and 24% for TXLC by mass. More than 90% of particles for all fuels were smaller than 300 μm. A large portion of very small particles was found in HAPCFB. It was found that the ash tended to make up most of the smaller particles of HAPCFB, and the combustibles were contained in larger particles of HAPCFB. Since TXLC, LAPCFB, and WYC contain low ash contents, most of the small particles may be presumed to be combustibles. Theoretically, the smaller particles would heat faster, release volatiles faster than the larger particles, and hence reduce the local O_2 concentration. The low O_2 concentration slows down NO_x formation and allows NO_x reduction to be dominant. The release rate of volatiles is higher with higher heating rates. Thus particle size is one of the important parameter for NO_x reduction.

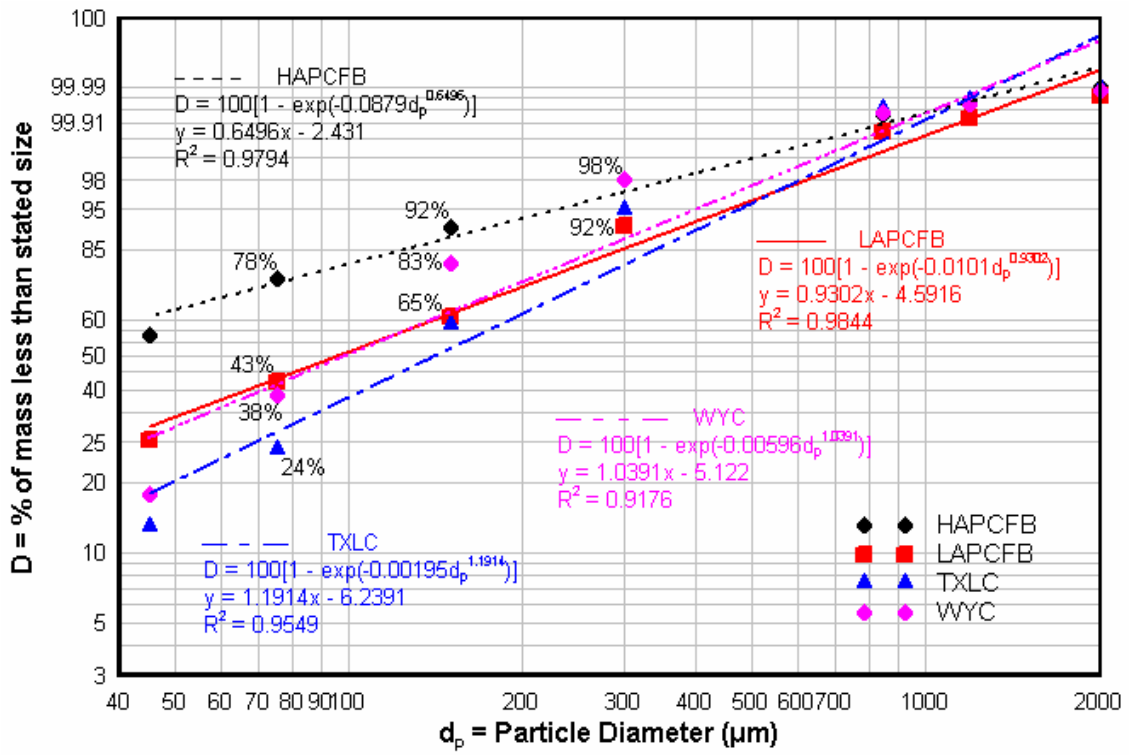

Figure 5.3. Particle size distributions of the reburn fuels for the FB reburning.

For the FB reburn experiments, mean size by mass and Sauter mean diameter (commonly abbreviated as SMD or d_{32}) of fuel particles are presented in Table 5.6. Mean size of reburn fuels was about 65 μm for HAPCFB, 112 μm for WYC, 147 μm for LAPCFB, and 156 μm for TXLC. HAPCFB had the smallest mean size of particles due the fact that it contained a larger portion of small particles made up of mostly ash than other fuels. The SMD is defined as the diameter of a sphere that has the same ratio of volume to surface area and used in almost exclusively to determine the average diameter of solid fuel particles. It is represented as Eq. (5.2). The SMD of reburn fuels was about 33 μm for HAPCFB, 56 μm for LAPCFB, 64 μm for WYC, and 81 μm for TXLC. The detailed calculations of the SMD are presented in Appendix A.

Table 5.6. Size distributions of fuel particles for the FB reburning.

Mean Diameter (μm) Between Sieves	HAPCFB (w%)	LAPCFB (w%)	TXLC (w%)	WYC (w%)
1596	0.01	0.05	0.01	0.013
1015	0.03	0.1	0.018	0.021
570	1.68	7.58	4.97	1.69
225	6.44	27.21	33.72	15.35
113	13.73	22.56	37.09	45.02
60	20.43	16.06	11.82	21.76
22.5	57.69	26.44	12.38	16.19
Mean Size by Mass (μm)	65.2	147.2	156.1	111.9
SMD (μm)	32.7	56.3	81	64.4

$$SMD \quad or \quad d_{32} = \frac{\sum_{i=1}^{n} d_i^{\,3} \cdot n_i}{\sum_{i=1}^{n} d_i^{\,2} \cdot n_i} \tag{5.2}$$

where d_i is the diameter of particles and n_i is the number of the particles.

For the DB reburn experiments, fuel samples of LASSDB, LAPCFB and TXLC were analyzed, and the results are presented in figure 5.4 and Table 5.7. Particles smaller than 75 μm (or 200-mesh screen) were about 49% for LAPCFB, 23% for TXLC and LASSDB by mass. More than 75% of particles for all fuels were smaller than 300 μm. LASSDB was coarser than LAPCFB. Mean size of reburn fuels was about 242 μm for LASSDB, 150 μm for LAPCFB, and 167 μm for TXLC. Since LASSDB contained about 22 w% of 570 μm, its mean size was the largest. The SMD of reburn fuels was about 89 μm for LASSDB, 50 μm for LAPCFB, and 95 μm for TXLC. LAPCFB contained about 49 w% particles less than 60 μm, and it made the SMD small.

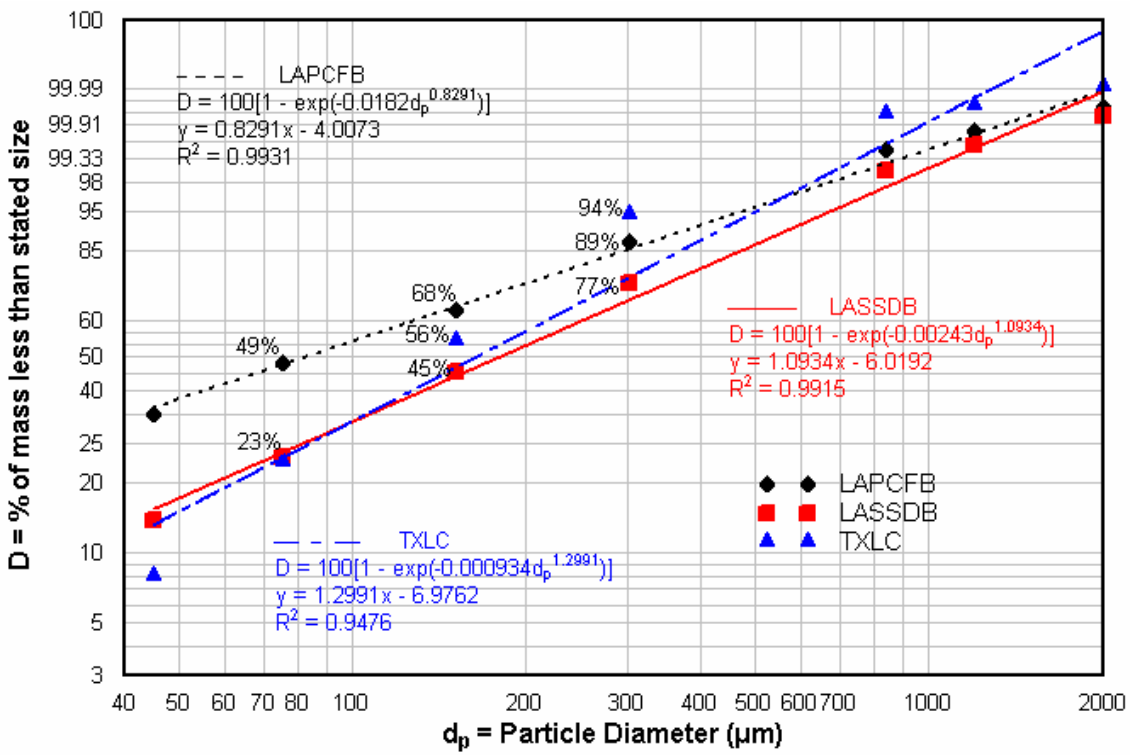

Figure 5.4. Particle size distributions of the reburn fuels for the DB reburning.

Table 5.7. Size distributions of fuel particles for the DB reburning.

Mean Diameter (µm) Between Sieves	LASSDB (w%)	LAPCFB (w%)	TXLC (w%)
1596	0.260	0.108	0.015
1015	0.841	0.263	0.02
570	21.815	10.367	5.595
225	31.451	21.557	37.986
113	22.880	19.091	34.204
60	9.602	15.912	14.857
22.5	13.110	32.680	7.320
Mean Size by Mass (µm)	242.2	150.4	166.8
SMD (µm)	88.8	50	94.7

5.1.5 Characteristics of Oxidation and Pyrolysis

Pyrolysis and oxidation of reburn fuels were characterized by Thermogravimetric Analysis (TGA). Five ranges of the particle size were selected as $D_p \leq 45$, $45 \leq D_p \leq 75$, $75 \leq D_p \leq 150$, $150 \leq D_p \leq 300$, and $300 \leq D_p \leq 840$ μm. Air was used as a main purge gas for the oxidation, and N_2 was used for some cases for the pyrolysis. Once air was used for the oxidation, the fuel sample first dried at 120ºC for 10 minutes and then heated at 950ºC for 15 minutes. Then it was cooled down to 575ºC, and the temperature was kept at 575ºC until the weight change was less than 0.3 mg/h. These procedures were selected based on the procedures of ASTM standards: ASTM E-872 and D-3175 for the estimation of the amount of VM and E-1755 for the estimation of the amount of ash. The release rate of volatiles is typically higher with higher heating rates. The average heating rate was 190ºC/min for the oxidation because the function "Equilibriate" was selected in a TGA operating program to increase the temperature as fast as possible, It was much lower than the actual heating rate when the fuel was injected into the reburn zone (about 1100ºC/s). For the pyrolysis using N_2, the fuel sample first dried at 120ºC for 10 minutes and then heated at 575ºC until the weight change was less than 0.3 mg/h. The average heating rate was 120ºC/min for the pyrolysis.

The oxidation results for LASSDB as a function of time and temperature on an as received basis are presented in figure 5.5. It is clear that there exit five distinct regions (*I* – *V*): Region *I* is for a moisture loss, Region *II* is for complete drying and heating to the oxidation (or pyrolysis) temperature, Region *III* is for a rapid release of volatiles (major amounts), Region *IV* is for a release of volatiles (minor amounts) and fixed carbon, and Region *V* is an ash portion. The moisture loss (Region *I*) was about 10% of the total weight for all particle sizes, and the amount of volatiles (Region *III*) released during the oxidation was about 30 to 55% of the total weight. For the better comparison, Regions *III*, *IV* and *V* are plotted on a dry basis in the next paragraph.

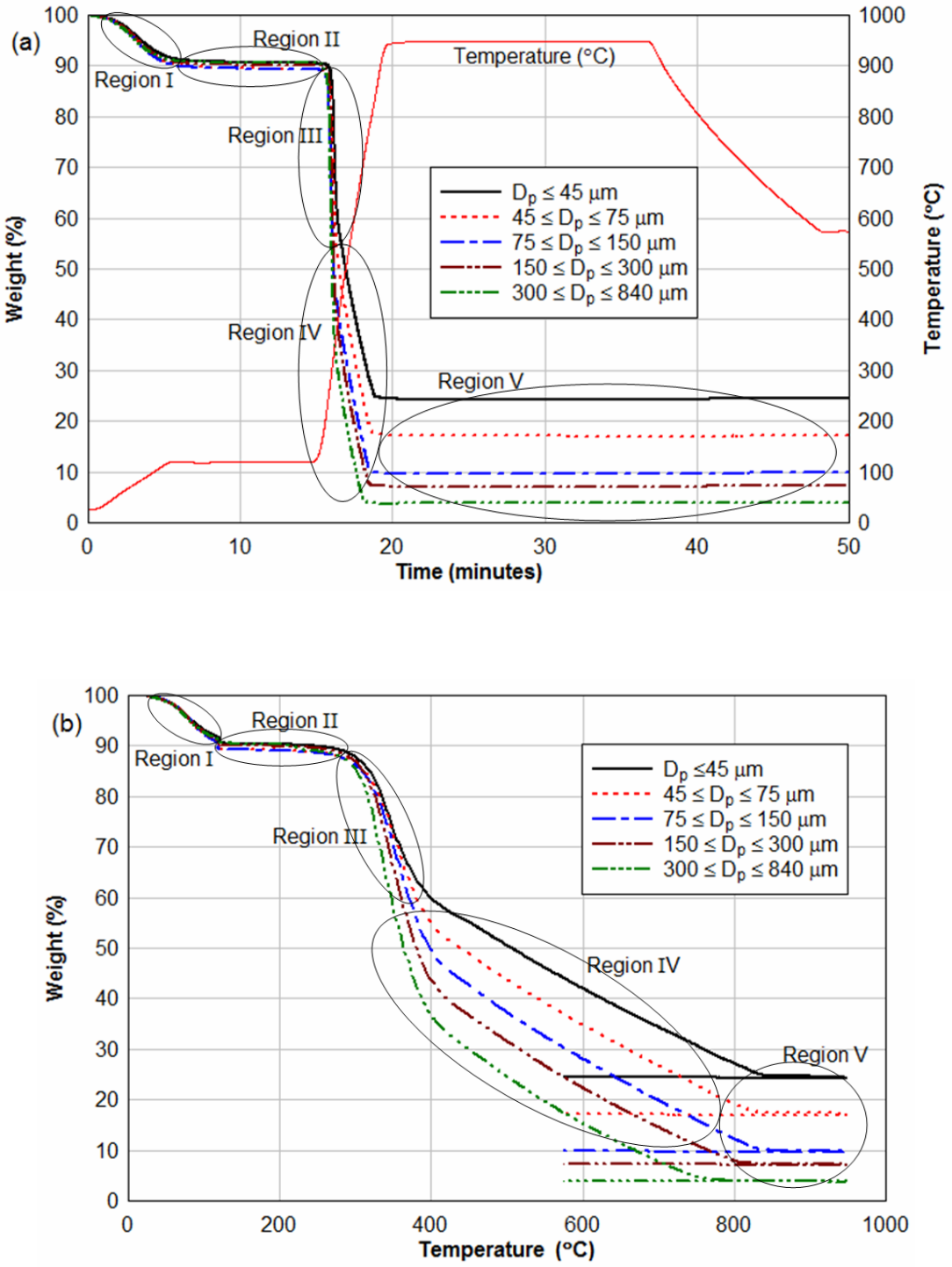

Figure 5.5. Oxidation results for various particle sizes of LASSDB using air on an as received basis: (a) Results as a function of time and (b) Results as a function of temperature.

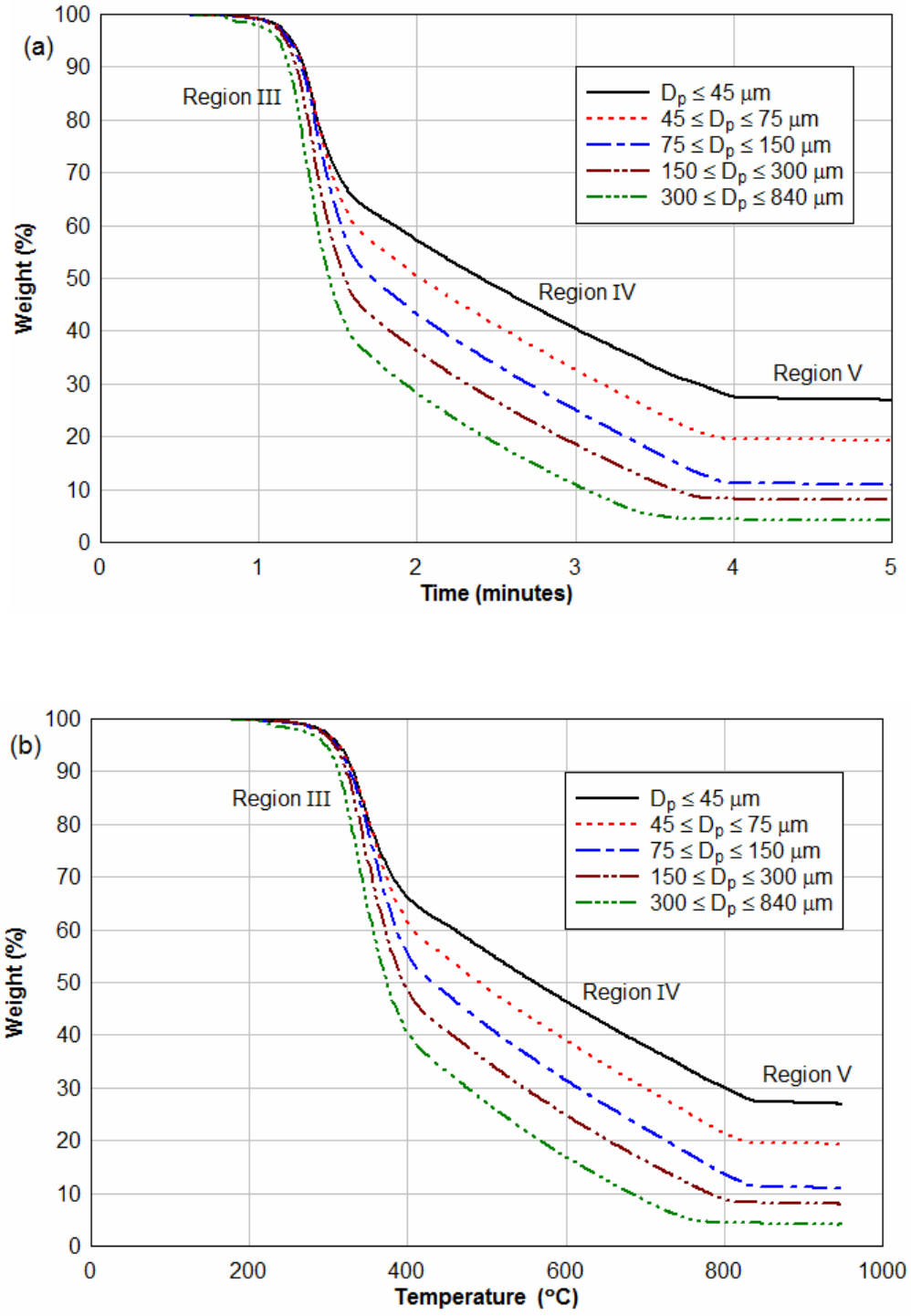

Figure 5.6. Oxidation results for various particle sizes of LASSDB using air on a dry basis: (a) Results as a function of time and (b) Results as a function of temperature.

Figure 5.6 presents the oxidation results for LASSDB on a dry basis. The major amounts of volatiles were released within one minute in Region *III*. Then, the remaining volatiles (minor amounts) and fixed carbon were released within two minutes in Region *IV*. Higher portions of ash were found in smaller particles. This result is consistent with the result reported by Rico, et al. [118], that is, the particles of ash are smaller than the particles of VM. It is interesting that the larger particles release volatiles more, slightly earlier and at lower temperature than the smaller particles. These phenomena can be explained by the heating rates and the particle structure in the testing pan. The heating rates were higher for the larger particles which increased the release rate of the VM. Because of the way the fuel sample was heated using the Equilibriate function in the TGA instrument, the heating rate was varied case by case. The heating rates and the release rates of the VM in Region *III* in figure 5.6 (a) were estimated and presented in Table 5.8. The structures of fuel particles in the testing pan are shown in figure 5.7. The pan filled with larger particles is more porous than the pan filled with smaller particles. More spaces are available for the larger particles, and thus the larger particles in the middle or bottom areas are heated faster at the same temperature. Ignition temperatures of several fuels were reported in Reference [119]. The ignition temperature was determined by the difference of the results of fuel oxidation and pyrolysis. The ignition temperature of LASSDB was found to be 250ºC.

Table 5.8. Heating rates and the release rates of the VM in Region *III*.

Particle Size (μm)	Heating Rate (ºC/min)	Release Rate of VM (w%/min)
$D_p \leq 45$	181.7	21.4
$45 \leq D_p \leq 75$	182.4	24.8
$75 \leq D_p \leq 150$	182.8	28.4
$150 \leq D_p \leq 300$	184.1	31.9
$300 \leq D_p \leq 840$	184.7	35.9

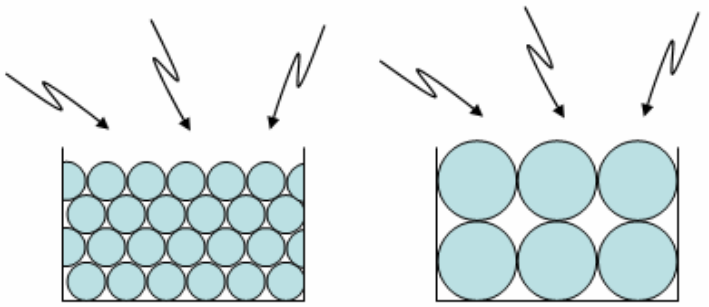

Figure 5.7. Structures of fuel particles in the testing pan.

Figure 5.8 presents oxidation results for TXLC on a dry basis. Similar regions and results were observed for TXLC. Though it is not clear to distinguish Regions *III* and *IV*, it can be seen that the amounts of volatiles released from TXLC are less than those from LASSDB, and the amounts of fixed carbons released from TXLC are more than those from LASSDB. It is consistent with the proximate analysis in Table 5.1. The release rates of the VM are lower than those for LASSDB. The ignition temperature of TXLC was 270ºC as reported in Reference [119] which was slightly higher than that of LASSDB. The ignition temperatures of reburn fuels were not determined in the current study because the oxidation and pyrolysis were conducted in different heating conditions.

Pyrolysis results for LASSDB, LAPCFB and TXLC on an as received basis are presented in figure 5.9. The results of LASSDB and LAPCFB are very similar each other. Both CBs released more amounts of the VM than TXLC. The release rates of both CBs were much faster than that of TXLC, and they are much smaller for the pyrolysis than the oxidation because of the heating rate. The pyrolysis stated at 240ºC for both LASSDB and LAPCFB and at 300ºC for TXLC. Pyrolysis temperatures of several fuels were also reported in References [60, 119]. The comparison of the ignition and pyrolysis temperatures shows that the particles of LASSDB were ignited during pyrolysis while the particles of TXLC were ignited before pyrolysis.

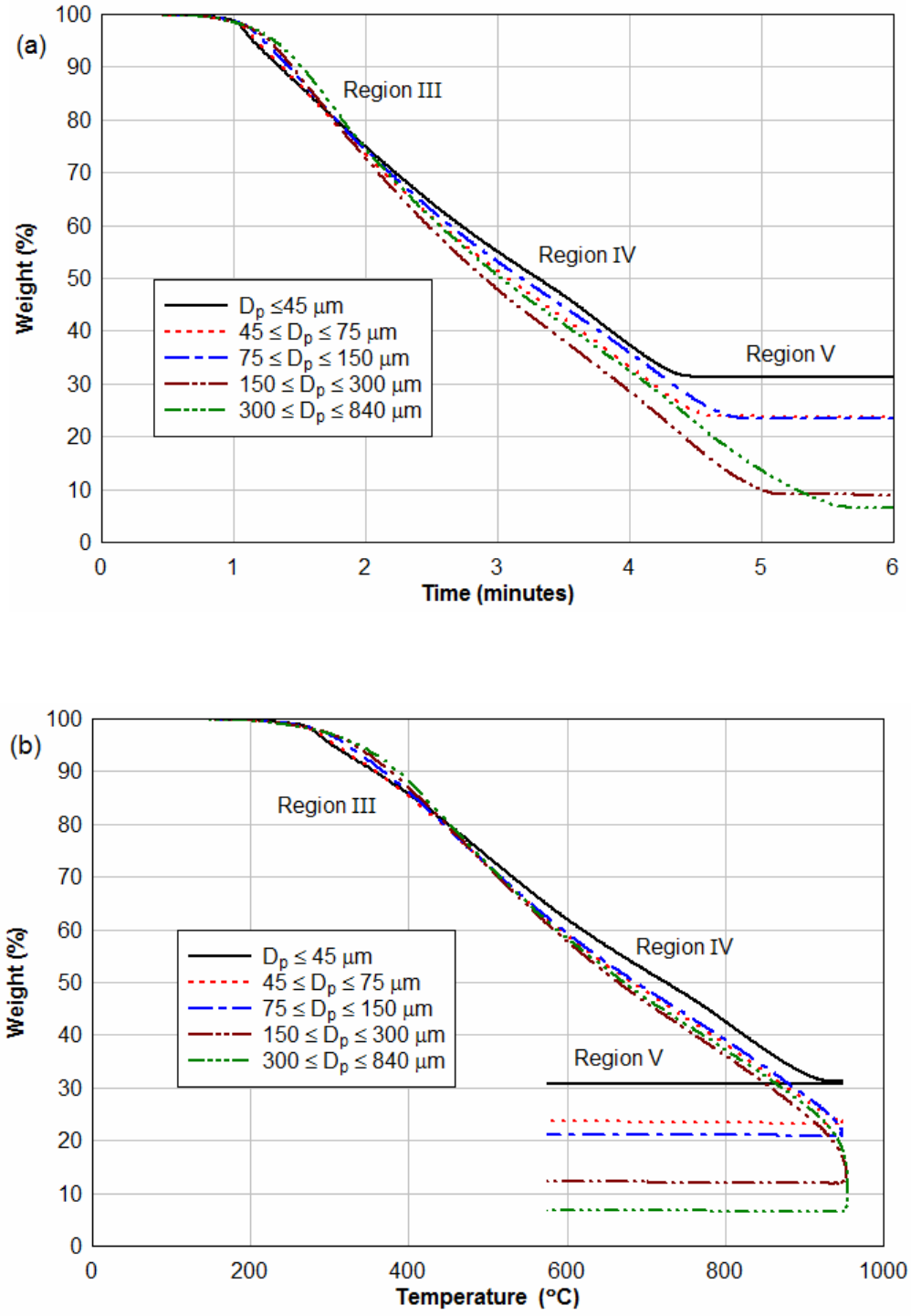

Figure 5.8. Oxidation results for various particle sizes of TXLC using air on a dry basis: (a) Results as a function of time and (b) Results as a function of temperature.

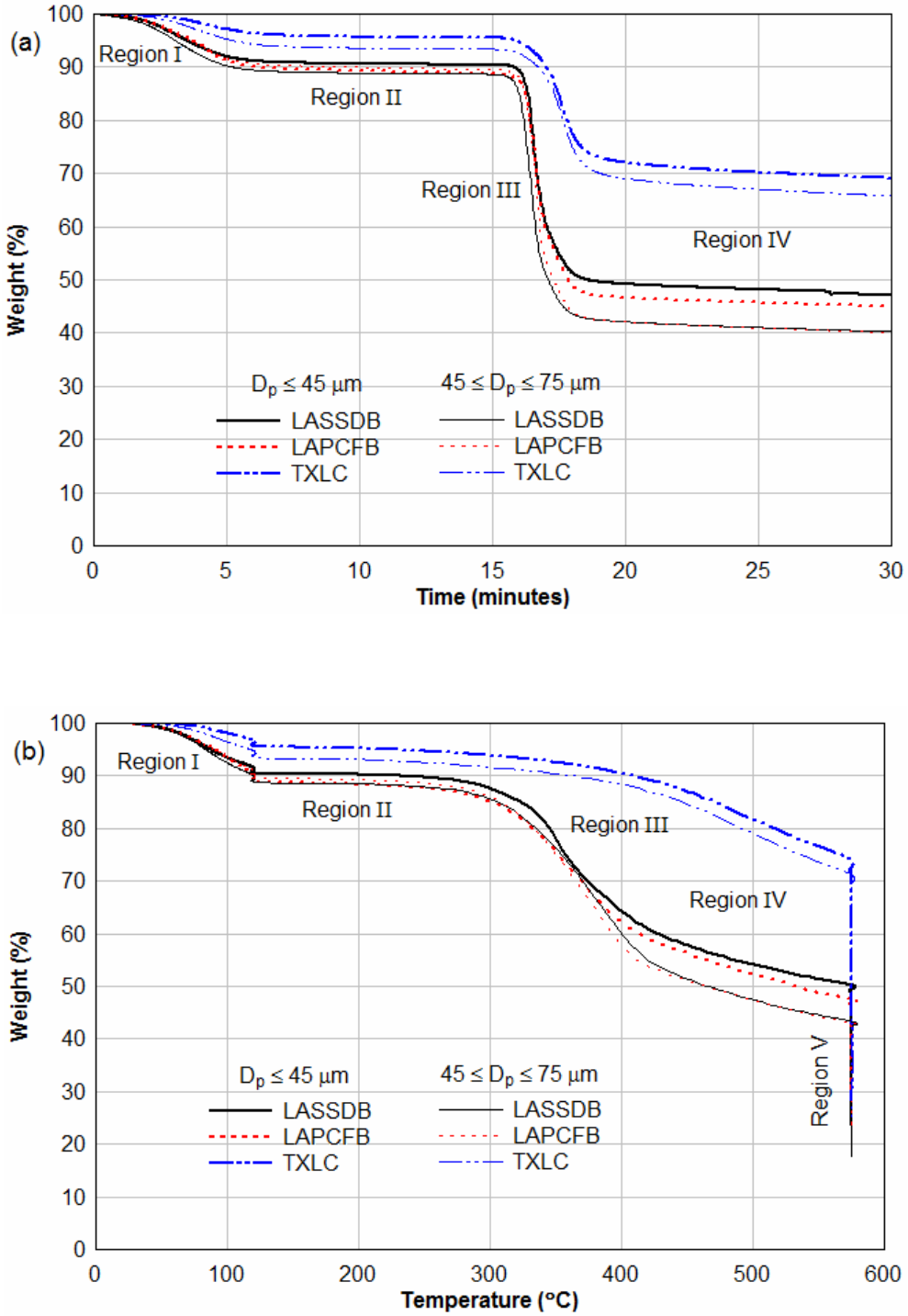

Figure 5.9. Pyrolysis results for various particle sizes of LASSDB using N_2 on an as received basis: (a) Results as a function of time and (b) Results as a function of temperature.

5.2 Fuel-Nitrogen (N) Analysis

Nitrogen species, HCN and NH_3 derived from fuel-N during combustion, are the main sources for the NO_x formation and reduction in homogeneous gas-phase reaction. The fuel-N mainly transforms to N_2 and NO_x during pyrolysis and devolatilization. It was found HCN was a main precursor for N_2O [120, 121]. Thus NH_3 was used as a main precursor for NO_x reduction in the current study as presented in Eq. (5.3).

$$NH_3 + 1.5NO \rightarrow 1.25N_2 + 1.5H_2O \tag{5.3}$$

Assuming that fuel-N releases NH_3, then it is very useful to estimate amounts of NH_3 and hence fuel-N required to reduce certain amounts of NO_x. A methodology of fuel-N analysis is briefly presented in this section and detailed presented in Appendix B. The analysis was performed based on the presumption that the sufficient fuel-N in the reburn fuels produced the necessary amount of NH_3 needed for 90% NO_x reduction. The assumptions required for the analysis are as follows (1) The fuel-N in biomass convert to 60% NH_3, 30% HCN and 10% N_2 on a mass basis, and (2) The fuel-N in coals convert to 30% NH_3, 60% HCN and 10% N_2 on a mass basis. For the analysis, Eq. (5.4) was used. The heat generated by the reburn fuels was considered as 30% (9 kW or 30,000 BTU/h) of the total heat. The fuel properties in Tables 5.1 and 5.2 and chemical forms listed as $C_cH_hN_nO_oS_s$ in Table 5.3 were used for the analysis. The blends of coal:biomass were determined by the combination of the fuel properties on a mass basis. The NO_x reduction in mole/s by reburning is calculated using Eq. (5.5).

$$CH_hN_nO_oS_s + a\left(O_2 + A \cdot H_2O + B \cdot N_2\right) \rightarrow CO_2 + bH_2O + cSO_2 + dO_2 + eN_2 \tag{5.4}$$

where A = 0.0234, B = 3.785, $a = \frac{(1+h/4+s-o/2)}{\phi}$, $b = \left(\frac{h}{2} + A\frac{(1+h/4+s-o/2)}{\phi}\right)$, $c = s$, $d = \left(1+\frac{h}{4}+s-\frac{o}{2}\right)\left(\frac{1}{\phi}-1\right)$, and $e = \left(\frac{B}{\phi}\left(1+\frac{h}{4}+s-\frac{o}{2}\right)+\frac{n}{2}\right)$.

$$\dot{N}_{NOx,reduced} = \dot{N}_{dry,PRZ} \times x_{NOx,PRZ} - \dot{N}_{dry,exit} \times x_{NOx,exit} \tag{5.5}$$

where $\dot{N}_{dry,PRZ}$ and $\dot{N}_{dry,exit}$ are mole flow rates on a dry basis in the primary zone and at the furnace exit, respectively, and $x_{NOx,pri}$ and $x_{NOx,exit}$ are mole fractions of NO_x measured before reburning and after reburning, respectively. The combustion efficiency, η_{comb}, should also be considered for the reburn combustion to make sure that all fuels are burnt. The minimum amount of NH_3 used for the NO_x reduction is calculated using Eq. (5.3). The reburn fuels contain N% nitrogen, M% moisture and A% ash on a DAF mass basis. The mole flow rate of the fuel-N in the reburn zone (RBZ) is

$$\dot{N}_{DAF,N\%} = \dot{N}_{NH_3,used} / k \tag{5.6}$$

where $\dot{N}_{DAF,N\%}$ is the mole flow rate on a dry ash free (DAF) basis, $\dot{N}_{NH_3,used}$ is the mole flow rate used for 90% NO_x reduction, and k is the amounts of NH_3 converted from the fuel-N. Finally, the minimum amounts of the reburn fuels required for 90% NO_x reduction are obtained, depending on the reburn fuels, and then the flow rate used in the experiments must exceed the minimum required.

5.3 NO_x Emission Analysis

For the measurement of NO_x emissions, the O_2 concentration should be analyzed at the same point and time as NO_x is analyzed and analyzed on the same basis (wet or dry). The NO_x concentration must be reported at standard or reference O_2 concentration. The representation of NO_x emissions at the exhaust based on a 3% O_2 concentration (which is called a reference O_2) is suggested by EPA standards while some European studies use 6% O_2. For gas turbines, the standard O_2 concentration is 15%. The conversion formula for the corrected NO_x concentration at 3% O_2 is represented as [122]:

$$[NO_x]_{corr} = [NO_x]_{meas} \times \frac{O_{2,amb} - O_{2,ref}}{O_{2,amb} - O_{2,meas}} \tag{5.7}$$

where $[NO_x]_{meas}$ is the measured NO_x concentration in [ppm], $O_{2,amb}$ is the ambient O_2 concentration (20.9%), $O_{2,ref}$ is the reference O_2 concentration (3%), and $O_{2,meas}$ is the measured O_2 concentration.

The dilution effect of the reburn air is significant on the measurement of NO_x emission in [ppm], thus it should be accounted in further discussion. The emissions of NO_x and SO_2 on a heat basis are described as below [12]:

$$NO_x \ in \ (kg/GJ) \ = \ \frac{46.01 \ \times \ x_{NO_x} \ \times \ C \ fraction}{12.01 \ \times \ x_{CO_2} \ \times \ HHV \ (GJ/kg)} \tag{5.8}$$

$$SO_2 \ in \ (kg/GJ) \ = \ \frac{64.06 \ \times \ x_{SO_2} \ \times \ C \ fraction}{12.01 \ \times \ x_{CO_2} \ \times \ HHV \ (GJ/kg)} \tag{5.9}$$

where the C fraction is a mass fraction of carbon in as received fuels, HHV is a higher heating value of the as received fuels, and *x* is a mole fraction. Note that (1) *C* fraction and *HHV* for the current study are the combination values of those in the primary and reburn fuels, and (2) a molecular weight of 46.01 is used for NO_x since all NO is eventually converted into NO_2 in the atmosphere. In Eq. (5.8) and (5.9), the amount of CO is neglected, otherwise $x_{CO_2} + x_{CO}$ is used instead of x_{CO_2}. The similar concentrations in [ppm] measured from two different cases can be converted to different values in g/GJ because concentrations of CO and CO_2 are different case by case.

The equivalence ratio (ϕ) was first calculated by measuring the air flows and average feed rate of fuel. This was further checked by gas analysis. The verification was performed for lean (ϕ < 1.0) and stochiometric (ϕ = 1.0) conditions based on the assumption of complete combustion. For lean combustion, it can be shown as $\phi \approx 1 - 4.76 X_{O_2}$ where X_{O2} is the mole fraction of oxygen in flue gas.

5.4 Heat Exchanger (HEX) Analysis

A brief overview of relevant heat transfer analysis for HEXs is presented. In the current setup, the entrance and exit temperatures of the hot flue gases and cold fluids are important and typically mentioned. Defining the overall heat transfer rate as,

$$\dot{Q} = UA\Delta T_{LM} \tag{5.10}$$

$$\Delta T_{LM} = F\Delta T_{lm} = F\frac{\Delta T_1 - \Delta T_2}{\ln\left(\frac{\Delta T_1}{\Delta T_2}\right)} \tag{5.11}$$

where U is an *overall heat transfer coefficient* (OHTC), A is a surface area of the HEX, ΔT_{LM} is a *log mean temperature difference* (LMTD), F is a correction factor used for the cross-flow HEX system, and ΔT_1 and ΔT_2 are the local temperature differences. The local temperatures are presented in figure 5.10, and the local temperature differences are defined as

$$\begin{pmatrix} \Delta T_1 = T_{hot,in} - T_{cold,exit} \\ \Delta T_2 = T_{hot,exit} - T_{cold,in} \end{pmatrix} \tag{5.12}$$

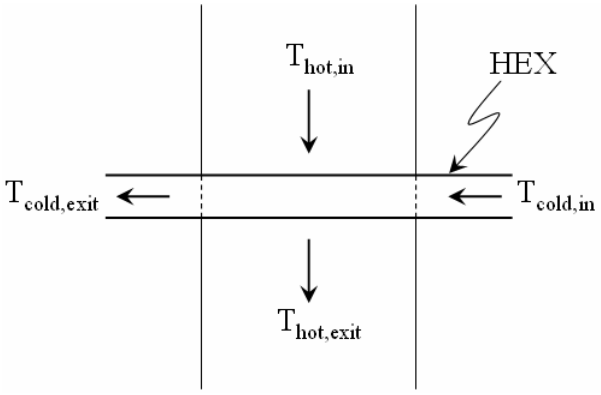

Figure 5.10. A sketch of local temperatures around the HEX.

If the temperature change of one fluid (e.g. hot flue gas) is negligible, then the correction factor, F is 1. The determination of F is explained elsewhere [123]. The hot fluid is the flue gas stream as generated by the current facility, and the cold fluid used in the study is air or water. The energy balance around the HEX yields the heat transfer rate as

$$\dot{Q}_{hot} = \dot{m}_{gas} c_{p,gas} (T_{hot,in} - T_{hot,exit}) \tag{5.13}$$

$$\dot{Q}_{cold} = \dot{m}_{cold} c_{p,cold} (T_{cold,exit} - T_{cold,in}) \tag{5.14}$$

where $\dot{m}$ is a mass flow rate (kg/s) and c_p is a specific heat (J/kg·K) which depends on the average temperatures at the entrance and exit of hot and cold fluids. If the reactor is well insulated and no radiation takes place, then the heat transfer rates of Eq. (5.13) and (5.14) are the same ($\dot{Q}_{hot} = \dot{Q}_{cold} = \dot{Q}$). If the temperature difference ($\Delta T = T_{cold,exit} - T_{cold,in}$) of the cold fluid increases, the heat transfer to the HEX also increases. The overall heat transfer coefficient (OHTC or U) [W/m^2·K] is now expressed as

$$U = \frac{\dot{m}_{cold} c_{p,cold} (T_{cold,exit} - T_{cold,in})}{A \Delta T_{LM}} \tag{5.15}$$

Governing equations from (5.10) to (5.15) are used in the heat exchanger analysis based on one-dimensional, steady-state conditions without ash depositions. Typical values and ranges of OHTC (U) in the steady-state condition without the fouling behavior based on types of hot and cold fluids are listed in Table 5.9. The typical range for the gas-to-gas HEX case is 5 to 50 W/m^2·K and for the gas-to-liquid HEX case is 10 to 100 W/m^2·K. With the growth of ash

depositions, thermal resistance which relies on the ash composition and particle size increases, and the OHTC causes the exit temperature of the cold fluid in the HEX to decrease. Equation (5.15) does not account for any "*in situ*" heat generation due to the oxidation of combustibles in ash deposited over the HEX.

Table 5.9. Typical values of OHTC (*U)* for HEXs [124].

Configuration	Typical Value of U [W/(m^2·K)]	Typical Range of U [W/(m^2·K)]
Gas-to-gas HEX at normal pressure	20	5 – 50
Gas-to-gas HEX at high pressure	200	50 – 500
Liquid-to-gas or gas-to-liquid HEX	50	10 – 100
Liquid-to-liquid tubular HEX	1000	200 – 2000
Liquid-to-liquid plate HEX	2500	500 – 5000
Condenser, to a gas	50	10 – 100
Condenser, to a liquid	3000	500 – 6000
Vaporiser, to a gas	50	10 – 100
Vaporiser, to a liquid	5000	500 – 10000
Vaporiser, to a condensing gas	3000	600 – 6000

Heat transfer from a hot fluid flow to a cold water/steam circulated through HEXs is performed by conduction through the wall of HEXs. Wall thickness and its thermal conductivity are very important to evaluate the efficiency of HEXs. Hence, the growth of ash fouling affects the heat transfer. The layer of ash is treated as another conduction resistance material in series with the wall as shown in figure 5.11.

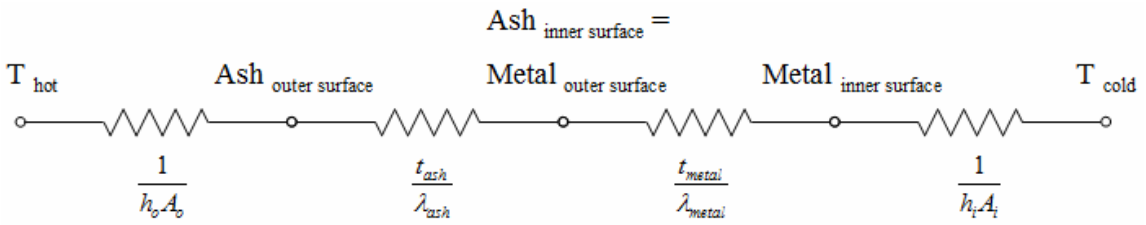

Figure 5.11. An equivalent thermal circuit for the HEX analysis.

$$R_{total} = \frac{1}{h_i A_i} + \frac{t_{metal}}{\lambda_{metal} A_{metal}} + \frac{t_{ash}}{\lambda_{ash} A_{ash}} + \frac{1}{h_o A_o} \tag{5.16}$$

$$\dot{Q} = \frac{\Delta T}{R_{total}} \tag{5.17}$$

$$\mathrm{U} = \frac{1}{R_{total} A} \tag{5.18}$$

where R_{total} is a total thermal resistance, h is a convective heat transfer coefficient, A is a surface area, t is a thickness, and λ is a thermal conductivity. As t_{ash} increases, R_{total} increases, and hence U decreases. As cold fluid is changed (e.g., air to water), h_i will change affecting U if $1/h_iA_i$ is a dominant term in R_{total}.

Ash deposition causes heat transfer rate to decrease with time and are more severe for the combustion with high ash fuels. Radiation also takes place in pulverized coal-fired boilers, and measurements of the emission properties of ash and deposits have been performed using bench-, pilot- and full-scale combustion systems [125, 126]. Ash deposits from western U.S. coals reflected up to 70% of incident radiation, and most eastern U.S. coals showed emissivity of 0.7 to 0.9 [125]. Emissivity and reflectivity of ash was primarily functions of particle size and composition of ash [126]. Equation (5.12) indirectly accounts for radiation since $T_{hot,exit}$ will be lower when there is more radiations loss.

The current bench-scale facility was operated under the transient condition and short-time operation with the ash deposition. The transient condition is defined as the condition in which all temperatures of the cold fluid and the hot flue gas stream increase as a function of time. Thus, T_{exit}, T_{in} and ΔT_{LM} are functions of time. In order to obtain the OHTC, temperatures of the cold fluid and the hot flue gas stream are monitored as a function of time, and the LMTD method is employed. Thus during the growth of the ash deposition on HEX surfaces, OHTCs and LMTDs of HEXs are determined as a function of time. The thickness of the ash deposition increases with time, so that the decrease of OHTC is typically expected under the steady-state condition. However, in the transient condition such as the current testing boiler burner, similar result may not be expected. Since temperatures of the hot gas stream keep increasing during the combustion, the heat transfer rate to the HEXs may increase with time. Hence results are interpreted using the results of actual temperature distributions of solid fuel combustion (ash deposition cases) and comparing distribution with reference distribution for NG combustion (ashless cases). Thus, the results of actual temperature distributions are used as a basis for evaluating the effect of presence of ash and deposition of ash from solid reburn fuels.

5.5 Ash Analysis

Loss on ignition (LOI) is a widely used method to estimate the carbon content of ash. Organic matter is oxidized to CO_2 and ash at 500 – 550ºC, and carbon remains at 900 – 1000ºC. LOI is typically obtained by the weight loss during the process by weighing the samples before and after heating. In the current study, the combustible loss which is defined as the ratio of unburnt combustibles in the ash to initial combustibles in the fuel is estimated instead of carbon contents. In order to determine the combustible loss of the current boiler facility, ash samples were collected from four locations: from surfaces of the top, middle, and bottom HEXs and from the ash port at the bottom of the furnace. The ash port was filled with water due to the water quenching system. All ash samples were dried in the lab and sent for analysis. The contents of moisture and combustible matter in the ash samples were measured. The measurement of the moisture content was performed by overnight drying at 105ºC to constant weight. For the measurement of the combustible matter, ash samples were placed in a 950ºC oven for 15 minutes and removed (adopted from ASTM E-872 and D-3175), and then heated in an oven at 575ºC overnight to a constant weight (adopted from ASTM E-1755).

The combustible loss can be expressed as [48]

$$Combustible\ loss = 1 - BF \tag{5.19}$$

$$BF = \frac{m_{F,0} - m_F}{m_{F,0}} = 1 - \frac{(1-A)A_0}{(1-A_0)A} \tag{5.20}$$

$$A_0 = \frac{m_{A,0}}{m_{A,0} + m_{F,0}} \quad and \quad A = \frac{m_A}{m_{A,0} + m_F} \tag{5.21}$$

where BF is a burnt fraction, $m_{F,0}$ is the initial mass of combustible in the dry solid fuel, m_F is the final mass of combustilbe in the dry solid fuel, A_0 denotes the initial ash fraction on a dry basis, A represents the ash fraction in a dry sample after combustion, $m_{A,0}$ is the initial mass of ash in the dry solid fuel, m_A is the final mass of ash in the dry solid fuel. The burnt fraction (BF) which is defined as the ratio of combustibles burnt to combustibles injected in the burner.

The prediction of the ash concentration [kg/m^3] on the surface of HEXs is briefly discussed in this section. The detailed description is presented in Appendix C. The ash concentration is defined as the amount of ash in the unit volume of the gas stream. With the assumptions of 1) complete release of ash from fuel and 2) the complete combustion with CO_2, O_2, H_2O, and mainly N_2, the ash concentration, C_{ash} can be expressed as

$$C_{ash} = \frac{\dot{m}_{ash}}{\dot{V}_{gas}} = \frac{\dot{m}_{Fuel} Y_{ash,Fuel}}{\dot{V}_{gas}} \tag{5.22}$$

where $\dot{m}_{ash}$ is a mass flow rate of the ash in the total gas stream, $\dot{V}_{gas}$ is the volume flow rate of the gas in the total gas stream, $\dot{m}_{Fuel}$ is a mass flow rate of the total fuel, and $Y_{ash,Fuel}$ is an ash fraction of the total fuel. Because the density of the gas stream is in inverse proportion to the gas temperature, the ash concentration increases with a decrease in the gas temperature. Therefore more ash deposition is likely on the surface of the HEX in the lower section of the combustor than in the upper section. Further the particles are mostly ash near the bottom HEX compared to the top HEX. Since fuel mass firing rate is higher for low "BTU" fuels, Eq. (5.22) reveals the increased ash concentration for low BTU fuels even under similar fuel ash contents.

5.6 Uncertainty and Repeatability Analyses

The following conditions of uncertainty existed during the reburn experiments. First, the refractory in the boiler could have been offset from the reactor center. Second, the refractory wall could have been thicker than the original thickness because of the accumulation of the ash fouling from previous experiments. Third, thermocouple probes could have been covered by ash particles which can lead lower readings of temperatures. Fourth, thermocouple probes may not have been located at the center of the HEX due to gravitational deflection. Fifth, the reburn feeding system made an unstable feed rate though the feed rate was calibrated for each fuel before experimentation. The solid fuel was fed to the system with a volumetric feeder. The fluctuation of the feed rate is caused by the density of the reburn fuel. Sixth, some of flow meters showed fluctuations during the operation.

Table 5.10. Uncertainty for reburn experiments.

Uncertainty Factor	Uncertainty of Each Factor (%)
Primary Air Flow Meter	± 0.31
Ammonia Flow Meter	± 0.50
NG Digital Flow Meter	± 0.66
RB Motive Air Flow Meter	± 0.83
RB Aspirated Air Flow Meter	± 0.71
Cold Fluid Flow Meter for HEX	± 0.91
Data Measurement	± 5.00

For the determination of the overall system uncertainty, possible error ranges of instruments and measurements were considered. During the tests, the error ranges of flow meters were observed and calculated for the primary air, reburn motive air, reburn aspirated air, NH_3, NG,

HEX air, and HEX water. As listed in Table 5.10, the uncertainty range of each flow meter was determined less than ± 1.0%. The unstable feed rates of the solid fuels were observed because of the errors of aspirated and motive air flow meters. The dominant parameter for the overall system uncertainty was the unstable reading of gas concentrations caused by the unstable feed rate. The fluctuation of data measurements was between ± 2.5 and ± 5%. Therefore, the final overall system uncertainty was determined in the range of ± 3.0 to ± 5.3% [127]. The repeatability was also estimated by two experimenters using the same reburn fuels in two different times. For the LAPCFB cases presented in figure 5.12, the mean repeatability was found to be about 96%.

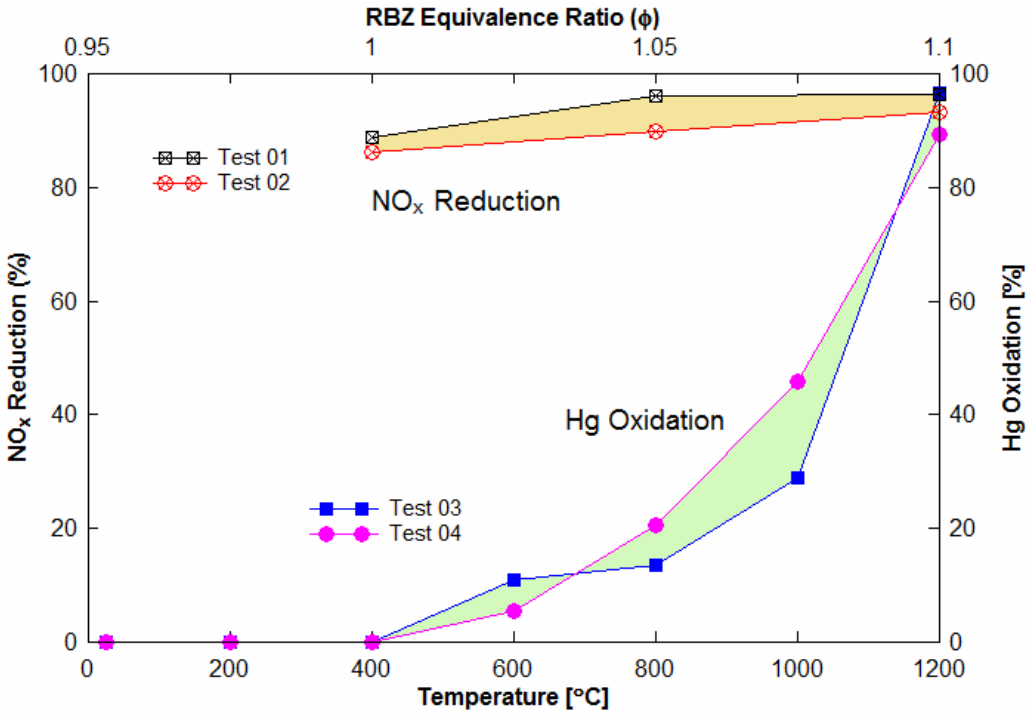

Figure 5.12. Repeatability analysis for reburn and Hg oxidation experiments.

In the Hg oxidation experiments using the flow reactor, the mercury vapor monitor measured less than 1.0 μg/m^3 in the background laboratory air. About 10 – 25 μg/m^3 Hg^0 was measured in the system without flowing Hg^0 because some Hg^0 were deposited in tubes (Tygon tubes were used between the systems) and metal connecters due to the tests previously performed. Experiments with HCl were carefully managed, monitored, and repeated to get proper measurements due to large fluctuations when using HCl. The temperature of the Hg^0 carrier gas in the Hg generator varied ± 0.3ºC from the set temperature, and this variation had a minor effect on the initial Hg^0 concentration. The measured gas temperature was close to the reactor set temperature. Almost all measurements were conducted for the steady-state condition which was defined that the measurement fluctuated ± 5 μg/m^3 over 5 minutes. For a few cases, the Hg^0 measurement was taken before it reached the steady-state condition. This was because of slow reactions, so that much more time was needed to be stabilized. In some cases, Hg oxidation did not appear immediately due to the time delay of the heating.

For the determination of the overall system uncertainty for the flow reactor experiments, possible error ranges of instruments and measurements were considered. Table 5.11 shows the uncertainty range of Case *VII* (HCl + NO + O_2). The uncertainty range of each mass flow controller (MFC) depended on gas concentrations, however, usually ± 0.5% or less. The measurements were taken in the range of ± 1 to ± 5 μg/m^3. The temperature fluctuation of the Hg generator was about ± 0.3ºC. The Hg permeation tube was certified ± 2% uncertainty. The final overall system uncertainty was in the range of ± 2.3 to ± 5.7% [127]. The repeatability was also estimated using the same simulated flue gas in two different times, and it is graphically presented in figure 5.12. The results of Case *VII* (HCl + NO + O_2) was compared, and the average error of the repeatability was found to be about 5.3% offset.

Table 5.11. Uncertainty for Case *VII* ($HCl + NO + O_2$) of the flow reactor experiments.

Uncertainty Factor	Uncertainty of Each Factor (%)
Hg^0 Permeation Tube	± 2.00
Hg^0 Generator Temperature	± 0.32
Balance N_2 MFC	± 0.15
Hg^0 Carrier N_2 MFC	± 0.11
HCl MFC	± 0.18
O_2 MFC	± 0.32
NO MFC	± 0.63
Data Measurement	± 5.26

6. RESULTS OF BIOMASS REBURNING ON NO_x CONTROL

The main focus of the current study is a reburning on NO_x reduction using a bench-scale boiler with coal and cattle biomass (CB). The CB includes feedlot biomass (FB) and dairy biomass (DB). Pure CB, pure coals and blends of coal:CB are used as reburn fuels. The results of NO_x reduction in the biomass reburning are presented and discussed based on a number of variables: reburn fuels, reburn equivalence ratios (ER_{RBZ}), reburn heat inputs, non-vitiated/vitiated reburn gases, heat exchangers (HEXs), reburn injection configurations, and baseline NO_x concentrations. The results of other gas emissions (CO, CO_2, SO_2, C_xH_y) are discussed as well.

6.1 Temperature Distribution

The flue gas temperatures of the vertically down-fired combustor were measured during the experiments. Since the temperature plays a very significant role on the NO_x formation and reduction, the temperature in the reburn zone (RBZ) was monitored and kept below 1600 K to prevent the high production of thermal NO_x. In figure 6.1 (a), the gas temperatures were measured at spaced intervals of 6 in (15.24 cm) below the reburn zone. The axial temperature linearly decreased along the reactor. After the reactor is fired, the temperatures in downstream gradually increased with time at any given axial distance while the temperature of the reburn zone remained relatively steady. The sampling probe was located at the center of the reactor and at the location of 1.37 m below the reburn zone, and the radial temperature of the sampling area is presented in figure 6.1 (b). The radial gas temperatures between the layers of the insulation and refractory were relatively steady and also almost flat across the reactor indicating a thin boundary layer.

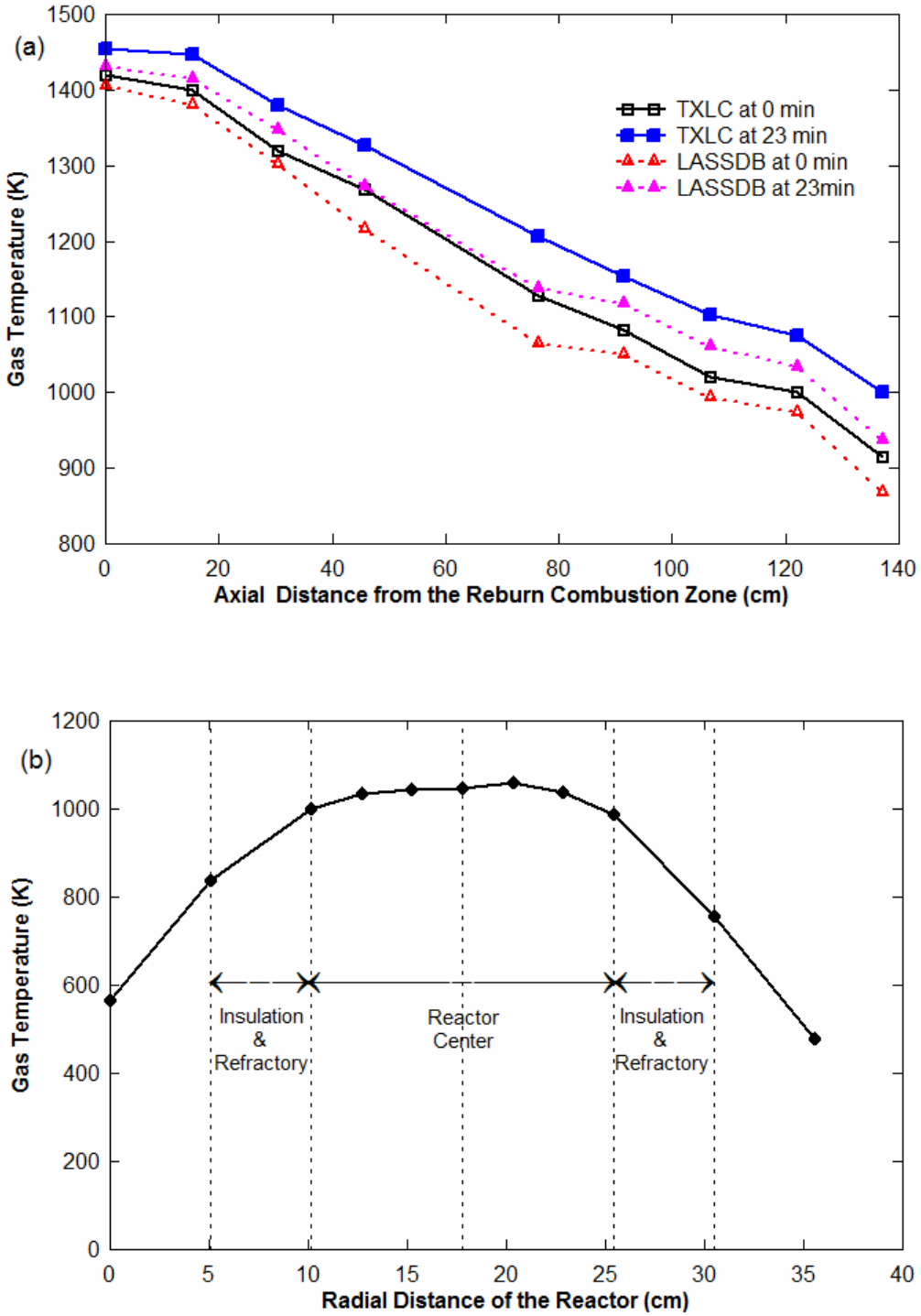

Figure 6.1. (a) Temperature distribution of the flue gas over the axial distance below the reburn nozzles and (b) Temperature distribution of the flue gas over the radial distance at the sampling port (at 137cm below the reburn nozzles).

6.2 NH_3 Slip and Dilution of Reburn Gases

Recall that NO_x was simulated by firing the NG and air with a trace amount of NH_3 in the primary burner. To ensure that all of injected NH_3 was converted to NO_x, the levels of NO_x were measured before and after the NH_3 injection during the NG combustion. The production of thermal NO_x without the NH_3 injection was measured between 50 and 70 ppm. After NH_3 was injected, the level of NO_x was measured between 420 and 440 ppm. This suggested that NH_3 was responsible for generating about 350 ppm of NO_x. The average amount of NH_3 injected into the system was 1.44 cm^3/s (0.18 SCFH) while the theoretical amount of NH_3 required to generate 350 ppm of NO_x is 1.82 cm^3/s (0.23 SCFH). It suggests that all NH_3 injected in the primary zone was converted into NO_x. The difference in the theoretical amount required and the amount injected may be attributed to measurement error or other errors inherent in the system.

The dilution effect of the reburn air is significant on the measurement of NO_x emission in [ppm], thus it should be accounted in further discussion. The initial gas emissions by NG combustion before the injection of the reburn air were 405 ppm of NO_x, 1.1% of O_2 and 12.06% of CO_2. The gas emissions measured after the reburn air injection were 252 to 262 ppm of NO_x, 7.9 to 9.2% of O_2 and 7.06 to 7.95% of CO_2 for $0.95 < ER_{RBZ} < 1.1$. Assuming that reburn fuel did not produce any NO_x, the addition of reburn gases with the primary gases will reduce the NO_x by one third; however, the dilution effect in NO_x emission is eliminated once the NO_x emission was measured on a heat basis [g/GJ]. The NO_x emission was 169 g/GJ (or 405 ppm) due to NG combustion, and if reburn air was added without reburn fuels, then the emission was measured in the range of 166 and 180 g/GJ (or 252 to 262 ppm) after the dilution. Therefore, the heat basis conversion eliminates the dilution effect and hence the results on a heat basis are used for the further discussion. The 3% O_2 correction by EPA also neutralized the dilution effect but it is more appropriate to fuel-lean condition.

6.3 Effects of Reburn Equivalence Ratio (ER_{RBZ} or ϕ_{RBZ})

The equivalence ratio (ER or ϕ) is typically defined as the ratio of the fuel-to-air ratio to the stoichiometric fuel-to-air ratio which is an inverse value of the stoichiometric ratio (SR). For the emission control of NO_x, several reburn fuels were tested at various ERs in the reburn zone under the operating conditions of the base case (see Tables 4.1 and 4.2). Figure 6.2 presents the NO_x emissions [g/GJ and lb/mmBTU] as a function of the ER_{RBZ}, and the error bars of each measurement are also shown. The error ranges were determined to be about ± 5 to ± 10 g/GJ for NO_x emissions, about ± 0.015 to ± 0.02 for the ER_{RBZ}, and about ± 3 to ± 5% for NO_x reductions, depending on the conditions. The baseline NO_x concentration varied from 175 to 186 g/GJ (or 420 to 440 ppm), depending on reburn fuels. The NO_x emission decreases with an increase of the ER_{RBZ}. The results showed decreases in NO_x emission such as about 143 to 92 g/GJ for TXLC, 139 to 66 g/GJ for 90:10 TXLC:LASSDB, 91 to 37 g/GJ for 80:20 TXLC:LASSDB, 17 to 8 g/GJ for LASSDB, and 43 to 13 g/GJ for LAPCFB. There were two observations: (1) Higher the percentage of LASSDB in the reburn fuel, lower the NO_x emission and (2) With increased ER_{RBZ}, the NO_x emission decreased due to the depletion of the oxygen in the reburn zone, and then the low O_2 concentration slows down the NO_x formation and allows the NO_x reduction to be dominant. The extent of NO_x reduction was found to be strongly dependent to the ER_{RBZ}, with greater reduction in fuel-rich combustion.

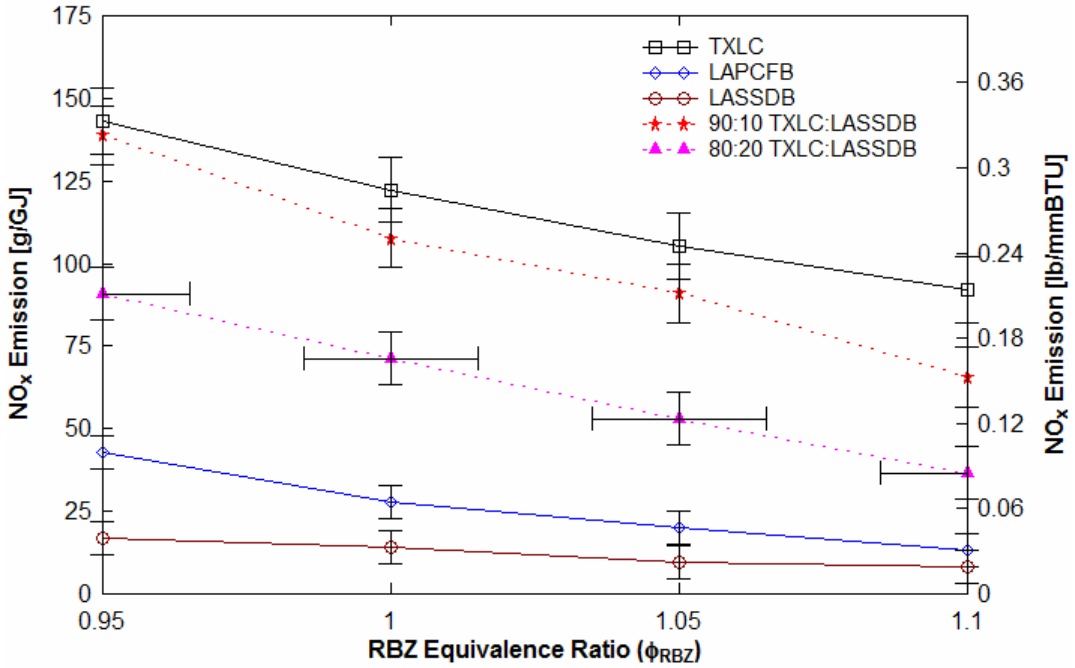

Figure 6.2. NO_x emission for several reburn fuels in the conditions of non-vitiation, 30% reburn heat input and 0° reburn injection with baseline NO_x between 179 and 186 g/GJ.

The verification of ER_{RBZ} in the fuel-lean combustion ($\phi < 1.0$) was performed by Eq. (6.1) based on the assumption of complete combustion [48].

$$\phi \approx 1 - 4.76 X_{O_2} \tag{6.1}$$

where X_{O2} is the mole fraction of O_2 in the flue gas. The ER_{RBZ} used in experiments was calculated by the flow rate of O_2 injected in to the primary and reburn zone. The ER_{RBZ} was predicted by Eq. (6.1) using the mole fraction of O_2 measured by the gas analyzer. The ER_{RBZ} predicted by Eq. (6.1) was close to or slightly higher than the ER_{RBZ} calculated by the O_2 flow rate, indicating more fuels were burnt than what it was expected. It may cause incomplete combustion and high CO emissions.

6.4 Effects of Biomass Blended with Coal

Figure 6.3 shows the NO_x reduction on a heat basis. Most interesting observation is that NO_x reductions were found to be about 91 to 96% for LASSDB as the highest, 77 to 93% for LAPCFB as the second highest and 19 to 48% for TXLC as the lowest depending on the ER_{RBZ}. It is because TXLC contains small amounts of VM while LASSDB and LAPCFB contain large amount of VM. Results of fuel blends are about 49 to 80% for 80:20 TXLC:LASSDB and 24 to 64% for 90:10 TXLC:LASSDB depending on the ER_{RBZ}. The results show that both LASSDB and LAPCFB are very effective in NO_x reduction. Blending of 10% DB with coal increased the NO_x reduction up to 16% more, and even up to 32% more for 80:20 TXLC:LASSDB. Results indicated NO_x reduction increased with an increase of the LASSDB proportion in reburn fuels. Consistent findings are reported in the results of feedlot biomass (FB) reburning discussed later. Therefore, the CB (LASSDB and LAPCFB) can be used a very effective reburn fuel for the NO_x emission control in coal-fired power plants. Theoretically finer particles heat faster and release volatiles faster, thus the emission control can be better.

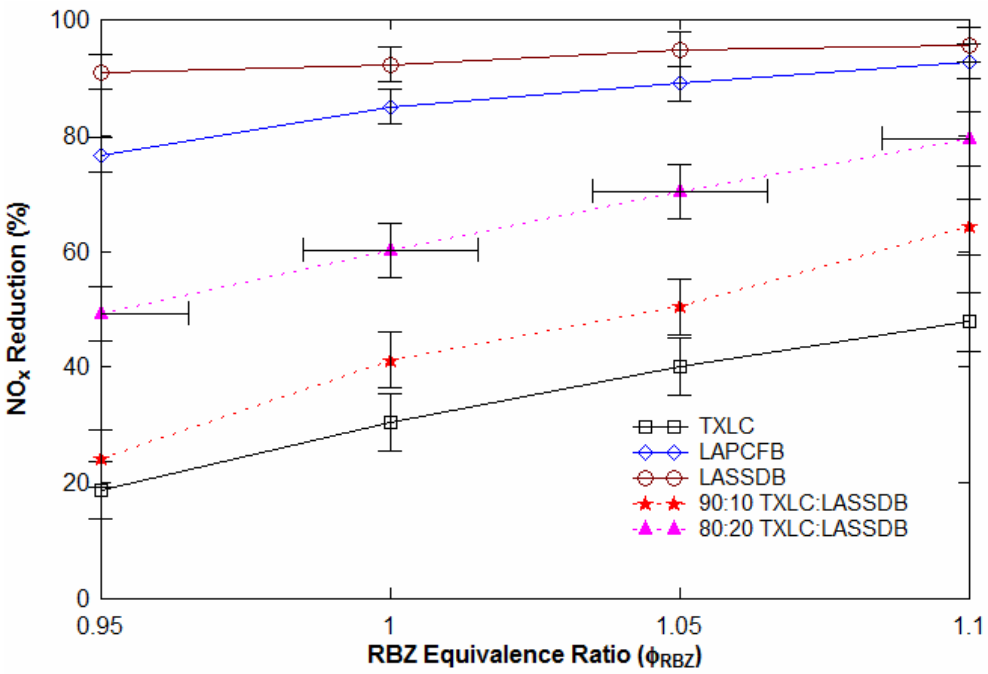

Figure 6.3. NO_x reduction on a heat basis for several reburn fuels in the conditions of non-vitiation, 30% reburn heat input and 0° reburn injection.

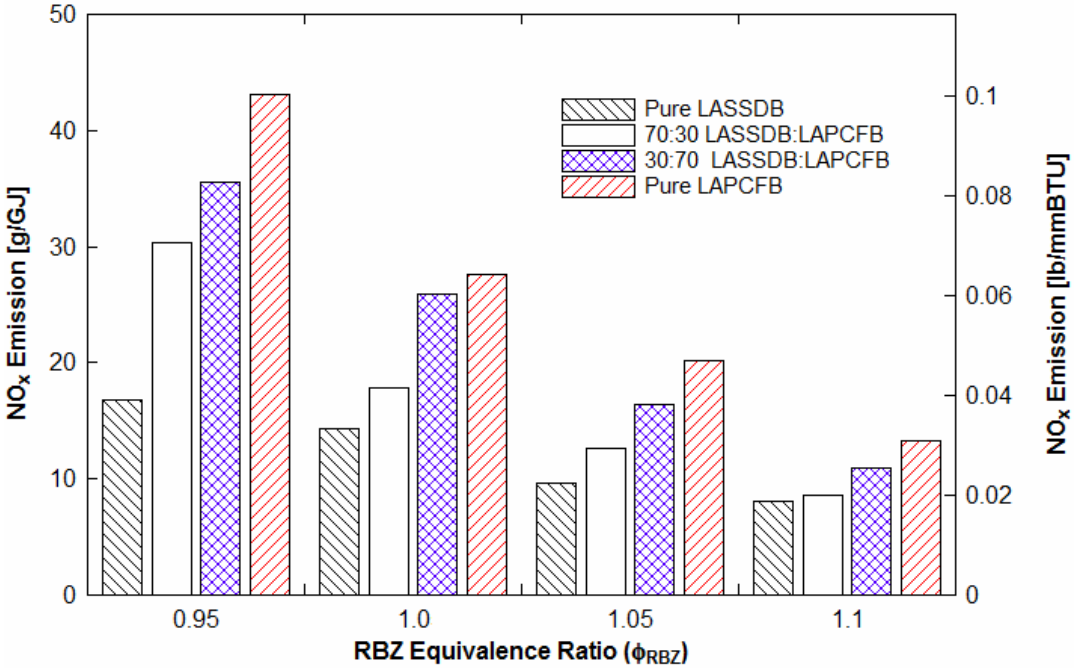

Figure 6.4. NO_x emission in [g/GJ] and [lb/mmBTU] with blends of DB and FB (non-vitiation, 30% heat input and 0° injection) with baseline NO_x between 177 and 186 g/GJ.

In the current study, the composition of the reburn fuel seems to play an important role in NO_x reduction. LASSDB contained more fuel-N and less fuel-oxygen which are responsible for NO_x reduction. NH_3 is one of the N containing compounds from fuel-N and reacts with NO_x to reduce the NO_x level, and lower O_2 increases NO_x reduction. With the 30% reburn heat input the injected amount of fuel-N was about the same in both LASSDB and LAPCFB (0.79 g/min in LASSDB and 0.78 g/min in LAPCFB) on a dry ash free (DAF) basis; however, lesser amounts of the fuel based oxygen were injected by LASSDB (7.86 g/min) than LAPCFB (9.52 g/min) on a DAF basis. Typically more CO will be produced by LAPCFB than LASSDB, thus stoichiometric O_2 required by the VM of LASSDB will be higher compared to the VM of LAPCFB. As such local O_2 will decrease faster for LASSDB. Therefore, LASSDB resulted in higher NO_x reduction than LAPCFB due to the higher fuel-N and lower fuel-oxygen. Figure 6.4 supports these results by showing the NO_x emission with blends of LASSDB and LAPCFB. The NO_x emissions increase with a decrease in LASSDB. For the TXLC case, the small amount of VM and low fuel-N (0.25 g/min) were the dominant factors for low NO_x reductions even though it contains low fuel-oxygen (3.55 g/min) on a DAF basis.

6.5 Effects of O_2 Concentration in Reburn Gas

The use of the flue gas recirculation (FGR) produces lesser NO_x emission than using air alone since the low O_2 concentration causes the NO_x formation rate to be slower. Though the vitiated reburn gas causes higher gas velocity and shorter residence time than the non-vitiated reburn gas, it allows the nitrogen species to be released in an oxygen deprived region, thus allowing more HCN and NH_3 to be available for NO_x reduction rather than NO_x generation. To simulate the reduced O_2 concentration through FGR, the N_2 gas was mixed with the reburn air. This vitiated reburn gas caused the O_2 concentration in the reburn zone to drop from 20.9 to 12.5%. The effect of the vitiation gas on NO_x reduction was investigated at 30% reburn heat input and 0° reburn injection. The results shown in figure 6.5 (a) indicated the vitiation decreased NO_x emissions, and the larger decrease in the NO_x emission occurred under fuel-rich combustions. In figure 6.5 (b) the vitiated reburn gas resulted in up to 6% more NO_x reduction at $\phi_{RBZ} = 1.0$, and resulted in up to 15% more NO_x reduction at $\phi_{RBZ} = 1.1$. The vitiation effect was stronger in fuel-rich conditions. It was found that the vitiated reburn gas played a significant role on the control of NO_x emission; however, it seems that vitiated reburn gas does not improve the NO_x reduction significantly when LASSDB was used. Note that the use of the real FGR gas can increase the levels of CO_2, H_2O and NO_x in the combustion zone. The CO_2 and H_2O can also react with hydrocarbon (HC) and $C_{(s)}$.

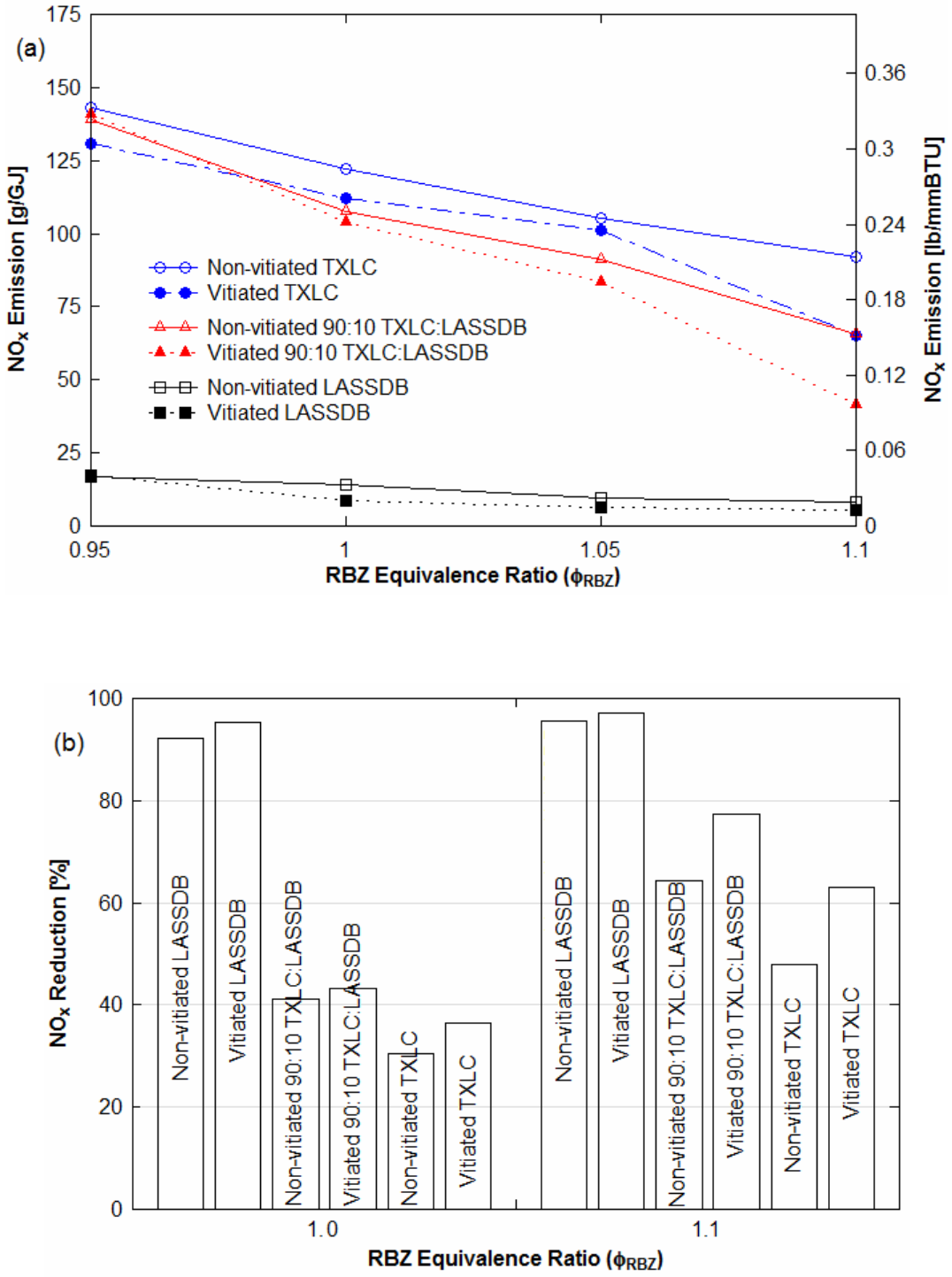

Figure 6.5. Effect of the vitiated reburn air (30% reburn heat input and 0° reburn injection): (a) NO_x emission and (b) NO_x reduction on a heat basis.

6.6 Effects of Reburn Injection

Several configurations of the reburn injection shown in figure 4.2 were tested using 80:20 and 90:10 TXLC:LASSDB fuels in the conditions of the non-vitiation and 30% reburn heat input. The tested cases were 1) 0° circular, 2) 45° circular and 3) 45° oval injections in the symmetric configuration and 4) 45° circular injection in the asymmetric configuration. Various reburn injection configurations provided different mixing conditions within the reburn zone. The 45° upward injection of the down-fired boiler provided more mixing time, residence time and reaction time within the reburn zone than the lateral (0°) injection. Better mixing with the primary gases promotes rapid heat up of fuel particles, faster release of volatiles along with rapid reduction in the local O_2 concentration because of the oxidation and increased residence time, and enhances the reaction selectivity. The reduced concentration of oxygen inhibits the NO_x formation. The mixing time of the hot flue gas in the reactor was estimated using CO_2 from the reburn port and air from the primary port. The detailed procedures and conditions are presented in Appendix D. The mixing time was found to be less than 350 ms for the 0° injection, which is very similar to the previous result reported in [128]. The previous result was 320 ms using N_2, and the residence time was estimated between 550 to 750 ms depending on the reburn fuel and temperature [128]. The optimum residence time is typically coupled to the mixing time.

The gas temperatures of 0° circular, 45° circular and 45° oval injections in the symmetric configuration are presented in figure 6.6. For the oval injection, the longer diameter of the nozzles is normal to the furnace axis. The temperatures of the 0° circular and 45° circular injections were relatively close to each other and higher than the temperatures of the 45° oval injection. It suggested the circular injection produced better mixing condition than the oval injection in these cases because better mixing with the primary gases promotes rapid heat up of fuel particles.

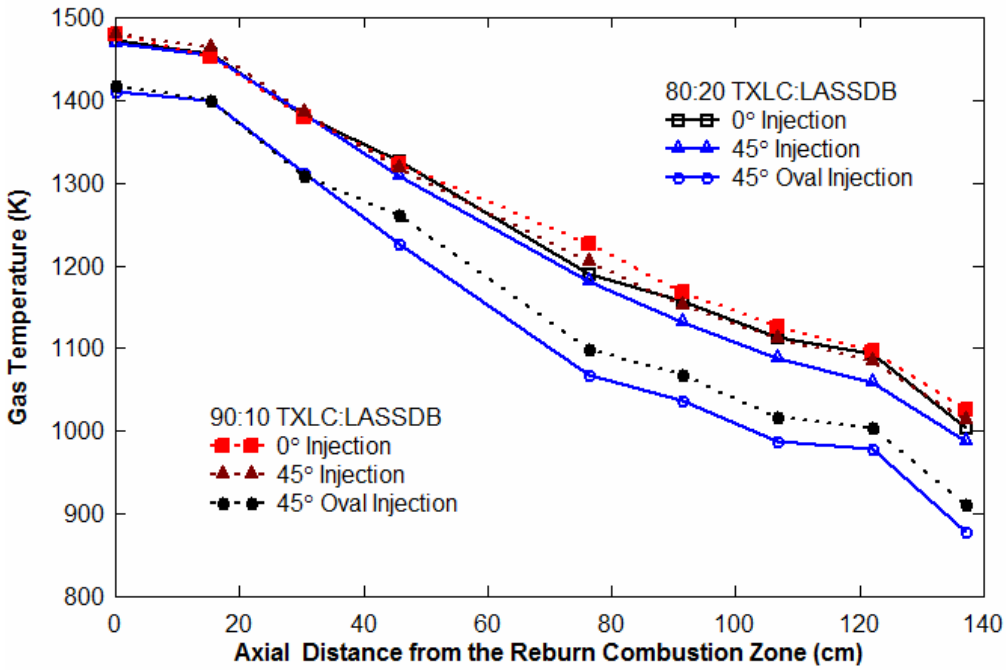

Figure 6.6. Gas temperature distribution for the effect of the reburn injection in the conditions of the non-vitiation and 30% reburn heat input.

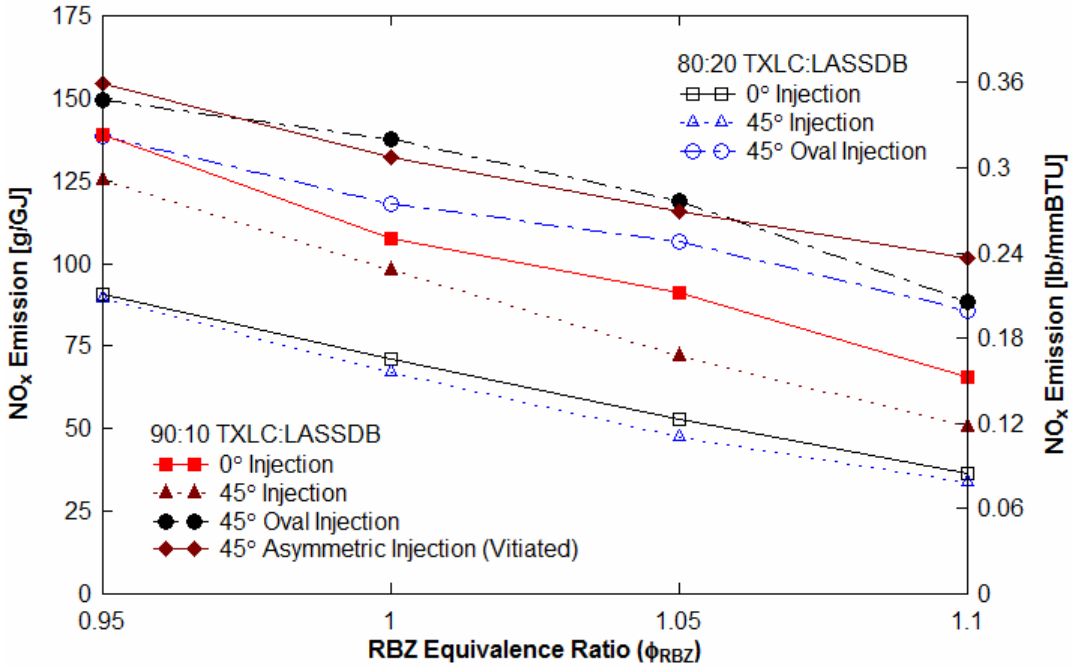

Figure 6.7. Effect of the reburn injection (0° circular, 45° circular and 45° oval injections in the symmetric configuration and 45° circular injection in the asymmetric configuration) in the conditions of the non-vitiation and 30% reburn heat input.

The results of NO_x emission are presented in figure 6.7. The 45° upward injection provided longer residence time than the lateral (0°) injection, and thus the 45° injection resulted in less NO_x emissions. The 45° circular injection with better mixing also resulted in less NO_x emissions than the 45° oval injection for both fuel blends. The previous experimental results showed a 0° flat spray (or oval) injector produced high NO_x reduction with higher gas temperatures than a 0° circular jet injector [27]. The current and previous results are inconsistent; however, the differences of the gas temperature can explain the inconsistent results. In the pervious results, the 0° flat spray injector caused a stagnation type flow of the reburn fuel and air for the opposite reburn fuel injectors, and thus probably the fuel particles were scattered very well burning rapidly. It resulted in higher gas temperatures than the 0° circular jet injector. However, in the current study, the 45° oval injector produced lower gas temperatures than the 45° circular injector. And thus, the 45° circular injector created better performance than the 45° oval injector.

The NO emissions in the asymmetric configuration are presented in figure 6.7. The 45° upward injection with circular nozzles in the vitiation case (12.5% O_2) was examined using 90:10 TXLC:LASSDB. As shown in figure 4.2 (c), reburn fuel and air (20.9% O_2) were injected from one nozzle, and N_2 was injected from the other nozzle. The asymmetric reburn injection resulted in very poor NO_x reduction compared to the vitiation case of the symmetric configuration. The 45° injection in the asymmetric case resulted in 16 to 45% NO_x reduction while the 0° injection in the symmetric case achieved 23 to 77%, depending on the ER_{RBZ}. It is because enough oxygen was available at the reburn fuel side to produce fuel NO_x instead of reducing NO_x emissions, and a good-mixing did not take place in the reburn zone. Therefore, the symmetric configuration of the reburn injection showed better NO_x reduction than the asymmetric configuration. This result for the asymmetric case is consistent with the result of pilot-scale tests performed in Southern Research Institute in Alabama [129].

6.7 Effects of Reburn Heat Input

Typical heat generated by combustion of reburn fuels in pulverized coal-fired boilers ranges from 10 to 30% of the total heat as listed in Table 2.1, but achieving high NO_x reductions with less reburn heat input is essential but challenged when the reburn fuel supply is limited. Further, the small heat fraction by reburning can reduce the problems of the high ash production, fouling, slagging, and the resource limitation of biomass, especially using CB for the long-time operation. Figure 6.8 presents the effect of the reburn heat input on NO_x emission using LASSDB in the conditions of the non-vitiation and lateral (0°) reburn injection in the symmetric configuration. The reburn heat input varied from 20 to 30% with the similar amount of the baseline NO_x concentration produced by the primary fuel combustion. Once the reburn heat input decreased from 30 to 20%, NO_x emissions increased about 2.5 to 4 times depending on the ER_{RBZ}. In fuel-lean combustion (ϕ_{RBZ} = 0.95), the increment of the NO_x emission was large (17 to 65 g/GJ) while it became smaller (8 to 19 g/GJ) in fuel-rich combustion (ϕ_{RBZ} = 1.1). Though it was found the high NO_x emissions in the 20% heat input compared to the 30% heat input, the high NO_x reductions were still achieved between 64 and 89% for the 20% heat input. Considering the results with problems caused by CB, the 20% reburn heat input can be the better operating condition than the 30% reburn heat input for the long-time operation. High NO_x reduction efficiency with low amounts of the CB injection per a boiler unit makes more boiler units use CB.

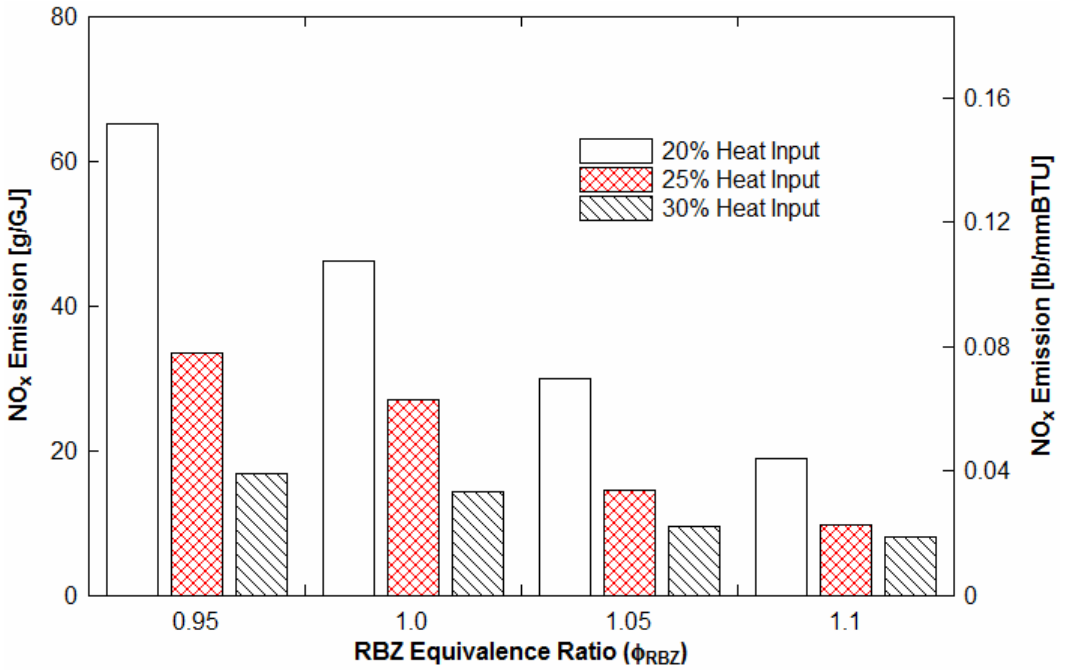

Figure 6.8. Effect of the reburn heat input using LASSDB (non-vitiation and lateral (0°) reburn injection) with baseline NO_x between 175 and 186 g/GJ.

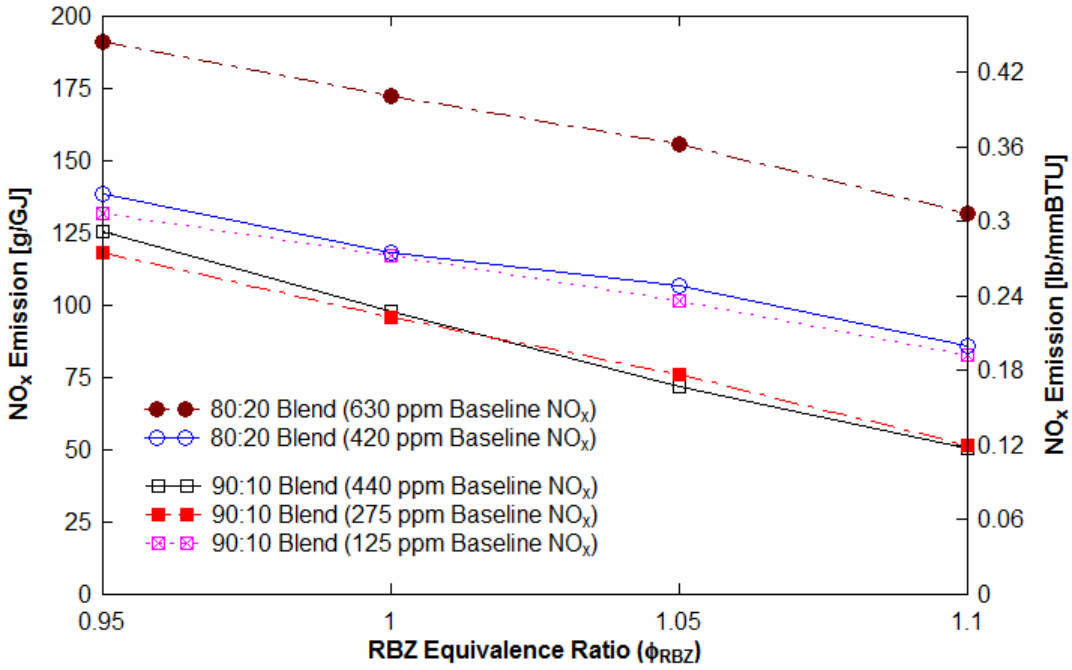

Figure 6.9. Effect of the initial or baseline NO_x (non-vitiation, 30% heat input and 45° injection): 90:10 blends for the circular injection & 80:20 blends for the oval injection.

6.8 Effects of Baseline NO_x Concentration

The effect of the initial or baseline NO_x concentration produced by primary fuel combustion was investigated in the conditions of the non-vitiation, 30% reburn heat input and 45° reburn injection. The results are presented in figure 6.9. For 90:10 TXLC:LASSDB, the 45° circular reburn nozzles were used, and three baseline NO_x concentrations (125, 275 and 440 ppm) were tested. For 80:20 TXLC:LASSDB, the 45° oval nozzles were used, and two baseline NO_x concentrations (420 and 630 ppm) were tested. The results of 440 ppm baseline NO_x (90:10 blend) and 420 ppm baseline NO_x (80:20 blend) were already presented in Effect of Reburn Injection. The NO_x emissions decreased from 191 to 132 g/GJ and 139 to 86 g/GJ for the 80:20 blends with the baseline NO_x of 630 and 420 ppm, respectively. For the 90:10 blends with the baseline NO_x of 440 and 275 ppm, NO_x emissions were very similar and decreased from 125 to 51 g/GJ and 118 to 51 g/GJ, respectively. The NO_x emissions for the 125 ppm baseline NO_x decreased from 132 to 83 g/GJ.

The results of NO_x reductions are presented in figure 6.10. For the baseline NO_x of 440 and 275 ppm, the NO_x reductions increased from 33 to 73% and 1 to 57 %, respectively, with an increase of the ER_{RBZ} in figure 6.10 (a). About 16 to 32% offset in NO_x reduction was found between the cases, and lower NO_x reductions were found with the lower baseline NO_x case. Though the case using the 125 ppm baseline NO_x showed the decrease in the NO_x emission, negative NO_x reductions (or NO_x formations) were measured as 150% at ER_{RBZ} = 0.95 and 57% at ER_{RBZ} = 1.1 shown in figure 6.10 (a). It indicated NO_x was formed instead of reduced during reburning.

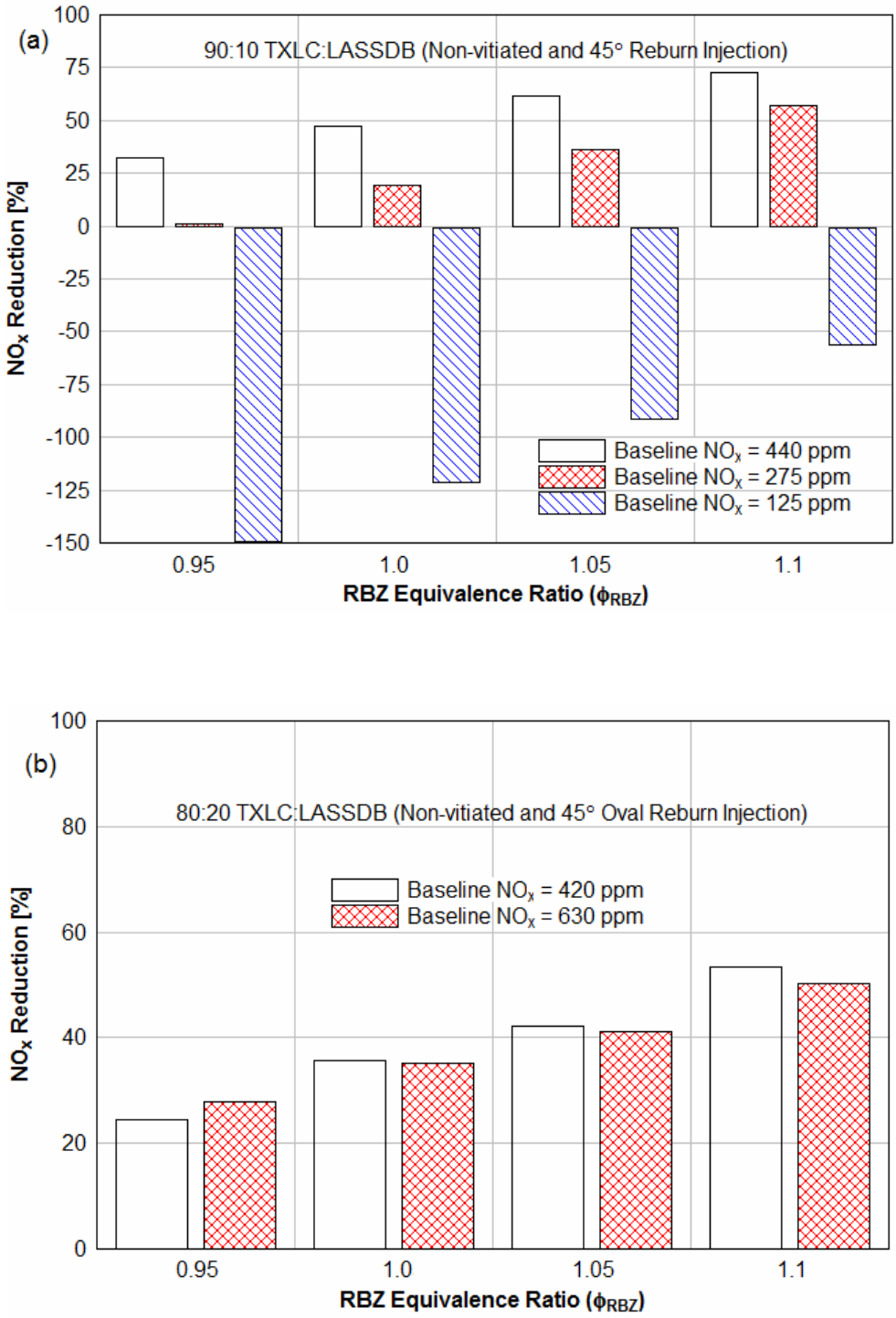

Figure 6.10. Effect of the initial or baseline NO_x produced by primary fuel combustion (non-vitiation, 30% heat input and 45° injection): (a) NO_x reduction [%] for 90:10 blends with the circular nozzles and (b) NO_x reduction [%] for 80:20 blends with the oval nozzles.

In figure 6.10 (b), no significant difference was found between the cases of 630 and 420 ppm baseline NO_x for 80:20 TXLC:LASSDB. Though the 630 ppm case showed higher NO_x emissions than the 420 ppm case, their offset in NO_x reduction was found to be about 3% for all ER_{RBZ}. These results indicated NO_x reductions took place with high baseline NO_x concentrations (i.e. 275, 420, 440, and 630 ppm) while NO_x formations took place with the low baseline NO_x concentration (i.e. 125 ppm). NO_x reduction with NH_3 slowed down compared to NO_x formation because of the low ambient NO_x levels. The change of NO_x reduction was not significant with baseline NO_x of about 400 ppm or higher, but it was significant with baseline NO_x less than 400 ppm. The result of the 125 ppm case showed even negative NO_x reductions. The results of 90:10 and 80:20 TXLC:LASSDB cases show a good agreement with previous findings in [32]. NO_x reduction typically takes place when NO_x molecules collide and react with NH_3 derived from fuel-N during fuel combustion. The small amount of NO_x has less probability of collisions and reactions with NH_3. Unlike the NO_x species, more O_2 is available in the reburn zone to react with NH_3 to form NO_x. Therefore, NO_x formations (or negative NO_x reductions) took place in the case of the baseline NO_x of 125 ppm.

It was also possible that CO had an effect on the NO_x formation. NO_x formations during HCN and NH_3 oxidation with high oxygen concentrations were studied at temperatures between 870 and 1270 K in fuel combustion [120]. It was found that approximately 22% HCN and 40% NH_3 were converted to NO_x by the addition of 1250 ppm CO at 1270 K. In the 125 ppm (90:10 TXLC:LASSDB) case of the current study, concentrations of O_2 [%], NO_x [ppm] and CO_2 [%] were higher than those in the 440 ppm case of 90:10 TXLC:LASSDB, but concentrations of CO [%] were lower. The CO concentrations in the 440 ppm case were found to be about 3700 to 8500 ppm more than those in the 125 ppm case, depending on the ER_{RBZ}. Based on the results reported by Wargadalam et al. [120], it can be deduced that approximately 3700 to 8500 ppm of

CO was used for the NO_x formation during HCN and NH_3 oxidation in the 125 ppm case, and it resulted in 57% to 150% more NO_x emission compared to its baseline NO_x concentration. Between 440 and 275 ppm cases, approximately 1800 to 5000 ppm more CO was found in the 440 ppm baseline NO_x case, and these CO concentrations reduced the extent of NO_x reduction much in the 275 ppm case.

In summary, these results reveal that baseline NO_x emissions higher than 275 ppm (or 119 g/GJ and 0.28 lb/mmBTU) are very effective on the NO_x emission control during reburning coal and DB. However, the DB reburning may not as powerful as other techniques to control NO_x emission for the boiler systems in which the baseline NO_x emission is lower than 275 ppm. Approximately 75% of all power plants in US have been already equipped low-NO_x burners (LNBs) which are able to achieve 70% NO_x reduction. Therefore, it should be carefully considered for designing new boiler systems with both LNBs and reburn systems or retrofitting old LNB systems by combining reburn systems because the low NO_x reduction efficiency can be obtained, even NO_x formation can be observed.

6.9 Effects of Heat Exchanger (HEX)

To investigate the fouling potential, either air cooled or water cooled HEXs were installed. The results on the fouling reported in Section 7. However, the presence of HEXs alters temperature distribution in the furnace and hence may affect NO_x emissions. The effects of HEXs on NO_x emission and reduction are reported here. The effect of HEX on NO_x emission was examined in the presence and absence of three single-passed air cooled HEXs in the coal-fired boiler. The operating conditions between these cases are almost identical in the conditions of the non-vitiation and lateral (0°) reburn injection. The distributions of the gas temperature for the cases in the presence and absence of HEXs are shown in figure 6.11. The local gas temperatures near the HEXs dropped faster in the presence of HEXs than the others because of the heat transfer to HEXs. The temperature drop was between 30 to 55 K for the cases without HEXs while it was between 70 to 110 K for the cases with HEXs.

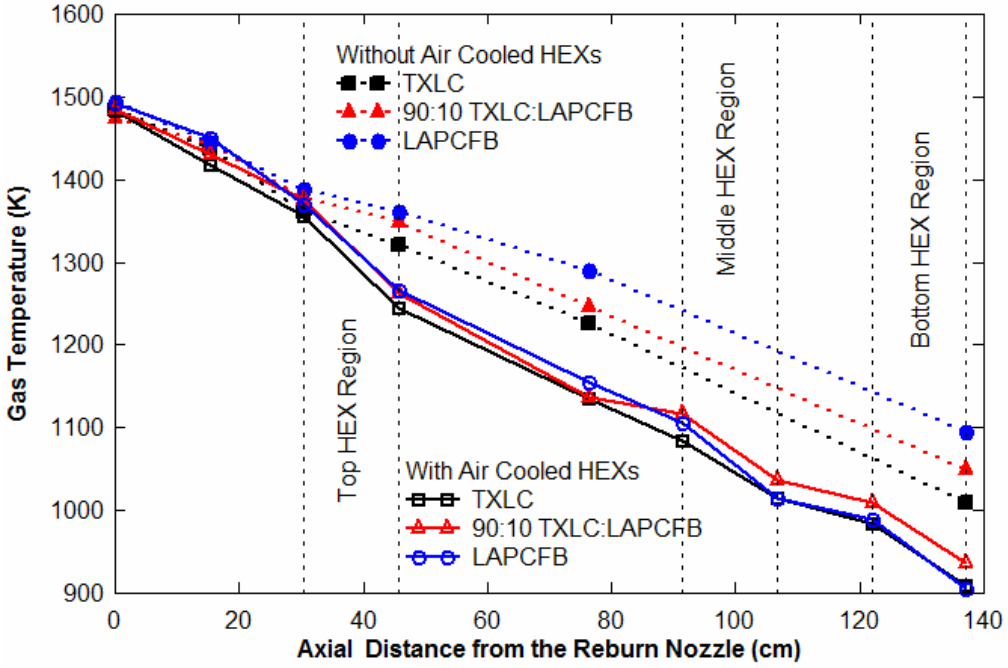

Figure 6.11. Temperature distributions of the flue gas along the axial distance from the reburn nozzle for the lateral (0°) reburn injection with and without HEXs.

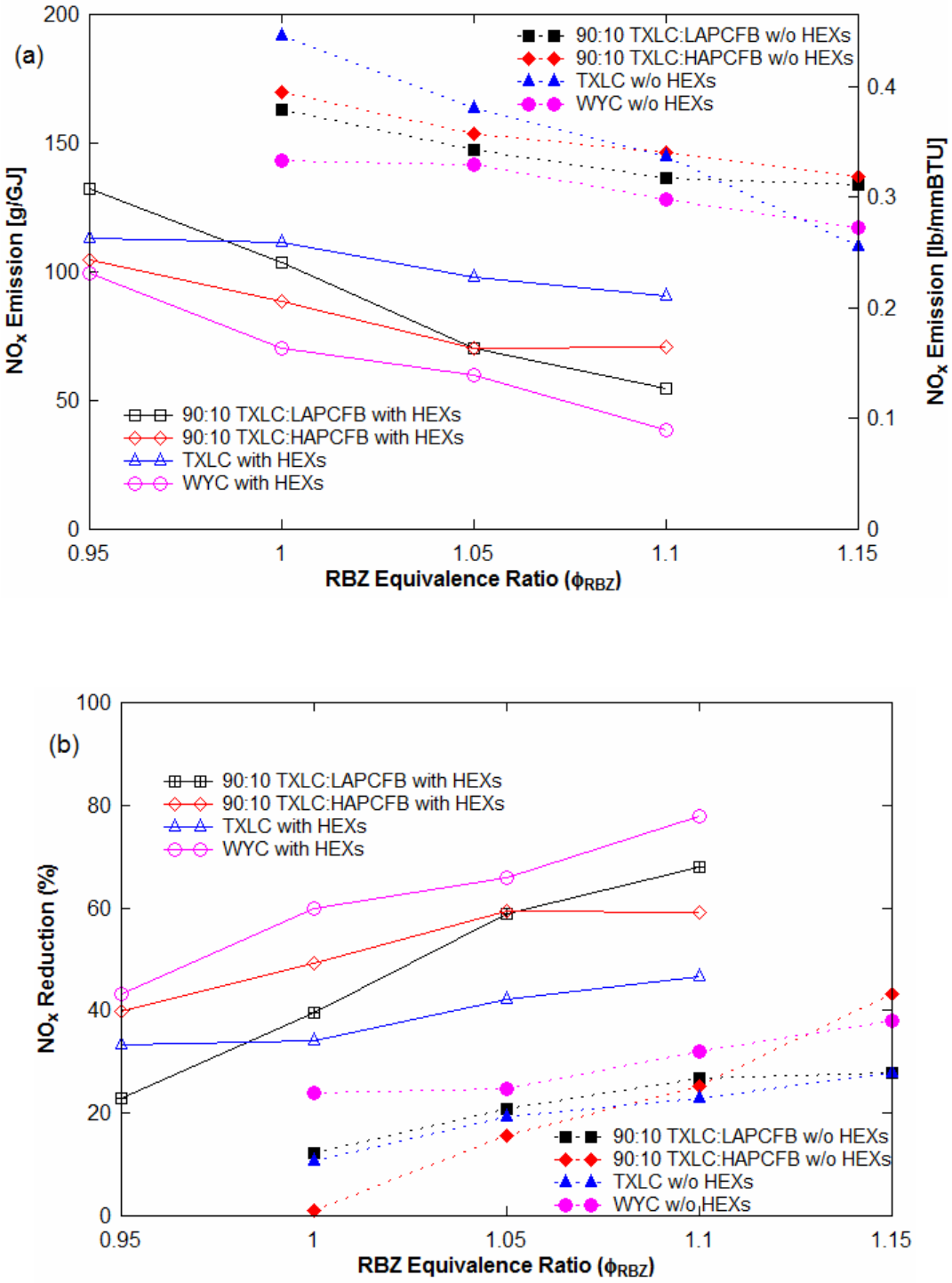

Figure 6.12. Comparison results of the cases with and without HEXs (non-vitiation and lateral (0°) reburn injection): (a) NO_x emission in [g/GJ] and [lb/mmBTU] and (b) NO_x reduction [%].

In figure 6.12, the effects of presence of HEXs on NO_x emission and reduction are presented. The results for the cases in the absence of HEXs were adopted from the previous cases performed by Goughnour [128] and compared with the results for the cases in the presence of air cooled HEXs obtained for the current study. The results adopted from previous cases were reanalyzed based on the current operating conditions and reconverted on a heat basis using the conversion equations reported in Section 5. The use of HEXs results in a significant effect on the NO_x reduction as shown in figure 6.12. It is found that NO_x emissions for the cases with HEXs are lower than those for the cases without HEXs. For example, at ER_{RBZ} of 1.1 in figure 6.12 (a), about 128 to 147 g/GJ of NO_x emission was found for the cases without HEXs depending on reburn fuels while about 39 to 91 g/GJ of NO_x emission was found for the HEX cases. For the NO_x reduction at ER_{RBZ} of 1.1 shown in figure 6.12 (b), about 23 to 32% was achieved for the cases without HEXs while about 47 to 78% was obtained for the HEX cases. The use of HEXs in the boiler increased NO_x reduction about 23 to 46% more. The possible cause for these results is the catalytic effect of the deposition of fly ash on HEXs. The fly ash in power plants can be used as a catalyst in SCR systems for NO_x and SO_x reductions since it contains high silica and alumina contents [130, 131]. During reburning, the injection of metal-containing compounds (Fe-, Na-, K-, and Ca-) with the primary fuel was effective on NO_x reduction, and the use of fly ash including metallic oxides (Fe_2O_3, Na_2O, K_2O, and CaO) was also somewhat effective on NO_x reduction [28, 132].

In the current study, it seemed that the catalytic effect of the fly ash produced from CB was stronger than that of the fly ash produced from TXLC. See figure 6.13 for the result comparison at ER_{RBZ} of 1.1. Approximately 24% NO_x reduction was increased for TXLC in the presence of HEXs, while about 41% for 90:10 TXLC:LAPCFB and 34% for 90:10 TXLC:HAPCFB were increased. It is because the BFs of the blended fuels were higher than the BF of TXLC (see the

BF results in the next section), and hence the amounts of ash produced from the blended fuels were higher indicating more metallic oxides were available during the similar combustion period. Also, a layer of ash depositions was formed on the surface of the HEX. The fuel particles on the surface kept burning during the combustion and finally became pure ash, thus even more metallic oxides in the ash was available for the cases in the presence of HEXs.

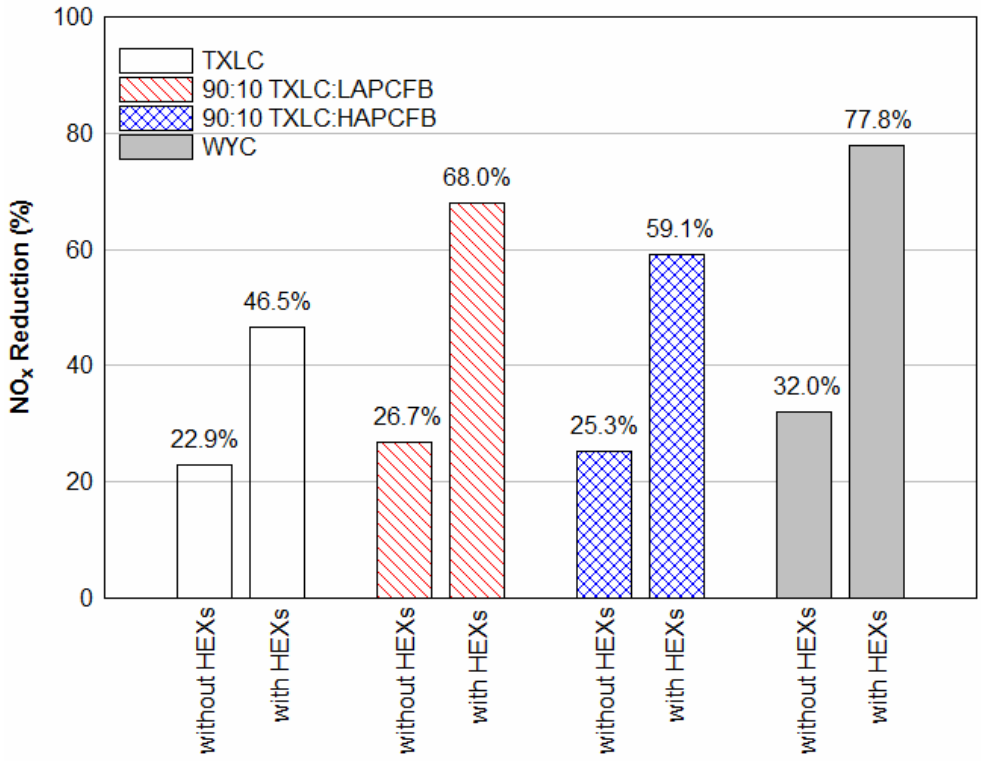

Figure 6.13. Result comparison at ER_{RBZ} = 1.1 for the cases with and without HEXs (non-vitiation and lateral (0°) reburn injection).

6.10 Emissions along the Distance from Reburn Nozzles

Emissions of NO_x [g/GJ] and CO [%] along the distance from reburn nozzles are presented in figure 6.14 in conditions of the non-vitiation and lateral (0°) reburn injection with HEXs. Four locations of the sampling ports are presented in figure 4.1. Volatiles are released very quickly during combustion, and NH_3 reacts with NO_x. The higher combustion temperatures, the faster volatile emissions. Most cases in figure 6.14 show less than 10% reduction along the distance from the reburn nozzles except 60:40 TXLC:LAPCFB (ER_{RBZ} = 1.0). It indicated almost all NO_x reduction took place around the reburn zone where the reburn fuel was injected into the boiler. Less oxygen was available in the downstream of the boiler, and hence less amount of CO was presented. Thus CO decreased along the distance as well.

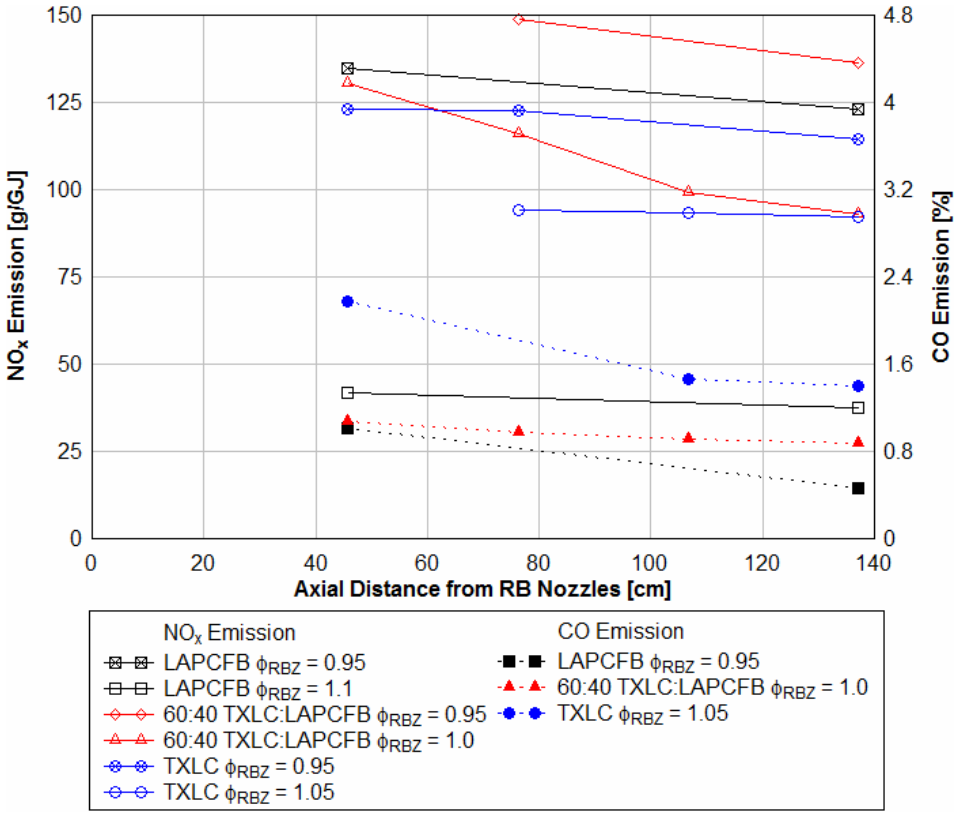

Figure 6.14. NO_x [g/GJ] and CO [%] emissions along the axial distance from reburn nozzles (non-vitiation and lateral (0°) reburn injection with HEXs).

6.11 Emissions of Other Gas Components

Gas emissions of CO, CO_2, SO_2, and C_xH_y were measured along with the NO_x emissions and the results are summarized. Figure 6.15 shows CO emissions in the conditions of the 30% reburn heat input and 0° reburn injection. During the reburn combustion, the fuel-rich environment presents in the reactor, so that high CO emissions were expected. Thus CO emissions increased with an increase of the ER_{RBZ}. High CO emissions in the fuel-lean combustion (ϕ_{RBZ} = 0.95) were measured due to the short residence time which caused incomplete combustion of CO. The effect of the reburn fuels are presented in figure 6.15 (a). It is seen that biomass fuels emitted more CO than both blends of coal:biomass and coal-only fuels since biomass particles contain more oxygen compared to coal particles. Further they release more VM. The higher VM also results in higher BF for blend fuels compared to coal. Figure 6.15 (b) presents the effect of the reburn heat input on CO emission. The 20% and 30% reburn heat inputs for LASSDB were compared in the conditions of the non-vitiation and lateral (0°) reburn injection. The higher reburn heat input, the higher CO emission.

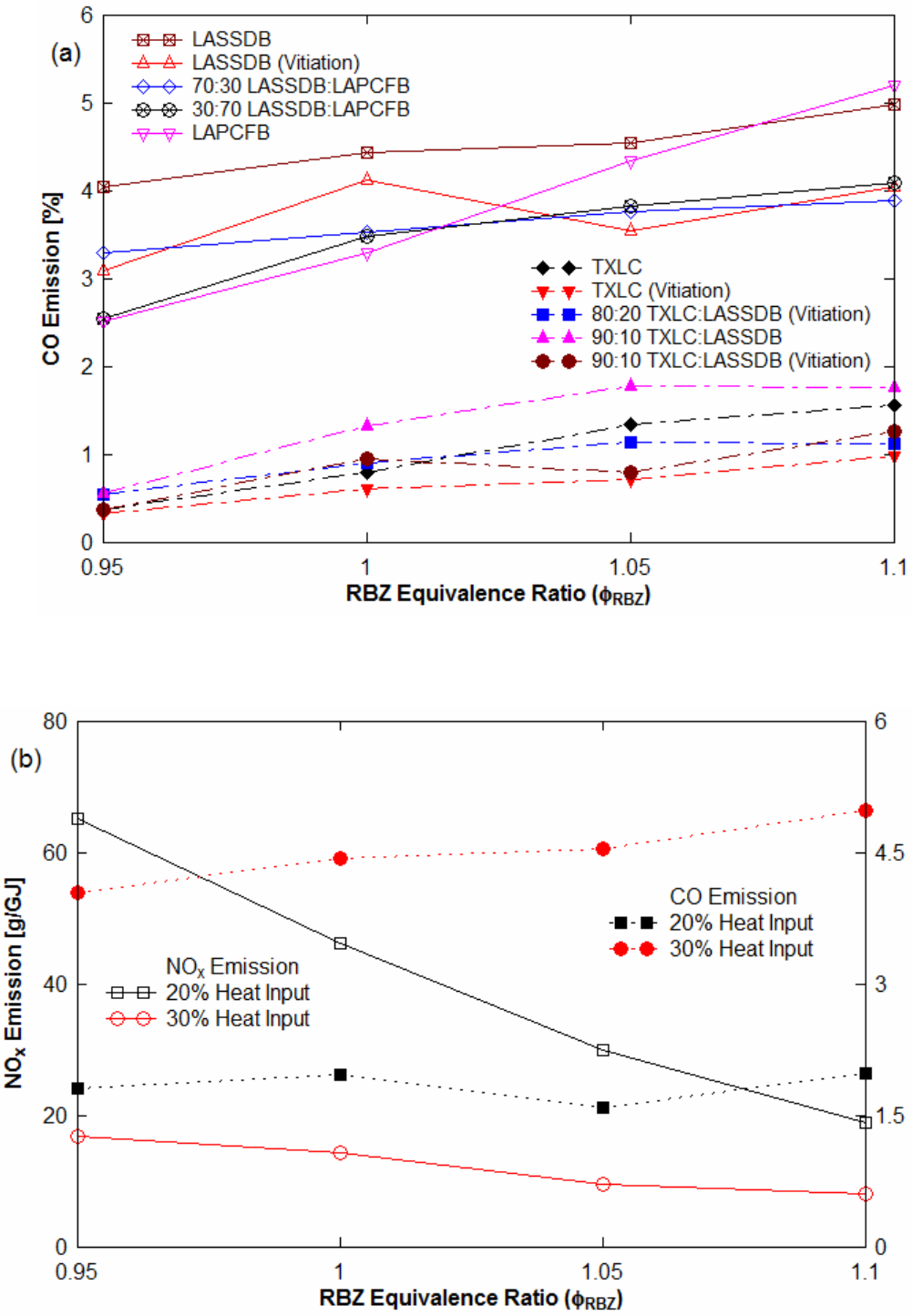

Figure 6.15. (a) Effect of the reburn fuels on CO emissions in different experimental conditions and (b) Effect of the reburn heat input using LASSDB.

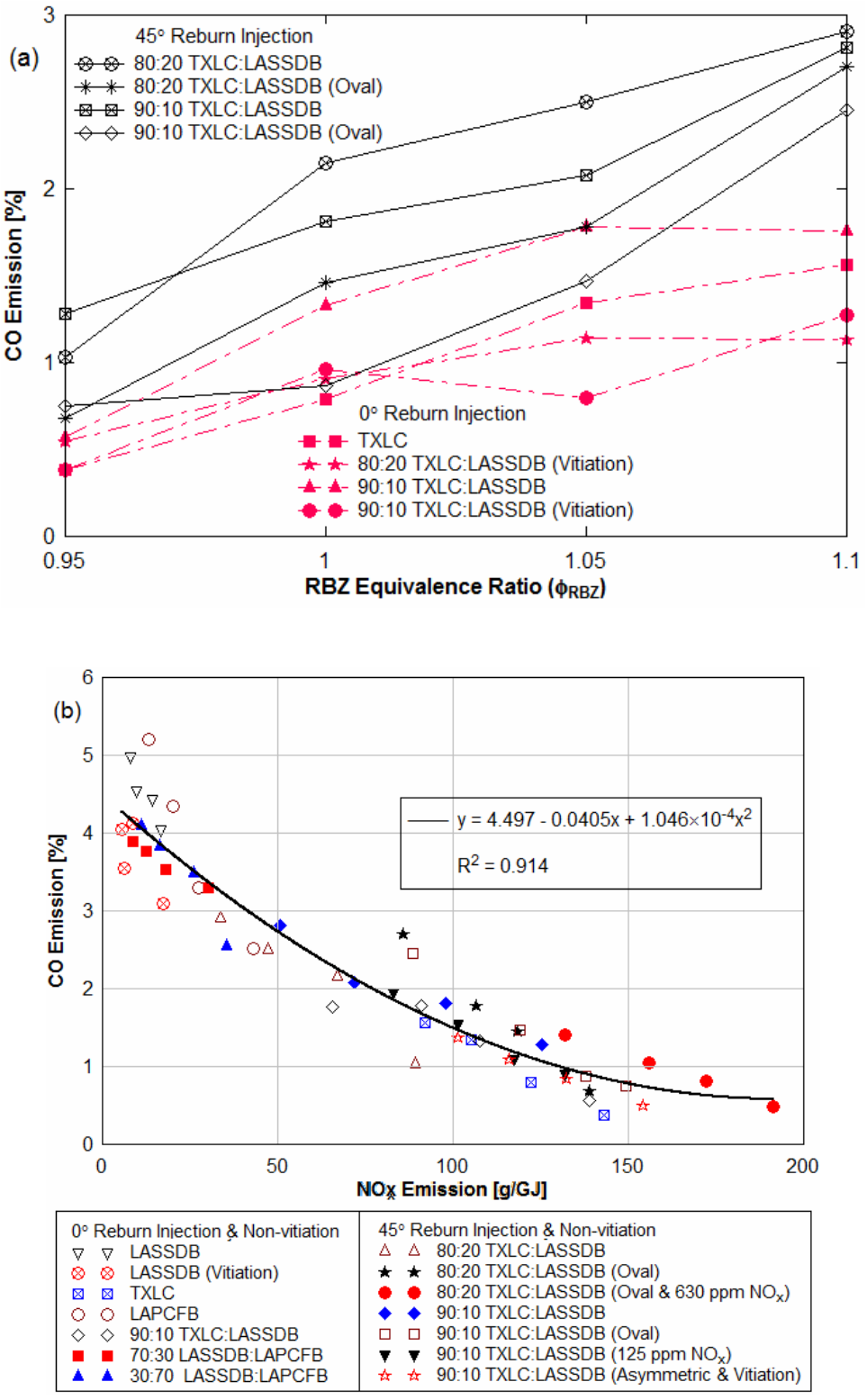

Figure 6.16. (a) Effect of the reburn injection on CO emissions and (b) Relation of CO and NO_x emissions in different experimental conditions.

Figure 6.16 (a) presents the effect of the reburn injection on CO emissions. The results showed the 45° upward reburn injection produced more CO emissions due to it increased the residence time which resulted in combustion of more fuel particles in the reburn zone. In the fuel-rich combustion, CO emissions typically increase while NO_x emissions decrease with an increase of the ER_{RBZ}. Figure 6.16 (b) presents CO and NO_x emissions as a function of the ER_{RBZ} in different experimental conditions, and it showed a linear relation between CO and NO_x emissions.

In figure 6.17 (a), CO_2 emissions decreased with an increase of the ER_{RBZ}. It is also noted that the N_2 addition for vitiation cases diluted the level of CO_2, thus the CO_2 level for non-vitiation cases were higher. The C_xH_y (unburned hydrocarbons) emissions increased with the increment of the ER_{RBZ} shown in figure 6.17 (b). C_xH_y is typically burned to CO_2 and water with enough O_2. When the ER_{RBZ} increases, the depletion of O_2 causes less combustion of C_xH_y and produces less CO_2 and water. The results showed combustion of biomass-only fuels produced much more C_xH_y than the other fuels. The results of the other fuels, blends of coal:biomass and coal-only fuels, showed less than 100 ppm independent on the ER_{RBZ}. Higher C_xH_y emission causes higher BF (note that BF implies gasification fraction in the event CO and C_xH_y are not burnt to CO_2 and H_2O).

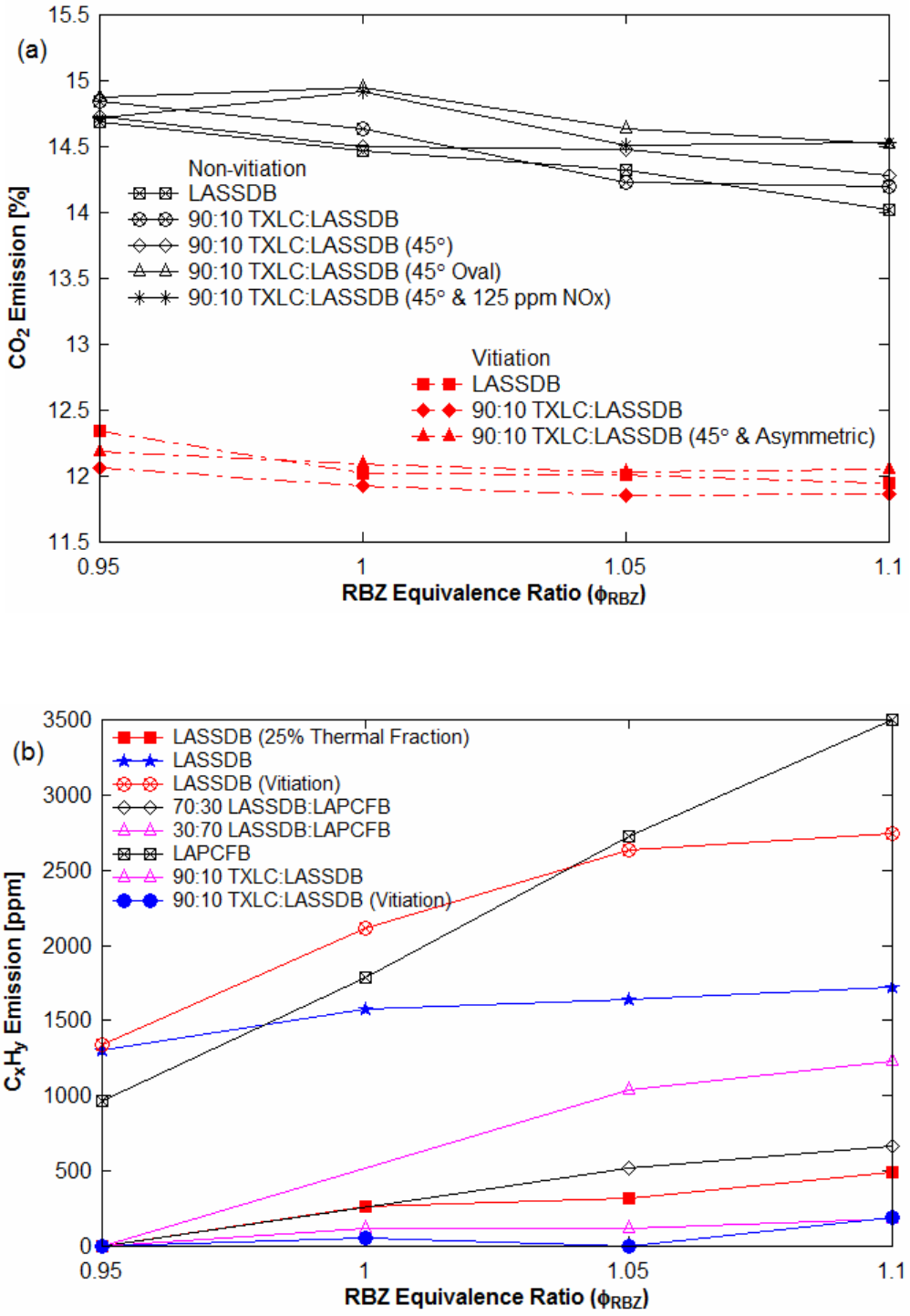

Figure 6.17. (a) CO_2 emissions and (b) C_xH_y emissions as a function of the ER_{RBZ} in different experimental conditions.

The SO_2 emissions in figure 6.18 increased with the increment of the ER_{RBZ}. The measurement of SO_2 was interfered by water condensed in the gas analyzer probe. The stable measurements of SO_2 emissions were presented in the figure 6.18. Since SO_2 is readily soluble to the cold water, more SO_2 emissions should be detected for the case the less water is produced. With the increment of ER_{RBZ}, less water was produced from C_xH_y, hence a higher level of SO_2 was presented.

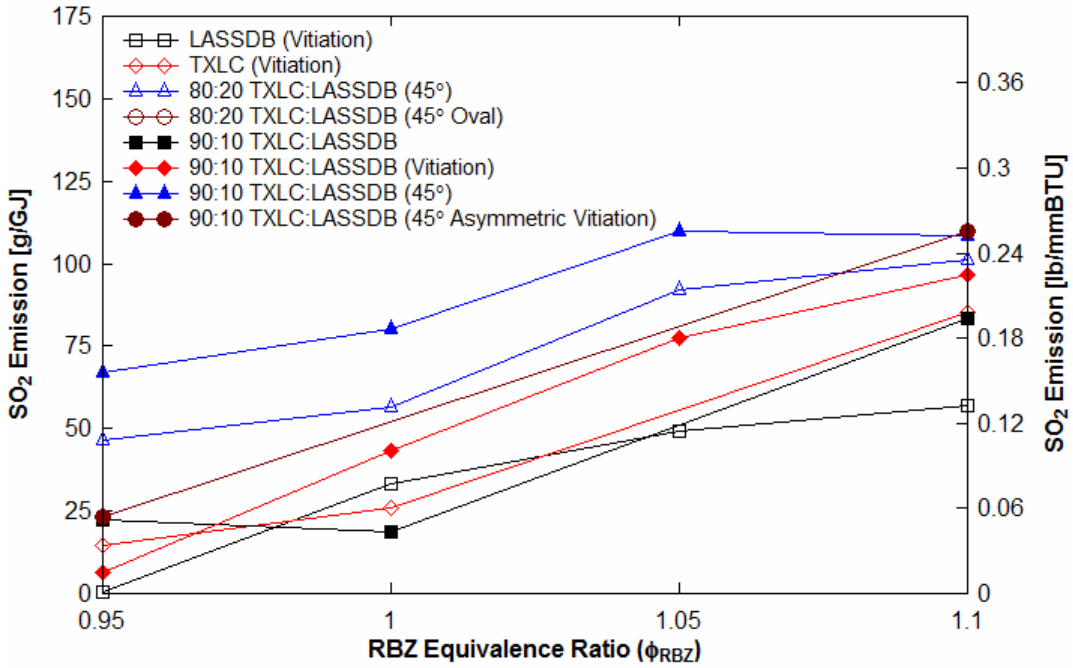

Figure 6.18. SO_2 emissions as a function of the ER_{RBZ} in different experimental conditions.

6.12 Burnt Fraction (BF)

As opposed to the DOE-NETL facility (500,000 BTU/h) operated over several hours [25], the current bench-scale (30 kW or 100,000 BTU/h) facility has operated over shorter duration (3 – 4 hours) due to the limited feeder capacity. Thus enough ash depositions were not formed to cause the slagging behavior. The proportions of moisture, ash, and combustibles (volatile matter and fixed carbon) for the reburn fuels are presented in Table 5.1. Combustibles in fuels are 80.03% for LASSDB, 79.47% for LAPCFB and 81.41% for TXLC on a dry basis. In order to determine the BF (or gasification fraction), the bottom ash was collected from the ash port filled with water at the furnace bottom after the furnace completely cooled down. During reburning the ER_{RBZ} varied from 0.95 to 1.1, and the combustion period was different case by case; however, it seems that the overall condition of reburning was slightly fuel-rich. The BF is defined as the ratio of combustibles burnt to the initial combustible mass. The ash samples were analyzed using ASTM methods (D-3175, E-872 and E-1755) and the BF was determined on a dry basis by the results of the ash analysis reported in Reference [48].

The results of the BF are listed in Table 6.1, and the elemental analysis of ash was presented in Table 5.4. The BF results of the bottom ash are somewhat low in Table 6.1; 64.15% for pure TXLC, 65.78% for 90:10 TXLC:LASSDB, 70.39% for 80:20 TXLC:LASSDB, 85.29% for LASSDB, 67.35% for 90:10 TXLC:LAPCFB, 87.70% for 70:30 TXLC:LAPCFB, and 88.90% for LAPCFB. The majority of lighter fly ash particles in the gas stream flowed into the exhaust duct, and most of heavy solid particles dropped into the water in the ash port. Thus the bottom ash collected from the ash port contained most of the heavy particles, and the BF calculated by the analysis of the heavy ash particles can be low. For the accurate BF estimation, both light fly ash and heavy bottom ash produced during the same period should be analyzed. It is found that the BF increased with the increase of the proportion of DB in the reburn fuels. It is because DB

has higher volatile matters (almost 80% on a DAF basis), and its particle sizes are smaller compared to TXLC. The BFs of LASSDB based fuels were lower than the BFs of LAPCFB based fuels since LASSDB contained bigger particles than LAPCFB shown in Table 5.7. When the HEXs were used during reburning, the BFs of the ash samples collected from all surfaces of HEXs were found to be about 100% (or pure ash) since the fuel particles on the surface kept burning during the combustion. The analyses of BF and combustible loss for ash collected from the surfaces of the HEXs are presented and discussed in Section 7.

Table 6.1. Ash analysis for burnt fraction (BF) on a dry basis for the bottom ash.

Reburn Fuel	Ash [w%]	Combustibles [w%]	Burnt Fraction [w%]
LASSDB	62.91	37.09	85.29
80:20 TXLC:LASSDB	43.77	56.23	70.39
90:10 TXLC:LASSDB	40.46	59.54	65.78
TXLC	38.91	61.09	64.15
LAPCFB	69.94	30.06	88.90
70:30 TXLC:LAPCFB	65.85	34.15	87.70
90:10 TXLC:LAPCFB	41.47	58.53	67.35

7. RESULTS OF ASH FOULING DURING REBURNING

This section summarizes the results of ash fouling in the biomass reburning under transient condition and short-time operation. The main focus of this study is to determine the heat transfer performance and combustion efficiency during the biomass reburning using the method proposed in Section 5. Many studies have been focused on fouling behavior in steady-state conditions presented in Section 2; however, this section deals with transient conditions in the bench-scale facility. The fouling experiment is a supplemental study to the biomass reburning.

7.1 Fouling Using Air Cooled HEXs

7.1.1. Temperature Profile

The flue gas temperatures of the vertically down-fired combustor were measured at spaced intervals of 6 in (15.24 cm) below the reburn nozzles as shown in figure 4.1. The temperature of the hot flue gas linearly decreases along the reactor, and the linear equation was used to measure flue gas temperatures above (at the inlet) and below (at the outlet) of heat exchangers (HEXs) as shown in figure 4.1 (d). The temperature is a very significant factor to the reaction rate of NO_x formation and reduction. The temperature of the reburn zone (RBZ) was monitored and kept below 1320ºC (2400ºF) to prevent the production of thermal NO_x. Radial temperatures in the reactor were measured and were similar to the results in figure 6.1 (b). The bench-scale facility was operated under the transient and short-time operation for the conditions of the non-vitiation, 30% reburn heat input and lateral (0°) reburn injection. The transient condition is defined as the condition in which all temperatures of the cold fluid and the hot flue gas increase as a function of time. The cold fluid in HEXs was air for most of cases and water for some cases of DB blends.

Figure 7.1 (a) presents temperature distributions of the hot flue gas measured at the gas inlet and outlet for the three air cooled HEXs (top, middle and bottom) when natural gas (NG) is fired for ashless cases. In the beginning, the primary fuel (NG) combustion produced 70% (21 kW, 70,000 BTU/h) of the total heat. After 65 minutes, the flow rates of the primary fuel and air were increased to generate 100% (30 kW or 100,000 BTU/h) of the total heat and the corresponding increase in gas temperatures. Figure 7.1 (b) shows temperature distributions of the cold gas (air) at each end of the HEXs. The exit temperature was higher than the inlet temperature. The air flowed into the HEXs after about 25 minutes, causing all temperatures to decrease, and then they increased again. After 65 minutes, when all temperatures increased the primary throughput was increased to 30 kW. The local temperature differences ($\Delta T = T_{exit} - T_{in}$) between the inlet and the exit of each HEX increased over time.

Figure 7.2 presents temperature profiles of the vertically down-fired combustor along the axis from the RBZ at certain times (90, 120, 150, and 180 minutes). The temperature linearly decreases along the axis and gradually increased with time at any given axial distance. The temperature distributions of NG combustion for the ashless cases shown in figures 7.1 and 7.2 are defined as reference temperature distributions for the future analyses and discussions.

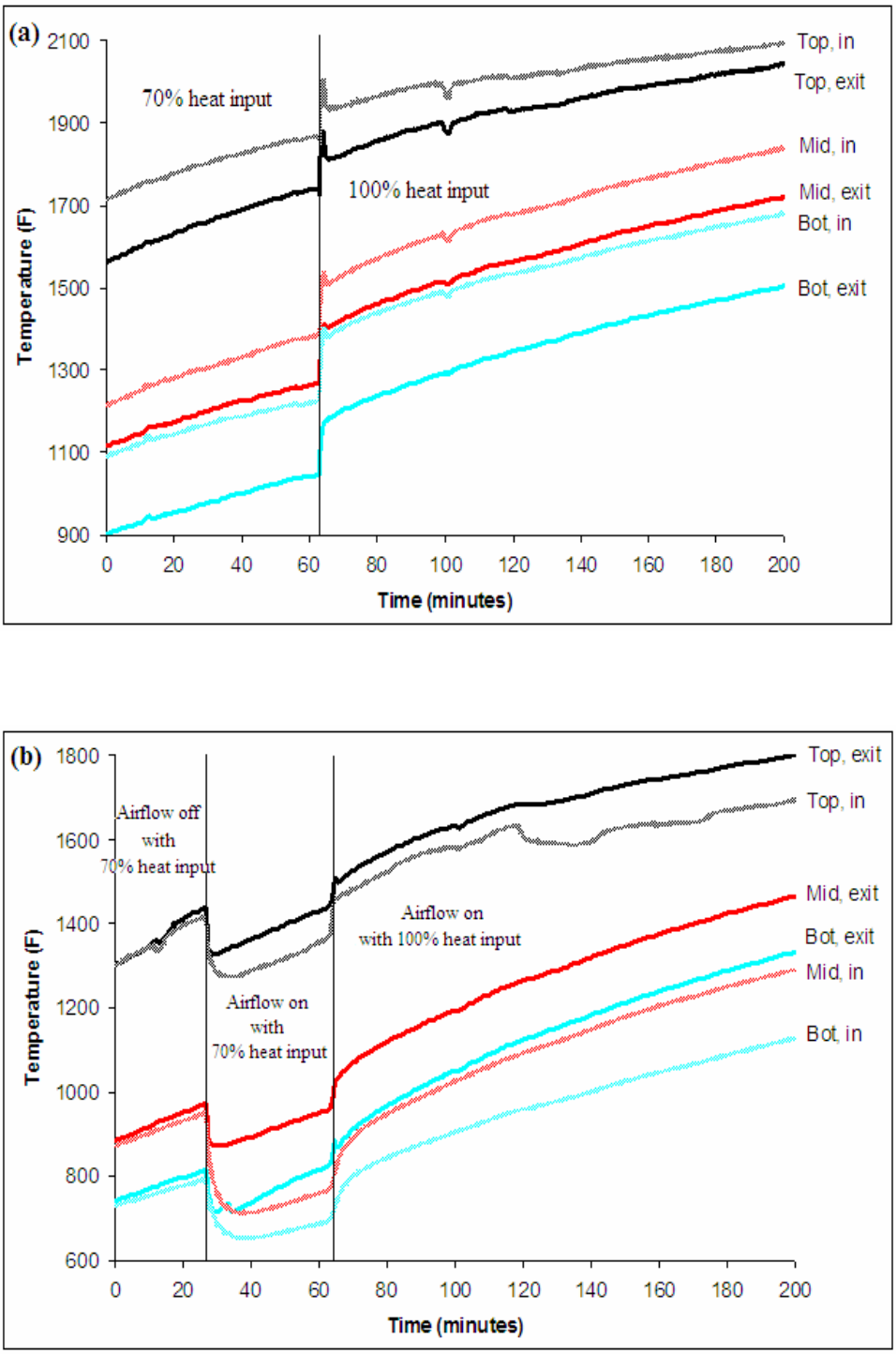

Figure 7.1. Temperature distributions of the hot and cold gases with the primary fuel (NG) to generate 100% of the total heat without ash depositions: (a) Hot flue gas stream and (b) Cold (airflow) gas.

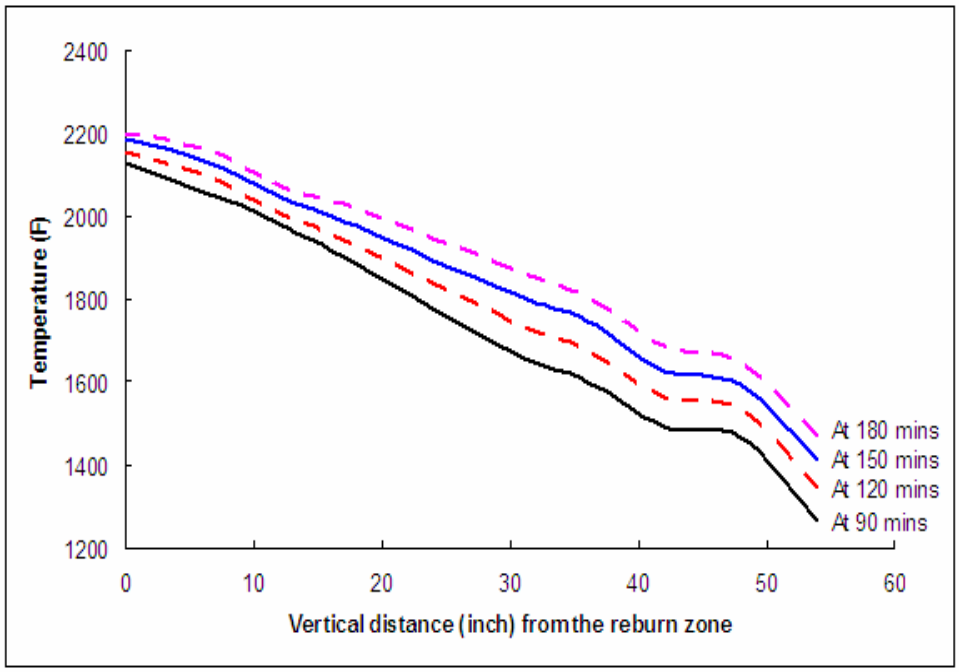

Figure 7.2. Temperature profile of the vertically down-fired combustor along the vertical distance from the reburn nozzles.

The experiments were then repeated with 70% of the heat rate supplied by the primary fuel (NG) and 30% by solid reburn fuels with ash in order to understand the transition of the cold gas temperatures under the condition with the ash deposition. The flue gas temperatures of the inlet and exit of HEXs are close to each other just before the cold gas starts. The reburn fuel and air (about 20% of total air) are injected in order to produce 30% of the total heat after 65 min. In the case of 100% LAPCFB, the local temperature differences (ΔT) of the cold gas in HEX for the top and middle HEXs were reduced while ΔT_{Bot} increased. As a result, when ΔT increases, the rate of increase of the exit temperature is higher than that of the inlet temperature. Hence the heat transfer rate ($\dot{Q}$) to the HEX increases over time. When ΔT decreases, the rate of increase of the inlet temperature is higher than the rate of increase of the exit temperature. This causes the heat transfer rate to the HEX to decrease over time.

7.1.2. Criteria for Fouling

Because of the growth the ash deposition, the decrease of overall heat transfer coefficients (OHTC) is typically expected under the steady-state condition with time. However, in the transient condition, a similar result may not be expected. Due to the smaller size of reactor, the temperature difference at the inlet and exit may not be steady unless the long period combustion; further the small scale reactor clogged when FB was burnt over longer periods, particularly with the combustion of high ash FB. Hence results are interpreted using the results of temperature distributions of the solid fuel combustion (ash deposition cases) and comparing distribution with reference distribution for NG combustion (ashless cases). Figure 7.3 shows results of OHTCs and log mean temperature differences (LMTDs) for ashless cases using the temperature data shown in figure 7.1. In particular, time dependant temperature functions (T(t)) were used after 100% heat input was generated. In figure 7.3 (a), the OHTC (U) increased with time. The sudden jump of U_{Top} appeared due to the decrease of the air temperature caused by the adjustment of the experimental settings. The OHTC of the top and middle HEXs slowly increased while that of the bottom HEX quickly increased. The heat transfer rate to the HEX increased with time since hot gas temperatures kept increasing during combustion. It was not the same phenomenon that occurred in steady-state conditions. The typical values of the OHTC under the steady-state condition are listed in Table 5.9. Figure 7.3 (b) shows the trend of the LMTD over time for the case of no ash depositions. It was observed that the LMTD decreased with time, and also varied with the position of the HEX. The decreasing tendency of the LMTD means that temperatures of the hot flue gas and the cold gas (air) became closer to each other over time due to the heat transfer from the flue gas to the HEX. Based on the temperature measurement, temperatures of the cold gas increased twice faster than temperatures of the flue gas. The LMTD of the middle HEX was the highest, and the LMTD of the top HEX was the lowest.

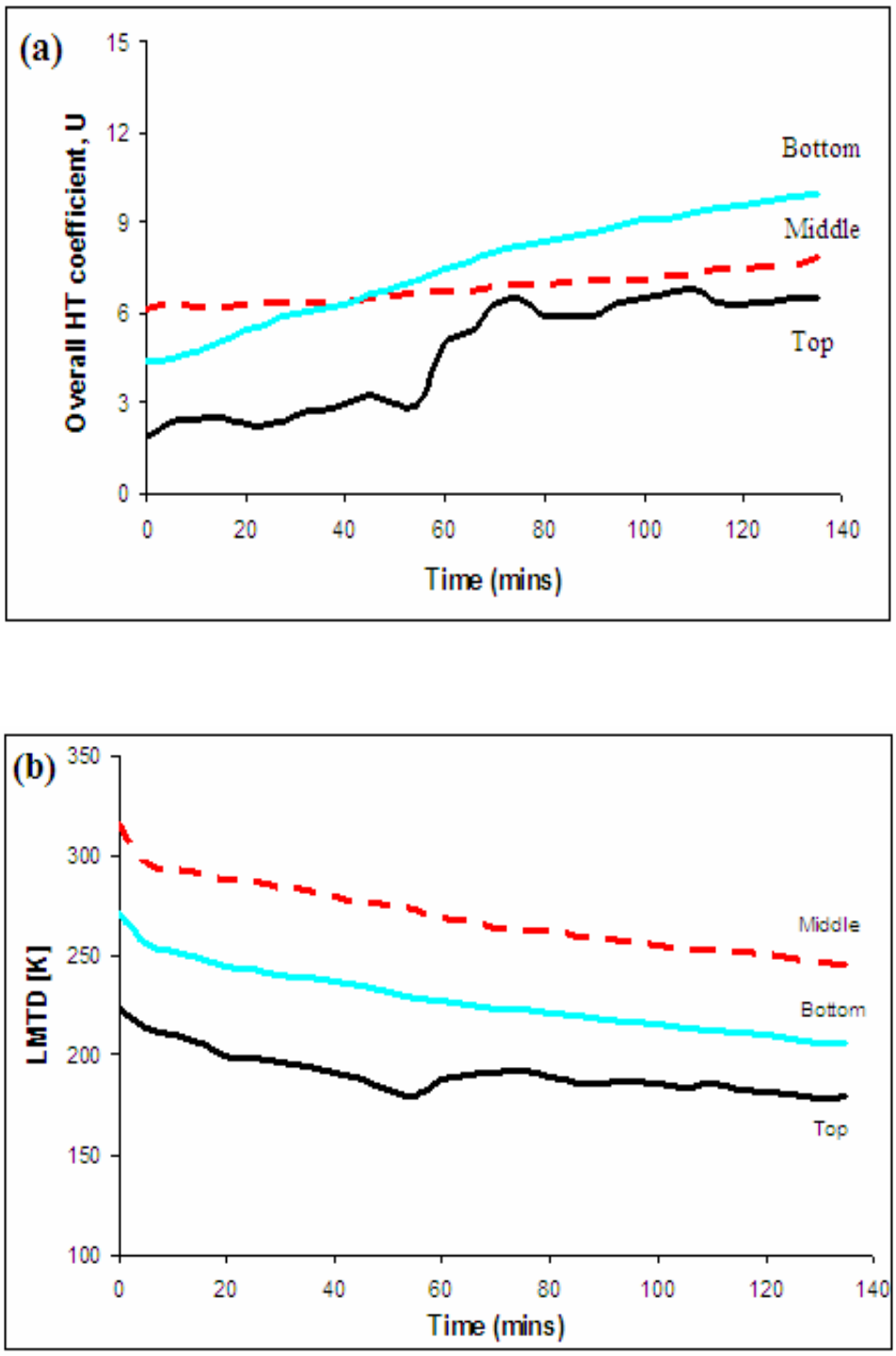

Figure 7.3. Overall heat transfer coefficients (OHTC) and log mean temperature differences (LMTD) in the conditions of 30 kW heat input for ashless cases: (a) OHTC (*U*) and (b) LMTD.

In order to verify the results mentioned above, a simple calculation was made using the data in figure 7.1. The average temperatures of both inlet and exit of the hot flue gas and those of the cold gas were obtained. The differences of the average temperatures of hot and cold gases were obtained as 391ºF (top), 520ºF (middle), and 472ºF (bottom) at 0 minutes and 322ºF (top), 405ºF (middle), and 366ºF (bottom) at 120 minutes. The values of the middle HEX were the highest, and those of the top HEX were the lowest. Figure 7.3 was used as a criterion for evaluating the effect of the presence of ash and the deposition of ash from solid reburn fuels. Particularly the rates of increase of the OHTC in ash deposition cases are compared with those in ashless cases.

7.1.3. TXLC

As a base case, TXLC was injected as a reburn fuel. It contains 11.46 % ash which is the lowest amount among the tested reburn fuels. It was seen that more ash deposits were formed on the surface of the bottom HEX than the surfaces of other HEXs since the ash concentration in the flue gas was high. The top HEX was covered by a thin layer of the black slag and little bit of powdered ash since the gas temperature was in the range of the solidified slag production. However, not much black slag was observed. The middle and bottom HEXs were mostly covered by a powdered ash layer because the coal was almost completely burnt below 800ºC (1470ºF). The powdered ash covered the top area of the HEXs, while their bottom areas were usually very clean. The ash deposition on the bottom areas of the HEXs was relatively hard to form since the gas stream flowed vertically downward. It was also possible some of ash depositions dropped off from the bottom of the HEX surfaces when the HEXs were detached from the boiler at the end of experiments.

The OHTC (U) of the HEXs are shown in figure 7.4 (a). The OHTC seem to be increase while the layer of ash formed on the surfaces of the HEXs. It was because the gas temperature

kept increasing with increasing heat transfer rate to the HEX during combustion of the solid fuels under transient conditions. The OHTC of the top and bottom HEXs increased, while the OHTC of the middle HEX decreased with time. Figure 7.4 (b) shows the ratio of the OHTC with and without ash deposits over time. Because operating temperatures were different case by case, data under the condition of the similar gas inlet temperature were selected and used. The results show the OHTC of the ash deposition case was lower than that of the ashless case. The ratios of OHTC(ash) to OHTC(no ash) for all HEXs decreased. Due to lower temperatures and thicker ash layer for the bottom HEXs, the OHTC ratio of the bottom HEX is expected to be the lowest value; however, the results shows somewhat higher values. The decreasing tendency of the OHTC ratio was still observed over time due to the growth of the ash deposition. The presence of ash in gas phase increased radiation heat transfer rate while the deposition reduced the conductive heat transfer rate. Apparently for TXLC, the deposition effect on heat transfer seemed to be dominant.

Figure 7.5 (a) presents the LMTD trend of the HEXs with TXLC. It was observed that the LMTD decreased with time, and also varied with the position of the HEX. The LMTD of the middle HEX was the highest, and the LMTD of the top HEX was the lowest. The results were similar to those found in the ashless case. Figure 7.5 (b) shows the ratio of the LMTD with and without ash depositions over time. An increasing tendency is expected due to the ash deposition. LMTD ratios of the top and bottom HEXs increased while that of the middle HEX decreased.

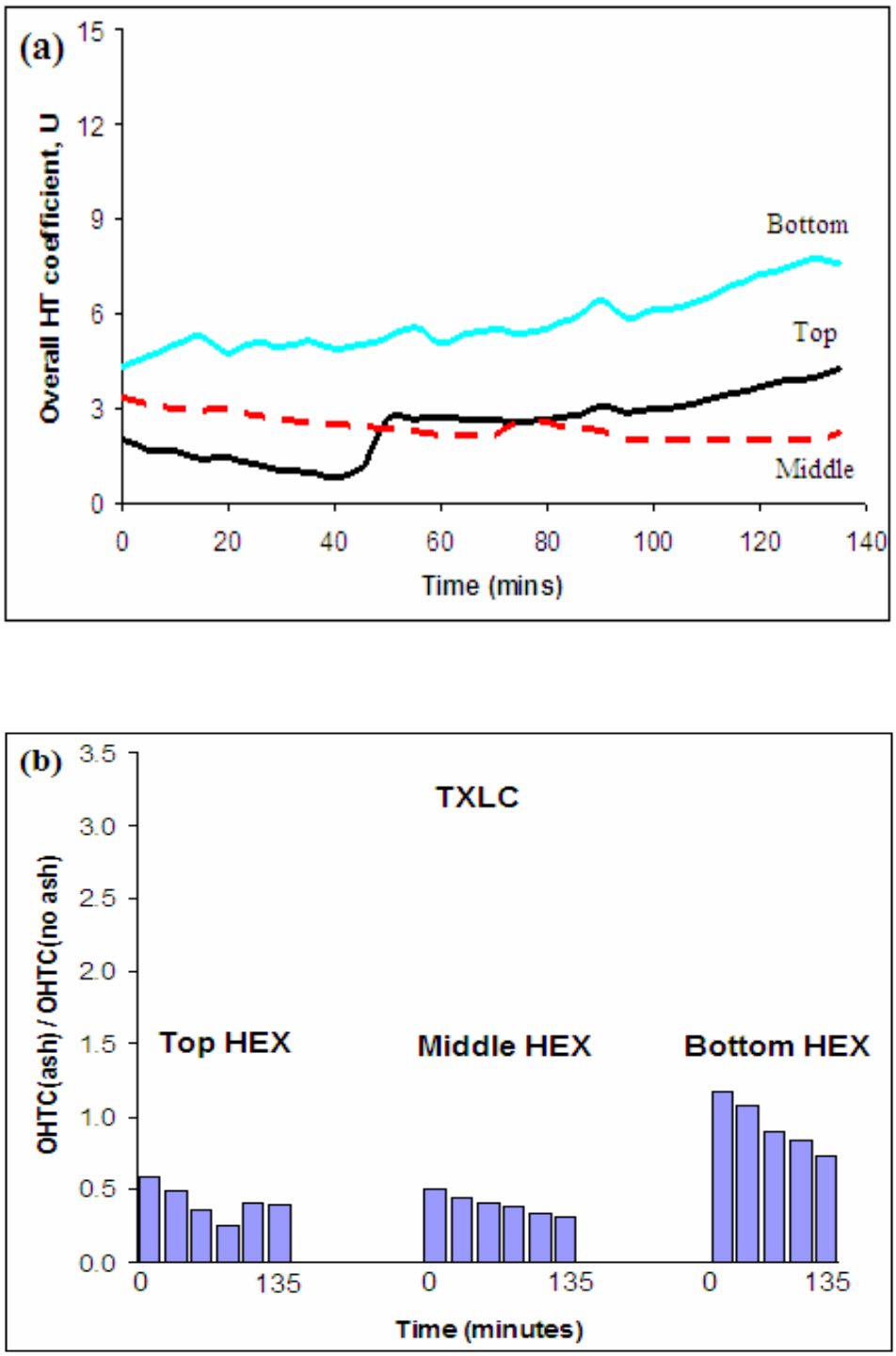

Figure 7.4. Overall heat transfer coefficients (OHTC) for pure TXLC as a reburn fuel: (a) OHTC (*U*) and (b) Ratios of the OHTC with and without ash deposition.

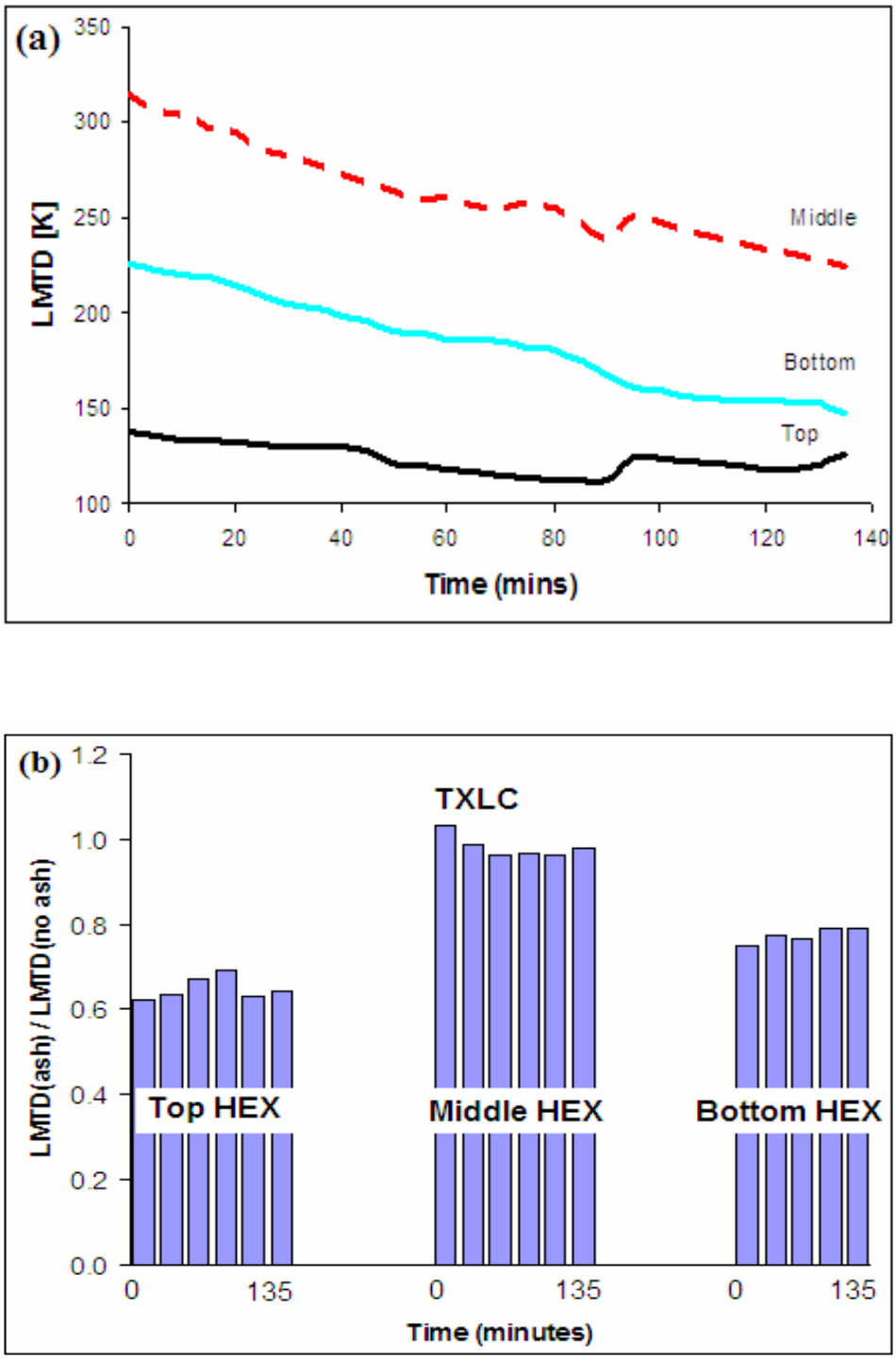

Figure 7.5. Log mean temperature differences (LMTD) for pure TXLC as a reburn fuel: (a) LMTD and (b) Ratios of the LMTD with and without ash deposition.

7.1.4. LAPCFB

Pure LAPCFB that contains 16.50 % of the ash content was injected into the reburn zone. As shown in figure 7.6, heavier ash depositions were formed compared to the pure TXLC. More ash was formed along the reactor from the top to the bottom. The top HEX was mostly covered by the thin layer of the black slag at the center and little bit of ash at both sides. However, the middle and bottom HEXs were mostly covered by the powdered ash layer. More black slag was observed for LAPCFB than TXLC. The top areas of the HEXs were heavily covered by ash particles, but their bottom areas were barely covered. It is likely that the fuel which contains more ash contents causes heavier ash deposition.

In figure 7.7 (a), the OHTC (U) of the middle and bottom HEXs increased while that of the top HEXs decreased. It was because the thin layer of the black slag had less thermal conductivity than that of the ash powder layer. Theoretically, the smaller particle sizes would burn faster and hence would produce hotter gases. The particles smaller than 75 μm are 43% for LAPCFB and 24% for TXLC as shown in figure 5.3. Thus the flue gas temperature of LAPCFB increased faster than that of TXLC and no ash deposition in the same time period. It is concluded that the ash deposition caused a decrease in OHTC on the top and bottom HEXs. The ratios of the OHTC with and without ash depositions over time are presented in figure 7.7 (b). For the ashless cases, there were no particles to transfer heat by radiation, and hence the OHTC ratios were more than 1 in the initial period. Note that the numerator in Eq. (5.15) represents heat gained by both heat radiation and convection. As more ash is being deposited, the growing ash layer become as an insulator, thus the OHTC ratios decrease. At the top section of the burner, the temperatures were high and ash became sticky tending to get high heat radiation; however, the gas temperatures in the middle of the boiler were lower than the top temperatures. Thus the radiation heat contribution to the middle HEX was less, and heat radiation to the bottom HEX was lowest.

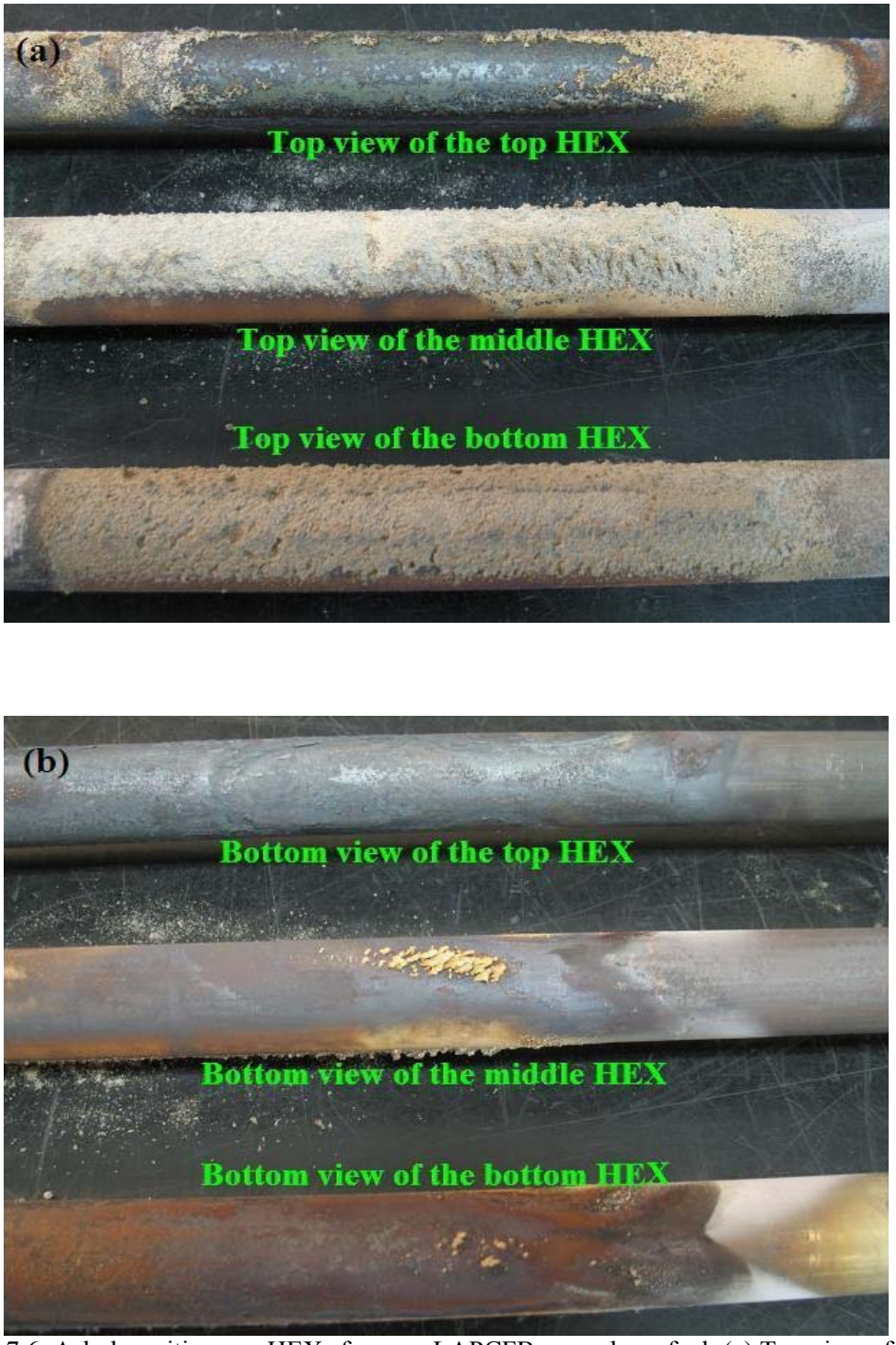

Figure 7.6. Ash depositions on HEXs for pure LAPCFB as a reburn fuel: (a) Top view of HEXs and (b) Bottom view of HEXs.

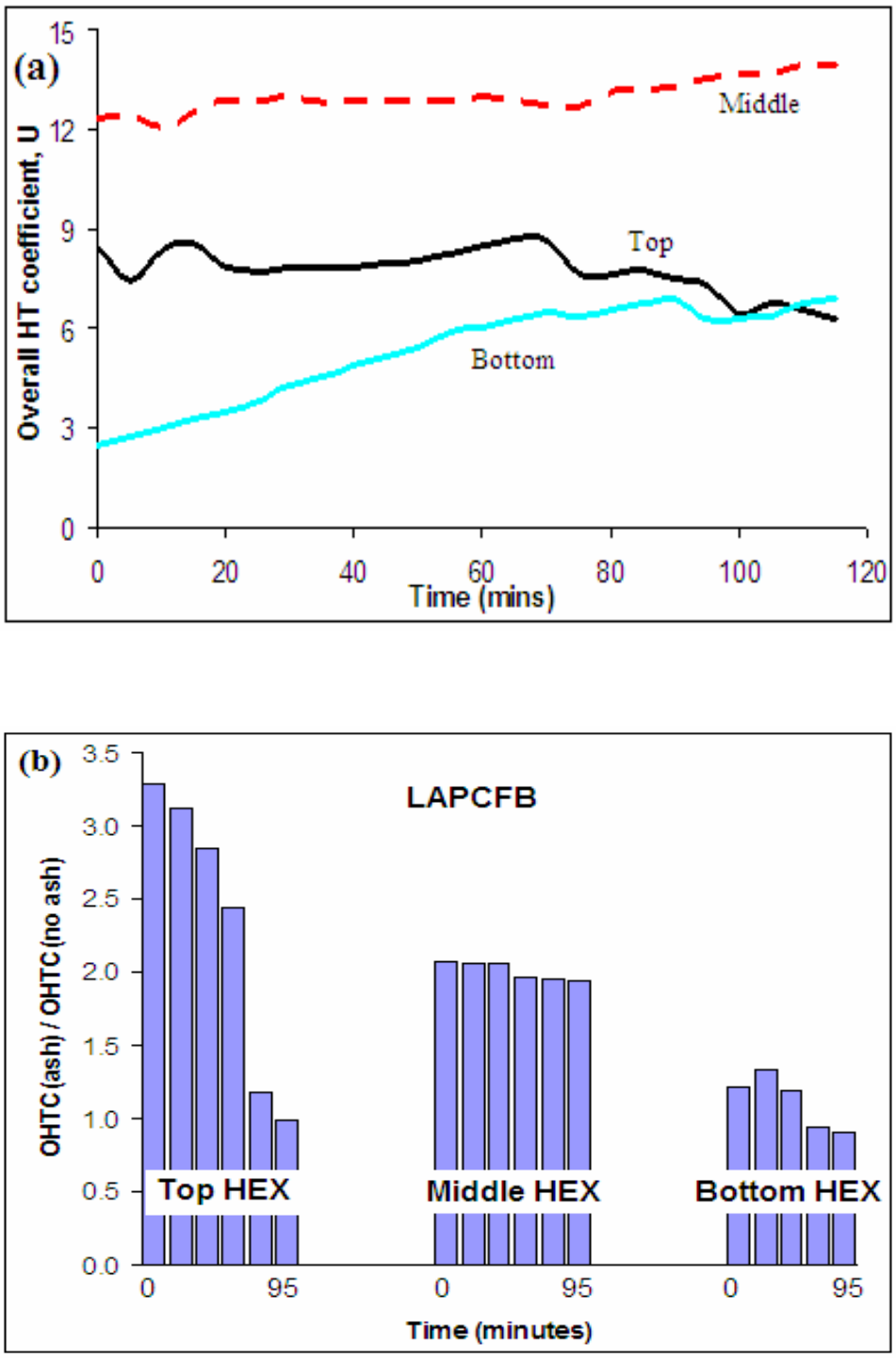

Figure 7.7. Overall heat transfer coefficients (OHTC) for the pure LAPCFB as a reburn fuel: (a) OHTC (*U)* and (b) Ratios of the OHTC with and without ash deposition.

The ratios of OHTC(ash) to OHTC(no ash) for LAPCFB were high compared to those of TXLC. This is explained as follows: The fuel feed rate for LAPCFB was almost 8 % more compared to TXLC to generate the same heat input; this coupled with increased fuel ash content results in ash loading almost 55% more compared to TXLC as shown in Table 5.3. The increased mass concentration in gas phase increased the radiation heat transfer rate. Thus the initial OHTC was much higher compared to the case for coal.

7.1.5. Blends of TXLC and LAPCFB

Several fuel blends (90:10 TXLC:LAPCFB, 70:30 TXLC:LAPCFB, 90:10 TXLC:HAPCFB, and 70:30 TXLC:HAPCFB) were tested. The HAPCFB has the highest amount of ash (53.85%) among the tested fuels. Due to safety reasons, combustion of TXLC:HAPCFB blends was tested over a shorter time period than that of TXLC:LAPCFB blends. The reactor clogged when FB was burnt over longer periods, particularly with combustion of pure HAPCFB, and its molten behavior was observed under the reburn nozzles shown in figure 7.8. More black slag, heavier ash depositions, and higher thermal resistances for 70:30 blends than those of 90:10 blends are expected for both types of FB, LAPCFB and HAPCFB. It is likely that the solid fuel with more ash contents causes heavier ash deposition. Since the short testing period of TXLC:HAPCFB blends, not much ash depositions were formed. The top HEX was covered by the thin layer of the black slag while other HEXs were mostly covered by the ash powder layer. More black slag and heavier ash depositions for 70:30 blends than for 90:10 blends were observed.

Figure 7.8. Molten behavior under the reburn burner with firing HAPCFB.

In figures 7.9 (a) and (b), the OHTC (*U)* of the top HEX of all fuel blends was reduced while the OHTCs of other HEXs were increased. The decrease of U_{Top} occurred since the thin layer of the black slag had less thermal conductivity than that of the powdered ash layer. The ratios of OHTC(ash) to OHTC(no ash) were more than 1 for the HEXs in the initial period due to heat radiation. The average OHTC ($OHTC_{avg}$) is defined as the mean value of the obtained OHTCs over time. The $OHTC_{avg}$ for fuel blends are listed in Table 7.1. Most of the $OHTC_{avg}$ were lower than those of no ash cases except the case of the bottom HEX of 70:30 TXLC:HAPCFB (0.049 $W/m^2 \cdot K \cdot min$). Since the short testing period of TXLC:HAPCFB blends, the result might not be enough to evaluate properly. The $OHTC_{avg}$ of the top and bottom HEXs of 70:30 TXLC:LAPCFB were as lower than those of 90:10 TXLC:LAPCFB. It was caused by higher thermal resistances and more ash depositions during combustion of 70:30 TXLC:LAPCFB. It is found that the effect of ash formation on OHTC depends on the proportion of FB in reburn fuels.

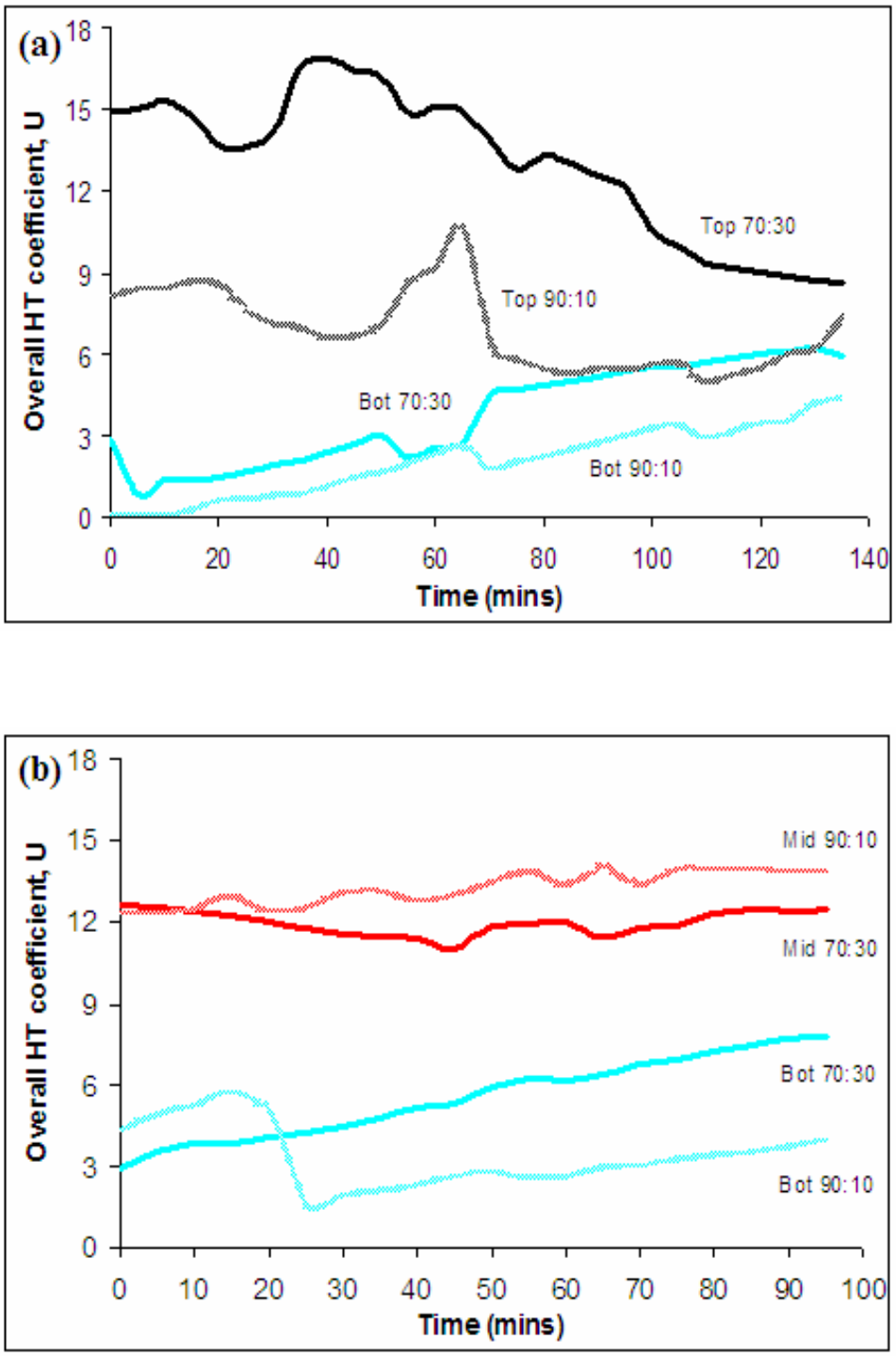

Figure 7.9. Overall heat transfer coefficients (OHTC) for fuel blends: (a) OHTC (*U*) of TXLC:LAPCFB and (b) OHTC (*U*) of TXLC:HAPCFB.

Table 7.1. Average OHTC rates [W/m^2·K·min] for 90:10 and 70:30 coal:FB blends.

HEX Location	No ash deposition	90:10 TXLC:LAPCFB	70:30 TXLC:LAPCFB	90:10 TXLC:HAPCFB	70:30 TXLC:HAPCFB
Top	0.026	-0.020	-0.058	-	-
Middle	0.012	-	-	0.005	0.010
Bottom	0.042	0.041	0.009	0.032	0.049

7.1.6. Burnt Fraction and Combustible Loss

As opposed to the pilot-scale DOE-NETL facility (500,000 BTU/h) [25] and more expensive operation over several hours, the current bench-scale (100,000 BTU/h) facility operates over shorter duration (2 – 3 hours) due to the limited feeder capacity. Thus ash depositions on HEXs were not formed enough to cause the slagging behavior. The proportions of moisture, ash, and combustibles for the reburn fuels are listed in Table 5.1. Combustibles in fuels are 79.47% for LAPCFB, 81.41% for TXLC and 35.12% for HAPCFB on a dry basis. In order to determine the combustible loss, ash were collected from four different places; surfaces of top, middle, and bottom air cooled HEXs and the ash port at the furnace bottom. After the furnace completely cooled down, the HEXs were detached from the boiler burner, and ash samples from the surfaces of HEXs and from the ash port at the furnace bottom were scraped off and sent for analysis. During the clean-up process of the HEXs, it was found that the bottom HEX in the low temperature zone was easier to be cleaned compared to the upper HEXs. The combustible loss was determined on a dry basis using the results of the ash analysis [48]. The combustible loss is defined as the ratio of unburnt combustibles in the ash to initial combustibles in the fuel. The burnt fraction (BF) is defined as the ratio of combustibles burnt to the initial combustible mass.

The ash deposits on the HEX surfaces commonly consist of small, sticky particles. Large ash particles may not adhere to the HEX surface due to impaction and bouncing off of surfaces. Due

to the round cross-section of the HEXs, the ash deposits build up around the top area of the HEXs which created temperature non-uniformity around the HEXs. Not all analysis results were presented due to some samples being too small for analysis. The results are listed in Table 7.2 which shows that almost 0% combustible loss and 100% BF were detected for all HEXs since the particles on the surfaces of the HEXs kept burning during combustion. Detailed elemental analysis of ash is presented in Table 5.4. The contents of alkali metals (sodium, Na and potassium, K) can make the ash more sticky. In current fouling tests, more ash depositions were formed during FB combustion than coal combustion. Since higher amounts of alkali metals in ash of HAPCFB and LAPCFB, more ash sticks on the surfaces of the HEXs.

Unlike the combustible loss obtained from the samples on the HEXs, the combustible loss obtained from the bottom ash collected from the ash port was somewhat high; 50.21% for pure TXLC, 11.1% for pure LAPCFB, 32.65% for 90:10 TXLC:LAPCFB, 12.3% for 70:30 TXLC:LAPCFB, 42.44% for 90:10 TXLC:HAPCFB, 17.45% for 70:30 TXLC:HAPCFB. The lighter fly ash particles in the flue gas flowed into the exhaust duct, and only heavy particles dropped into the water in the ash port. Thus the bottom ash contained most of heavy particles, and the combustible loss calculated by the analysis of heavy ash particles can be high. For the accurate estimation of the combustible loss, both lighter fly ash and heavier bottom ash produced during the same period should be analyzed. It is found that the combustible loss decreases with the increase of the proportion of FB in reburn fuels. It is because FB has higher volatile matters (almost 80% on a DAF basis), and also its particle sizes are smaller than TXLC. Thus higher BF was obtained when more FB was present in reburn fuels. In Table 7.2, the BF was much higher for LAPCFB and 70:30 TXLC:LAPCFB. The BF of LAPCFB blends was higher than that of HAPCFB blends due to smaller particles in LAPCFB.

Table 7.2. Ash analysis results of FB fuels for burnt fraction (BF) and combustible loss.

Fuel	Ash from	Ash (w%)	Combustibles (w%)	Burnt Fraction, BF (w%)	Combustible Loss (w%)
Pure TXLC	Top HEX	100	0	100	0
	Mid HEX	100	0	100	0
	Bot HEX	100	0	100	0
	Ash Port	31.26	68.74	49.79	50.21
90:10 TXLC:LAPCFB	Top HEX	100	0	100	0
	Mid HEX	99.94	0.06	99.99	0.01
	Bot HEX	99.88	0.12	99.97	0.03
	Ash Port	41.47	58.53	67.35	32.65
70:30 TXLC:LAPCFB	Top HEX	100	0	100	0
	Mid HEX	100	0	100	0
	Bot HEX	99.90	0.10	99.98	0.02
	Ash Port	65.85	34.15	87.70	12.30
Pure LAPCFB	Top HEX	99.91	0.09	99.98	0.02
	Mid HEX	99.49	0.51	99.87	0.13
	Bot HEX	99.39	0.61	99.84	0.16
	Ash Port	69.94	30.06	88.90	11.10
90:10 TXLC:HAPCFB	Top HEX	-	-	-	-
	Mid HEX	100	0	100	0
	Bot HEX	100	0	100	0
	Ash Port	41.61	58.39	57.56	42.44
70:30 TXLC:HAPCFB	Top HEX	-	-	-	-
	Mid HEX	100	0	100	0
	Bot HEX	100	0	100	0
	Ash Port	73.38	26.62	82.55	17.45
Pure HAPCFB	Top HEX	100	0	100	0
	Mid HEX	99.89	0.11	99.80	0.20
	Bot HEX	99.61	0.39	99.28	0.72
	Ash Port	-	-	-	-

7.2 Fouling Using Water Cooled HEXs

In the previous section, air cooled HEXs were used for the fouling studies for the following reasons; 1) The temperature rise is much higher with air compared to water for the same mass flow due to the reduced specific heat and reduced error in temperature values, 2) Because of the high temperature rise, the air temperature is much hotter with air cooling and, as such, the average temperature of an ash layer will increase in a short amount of time so that slagging tendency, if any, can be detected, and 3) Results of NO_x reduction with hotter ash layers on the air cooled HEXs were obtained as a function of the ER_{RBZ} during the fouling tests. In this section, however, water (about 295 K) was used as a cold fluid in HEXs, and the change is expected to cause higher heat transfer rates but lower temperatures of the hot and cold fluids than those for air cooled HEXs because of the higher specific heat of water. Fouling tests were performed only at ER_{RBZ} = 1.05 to produce more ash particles and stabilize test conditions. The parametric studies include various types of the reburn fuel, but at 30% reburn heat input and 45° upward reburn injection in the symmetric configuration. The tested reburn fuels were TXLC, LASSDB, 90:10 TXLC:LASSDB, and 80:20 TXLC:LASSDB.

7.2.1. Temperature Profile

In figure 7.10, inlet and exit temperatures of both hot flue gas and water are presented as TXLC was fired as a reburn fuel. The gas temperatures at inlets and exits kept increasing as a function of time due to the combustion of the reburn fuel. The differences between the inlet and exit temperatures were 10 to 15 K, and they were steady with time. The ranges and behaviors of gas temperatures for 90:10 TXLC:LASSDB and 80:20 TXLC:LASSDB were very similar to those for TXLC in figure 7.10 (a). The overall ranges of gas temperatures for LASSDB were 50 to 150 K less than those for TXLC depending on the HEX locations. Note that all of the flue gas

temperatures measured during tests for water HEX cases are about 100 to 200 K less than those for air HEX cases in the similar conditions.

In figure 7.10 (b), the water temperatures decreased since the growth of ash depositions on the surface of HEXs. The temperatures of the cold fluid (water) were much lower than those of the cold fluid (air) because of the high specific heat of water compared to air: between 300 and 330 K for water HEX cases while 650 and 1340 K for air HEX cases. There exit two distinct behaviors of water temperature difference ($T_{w,exit}$ - $T_{w,in}$) at the inlets and exits: increasing and decreasing. The water temperatures show the increasing temperature difference condition for each HEX in figure 7.10 (b). It causes the OHTC to increase while the decreasing temperature difference causes the OHTC to decrease. Because of the decreased heat input, the latter behavior was observed for the top HEX of the 80:20 TXLC:LASSDB case in figure 7.11. Results in figures 7.10 (a) and (b) indicate that heat transfer rate from the hot gas to the HEXs is very high due to colder water temperature; further the water temperatures for all fuels typically decreased with time, and the ranges of the water temperatures were between 300 and 330 K depending on the HEX locations. Prior to water flows into the HEXs, the HEXs are very hot. As the water flow starts, the water temperature is initially high. And then as time progresses, the HEX temperature starts decreasing coupled with decreasing the water temperature due to the growth of the ash depositions.

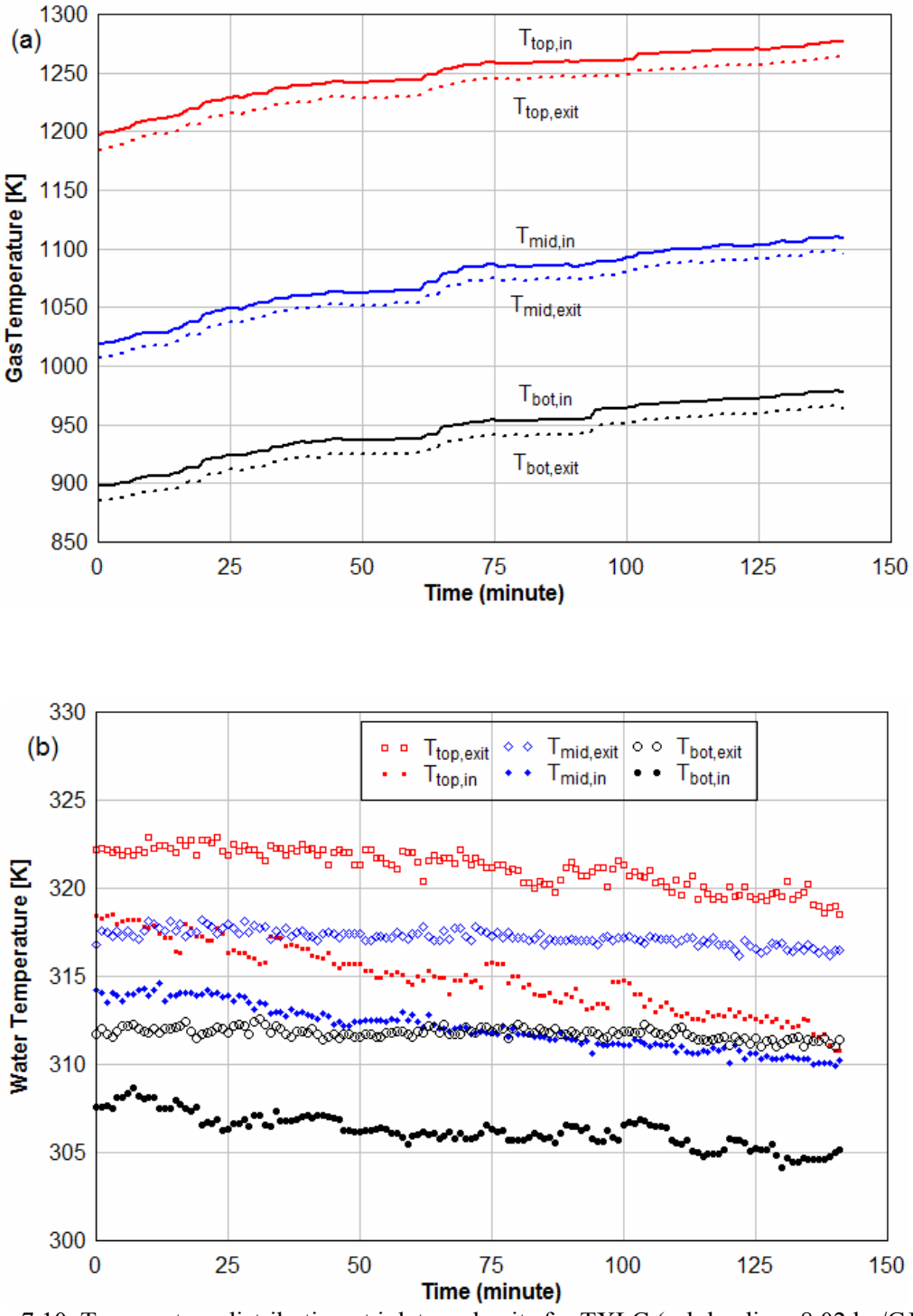

Figure 7.10. Temperature distribution at inlets and exits for TXLC (ash loading: 8.02 kg/GJ): (a) Flue gas temperature and (b) Water temperature in HEXs (Top: top HEX, Mid: middle HEX, and Bot: bottom HEX).

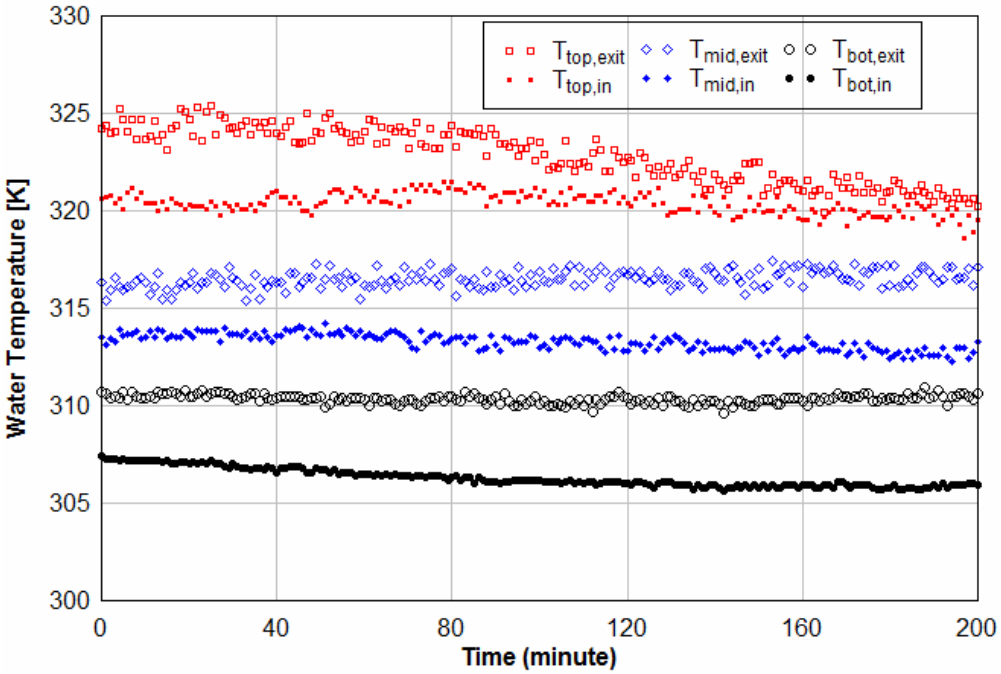

Figure 7.11. Temperature distribution at inlets and exits of water HEXs for 80:20 TXLC:LASSD (ash loading: 8.74 kg/GJ).

7.2.2. LMTD and OHTC

Log mean temperature differences (LMTD) were calculated using Eq. (5.11) for the top, middle and bottom water HEXs for cases firing TXLC as a reburn fuel, and the results are presented in figure 7.12. Because both increasing gas temperatures and decreasing water temperatures as a function of time as shown in figure 7.10, the LMTD increased, and the increasing rates were relatively similar for all cases. Unlike the water HEX cases, the decrease of the LMTD was observed for the air HEX cases because both gas and air temperatures increased. The LMTD for the water HEX cases was three times larger than that for the air HEX cases. The behaviors of the LMTD for 90:10 TXLC:LASSDB and 80:20 TXLC:LASSDB were very similar to those for TXLC. The overall variations of the LMTD for LASSDB were 50 to 100 K less than those for TXLC depending on the HEX locations.

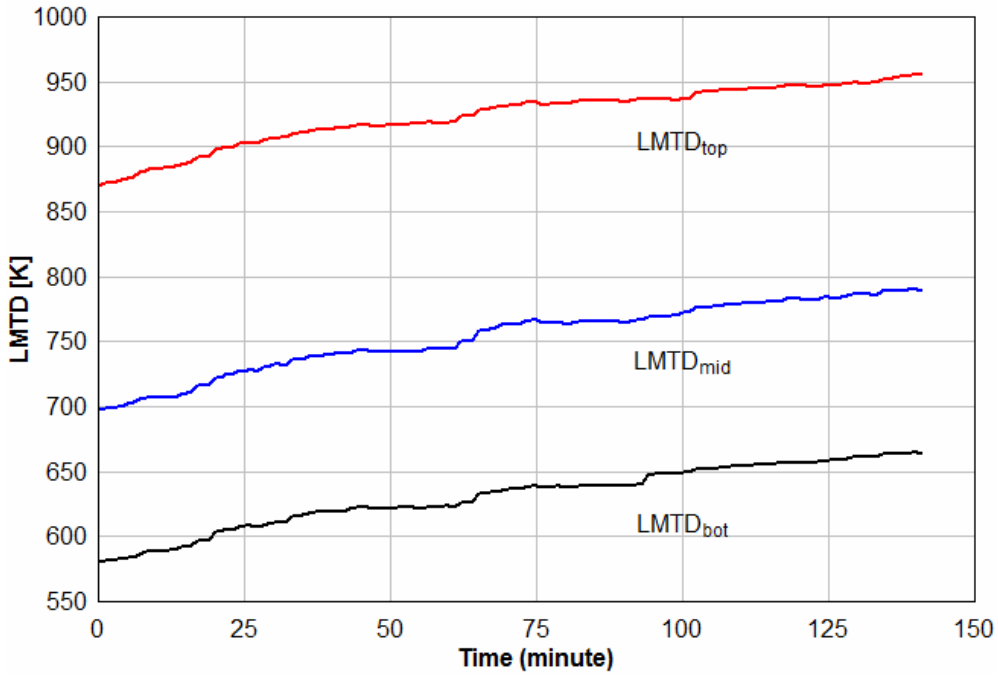

Figure 7.12. Log mean temperature differences (LMTD) for water HEXs using TXLC as a reburn fuel.

Figure 7.13. Ash depositions on bottom HEXs for several reburn fuels.

In figure 7.13, the extent of ash depositions on the bottom HEX for several reburn fuels were presented. The HEX was mostly covered by a powdered ash layer, and the ash layer was almost uniformly deposited on the HEX. Some of ash depositions dropped off from HEX surfaces when the HEXs were detached from the boiler burner at the end of experiments. Though the missing areas of ash layers were observed, the extent of ash depositions for LASSDB was still higher than the others. It is likely that the fuel with higher ash contents causes heavier ash deposition. Unlike the ash depositions on middle and bottom HEXs, a thin layer of solidified slag was formed on the surfaces of the top HEXs.

Overall heat transfer coefficients (OHTC) were calculated using Eq. (5.15) and presented in figure 7.14 for the bottom HEX with ash depositions using several reburn fuels. The typical range of the OHTC in the steady-state condition is between 10 and 100 $W/m^2 \cdot K$ as listed in Table 5.9. In the beginning without ash depositions, the range of the $OHTC_{bot}$ was between 100 and 140 $W/m^2 \cdot K$ which was little higher than the result of the steady-state condition. During the ash buildup, the $OHTC_{bot}$ decreased for LASSDB but increased for TXLC. For 90:10 TXLC:LASSDB and 80:20 TXLC:LASSDB the $OHTC_{bot}$ is almost flat. There are two competing effects: The increasing temperature causes the increase in OHTC, and the ash deposition causes the decrease in OHTC. For TXLC, the ash loading (8.02 kg/GJ) is small, so the effect of the gas temperature is dominant. For LASSDB, however, the effect of ash deposition is dominant because the ash loading (11.62 kg/GJ) is higher. The increase of the OHTC with the growth of ash depositions was observed since heat transfer rates to HEXs kept increasing during fuel combustion under the transient condition in which the gas temperatures increased. Further the high amounts of alkali metals (sodium, Na and potassium, K) in the ash of LASSDB caused the ash more sticky.

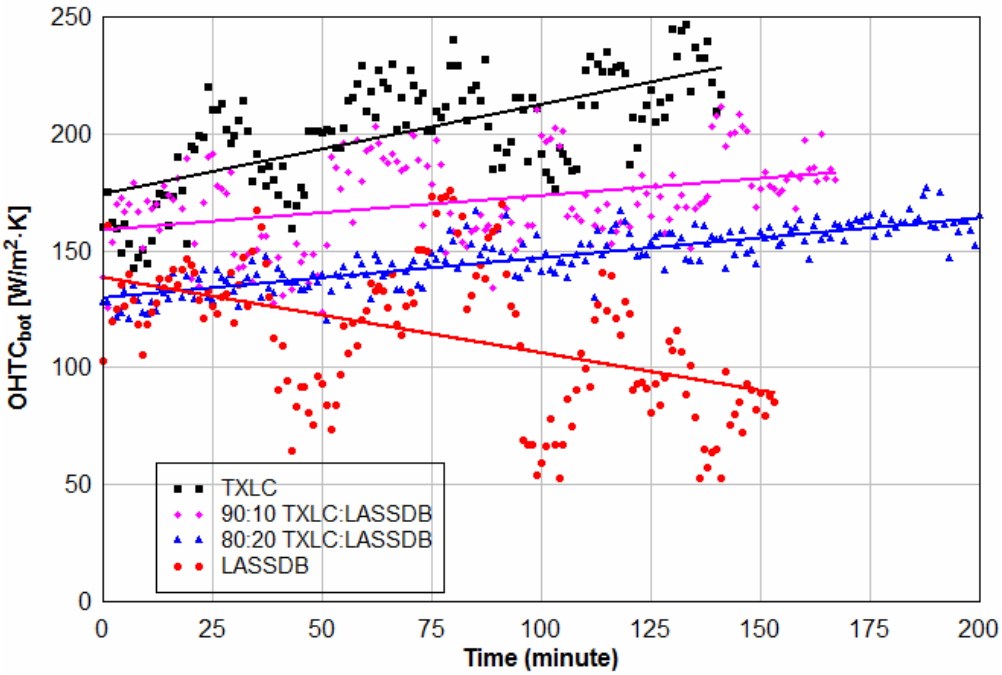

Figure 7.14. Overall heat transfer coefficient ($OHTC_{bot}$) for the bottom HEX in the cases of ash depositions using several reburn fuels.

Results of the OHTC were presented in figures 7.15 for the middle HEX and figure 7.16 for the top HEX in the cases of ash depositions. In the beginning without ash depositions, the $OHTC_{mid}$ and $OHTC_{top}$ ranged from 70 to 95 $W/m^2 \cdot K$ and 65 to 105 $W/m^2 \cdot K$, respectively, which were close to the results of the steady-state condition as listed in Table 5.9. During the ash deposition, all of the $OHTC_{mid}$ increased in figure 7.15 while both increase and decrease of the $OHTC_{top}$ were observed in figure 7.16. During the reburn tests in the presence of ash depositions, it was generally observed as $OHTC_{bot} > OHTC_{mid} > OHTC_{top}$ for each fuel. This is due to two different ash deposition behaviors: solidified slag and powdered ash depending on the combustion temperature. The thin layer of solidified slag was formed on the top HEXs while the powdered ash layer was formed on the middle and bottom HEXs. It was found the thin layer of the solidified slag had less thermal conductivity than that of the powdered ash layer.

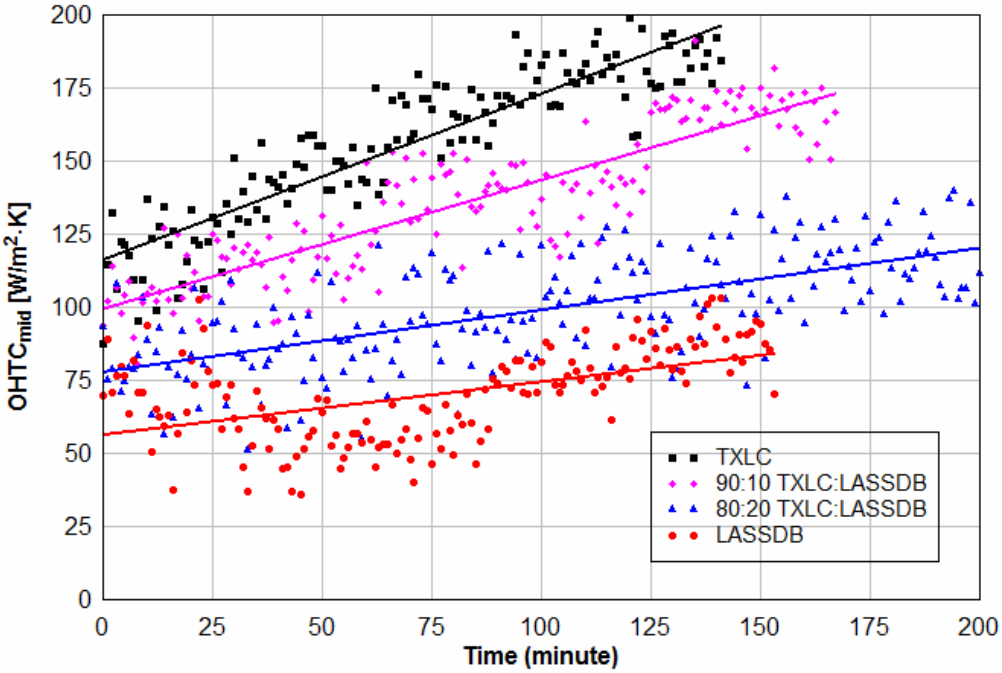

Figure 7.15. Overall heat transfer coefficient ($OHTC_{mid}$) for the middle HEX in the cases of ash depositions using several reburn fuels.

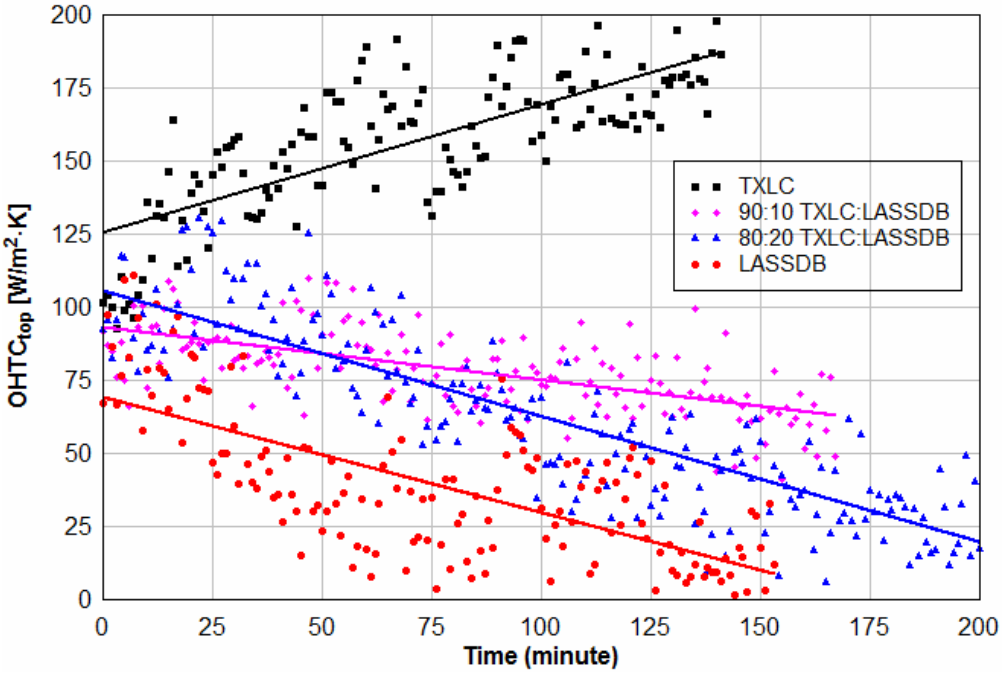

Figure 7.16. Overall heat transfer coefficient ($OHTC_{top}$) for the top HEX in the cases of ash depositions using several reburn fuels.

7.2.3. Ratio of OHTC

According to the results presented in figures 7.14 to 7.16, both increase and decrease of the OHTC were observed. Its decrease resulted in the effect of ash deposition; however, its increases occurred since the increased of the heat transfer rates to water HEXs during the transient and short-time operation. In order to observe the effect of the ash deposition, the ratio of the OHTC in the presence of ash depositions to the OHTC in the absence of ash depositions was determined. The results are presented in figures 7.17 to 7.19, and the OHTC ratios of all cases decreased with time. It indicated the thickness of the ash layer on HEXs increased with time, so that heat transfer to the HEXs decreased with the growth of ash depositions. The overall ranges of the OHTC ratios were TXLC > 90:10 TXLC:LASSDB > 80:20 TXLC:LASSDB > LASSDB. It resulted in higher ash loading in LASSDB than TXLC caused more ash deposition.

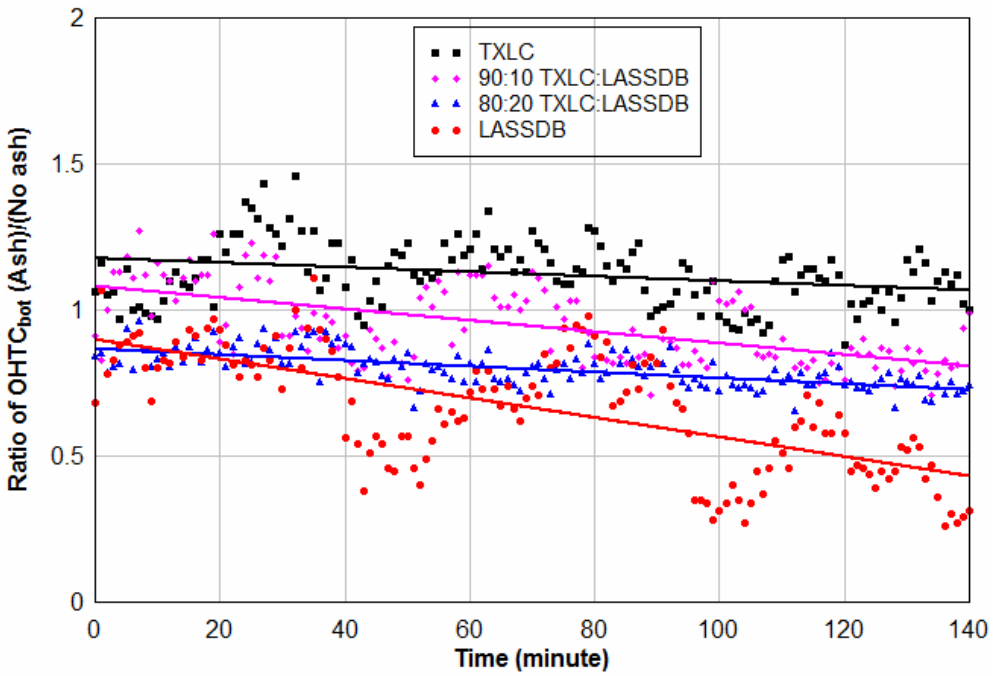

Figure 7.17. Ratios of $OHTC_{bot}$ (ash cases) to $OHTC_{bot}$ (no ash cases) for several reburn fuels.

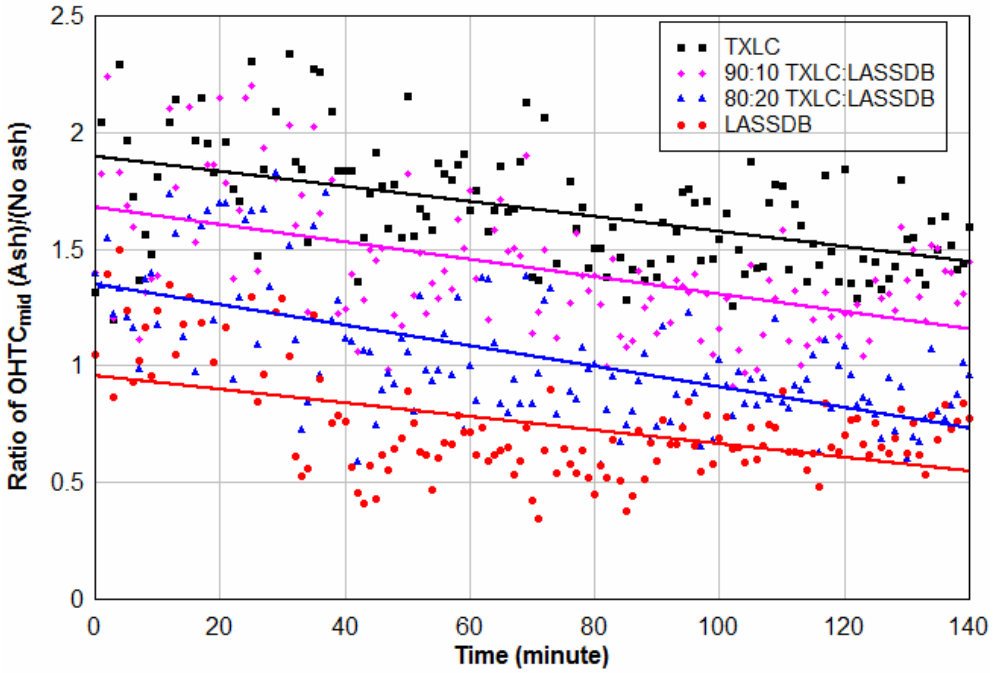

Figure 7.18. Ratios of $OHTC_{mid}$ (ash cases) to $OHTC_{mid}$ (no ash cases) for several reburn fuels.

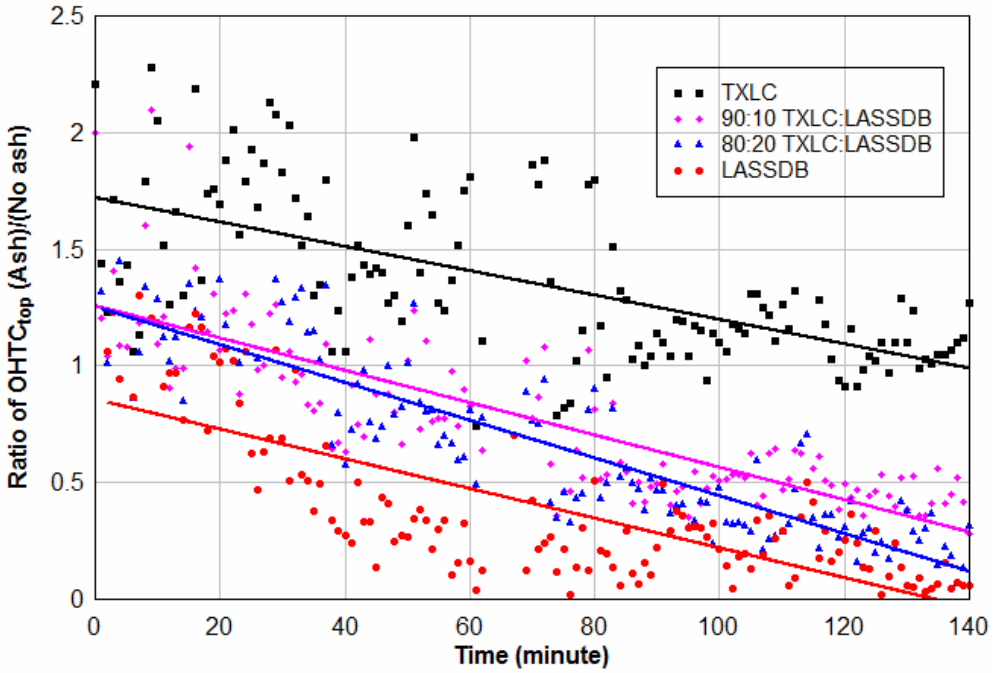

Figure 7.19. Ratios of $OHTC_{top}$ (ash cases) to $OHTC_{top}$ (no ash cases) for several reburn fuels.

7.2.4. Burnt Fraction and Combustible Loss

The proportions of moisture, ash, and combustibles for the reburn fuels are listed in Table 5.1. Proximate analysis shows that the combustibles in LASSDB and TXLC are very similar on a dry basis: 80.03% for LASSDB and 81.41% for TXLC. Burnt fraction (BF) and combustible loss were determined on a dry basis and presented in Table 7.3. The results show 97 to 100% BF and 0 to 3% combustible loss for all HEXs at ER_{RBZ} = 1.05. High BF was found in the fuel-rich condition due to the fuel particles on the HEX surfaces kept burning during combustion. Heavier ash depositions were formed during DB combustion than coal combustion. The BF results of the bottom ash were low since the bottom ash contained most of the heavy and big particles which lowered the combustion efficiency. It is found that the BF increased with an increase of the DB portion in reburn fuels. It is because DB has higher volatile matters (almost 80% on a DAF basis), and its particle sizes are smaller compared to TXLC.

Table 7.3. Ash analysis of DB fuels for burnt fraction (BF) and combustible loss.

Fuel	Ash Location	Burnt Fraction, BF (w%)	Combustible Loss (w%)
LASSDB	Top HEX	97.82	2.18
LASSDB	Mid HEX	97.84	2.16
LASSDB	Bot HEX	97.06	2.94
LASSDB	Bottom Ash	81.84	18.16
80:20 TXLC:LASSDB	Top HEX	98.06	1.94
80:20 TXLC:LASSDB	Mid HEX	98.49	1.51
80:20 TXLC:LASSDB	Bot HEX	98.32	1.68
80:20 TXLC:LASSDB	Bottom Ash	76.94	23.06
90:10 TXLC:LASSDB	Top HEX	99.69	0.31
90:10 TXLC:LASSDB	Mid HEX	99.44	0.56
90:10 TXLC:LASSDB	Bot HEX	99.20	0.80
90:10 TXLC:LASSDB	Bottom Ash	71.55	28.45
TXLC	Top HEX	98.56	1.44
TXLC	Mid HEX	98.50	1.50
TXLC	Bot HEX	97.83	2.17
TXLC	Bottom Ash	68.45	31.55

8. RESULTS ON MERCURY REDUCTION USING A FLOW REACTOR

In this section, the result of Hg emission from the bench-scale reburn boiler is evaluated, and the fundamental study of Hg oxidation or reduction using a flow reactor is investigated in homogeneous and heterogeneous conditions. The study of Hg reduction is the supplemental study to the biomass reburning.

8.1 Hg Reduction During Coal Combustion

Emission controls of mercury (Hg) using coal and biomass as fuels during co-firing were previously investigated, and the results were reported elsewhere [104]. The concentrations of gaseous total mercury (Hg^T) and elemental mercury (Hg^0) were measured, and the amounts of gaseous oxidized forms (Hg^{2+}) were calculated as the difference of Hg^T and Hg^0. Particle-bound forms (Hg_p) were not collected or analyzed in the study. Table 8.1 shows Hg emissions for coal combustion as a function of the equivalence ratio (ER). These results were adopted from Reference [104]. The typical range of Hg^T from the coal combustion was about 1.5 to 2.0 $\mu g/m^3$, and approximately 43 to 62% of Hg^T was oxidized. The results of blending fuels of coal and DB reported in Reference [104] increased the chlorine (Cl) content in the fuel and reduced Hg emissions during co-firing. It was suggested the presence of high ash content in the fuel provided great suitable site for the Hg oxidation. Large variations of Hg^T concentrations were observed during fuel-lean combustion while small variations were found at stoichiometry and fuel-rich conditions. It might be attributed that unburnt carbon adsorbed Hg during fuel-rich conditions while there is negligible unburnt carbon for the fuel-lean combustion.

Table 8.1. Hg emissions for coal combustion using a boiler.

Fuel	Equivalence Ratio, ER	Total mercury, Hg^T, [$\mu g/m^3$]	Elemental mercury, Hg^0, [$\mu g/m^3$]	Oxidized mercury, Hg^{2+}, [$\mu g/m^3$]
TXLC	0.8	1.8	1.0	0.8
	0.9	3.1	1.2	1.9
	1.0	1.9	0.8	1.1
	1.1	1.8	0.8	1.0
	1.2	1.7	0.7	1.0
WYC	0.8	1.6	0.9	0.7
	0.9	1.8	0.7	1.1
	1.0	1.5	0.6	0.9
	1.1	1.6	0.8	0.8
	1.2	1.4	0.8	0.6

8.2 Homogeneous Hg Oxidation

The Hg emissions using the coal-fired boiler were very low as shown in Table 8.1, and showed high experimental uncertainties because of very small amounts of Hg [ppb]. In order to understand the behavior of Hg oxidation with chlorinated compound, a fundamental study of the Hg chemistry was performed using a flow reactor in the homogeneous phase. Higher amount of Hg was simulated in the plug flow reactor (PFR) in order to reduce the errors of measurements and the experimental uncertainty. Several mixtures of chlorinated species, NO and O_2 were selected as shown in Table 4.4 and evaluated in the current study. The Hg compound formed includes HgCl, $HgCl_2$ and HgO. Typically the dominant oxidized form of Hg is $HgCl_2$. In the current study, only Hg^0 is measured; thus, the Hg oxidation is defined as the ratio of the amount of Hg^0 removed to the amount of Hg^0 supplied.

8.2.1 Cases *I* (NO), *II* (O_2), and *III* (NO + O_2)

The effects on Hg oxidation in the presence of NO (Case *I*), O_2 (Case *II*), and NO + O_2 (Case *III*) in the gas stream of N_2 were studied. The baseline concentration of Hg^0 was between 61 and 63 ppb at the reactor temperature of about 25ºC. Chlorine species such as HCl and Cl_2 were not used for these cases. The results of Hg emissions and oxidations were listed in Table 8.2. At 700ºC, the concentration of NO varied from 0 to 300 ppm for Case *I* and the concentration of O_2 varied from 0 to 5% for Case *II*. In the presence of both NO and O_2 for Case *III*, the NO concentration varied 0 to 300 ppm with the constant concentration of O_2 (3%). The residence time (RT) calculated at 700ºC was 0.16 *s* for all cases. The results shows that minor oxidations occurred for all cases, and the extents of Hg oxidation were less than 1% with an increase of NO or O_2 concentrations.

Table 8.2. Hg oxidation results for Cases *I*, *II*, and *III* with 0.16 *s* RT at 700ºC.

Case *I* 0 to 300 ppm NO		Case *II* 0 to 5% O_2		Case *III* 3% O_2 + 0 to 300 ppm NO	
NO [ppm]	Hg oxidation [%]	O_2 [%]	Hg oxidation [%]	NO [ppm]	Hg oxidation [%]
0	0.0	0	0.0	0	0.0
50	0.6	1	0.4	50	0.6
100	0.6	3	0.6	100	0.4
200	0.6	5	0.8	200	0.6
300	0.4	-	-	300	0.6

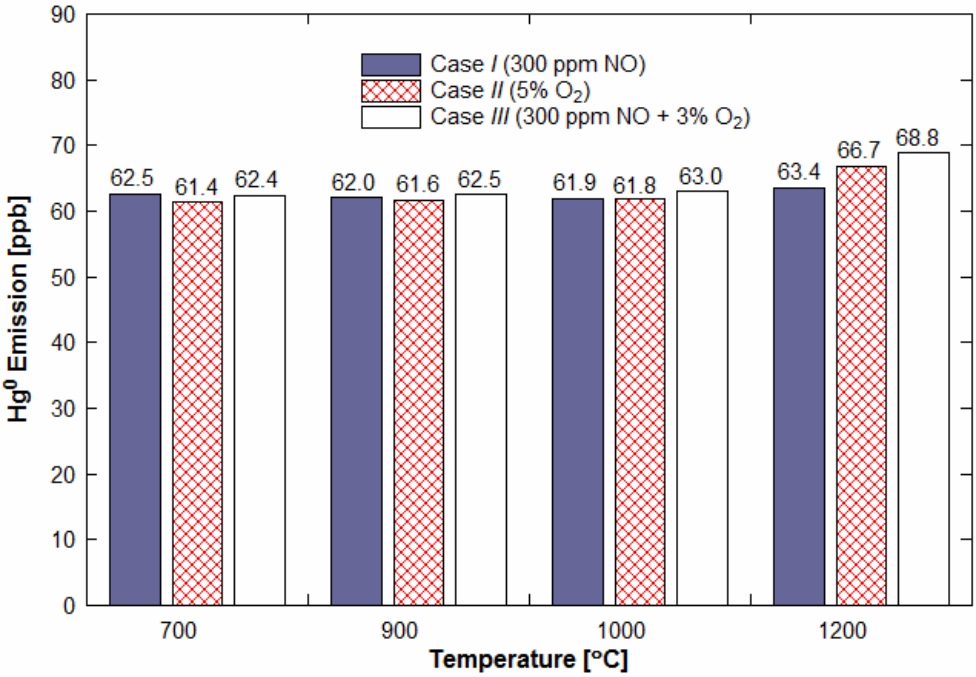

Figure 8.1. Hg emissions as a function of temperatures for Cases *I* (NO), *II* (O_2), and *III* (NO + O_2) with 0.16 *s* RT (Baseline Hg^0 = 61 – 63 ppb).

Hg emissions as a function of the reactor temperature for Cases *I*, *II* and *III* between 700 to 1200ºC are presented in figure 8.1. The effect of the temperature on Hg oxidation was within experimental scatter. The small increases in Hg emissions at 1200ºC were caused by the release

of Hg^0 deposited in the metal connectors or the transport tubes near the flow reactor. For the conditions in the absence of HCl, the homogeneous Hg oxidation in reactions (8.1) and (8.2) barely took place up to 1200ºC with NO concentrations up to 300 ppm or with O_2 concentrations up to 5%. Though the thermal decomposition of O_2 and NO typically occurs at high temperatures, the result shows minor effects on Hg oxidation below 1200ºC. The bond energy of O_2 and NO is known as 498 and 607 MJ/kmol, respectively. It was found that both NO and O_2 hardly reacted with Hg^0 directly.

$$Hg^o + NO \quad produces \quad HgO \tag{8.1}$$

$$Hg^o + O_2 \quad produces \quad HgO \tag{8.2}$$

8.2.2 Case *IV* (HCl)

Hg oxidation in the presence of HCl in the gas stream of N_2 was investigated. Table 8.3 shows the results of Hg emissions and oxidations as a function of the HCl concentration at 700ºC. The different RTs were estimated because of different flow rates. The level of HCl varied 0 to 90 ppm for the case with the total flow rate of 1100 SCCM, and 0 to 150 ppm HCl for the case with the total flow rate of 700 SCCM. In the case of 1100 SCCM, no oxidation was observed up to 70 ppm HCl, and about 17% Hg oxidation was found with 90 ppm HCl. For the case of 700 SCCM, about 14% Hg oxidation was found with 90 ppm HCl, and about 30% Hg oxidation was measured for HCl concentrations higher than 110 ppm. For both cases, Hg oxidation started with the addition of 90 ppm HCl which represented about 1.1×10^{-8} moles of HCl. The result is very similar to the results obtained by Ghorishi et al. [112]; the gas-phase oxidation by HCl took place at temperatures higher than 700ºC with HCl in the range of 100 to 200 ppm. According to

the results mentioned above, a certain amount of HCl is required to cause Hg oxidations. In the current cases, more than 90 ppm or 1.1×10^{-8} moles of HCl was required when no other gas presented in the system but HCl. The current result also shows the Hg oxidation increased with an increase of the concentration of HCl. The reactions of Hg + HCl were reported by Hall et al. [80], and their results presented significant increases in Hg oxidation with HCl concentrations from 0 to 150 ppm; however, oxygen presented in their stream. The Hg + HCl case by Hall et al. [80] is compared with the case of Hg + HCl + O_2 (Case *VI*) in the current study.

Table 8.3. Hg oxidation results for Case *IV (HCl)* at 700ºC (Baseline Hg^0 = 62.7 – 62.8 ppb).

700 SCCM with 0.26 *s* RT at 700ºC			1100 SCCM with 0.16 *s* RT at 700ºC		
HCl [ppm]	Hg measured [ppb]	Hg oxidation [%]	HCl [ppm]	Hg measured [ppb]	Hg oxidation [%]
0	62.8	0.0	0	62.7	0.0
50	62.5	0.4	30	63.1	0.0
90	53.9	14.2	50	63.4	0.0
110	44.5	29.1	70	63.9	0.0
130	44.7	28.7	90	51.8	17.3
150	44.0	29.9	-	-	-

Figure 8.2 shows effects of temperature on Hg oxidation in the presence of 50 ppm HCl for temperatures from 700 to 1200ºC, the RT of 0.16 *s* and the flow rate of 1100 SCCM. The results show the temperature had a significant effect on the Hg oxidation. Though no oxidation occurred below 700ºC, the Hg emissions decreased with an increase in the temperature higher than 700ºC, thus, more Hg oxidation took place at higher temperatures: 17% oxidation (52.7 ppb) at 900ºC, 24% (48.3 ppb) at 1000ºC, 55% (28.5 ppb) at 1100ºC, and 88% (7.9 ppb) at 1200ºC. The results show that not all Hg^0 was oxidized, and some of Hg^0 and HCl still remained in the system.

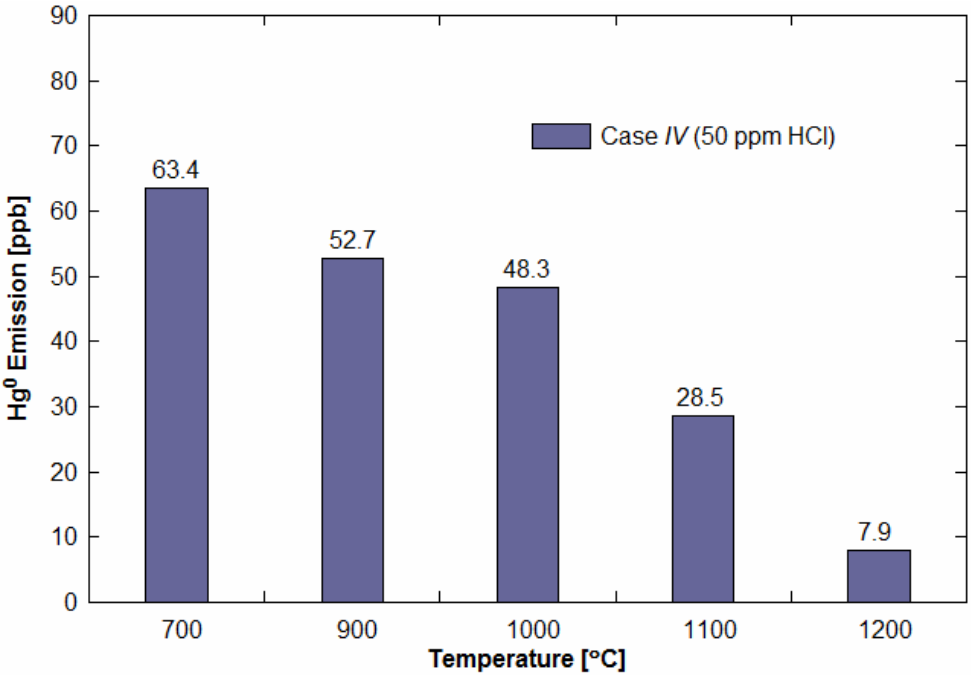

Figure 8.2. Hg emissions in the presence of 50 ppm HCl for Case *IV* in the conditions with the RT of 0.16 *s* and the flow rate of 1100 SCCM.

The reactions for Hg oxidations are summarized in Table 8.4. Since HCl was only chlorine species in the system in Case *IV*, the direct oxidation in reactions (8.3) and (8.4) should be considered. It is, however, reported that the reaction (8.3) is slow and unlikely to be important [80, 105, 112]. Because of the low production of HgCl by the reaction (8.3), the reaction (8.4) becomes unimportant for Case *IV*. Therefore, a possible mechanism of Hg oxidations in Case *IV* was that the thermal decomposition of HCl (bond energy: 432 MJ/kmol) produced chlorine atoms (HCl → H + Cl). The bond energy is less than that for O_2 and NO. The thermal decomposition of HCl was investigated at temperatures between 2500 and 4600 K [133, 134]; however, it is not well understood at temperatures lower than 2000 K. Using a plasma generator, the decomposition of HCl above 2000 K was achieved at least 95% on a mass basis by cooling the constituents to form H_2 and Cl_2 in the system downstream [135], and it was found that the

decomposition rate of HCl increased with an increase of the temperature. Radicals (i.e., atoms) are usually more reactive than stable species. Thus the H atoms react with HCl to produce more chlorine atoms (HCl + H → H_2 + Cl) [136]. Note that the bond energy of H_2 is 436 MJ/kmol comparable to HCl. The Cl atoms or species derived from HCl react with Hg species as shown in reactions (8.5) to (8.8). The reaction (8.5) is extremely rapid while the reactions (8.6) to (8.8) are slow.

Table 8.4. Detailed kinetic mechanisms, $k = AT^n \exp(-E_a/R \cdot T)$.

Reaction #	Reaction	A [cm^3/gmol·s]	n	E_a [J/mol]	Ref.
8.3	$Hg^o + HCl \rightarrow HgCl + H$	4.94×10^{14}	0	332000	[136]
8.4	$HgCl + HCl \rightarrow HgCl_2 + H$	4.94×10^{14}	0	90000	[136]
8.5	$Hg^o + Cl \rightarrow HgCl$	2.4×10^{8}	1.4	-60300	[136]
8.6	$Hg^o + Cl_2 \rightarrow HgCl + Cl$	1.39×10^{14}	0	142400	[136]
8.7	$HgCl + Cl \rightarrow HgCl_2$	2.19×10^{18}	0	13000	[136]
8.8	$HgCl + Cl_2 \rightarrow HgCl_2 + Cl$	1.39×10^{14}	0	4200	[136]

In Case *IV*, since no Hg oxidation was found below 700ºC and high Hg oxidations above 900ºC, it is suggested that the thermal decomposition of HCl occurred above 700ºC. The Hg oxidation was increased with an increase in temperatures because the thermal decomposition of HCl was increased with temperatures higher than 700ºC. The results in figure 8.2 show that HCl is very effective for Hg oxidation above 700ºC. According to the results, it is also suggested that Cl and Cl_2 are derived from HCl and key components in Hg oxidation during coal combustion. Because the reactions between HCl and other gas species during coal combustion are important, further investigations have been conducted as shown in the next section.

8.2.3 Case *V* (HCl + NO)

It is known that NO inhibits the homogeneous Hg oxidation by chlorine species when some other gas components (i.e. CO, CO_2, SO_2, H_2O, O_2, etc.) are presented in the gas stream [8]. In the current study, the effects of HCl + NO on Hg oxidation in the absence of other gas components were investigated in the conditions with the RT of 0.16 *s* and the flow rate of 1100 SCCM. The results of Hg emissions and oxidations are presents in Table 8.5 as a function of the gas concentration at 700ºC. In Case *V* (HCl + NO), the concentration of NO varied 0 to 300 ppm with 50 ppm HCl. The addition of 50 ppm NO increased Hg oxidation to about 35%; however, the Hg oxidation decreased with NO concentrations higher than 50 ppm. It indicated that Hg oxidation increased when NO was first added into the system; however, its high concentration inhibited Hg oxidation.

Table 8.5. Hg oxidation in Cases *V (HCl + NO)* with the RT of 0.16 *s* at 700ºC (Baseline Hg^0 = 62.4 ppb).

NO	Hg measured at exit	Hg oxidation
0 ppm	62.4 ppb	0.0 %
50 ppm	40.5 ppb	35.2 %
100 ppm	42.7 ppb	31.6 %
200 ppm	42.3 ppb	32.2 %
300 ppm	42.9 ppb	31.3 %

Figure 8.3 presents Hg emissions as a function of temperatures for Case *V* with 50 ppm HCl and 300 ppm NO. For temperatures up to 600ºC, the changes in the concentration of Hg^0 were less than about 3%. In contrast, high oxidations of Hg were found to be about 31% (43.3 ppb) at 800ºC, 50% (31.6 ppb) at 1000ºC, and 86% (8.5 ppb) at 1200ºC. The Hg oxidation significantly increased with an increase in temperatures when the temperatures are higher than 600ºC.

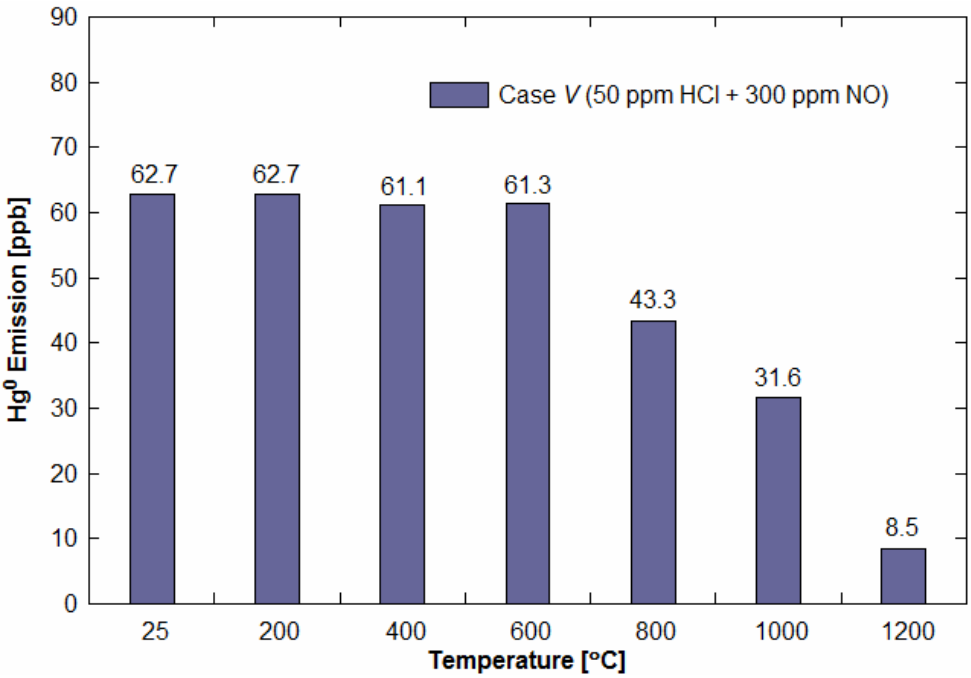

Figure 8.3. Hg emissions for Cases *V* (HCl + NO) in the conditions with the RT of 0.16 *s* and the flow rate of 1100 SCCM (Baseline Hg^0 = 62.7 ppb).

The comparison results of Cases *V* (HCl + NO) and *IV* (HCl) show that Hg oxidation started between 600 and 800ºC in Case *V* which was a lower temperature range than that of Case *IV* (700 and 900ºC). Since the thermal decomposition of HCl occurred at temperatures higher than 700ºC, it stimulated Hg oxidation first. Higher oxidations are found for Case *V* than Case *IV*; therefore, the addition of the NO concentration (300 ppm) in Case *V* promoted the Hg oxidation. It is probably because the reaction (8.9) produces Cl atoms and reduces some of NO emissions. Therefore, the production of Cl atoms was more in Case *V* (HCl + NO) than Case *IV* (HCl). The thermal decomposition of HCl and the production of Cl atoms by the NO addition caused more Hg^0 to be oxidized compared to Case *IV*.

$$HCl + NO \rightarrow HNO + Cl \tag{8.9}$$

8.2.4 Case *VI* (HCl + O_2)

The effects of O_2 on Hg oxidation in the presence of 50 ppm HCl in the gas stream of N_2 were studied in the conditions of the RT of 0.16 *s* and the flow rate of 1100 SCCM. Table 8.6 shows the results of Hg emissions and oxidations as a function of the gas concentration at 700ºC. In Case *VI* (HCl + O_2), the level of O_2 varied 0 to 5% with 50 ppm HCl. Approximately 34% Hg oxidation was found by the addition of 1% O_2. The Hg oxidation was increased with an increase of the concentration of O_2. About 40% oxidation was found in the presence of 5% O_2. Hg oxidations by the addition of various HCl concentrations with 10% O_2 were studied [80]. The results showed about 30% oxidation in the presence of 50 ppm HCl and 10% O_2 at 500ºC. The current results showed higher Hg oxidation such as 40% in the presence of 50 ppm HCl and 5% O_2 at 700ºC. The higher oxidation was reasonable due to the temperature was higher for the current case.

Table 8.6. Hg oxidation in Cases *VI (HCl + O_2)* with the RT of 0.16 *s* at 700ºC (Baseline Hg^0 = 61.7 ppb).

O_2	Hg measured at exit	Hg oxidation
0 %	61.7 ppb	0.0 %
1 %	40.6 ppb	34.2 %
3 %	38.0 ppb	38.3 %
5 %	36.9 ppb	40.1 %

Figure 8.4 presents the results of Hg emissions for Case *VI* as a function of the temperature. Hg oxidations increased with an increase of the temperature: about 12% (55.8 ppb) at 400ºC, 18% (51.9 ppb) at 600ºC, 36% (40.3 ppb) at 800ºC, 54% (29.3 ppb) at 1000ºC, and 92% (5.2 ppb) at 1200ºC. Some $HgO_{(s)}$ deposits appeared in the entrance tube of the Hg vapor monitor indicating the contribution of HgO in Hg oxidation.

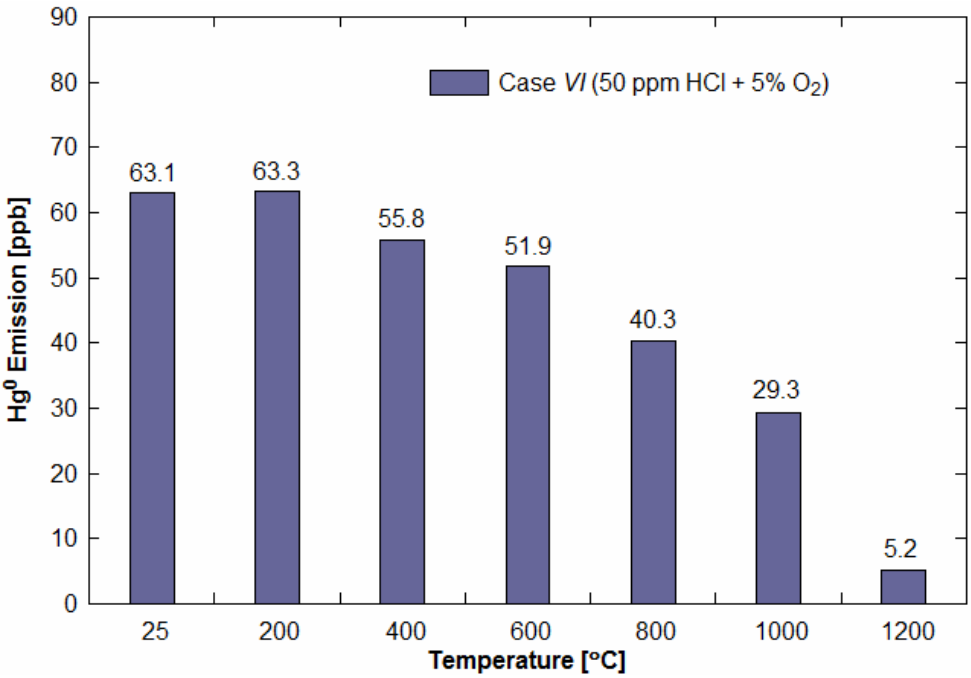

Figure 8.4. Hg emissions for Cases *VI* (HCl + O_2) in the conditions with the RT of 0.16 *s* and the flow rate of 1100 SCCM (Baseline Hg^0 = 63.3 ppb).

The comparison of results for Cases *IV* (HCl) and *VI* (HCl + O_2) shows that the high Hg oxidation first appeared at 400ºC in Case *VI* which was lower temperature than that of Case *IV* (900ºC). Therefore, the reactions between HCl and O_2 in Case *VI* took place at temperatures higher than 400ºC, and the thermal decomposition of HCl helped the Hg oxidation at the temperatures higher than 700ºC. The results suggested that the reaction between HCl and O_2 expressed in the reaction (8.10) produced chlorine species and OH radicals, and the reaction (8.11) participated to produce Cl atoms. The reaction (8.11) is very fast; A is 2.71×10^7 cm^3/gmol·s and E_a is -921 J/mol [136]. Therefore, the production of chorine species is expected more in Case *VI* (HCl + O_2) than both Cases *V* (HCl + NO) and *IV* (HCl). The production of HgO in Case *VI* contributed to the increase of the Hg oxidation as shown in reaction (8.12). The direct reaction by HCl in reaction (8.13) was also favorable to Hg oxidation [80]. About 30%

more oxidation at 1000ºC and 4% more oxidation at 1200ºC were found for Case *VI* than Case *IV*. Both the thermal decomposition of HCl and the reactions between HCl and O_2 increased Cl atoms, and thus more Hg oxidation. The results show the addition of O_2 shifted the reaction temperature lower from 900 to 400ºC. The Hg^0 appears to be oxidized when the reactor temperature reached 400ºC for Case *VI* while 800ºC for Case *V*. The Hg oxidations in the range of temperatures investigated were higher for Case *VI* than Case *V*. Due to high Hg oxidation and lower reaction temperatures, it was concluded that O_2 was more effective to produce Cl atoms than NO.

$$HCl + O_2 \rightarrow ClO + OH \tag{8.10}$$

$$HCl + OH \rightarrow Cl + H_2O \tag{8.11}$$

$$Hg^0 + ClO \rightarrow HgO + Cl \tag{8.12}$$

$$2Hg^0 + 4HCl + O_2 \rightarrow 2HgCl_2 + 2H_2O \tag{8.13}$$

8.2.5 Case *VII* (HCl + NO + O_2)

The study of Hg oxidation in the presence of HCl, NO and O_2 were performed for Case *VII*. Figure 8.5 shows Hg emissions as a function of time for the temperatures from ambient (25ºC) to 1200ºC in the presence of 50 ppm HCl, 300 ppm NO and 3% O_2 with the RT of 0.16 *s* and the flow rate of 1100 SCCM. The baseline concentration of Hg^0 at the ambient temperature was about 540 μg/m^3 (65.6 ppb). Hg emissions were reduced to about 480 μg/m^3 (58.4 ppb) at 600ºC, 465 μg/m^3 (56.7 ppb) at 800ºC, 380 μg/m^3 (46.6 ppb) at 1000ºC, and 19 μg/m^3 (2.3 ppb) at 1200ºC. The oxidation at 600ºC did not appear immediately due to the time delaying of the reactor heating. The temperature shows a significant effect on Hg emission in the presence of

HCl, NO and O_2. The Hg emission was decreased with an increase of the temperature. High Hg oxidation first appeared at 600ºC. It is found that Hg oxidations in Case *VII* were higher than Hg oxidations in Case *IV* (HCl) in the whole range of the temperature. The thermal decomposition of HCl occurred at the temperatures higher than 700ºC as mentioned above. The reactions among HCl, NO and O_2 as shown in reactions (8.9) to (8.12) are expected to produce Cl atoms at the temperatures higher than 600ºC.

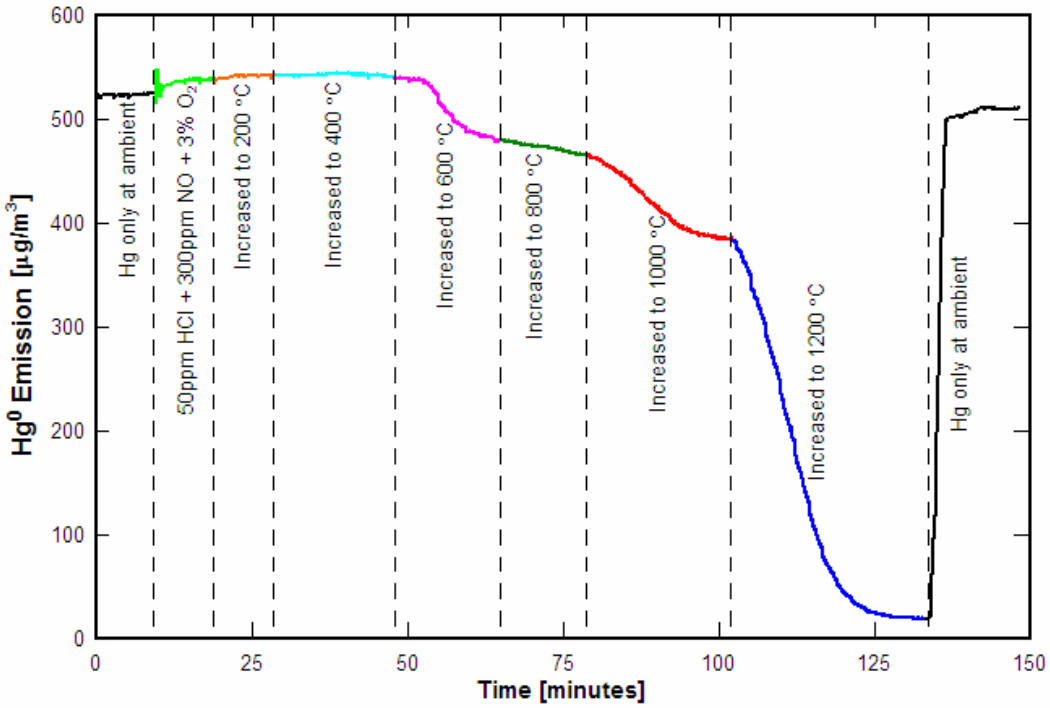

Figure 8.5. Hg emissions for Case *VII* (HCl + NO + O_2) in the conditions with the RT of 0.16 *s* and the flow rate of 1100 SCCM.

Figure 8.6 presents all of the results on Hg oxidation in the presence of HCl. High Hg oxidation first appeared at 900ºC for Case *IV* (HCl), at 800ºC for Case *V* (HCl + NO), at 400ºC for Case *VI* (HCl + O_2), and at 600ºC for Case *VII* (HCl + NO + O_2). Comparing the results of Cases *VI* (HCl + O_2) and *VII* (HCl + NO + O_2), the addition of NO inhibited the overall reaction,

and thus the Hg oxidation was observed at 600ºC. NO also inhibited the Hg oxidation at all temperatures. The addition of NO shifted the reaction temperature higher from 400 to 600ºC. The inhibition of Hg oxidation by NO is a well-known effect in the gas stream in the presence of other gas components (e.g. H_2O, O_2, SO_2, and CO_2) [74]. In the current case, the reactions causing the inhibition are suggested in reaction (8.14) for reducing OH radicals, and hence chlorine species. The three-parameter Arrhenius form of the reaction (8.14) is A = 1.3 × 10^4 m^3/kmol·s, n = 1.88, and E_a = -4003 kJ/kmol [136].

$$HNO + OH \rightarrow H_2O + NO \tag{8.14}$$

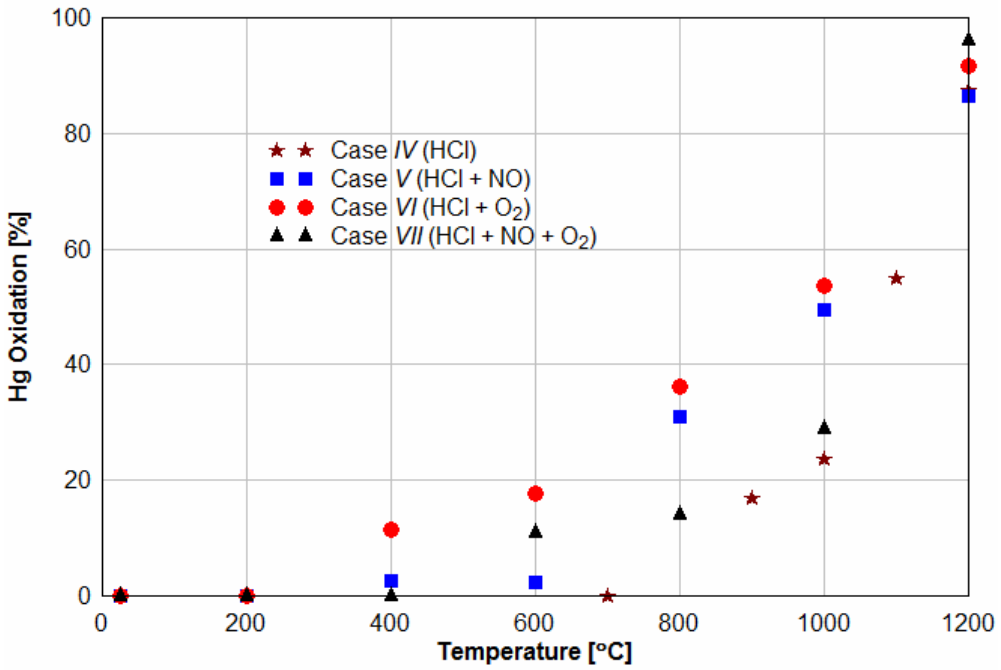

Figure 8.6. Results of Hg oxidation for all cases in the presence of HCl in the conditions with the RT of 0.16 s and the flow rate of 1100 SCCM.

Based on the comparison results between Cases *V* (HCl + NO) and *VII* (HCl + NO + O_2), the addition of O_2 promoted the overall reaction and Hg oxidation. The addition of O_2 lowered the reaction temperature from 800 to 600ºC. At 1200ºC in all cases in the presence of HCl, the results of Hg oxidations were found between 86% and 97%. Therefore, the optimum temperature for Hg oxidation can be near 1200ºC since the temperatures higher than 1200ºC will cause other emission problems in coal-fired combustors such as the production of thermal NO_x.

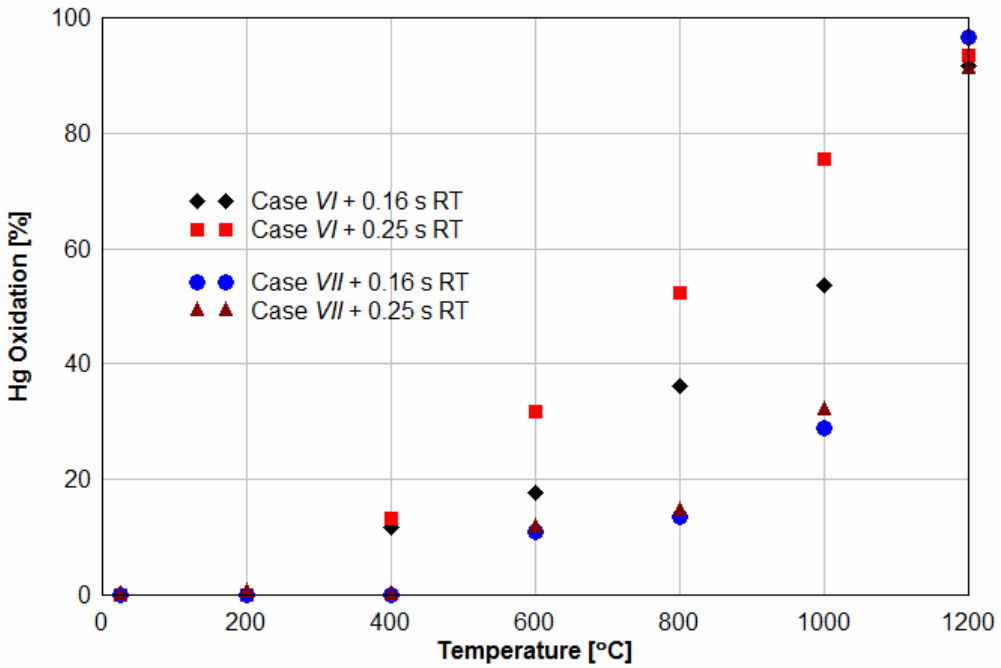

Figure 8.7. Hg oxidations as a function of temperatures for the different residence times with 1100 SCCM: (a) Case *VI* (HCl + O_2) and (b) Case *VII* (HCl + NO + O_2).

8.2.6 Effects of Residence Time (RT)

In figure 8.7, the effect of the RT on Hg oxidations was examined as a function of the temperature with the total flow rate of 1100 SCCM. The RT at 700ºC was estimated as 0.16 *s* when heating zones 2 & 3 are activated and 0.25 *s* when all three heating zones are activated.

The longer RT promoted Hg oxidations in all ranges of the temperature. The extent of the increase was greater for higher temperatures such as 600, 800 and 1000ºC. The longer RT provided enough time for the reactions among gas components and the thermal decompositions of HCl, and hence high Hg oxidations. For Case *VII* (HCl + NO + O_2) in figure 8.7 (b), small increases were observed, and it resulted in the inhibition effect of NO was stronger than the effect of RT on Hg oxidation. Regardless of the residence time, the Hg oxidations were first observed at 400ºC for Case *VI* and at 600ºC for Case *VII*. The increase of the RT helped to promote Hg oxidations, but caused no effect on the temperature corresponding to the oxidation.

8.2.7 Chemical Equilibrium Calculation

Since the Cl atom is key species for Hg oxidation, the high production of Cl atoms is required to achieve high Hg oxidation. It has been shown that the reaction of Cl atom and Hg^0 expressed in the reaction (8.5) is extremely rapid [136, 137]. Further Cl atom can be produced by the reactions of HCl and OH radical. In the current study, chemical equilibrium calculations [138] were performed to determine concentrations of Cl atoms and OH radicals for several cases: Case *IV* (HCl), Case *V* (HCl + NO), and Case *VI* (HCl + O_2). Figure 8.8 shows the results of equilibrium calculations for Case *IV* as a function of temperatures. Minor changes were observed until 800ºC; however, above 800ºC the concentrations of chlorine species (Cl and Cl_2) increased while the amounts of HCl decreased. The concentrations of the Cl and Cl_2 increased to a maximum of 26 ppb and 6 ppb at 1200ºC, respectively. Thus for Case *IV* (62 ppb Hg^0 and 50 ppm HCl), the reaction ($Hg + 2Cl \rightarrow HgCl_2$) will yield and hence about 31% Hg oxidation will occur. Though the measurement of chlorine species was not performed during the experiments, the indirect comparisons can be noted. If the RT used in the experiments are too short to reach the equilibrium condition, the extent of the production and reduction of the chlorine species

shown in the calculation results can be higher than those in the experimental results. If the kinetics suggests the RT used in the experiments are long enough, then the equilibrium may be reached.

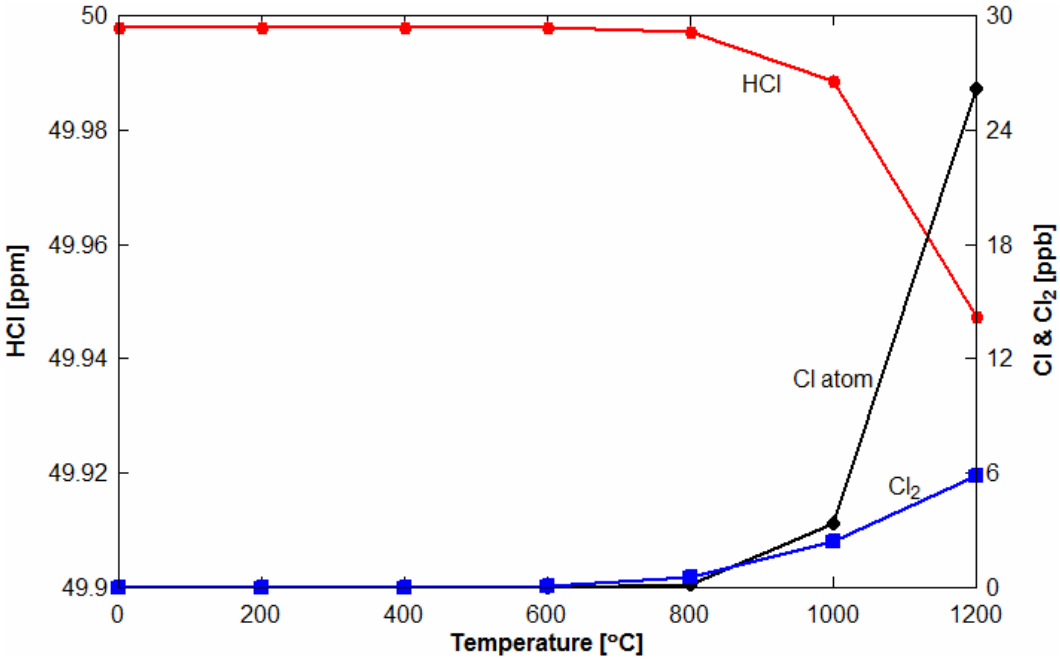

Figure 8.8. Calculation results in the condition of the chemical equilibrium for Case *IV* (HCl).

$$HCl + M \leftrightarrow H + Cl \tag{8.15}$$

$$HCl + H \rightarrow H_2 + Cl \tag{8.16}$$

A simple kinetic study was performed using reaction rates of reactions (8.15) and (8.16). These two reactions are suggested as the main precursory reactions to cause the Hg oxidation in Case *IV* (HCl) in the current study. The reaction (8.15) represented the thermal decomposition of HCl. Its reaction rate used for the kinetic calculation was adopted from elsewhere [133]. The Arrhenius form of the reaction (8.16) is A = 1.69×10^{10} m^3/kmol·s and E_a = 17333 kJ/kmol

[136]. The results of the calculation were presented in figure 8.9 as a function of time at 1200ºC. Approximately 20 ppb of Cl atoms was produced after 30 seconds when the reaction started at 1200ºC. Thus, more than 30 seconds of reaction time is required to reach 26 ppb obtained by the equilibrium calculation. Based on the results of the kinetic calculation, the production of the chlorine atoms during the experiments with the RT of 0.16 or 0.25 *s* was much lower than the results of the equilibrium calculation.

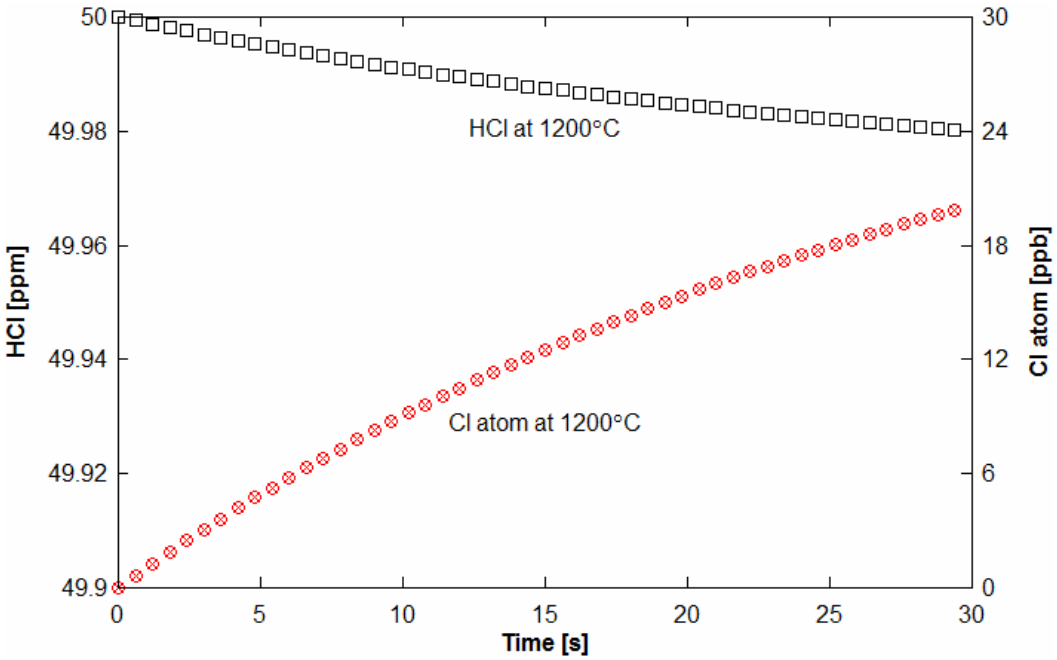

Figure 8.9. Calculation results using the reaction rates of Case *IV* (HCl) at 1200ºC.

Unlike Case *IV* (HCl), for Cases *V* (HCl + NO) and *VI* (HCl + O_2), enough oxygen atoms were available to produce OH radicals which can increase the concentration of Cl atoms. Figure 8.10 shows the results of equilibrium calculations [138] in the production of Cl atoms for Cases *V* and *VI* at various temperatures. The results show significant increases of Cl atoms probably because of the reactions of HCl and OH radicals expressed in the reaction (8.11). At 1200ºC, the

concentration of Cl atom was about 13 ppm for Case *V* and 26 ppm for Case *VI*. For all ranges of the temperature, the concentrations of Cl atom in Case *VI* were higher than those in Case *V*. Since higher level of Cl atom can cause higher Hg oxidation, the Hg oxidation for Case *VI* can be higher than that for Case *V*.

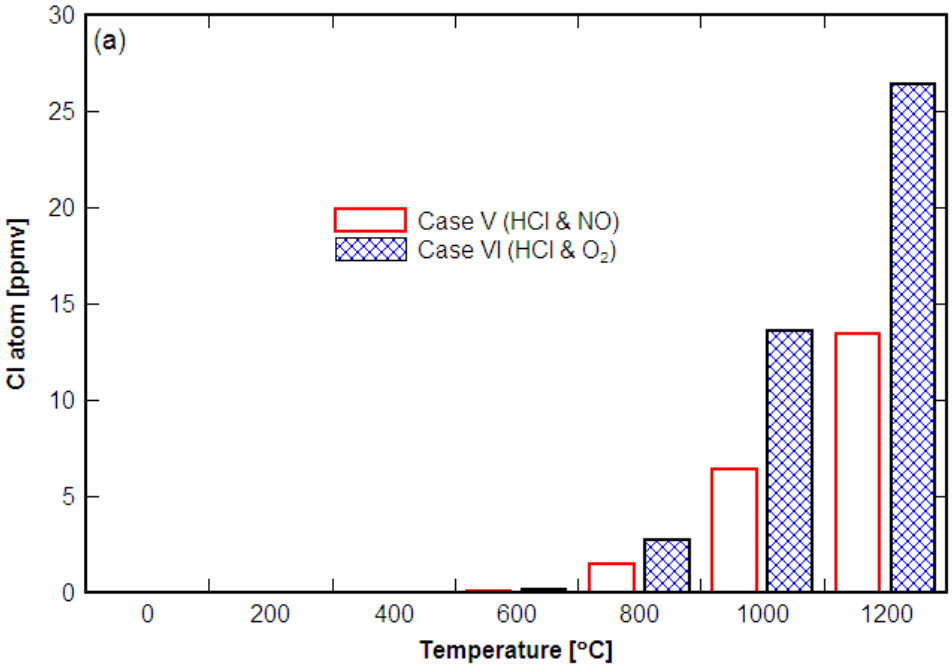

Figure 8.10. Calculation results in the condition of the chemical equilibrium for Case *V* (HCl + NO) and Case *VI* (HCl + O_2).

8.3 Heterogeneous Hg Reduction Using a Catalyst

8.3.1 Case *VIII* (HCl), *IX* (HCl + O_2) and *X* (HCl + NO + O_2)

Heterogeneous reactions in Hg reduction or capture were investigated using the VWT honeycomb monolithic catalyst. The VWT catalyst was placed in the middle of the center heating zone of the flow reactor. The residence time of 0.25 s, the space velocity of 70000 h^{-1}, the total flow rate of 1100 SCCM, the baseline Hg^0 concentration of 50 μg/m^3 (6 ppb), and the temperature range of 25 to 400ºC were prepared for the tests. The phenomena of absorption and emission of the VWT catalyst using ammonia were reported elsewhere [116]. The effect of Hg capture was observed during the current tests. About 60 to 70% of the baseline concentration of Hg^0 was captured and stored at the ambient temperature for all cases tested. The re-emission of Hg^0 stored in the catalyst was not observed during the total period (about 100 hours) of experiments.

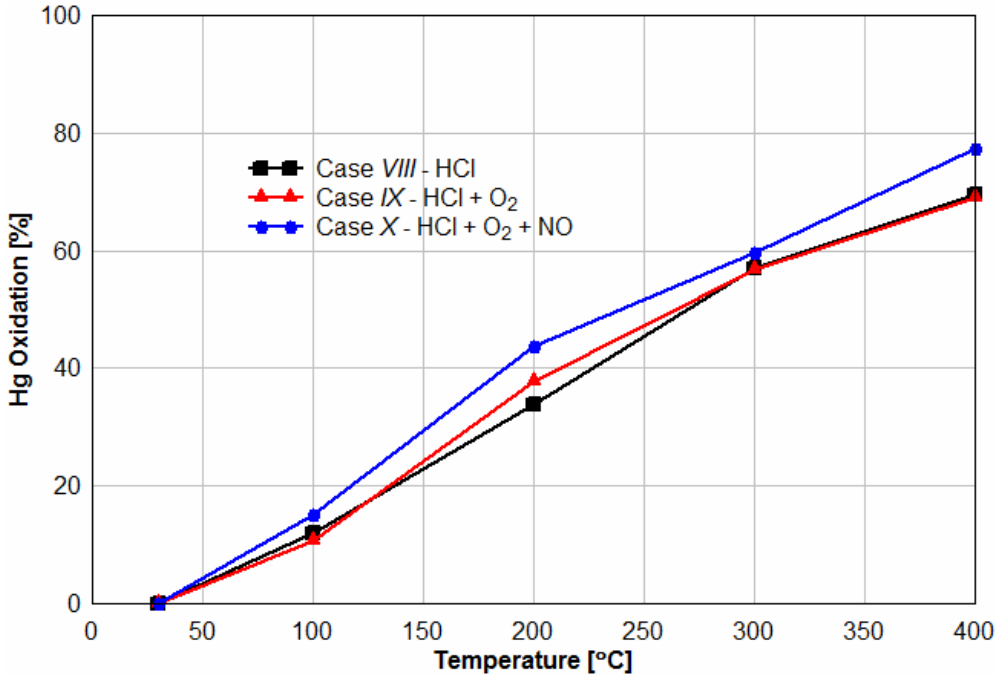

Figure 8.11. Results of Hg oxidation in heterogeneous reactions with the VWT catalyst in the conditions with the RT of 0.25 s and the flow rate of 1100 SCCM.

The results of heterogeneous reactions are presented in figure 8.11 for Cases *VIII* (HCl), *IX* (HCl + O_2) and *X* (HCl + NO + O_2). The extent of Hg reductions for all cases was relatively similar. The Hg reductions were found to be about 11 to 15% at 100ºC, 34 to 45% at 200ºC, 57 to 60% at 300ºC, and 69 to 77% at 400ºC. The results in Case *X* showed the highest Hg reduction, and thus it seemed that the catalytic effect was very strong and overcame the inhibition effect by NO. The use of the VWT catalyst promoted the reduction of Hg^0 and shifted the effective temperature lower than the homogeneous cases.

9. CONCLUSIONS AND FUTURE WORKS

In this final section, the conclusions of biomass reburning, fouling and Hg oxidation are summarized and emphasized. Furthermore, it includes recommendations for future researches.

9.1 Conclusions

9.1.1 Biomass Reburning on NO_x Reduction

NO_x reduction studies using a bench-scale 30 kW (100,000 BTU/h) boiler burner facility with coal and cattle biomass (CB) as reburn fuels were conducted. The major findings of the current research are summarized below:

1. The extent of NO_x reduction is function of types of the reburn fuel, ER_{RBZ}, O_2 concentrations in the reburn gas, injection angles of the reburn fuel, cross-sectional geometries of the reburn nozzles, symmetric and asymmetric reburn injections, reburn heat inputs, baseline NO_x concentrations, presence and absence of the HEXs.
2. The significance of each parameter is listed in the order of the significance on NO_x reduction: (1) ER_{RBZ}, (2) Types of the reburn fuel, (3) Reburn heat inputs, (4) Presence and absence of the HEXs, (5) Symmetric and asymmetric reburn injections, (6) Cross- sectional geometries of the reburn nozzles, (7) Baseline NO_x concentrations, (8) Injection angles of the reburn fuel, and (9) O_2 concentrations in the reburn gas.
3. The results showed that CB was a very effective fuel in NO_x reduction during reburning since the reburning with pure biomass achieved about 96% NO_x reduction at ER_{RBZ} = 1.1 while blended fuels resulted in 80% (80:20 TXLC:LASSDB) and 64% (90:10 TXLC:LASSDB). TXLC only achieved 48% at ER_{RBZ} = 1.1.

4. The use of 12.5% O_2 concentration in the reburn gas for the vitiation cases decreased combustion temperatures, caused better mixing, decreased the O_2 concentration, and decreased the rate of oxidizing of N compounds and hence high NO_x reductions.
5. Among several tested configurations of the reburn injection (0° and 45°, circular and oval, symmetric and asymmetric), the 45° upward injection provided longer residence time and better mixing, hence the highest reduction of NO_x emissions. The results by using the circular reburn nozzles showed higher NO_x reductions than those of oval cases. The results of the symmetric cases also showed higher NO_x reductions than those of asymmetric cases.
6. It was found that NO_x emissions with the presence of HEXs were lower than those with absence of HEXs probably due to the catalytic effect of the fly ash.
7. Higher NO_x reductions were obtained for higher reburn heat input. Considering the fouling problems caused by the high reburn heat input, the 20% heat input was considered to be better than the 30% heat input for the long-time operation.
8. High NO_x reductions were obtained with the baseline NO_x emissions higher than 275 ppm (or 230 g/GJ and 0.5 lb/mmBTU) while NO_x formations took place with the baseline NO_x of 125 ppm (or 105 g/GJ and 0.24 lb/mmBTU). The baseline NO_x level should be carefully considered for designing boilers particularly with low-NO_x burners.
9. Burnt fractions increased with the increase of the proportion of CB in reburn fuels because CB had higher volatile matter and its particle sizes were smaller compared to TXLC.
10. According to the results mentioned all of above, the optimum conditions of the boiler operation for biomass reburning are recommended as follows: ER_{RBZ} = 1.1, 45° upward circular reburn nozzles, 12.5% O_2 in the reburn gas, symmetric injection, and presence of HEXs. In order to make an effective reburn process, the baseline NO_x concentrations must be higher than 230 g/GJ (0.5 lb/mmBTU) and the reburn heat input higher than 20%.

9.1.2 Fouling Study

A study of the fouling potential in coal-fired boilers was conducted during biomass reburning under the transient and short-time operations. The results are summarized as follows:

1. A diagnostic method for the study of the ash fouling behavior in transient boiler operations was developed.
2. The presence of ash in the hotter parts of the furnace seemed to promote heat radiation from burning particles thus augmenting the heat transfer rate to HEXs.
3. The growth of the ash layer on the HEX surfaces over longer periods typically lowered the OHTC.
4. Ash analysis was performed using the bottom ash. The results showed lesser percentage of combustibles with higher percentage of CB in the blended fuels indicating better BF.
5. The results indicated almost 100% BF were detected for the samples from all HEX surfaces since the fuel particles on the surface kept burning during the combustion.
6. The behavior of the ash fouling was ranked as follows: LAPCFB (severe) > 70:30 TXLC:LAPCFB > 90:10TXLC:LAPCFB > TXLC (low).
7. The use of water instead of air decreased the gas temperatures about 100 to 200 K in the similar conditions. The changes of the OHTC were clearly observed with water HEXs.
8. The OHTC decreased as a function of time by about 26 – 33% with air cooled HEXs and about 17 – 82% with water cooled HEXs, and the highest reduction of the OHTC was observed for the bottom HEX.

9.1.3 Hg Reduction

A fundamental study of homogeneous and heterogeneous Hg reduction/oxidation was conducted using a plug flow reactor (PFR). The results are summarized as follows:

1. Homogeneous Hg oxidations barely took place in the absence of chlorine-containing species while the addition of HCl significantly increased Hg oxidations.
2. A certain amount of HCl (more than 90 ppm or 1.1×10^{-8} moles) was required to cause Hg oxidations when only HCl, N_2 and Hg were presented in the system.
3. Hg oxidation increased when NO or O_2 was first added into the system, but the further addition of high NO concentrations inhibited Hg oxidation. The addition of NO inhibited the overall reaction and shifted the reaction temperature higher while the addition of O_2 promoted Hg oxidations and lowered the reaction temperature.
4. Hg emissions decreased with an increase in the temperature indicating that more oxidation took place when the temperature was increased. A mechanism was suggested to explain Hg oxidation: the reaction HCl → H + Cl may occur between 700 and 900ºC.
5. During the heterogeneous reactions, about 60 to 70% of the baseline concentration of Hg^0 was captured and stored by the VWT catalyst. The use of the VWT catalyst promoted the reduction of Hg^0 and shifted the reaction temperature lower, and it seemed that the catalytic effect was very strong, and inhibition effects by NO were not significant.

9.2 Future Works

9.2.1 Biomass Reburning on NO_x Reduction

Though extensive study was conducted in the current work, several recommendations are presented as future work in order to better understand the reburn technology with cattle waste/biomass.

1. The extent of formations and destructions of NH_3 and HCN derived from fuel-N in CB are still unknown. Thus the amounts of NH_3 and HCN formed must be measured.
2. More studies are needed on the effects of the baseline NO_x concentration on the NO_x reduction.
3. The effects of the particle size of reburn fuels need to be investigated, and the use of finer fuels is recommended as 70% of the mass must pass through a 75 μm (200-mesh) sieve.
4. A study must be conducted on the extent of reburn fuel mixing in the reactor.
5. The NG composition was assumed to be pure CH_4 for all calculations performed in the current research. Though this change has negligible effects on experimental conditions, the overall empirical chemical formula ($CH_hN_nO_o$) of NG needs to be used.
6. Include overfire air or advanced reburning, and compare the results with the finding from the current work.
7. Study the effects of moisture and ash in CB or coals on NO_x reduction and combustion performance.

9.2.2 Fouling Study

Recommendations for the future fouling study are as follows.

1. Coal-fired combustion produces both bottom and fly ash. The ash from CB combustion is typically different from ash from coal combustion. The proportions of bottom ash and fly ash

must be determined. A sampling system with filter may be used in the gas stream to determine amount of fly ash.

2. The ash fouling results under the steady-state condition should be investigated and compared to the transient results in the current work.
3. Determine the thickness, uniformity and stickiness of ash layer.
4. Determine the elemental components of the CB ash collected and the loss on ignition (LOI).

9.2.3 Hg Reduction

Recommendations for the Hg study are as follows.

1. The species of the oxidized Hg were not detected; only elemental Hg was measured. For future study, either Ontario Hydro method or wet chemistry method is suggested to be used to detect oxidized mercury.
2. In order to simulate the realistic flue gas from coal-fired boilers, more gas components such as CO, CO_2, NO_2, H_2, SO_2, and H_2O in the simulated gas in the flow reactor must be introduced.
3. The concentration of HCl from the flue gas of coal-fired boilers must be measured and the effects of other chlorine species such as Cl_2 can be studied. The effects of NO_2, SO_2 or H_2O are also recommended for further study.
4. An integrated gas analyzer is needed to measure concentrations of HCl and/or Cl_2 as well as NO, NO_2, SO_2, CO, and/or CO_2.
5. It is also not known whether Hg reacted in the reactor or in the cooling region. Studies must be conducted to determine the extent of Hg absorption in the cooling region.

REFERENCES

[1] Environmental Protection Agency (EPA) – National Air Quality and Emissions Trends Report, 2003 Special Studies Edition, EPA 454/R-03-005, Research Triangle Park, NC, September 2003. Accessed in March 2007 at www.epa.gov/air/airtrends/reports.html.

[2] Frazzitta, S., Annamalai, K. and Sweeten, J. Performance of a Burner with Coal and Coal-Bio-Solid Fuel Blends. *Journal of Propulsion and Power,* v 15, n 2, 1999, 181-186.

[3] Department of Energy (DOE) – Clean Coal Technology: Reburning Technologies for the Control of Nitrogen Oxides Emissions from Coal-fired Boilers. Topical Report Number 14, May 1999. Accessed in March 2007 at www.fossil.energy.gov/programs/powersystems/publications.

[4] Energy Information Administration (EIA) – Annual Energy Outlook 2007 with Projections to 2030. Report #: DOE/EIA-0383(2007), Washington, DC, February 2007. Accessed in June 2007 at www.eia.doe.gov/oiaf/aeo/emission.html.

[5] Department of Environmental Protection in New Jersey (DEPNJ). Chapter III - Atmospheric Transport and Mercury Deposition, 2002. Accessed in February 2007 at www.state.nj.us/dep/dsr/vol2-chapter3.pdf.

[6] Carpi, A. Mercury from Combustion Sources: A Review of the Chemical Species Emitted and Their Transport in the Atmosphere. *Water, Air and Soil Pollution*, v 98, n 3-4, 1997, 241-254.

[7] US Geological Survey (USGS) – Mercury Contamination of Aquatic Ecosystems, 1997. Accessed in February 2007 at http://wi.water.usgs.gov/pubs/FS-216-95.

[8] Agarwal, H., Stenger, H.G., Wu, S., and Fan, Z. Effects of H_2O, SO_2 and NO on Homogeneous Hg Oxidation by Cl_2. *Energy and Fuels*, v 20, 2006, 1068-1075.

[9] Kilgroe, J.D., Sedman, C.B., Srivastava, R.K., Ryan, J.V., Lee, C.W., and Thorneloe, S.A. Control of Mercury Emissions from Coal-Fired Electric Utility Boilers: Interim Report: EPA-600/R-01-109, U.S. Environmental Protection Agency, U.S. Government Printing Office, Washington, DC, December 2001.

[10] Senior, C.L., Sarofim, A.F., Zeng,T., Helble, J.J., and Mamani-Paco, R. Gas-Phase Transformations of Mercury in Coal-Fired Power Plants. *Fuel Processing Technology,* v 63, n 2-3, 2000, 197-213.

[11] Dajnak, D. and Lockwood, F.C. Modeling of Toxic Heavy Metal Mercury Partitioning from Pulverized Fuel Combustion. *IFRF Combustion Journal,* Article Number 200103, 2001, 1-31.

[12] Annamalai, K., Thien, B. and Sweeten, B. Co-firing of Coal and Cattle Feedlot Biomass (FB) Fuels. Part II. Performance Results from 30 kW (100,000) BTU/h Laboratory Scale Boiler Burner. *Fuel*, v 82, 2003, 1183-1193.

[13] Sweeten, J.M., Annamalai K., Thien B., and McDonald L.A. Co-firing of Coal and Cattle Feedlot Biomass (FB) Fuels. Part I. Feedlot Biomass (Cattle Manure) Fuel Quality and Characteristics. *Fuel*, v 82, n 10, 2003, 1167-1182.

[14] Jenkins, B.M., Thy, P., Turn, S.Q., Blevins, L.G., Baxter L.L., Jakeway, L.A., Williams, R.B., Blunk, S.L., Yore, M.W., Wu, B.C., and Lesher, C.E. Composition and Microstructure of Ash Deposits from Co-firing Biomass and Coal. *Proceedings of Bioenergy 2002*, Boise, Idaho, 2002.

[15] Sami, M., Annamalai, K. and Wooldridge, M. Co-firing of Coal and Biomass Fuel Blends. *Progress in Energy and Combustion Science*, v 27, n 2, 2001, 171-214.

[16] Di Nola, G. Biomass Fuel Characterization for NO_x Emissions in Co-firing Applications. *Ph.D. Dissertation*, Mechanical Engineering, Universita' degli studi di Napoli, Italy, 2007.

[17] Spliethoff, H. and Hein, K.R.G. Effect of Co-Combustion of Biomass on Emissions in Pulverized Fuel Furnaces. *Fuel Processing Technology*, v 54, 1998, 189-205.

[18] Savolainen, K. Co-firing of Biomass in Coal-Fired Utility Boilers. *Applied Energy*, v 74, 2003, 369-381.

[19] Hartmann, D. and Kaltschmitt, M. Electricity Generation from Solid Biomass via Co-Combustion with Coal. Energy and Emission Balances from a German Case Study. *Biomass and Bioenergy*, v 16, n 6, 1999, 397-406.

[20] Kaer, S.K., Rosendahl, L. and Overgaard, P. Numerical Analysis of Co-firing Coal and Straw in a Utility Boiler at MIDCRAFT ENERGY COMPANY, Denmark. *Proceeding of the 4th European Computational Fluid Dynamics Conference*, Athens, Greece, 1998, 1194-1199.

[21] Sampson, G.R., Richmond, A.P. and Brewster, G.A. Co-firing of Wood Chips with Coal in Interior Alaska. *Forest Products Journal*, v 41, n 5, 1991, 53-56.

[22] Annamalai, K., Sweeten, J.M., Mathur, M., Thien, B., Wei, G., Priyadarsan, S., Arumugam, S., and Heflin, K. Co-firing Coal: Feedlot and Litter Biomass (CFB and CLB) Fuels in Pulverized Fuel and Fixed Bed Burners. Final Report: National Energy Technology Laboratory (NETL) and Department of Energy (DOE), 2003. Accessed in September 2007 at www.osti.gov/bridge/servlets/purl/822025-otOX2Z/native/822025.pdf.

[23] Wu, K.T., Lee, H.T., Juch, C.I., Wan, H.P., Shim, H.S., Adams, B.R., and Chen, S.L. Study of Syngas Co-firing and Reburning in a Coal Fired Boiler. *Fuel*, v 83, n 14-15 SPEC. ISS., 2004, 1991-2000.

[24] Sable, S.P., de Jong, W., Meij, R., and Spliethoff, H. Effect of Secondary Fuels and Combustor Temperature on Mercury Speciation in Pulverized Fuel Co-Combustion: Part 1. *Energy and Fuels*, v 21, n 4, 2007, 1883-1890.

[25] Annamalai, K., Sweeten, J., Freeman, M., Mathur, M., O'Dowd, W., Walbert, G., and Jones, S. Co-firing of Coal and Cattle Feedlot Biomass (FB) Fuels, Part III: Fouling Results from a 500,000 BTU/h Pilot Plant Scale Boiler Burner. *Fuel*, v 82, n 10, 2003, 1195-1200.

[26] Pronobis, M. Evaluation of the Influence of Biomass Co-combustion on Boiler Furnace Slagging by Means of Fusibility Correlations. *Biomass and Bioenergy*, v 28, n 4, 2005, 375-383.

[27] Thien, B. and Annamalai, K. Reduction of NO through Reburning with Coal and Feedlot Biomass. *National Combustion Conference*, Oakland, CA. March 25th – 27th, 2001.

[28] Lissianski, V.V., Zamansky, V.M. and Maly, P.M. Effect of Metal-Containing Additives on NO_x Reduction in Combustion and Reburning. *Combustion and Flame*, v 125, n 3, 2001, 1118-1127.

[29] Hall, R.E., Miller, C.A., Payne, R., Yakushin, E., and Mespan, J. Application of Multifuel Reburn for NO_x Control on a 300 MWe Boiler in Ukraine. *Proceedings of the Air & Waste Management Association's Annual Meeting & Exhibition*, 1996, 1-13.

[30] Spliethoff, H., Greul, U., Rudiger, H., and Hein, K.R.G. Basic Effects on NO_x Emissions in Air Staging and Reburning at a Bench-Scale Test Facility. *Fuel*, v 75, n 5, 1996, 560-564.

[31] Flosom B.A., Engelhardt, D.A., Moyeda, D.K., Chang, S.S, Janik, G.S., and Whelan, M.P. Gas Reburning and Advanced Gas Reburning for NO_x Emissions Control. *The 90th Annual Meeting and Exhibition at Air and Waste Management Association*, 97-TA30A.06, 1997, 1-7.

[32] Yang, Y.B., Naja, T.A., Gibbs, B.M., and Hampartsoumian, E. Optimisation of Operating Parameters for NO Reduction by Coal Reburning in a 0.2 MW Furnace, *Journal of the Institute of Energy*, v 70, 1997, 9-16.

[33] Miller, C.A., Touati, A.D., Becker, J., and Wendt, J.O.L. NO_x Abatement by Fuel-Lean Reburning: Laboratory Combustor and Pilot-Scale Package Boiler Results. *Symposium (International) on Combustion*, v 2, 1998, 3189-3195.

[34] Adams, B.R. and Harding, N.S. Reburning Using Biomass for NO_x Control. *Fuel Processing Technology*, v 54, n 1-3, 1998, 249-263.

[35] Maly, P.M., Zamansky, V.M., Ho, L., and Payne, R. Alternative Fuel Reburning. *Fuel*, v 78, n 3, 1999, 327-334.

[36] Zamansky, V.M., Maly, P.M., Lissianski, V.V., and Freeman, M.C. Advanced Biomass Reburning. Report: Department of Energy ad Agridulture, 2000. Accessed in September 2007 at www.netl.doe.gov/publications/proceedings/98/98ps/pspa-5.pdf.

[37] Sweterlitsch, J.J. and Brown, R.C. Fuel Lean Biomass Reburning in Coal-Fired Boilers. Final Technical Report: DOE Award No: DE-FG26-00NT40811, 2002.

[38] Shen, B., Yao, Q., and Xu, X. Kinetic Model for Natural Gas Reburning. *Fuel Processing Technology*, v 85, n 11, 2004, 1301-1315.

[39] Arumugam, S. Nitrogen Oxides Emission Control through Reburning with Biomass in Coal-Fired Power Plants. *MS Thesis*, Mechanical Engineering, Texas A&M University, College Station, TX, 2004.

[40] Storm, C., Spliethoff, H., and Hein, K.R.G. Generation of a Gaseous Fuel by Pyrolysis of Biomass and Sewage Sludge for Use as Reburn Gas in Coal-Fired Boilers. *Clean Air*, v 6, n 3, 2005, 289-328.

[41] Annamalai, K., Goughnour, P.G., Oh, H., Arcot V, U., and Sweeten, J.M. NO_x and Hg Capture using Coal, Feedlot Biomass (Cattle Manure) as Reburn Fuels – Task 2: Reburn Experiments for NO_x and Hg Reduction. Final Report: Texas Commission on Environmental Quality (TCEQ), Austin, TX, 2006.

[42] Liesa, F., Alzueta, M.U., Millera, A., and Bilbao, R. Influence of Reactant Mixing in a Laminar Flow Reactor: The Case of Gas Reburning. 1. Experimental Study. *Industrial and Engineering Chemistry Research*, v 46, n 11, 2007, 3520-3527.

[43] Li, S., Xu, T., Zhou, Q., Tan, H., Hui, S., and Hu, H. Optimization of Coal Reburning in a 1 MW Tangentially Fired Furnace. *Fuel*, v 86, n 7-8, 2007, 1169-1175.

[44] Singh, V. Biomass. Renewable Energy Policy Project, 2001. Accessed in June 2007 at www.crest.org/articles/static/1/1004994679_6.html#bioa.

[45] Energy and Natural Resources Committee. Natural Gas Prices Result in More Coal Plants - Amid Complaints from Enviros Worried About Air Quality, *Press Releases*, March 22nd, 2004. Accessed in January 2008 at http://energy.senate.gov/public/index.cfm.

[46] Annamalai, K., and Sweeten, B. Reburn System with Feedlot Biomass. US Patent # 6,973,883 issued to Annamalai and Sweeten on December 31st, 2005. Accessed in March 2007 at www.patentstorm.us/patents/6973883-fulltext.html.

[47] Sweeten, J.M. Composting Manure and Sludge. Publication L-2289, Texas Agricultural Extension Service Texas A&M University, College Station, TX, 1988.

[48] Annamalai, K. and Puri, I.K. Combustion Science and Engineering, CRC Series in Computational Mechanics and Applied Analysis, CRC Press, FL, 2005.

[49] Carlin, N., Annamalai, K., Sweeten, J., and Mukhtar, S. Thermo-Chemical Conversion Analysis on Dairy Manure-Based Biomass Through Direct Combustion. *International Journal of Green Energy*, v 4, 2007, 133-159.

[50] Annamalai, K.T., Carlin, N.T., Oh, H., Gordillo Ariza, G., Lawrence, B., Arcot V, U., Sweeten, J.M., Heflin, K., Harman, W.L. Thermo-Chemical Energy Conversion of Coal, Animal Waste Based Biomass, and Coal:Biomass Blends. *19th National and 8th ISHME-ASME, Heat and Mass Transfer Conference*, JNTU Hyderabad, India, January 3rd – 5th, 2008.

[51] Hurley, J.P. and Benson, S.A. Ash Deposition at Low Temperatures in Boilers Burning High-Calcium Coals. 1. Problem Definition. *Energy & Fuels*, v 9, n 5, 1995, 775-781.

[52] Walsh, P.M., Sarofim, A.F., and Beer, J.M. Fouling of Convection Heat Exchangers by Lignitic Coal Ash. *Energy & Fuels*, v 6, n 6, 1992, 709-715.

[53] Kalisz, S. and Pronobis, M. Investigations on Fouling Rate in Convective Bundles of Coal-Fired Boilers in Relation to Optimization of Sootblower Operation. *Fuel*, v 84, n 7-8, 2005, 927-937.

[54] Abd-Elhady, M.S., Rindt, C.C.M., Wijers, J.G., van Steenhoven, A.A., Bramer, E.A., and van der Meer, Th.H. Minimum Gas Speed in Heat Exchangers to Avoid Particulate Fouling. *International Journal of Heat and Mass Transfer*, v 47, n 17-18, 2004, 3943-3955.

[55] Van Doorn, J., Bruyn, P. and Vermeij, P. Combined Combustion of Biomass, Municipal Sewage Sludge and Coal in an Atmospheric Fluidized Ben Installation. *Proceeding of the 9th European Bioenergy Conference*, Copenhagen, Denmark, v 2, 1996, 1007-1012.

[56] Patumsawad, S. and Cliffe, K.R. Experimental Study on Fluidized Bed Combustion of High Moisture Municipal Solid Waste. *Energy Conversion and Management*, v 43, n 17, 2002, 2329-2340.

[57] Brouwer, J. Cofiring Waste Biofuels and Coal for Emissions Reduction. *Fuel and Energy Abstracts*, v 36, n 6, 1995, 437-437.

[58] Eghball, B. and Power, J.F. Beef Cattle Feedlot Manure Management. *Journal of Environmental Quality*, v 49, 1994, 113-122.

[59] Thien, B. Cofiring with Coal – Feedlot Biomass Blends. *Ph.D. Dissertation*, Texas A&M University, College Station, TX, 2002.

[60] Martin, B.R. Pyrolysis and Ignition Behavior of Coal, Cattle Biomass, and Coal/Cattle Biomass Blends. *M.S. Thesis*, Mechanical Engineering, Texas A&M University, College Station, TX, December 2006.

[61] Department of Energy/Energy Information Administration (DOE/EIA). *U.S. Coal Reserve: 1997 Update*. DOE/EIA-0529(97). Office of Coal, Nuclear, Electric and

Alternate Fuels, Office of Integrated Analysis and Forecasting, Washington, DC, February 1999. Accessed in March 2007 at www.eia.doe.gov/cneaf/coal/reserves/front-1.html.

[62] Smoot, L.D. Pulverized Coal Diffusion flames: A Perspective through Modeling. *18th Symposium on Combustion*, The Combustion Institute, Pittsburgh, PA, 1981, 1185-1202.

[63] Asay, B.W. Effect of Coal Type and Moisture Centent on Burnout and Nitrogenous Pollutant Formation. *Ph.D. Dissertation*, Brigham Young University, Provo, UT, 1982.

[64] Tillman, D.A. Cofiring Biomass with Coal: Issues for Technology Commercialization. *16th Annual Coal Conference*, Paper # 21-4, Pittsburgh, PA, 2000.

[65] Kobayashi, H. Rapid Decomposition Mechanisms of Pulverized Coals. *Ph.D. Dissertation*, Chemical Engineering Department, MIT, Cambridge, MA, 1977.

[66] Sami, M. Numerical Modeling of Coal-Feedlot Biomass Blend Combustion and NO_x Emission in Swirl Burner. *Ph.D. Dissertation*, Texas A&M University, College Station, TX, 2000.

[67] Xiangyang, D. Ignition and combustion of a Dense Stream of Coal Particles, *Ph.D. Dissertation*, Texas A&M University, College Station, TX, 1995.

[68] Ferguson, C. R. and Kirkpatrick, A. T. Internal Combustion Engines: Applied Thermodynamics, Second Edition, New York, John Wiley & Sons, Inc., 2001.

[69] Heywood, J.B. Internal Combustion Engine Fundamentals, New York, McGraw-Hill, 1988.

[70] Glarborg, P., Miller, J.A. and Kee, R.J. Kinetic Modeling and Sensitivity Analysis of Nitrogen Oxide Formation in Well-Stirred Reactors. *Combustion and Flame*, v 65, 1986, 177-202.

[71] Degobert, P. Automobiles and Pollution. Warrendale, PA., Society of Automotive Engineers, Inc., 1995.

[72] Lyon, R.K. and Hardy, J.E. Discovery and Development of the Thermal DeNOx Process. *Industrial and Engineering Chemistry Fundamentals*, v 25, 1986, 19-24.

[73] Miller, J.A. and Bowman, C.T. Mechanisms and Modeling of Nitrogen Chemistry in Combustion. *Progress in Energy and Combustion Science*, v 15, 1989, 287-338.

[74] Niksa, S., Helble, J.J., and Fujiwara, N. Kinetic Modeling of Homogeneous Mercury Oxidation: The Importance of NO and H_2O in Predicting Oxidation in Coal-Derived Systems. *Environmental Science and Technology*, v 35, n 18, 2001, 3701-3706.

[75] Brown, T.D., Smith, D.N., Hargis Jr., R.A., and O'Dowd, W.J. Mercury Measurement and Its Control: What We Know, Have Learned, and Need to Further Investigate. *Journal of the Air & Waste Management Association*, 1999, 1-97.

[76] Larjava, K. On the Measurement of Volatile Metal Species at Elevated Temperatures. *Thesis*, Espoo, Technical Research Center of Finland, VTT Publications 137, 1994.

[77] Wang, J., Xiao, Z. and Lindqvist, O. On-line Measurement of Mercury in Simulated Flue Gas. *Water, Air, and Soil Pollution*, v 80, 1995, 1217-1226.

[78] DeVito, M.S. and Rosenhoover, W.A. Flue Gas Hg Measurements from Coal-Fired Boilers Equipped with Wet Scrubbers. *92nd Annual Air & Waste Management Association Meeting and Exhibition*, St. Louis, MO, June 20th – 24th, 1999.

[79] Sliger, R.N., Kramlich, J.C. and Marinov, N.M. Towards the Development of a Chemical Kinetic Model for the Homogeneous Oxidation of Mercury by Chlorine Species. *Fuel Processing Technology*, v 65, 2000, 423-438.

[80] Hall, B., Schager, P., and Lindqvist, O. Chemical Reactions of Mercury in Combustion Flue Gases. *Water, Air, and Soil Pollution*, v 56, 1991, 3-14.

[81] Lighty, J.S., Silcox, G., Fry, A., Senior, C., Helble, J., and Krishnakumar, B. Fundamentals of Mercury Oxidation in Flue Gas. Technical Annual Report: DOE Grant Number DE-FG26-03NT41797, 2005, 1-23.

[82] Environmental Protection Agency (EPA) – Continuous Emission Monitoring – Information, Guidance, etc., 2006. Accessed in February 2007 at www.epa.gov/ttn/emc/cem.html.

[83] Department of Energy (DOE) - Advanced Nitrogen Oxide (NO_x) Controls, Pollution Control Innovations for Power Plants, Clean Coal & Natural Gas Power Systems, 2006. Accessed in March 2007 at www.fe.doe.gov/programs/powersystems/pollutioncontrols.

[84] Central Research Institute of Electric Power Industry (CRIEPI) – Development of a New Low-NO_x Wide-range Burner for Applications in Coal-fired Thermal Power Stations, 2004. Accessed in May 2007 at http://criepi.denken.or.jp/en/e_publication/a1997/97seika15.pdf.

[85] Hampartsoumian, E., Folayan, O.O., Nimmo, W., and Gibbs, B.M. Optimization of NO_x Reduction in Advanced Coal Reburing Systems and the Effect of Coal Type. *Fuel*, v 82, 2003, 373-384.

[86] Patsias, A.A., Nimmo, W., Gibbs, B.M., and Williams, P.T. Calcium-Based Sorbents for Simultaneous NO_x/SO_x Reduction in a Down-Fired Furnace. *Fuel*, v 84, n 14-15, 2005, 1864-1873.

[87] Ham, S.W. and Nam, I.S. The Royal Society of Chemistry, "Catalysis," v 16, Senior Reporter: Kemball, C. and Reporter: Caunt, A.D., London, Chemical Society, 2002.

[88] Environmental Protection Agency (EPA) – Database of Information Collected in the Electric Utility Steam Generating Unit Mercury Emissions Information Collection Effort.

OMB Control No. 2060-0396. Office of Air Quality Planning and Standards. 2001. Accessed in February 2007 at www.epa.gov/ttn/atw/combust/utiltox/utoxpg.html.

[89] Norton, G.A., Yang, H., Brown, R.C., Laudal, D.L., Dunham, G.E., and Erjavec, J. Heterogeneous Oxidation of Mercury in Simulated Post Combustion Conditions. *Fuel*, v 82, n 2, 2003, 107-116.

[90] Laudal, D.L., Heidt, M.K., Galbreath, K.C., Nott, B.R., and Brown, T.D. State of the Art: Mercury Speciation Measurement in Coal Combustion Systems. *Proceedings of the Air & Waste Management Association's Annual Meeting & Exhibition*, 1997, 12.

[91] Environmental Protection Agency (EPA) – Mercury, 2005. Accessed in June 2005 at www.epa.gov/mercury.

[92] Richardson, C., Machalek, T., Miller, S., Dene, C., and Chang, R. Effect of NO_x Control Processes on Mercury Speciation in Utility Flue Gas. *Journal of the Air & Waste Management Association*. v 52, n 8, 2002, 941-947.

[93] Feeley, T.J. III, Murphy, J., Hoffmann, J., and Renninger, S.A. A Review of DOE/NETL's Mercury Control Technology R&D Program for Coal-Fired Power Plants. DOE/NETL Hg R&D Program Review, April 2003. Accessed in May 2008 at http://www.netl.doe.gov/technologies/coalpower/ewr/pubs/DOENETL_HgR&D_WhitePaper_Final.pdf.

[94] Lee, C.W., Srivastava, R.K., Ghorishi, S.B., Hastings, T.W., and Stevens, F.M. Investigation of Selective Catalytic Reduction Impact on Mercury Speciation under Simulated NO_x Emission Control Conditions. *Journal of the Air and Waste Management Association*, v 54, n 12, 2004, 1560-1566.

[95] Coutts, P.T. and Young, J.W.S. Evaluation of Technologies for Reducing Mercury Emissions from the Electric Power Generation Sector – Final Report for Canadian Council of Ministers of the Environment by Specialists in Energy Nuclear and Environmental Sciences (SENES) Consultants Limited, Richmond Hill, Ontario, Canada, February 2002. Accessed in May 2008 at http://www.ccme.ca/assets/pdf/senes_fnlrpt_feb2002_e.pdf.

[96] Laudal, D.L., Thompson, J.S., Pavlish, J.H., Brickett, L., Chu, P., Srivastava, R.K., Kilgroe, J., and Lee, C.W. Mercury Speciation at Power Plants Using SCR and SNCR Control Technologies. *EM: Air and Waste Management Association's Magazine for Environmental Managers*, February 2003, 16-22.

[97] Air Pollution Prevention and Control Division (APPCD) – National Risk Management Research Laboratory, Office of Research and Development, U.S. Environmental Protection Agency. Control of Mercury Emissions from Coal Fired Electric Utility Boilers: An Update. Research Triangle Park, NC, February, 2005.

[98] Galbreath, K.C. and Zygarlicke, C.J. Mercury Transformations in Coal Combustion Flue Gas. *Fuel Processing Technology*, v 65, 2000, 289-310.

[99] Meischen, S.J., Van Pelt, V.J., Zarate, E.A., and Stephens Jr., E.A. Gas-phase Mercury Reduction to Measure Total Mercury in the Flue Gas of a Coal-Fired Boiler. *Journal of the Air and Waste Management Association*, v 54, n 1, 2004, 60-67.

[100] Zhuang, Y., Thompson, J.S., Zygarlicke, C.J., and Pavlish, J.H. Development of a Mercury Transformation Model in Coal Combustion Flue Gas. *Environmental Science and Technology*, v 38, n 21, 2004, 5803-5808.

[101] Serre, S.D., Gullett, B.K. and Ghorishi, S.B. The Effect of Water (Vapor-phase) and Carbon on Elemental Mercury Removal in a Flow Reactor. *93rd Annual Meeting on the Air and Waste Management Association*, Paper # 164, 2001.

[102] Gibb, W.H., Clarke, F., and Mehta, A.K. Fate of Coal Mercury During Combustion. *Fuel Processing Technology*, v 65, 2000, 365-377.

[103] Cao, Y., Duan, Y., Kellie, S., Li, L., Xu, W., Riley, J.T., Pan, W.P., Chu, P., Mehta, A.K., and Carty, R. Impact of Coal Chlorine on Mercury Speciation and Emission from a 100-MW Utility Boiler with Cold-Side Electrostatic Precipitators and Low-NO_x Burners. *Energy and Fuels*, v 19, n 3, 2005, 842-854.

[104] Arcot V, U. Mercury Emission Control for Coal Fired Power Plants using Coal and Biomass. *M.S. Thesis*, Mechanical Engineering, Texas A&M University, College Station, TX, December 2007.

[105] Kramlich, J.C. and Sliger, R.N. Reduction of Inherent Mercury Emissions in PC Combustion. Final Technical Report, DOE Grant No. DE-FG22-95PC95216-09, 2000.

[106] Widmer, N.C., Cole, J.A., Seeker, W.R., and Gaspar, J.A. Practical Limitation of Mercury Speciation in Simulated Municipal Waste Incinerator Flue Gas. *Combustion Science and Technology*, v 134, 1998, 315-326.

[107] Ghorishi, S.B. Fundamentals of Mercury Speciation and Control in Coal-Fired Boilers. EPA-600/R-98-014, February 1998.

[108] Granite, E.J. and Pennline, H.W. Photochemical Removal of Mercury from Flue Gas. *Industrial and Engineering Chemistry Research*, v 41, n 22, 2002, 5470-5476.

[109] Ghorishi, S.B., Keeney, R.M., Serre, S.D., Gullett, B.K., and Jozewicz, W.S. Development of a Cl-Impregnated Activated Carbon for Entrained-Flow Capture of Elemental Mercury. *Environmental Science and Technology*, v 36, n 20, 2002, 4454-4459.

[110] Lee, T.G., Hedrick, E., and Biswas, P. Hg Reactions in the Presence of Chlorine Species: Homogeneous Gas Phase and Heterogeneous Gas-Solid Phase. *Journal of the Air and Waste Management Association*, v 52, n 11, 2002, 1316-1323.

[111] Lu, D.Y., Granatstein, D.L., and Rose, D.J. Study of Mercury Speciation from Simulated Coal Gasification. *Industrial and Engineering Chemistry Research*, v 43, n 17, 2004, 5400-5404.

[112] Ghorishi, S.B., Lee, C.W., Jozewicz, W.S., and Kilgroe, J.D. Effects of Fly Ash Transition Metal Content and Flue Gas HCl/SO_2 Ratio on Mercury Speciation in Waste Combustion. *Environmental Engineering Science*, v 22, n 2, 2005, 221-231.

[113] Bell, K.J. and Mueller, A.C. Wolverine Engineering Data Book II. Wolverine Tube, Inc. Research and Development Team, 2001.

[114] Annamalai, K., Sweeten, J.M. and Martin, B. Pyrolysis, Ignition, and Fuel Characteristics of Coal, Feedlot Biomass, and Coal:Feedlot Biomass Blends. Final Report to Texas Commission on Environmental Quality (TCEQ), 2006. Accessed in May 2007 at http://search.tceq.state.tx.us/.

[115] Cho, Y.I. and Choi, B.G. Validation of an Electonic Anti-Fouling Technology in a Single-Tube Heat Exchanger. *International Journal of Heat and Mass Transfer*, v 42, 1999, 1491-1499.

[116] Oh, H.J. Selective Catalytic Reduction (SCR) of Nitric Oxide (NO) with Ammonia over Vanadia-Based and Pillared Interlayer Clay-Based Catalysts. *M.S. Thesis*, Mechanical Engineering, Texas A&M University, College Station, TX, May 2004.

[117] Bobcock, G.H. and Wilcox, S. Steam/Its Generation and Use, 39^{th} Edition. Bobcock and Wilcox Company, NY, 1978.

[118] Rico, J.L., Garcia, H., Rico, C., Tejero, I. Characterisation of Solid and Liquid Fractions of Dairy Manure with regard to Their Component Distribution and Methane Production. *Bioresource Technology*, v 98, n 5, 2007, p 971-979.

[119] Lawrence, B.D. Cofiring of Coal and Dairy Biomass in a 100,000 BTU/hr Furnace. *M.S. Thesis*, Mechanical Engineering, Texas A&M University, College Station, TX, December 2007.

[120] Wargadalam, V.J., Loffler, G., Winter, F., and Hofbauer, H. Homogeneous Formation of NO and N_2O from the Oxidation of HCN and NH_3 at 600-1000°C. *Combustion and Flame*, v 120, n 4, 2000, 465-478.

[121] Svoboda, K., Cermák, J. and Hartman, M. Chemistry of Nitrogen Oxides (NO, NO_2, N_2O) in Combustion of Solid Fuels. II. Heterogeneous Reactions - N_2O. *Chemical Papers*, v 54, n 2, 2000, 118-130.

[122] Feather River Air Quality Management District (FRAQMD) – Rule 3.21: Industrial, Institutional, and Commercial Boilers, Steam Generators, and Process Heaters, June 2006. Accessed in May 2007 at http://arbis.arb.ca.gov/DRDB/FR/CURHTML/R3-21.PDF.

[123] Incropera, F.P., and DeWitt, D.P. Fundamentals of Heat and Mass Transfer, Fourth Edition, John Wiley and Sons, Inc., NY, 1996.

[124] Martínez, I. Heat and Mass Convection - Heat Exchangers, 2007. Accessed in January 2008 at http://imartinez.etsin.upm.es/bk3/c12/Heat%20exchangers.htm.

[125] Richards, C.H., Harb, J.H., Baxter, L.L., Bhattacharaga, S., Gupta, R.P., and Wall, T.F. Radiative Heat Transfer in Pulverized-Coal-Fired Boilers-Development of the Absorbptive/Reflective Character of Initial Ash Deposits, *International Symposium on Combustion*, Irvine, CA, 1994, 1-24.

[126] Zygarlicke, C.J., McCollor, D.P., and Crocker, C.R. Ash Emissivity Characterization and Prediction. Final Report, 1999, Energy & Environmental Research Center. Accessed in February 2007 at www.osti.gov/bridge/servlets/purl/778529-ZIRNMy/native/778529.pdf.

[127] Kline, S.J. and McClintock, F.A. Describing Uncertainties in Single-Sample Experiments. *Mechanical Engineering*, v 75, n 1, 1953, 3-8.

[128] Goughnour, P.G. NO_x Reduction with the Use of Feedlot Biomass as a Reburn Fuel. *M.S. Thesis*, Mechanical Engineering, Texas A&M University, College Station, TX, August 2006.

[129] Annamalai, K., Sweeten, J.M., Heflin, K., and Gale, T.K. Pilot-Scale Testing of Coal and Biomass as Reburn Fuels – Task 3: Pilot Scale Tests. New Technology Research and Development Program Grant Contract 582-5-65591-0015, Texas Commission on Environmental Quality (TCEQ), July 2007. Accessed in January 2008 at http://www.tceq.state.tx.us/assets/public/implementation/air/terp/ntrd/prog_rpts/58256559 10015teestask3report.pdf.

[130] Xuan, X., Yue, C., Li, S., and Yao, Q. Selective catalytic reduction of NO by ammonia with fly ash catalyst. *Fuel*, v 82, n 5, March 2003, 575-579.

[131] Wang, W., Zhao, Z., Liu, F., and Wang, S. Study of NO/NO_x Removal from Flue Gas Contained Fly Ash and Water Vapor by Pulsed Corona Discharge. *Journal of Electrostatics*, v 63, n 2, 2005, 155-164.

[132] Zamansky, V.M., Ho, L., Maly, P.M., Randall Seeker, W. Reburning Promoted by Nitrogen- and Sodium-Containing Compounds. 26th *International Symposium on Combustion*, v 2, 2075-2082, Napoli, Italy, July 28th – August 2nd 1996.

[133] Schading, G.N. and Roth, P. Thermal Decomposition of HCl Measured by ARAS and IR Diode Laser Spectroscopy. *Combustion and Flame*, v 99, n 3-4, 1994, 467-474.

[134] Jacobs, T.A., Cohen, N. and Giedt, R.R. Kinetics of Hydrogen Halides in Shock Waves: HCl and DCl. *Journal of Chemical Physics*, v 46, n 5, 1967, 1958-1968.

[135] Felix, V.M. and Paskalov, G. Producing Chlorine and Hydrogen from Hydrogen Chloride by Plasma Process. US Patent # 5935390, 1999.

[136] Xu, M., Qiao, Y., Zheng, C., Li, L., and Liu, J. Modeling of Homogeneous Mercury Speciation using Detailed Chemical Kinetics. *Combustion and Flame*, v 132, n 1-2, 2003, 208-218.

[137] Senior, C., Lignell, D., Shiley, B., Chen, Z., and Sarofim, A. Kinetic Models for Predicting the Behavior of Mercury in Coal-Fired Power Plants. *Presented at the ACERC Annual Conference*, Salt Lake City, UT, 2003.

[138] NASA Computer Program CEA (Chemical Equilibrium with Applications). Additional information is available at www.lerc.nasa.gov/WWW/CEAWeb/.

APPENDIX A

SAUTER MEAN DIAMETER (SMD) CALCULATION

Sauter mean diameter (commonly abbreviated as SMD or d_{32}) is commonly used for estimating the average size of solid fuel particles. The SMD is defined as the diameter of a sphere that has the same ratio of volume to surface area. It is represented as Eq. (A.1).

$$SMD \quad or \quad d_{32} = \frac{\sum_{i=1}^{n} d_i^{\,3} \cdot n_i}{\sum_{i=1}^{n} d_i^{\,2} \cdot n_i} \tag{A.1}$$

where d_i is the diameter of particles and n_i is the number of the particles. The sample calculation is presented for LASSDB, and the same method was used for other reburn fuels.

Table A.1. SMD calculations for LASSDB.

Mesh #	Sieve Dia. D (μm)	Mean Size, D_m (μm)	Bigger than D (g)	Bigger than D (w%)	Less than D (w%)
10	2000	-	0.182	0.0420	99.9580
16	1190	1595	1.125	0.2598	99.6981
20	840	1015	3.64	0.8407	98.8575
50	300	570	94.458	21.8150	77.0425
100	150	225	136.181	31.4509	45.5916
200	75	112.5	99.068	22.8797	22.7120
325	45	60	41.575	9.6017	13.1103
Pan	0	22.5	56.767	13.1103	0
Total			432.996	100	-

Table 5.7. SMD calculations for LASSDB (continued).

Mesh #	$D_m \times w\%$ (μm)	Volume, V (μm^3)	Surface Area, A_s (μm^2)	A_s / V (1/μm)	$A_s / V \times (w\% / 100)$ (1/μm)
10	-	-	-	-	-
16	4.1441	2.125E+09	7.992E+06	0.0038	9.774E-06
20	8.5326	5.475E+08	3.237E+06	0.0059	4.969E-05
50	124.3454	9.697E+07	1.021E+06	0.0105	0.0023
100	70.7645	5.964E+06	1.590E+05	0.0267	0.0084
200	25.7396	7.455E+05	3.976E+04	0.0533	0.0122
325	5.7610	1.131E+05	1.131E+04	0.1000	0.0096
Pan	2.9498	5.964E+03	1.590E+03	0.2667	0.0350
Mean Size by Mass = $\Sigma (D_m \times w\%)$ = 242.237 μm					

Table 5.7. SMD calculations for LASSDB (continued).

Mesh #	$(w\% / 100) / D_m$ (μm)	V of each group (cm^3)	V of each particle (cm^3)	# of particle in each group (n_i)
10	-	0.5635	-	-
16	1.629E-06	3.4830	2.125E+09	1.639E+09
20	8.282E-06	11.2693	5.475E+08	2.058E+10
50	0.0004	292.4396	9.697E+07	3.016E+12
100	0.0014	421.6130	5.964E+06	7.069E+13
200	0.0020	306.7121	7.455E+05	4.114E+14
325	0.0016	128.7152	1.131E+05	1.138E+15
Pan	0.0058	175.7492	5.964E+03	2.947E+16
SMD = $\Sigma (D_{m,i}^3 \times n_i) / \Sigma (D_{m,i}^2 \times n_i)$ = 88.8415 μm				

APPENDIX B

FUEL-NITROGEN (N) ANALYSIS

In order to remove certain amounts of NO_x, it is very useful to know how much of NH_3 is required because of the limited amounts of biomass sources which NH_3 comes from. The combustion of the primary and the reburn fuels is represented as Eq. (B.1).

$$CH_hN_nO_oS_s + a(O_2 + A\cdot H_2O + B\cdot N_2) \rightarrow CO_2 + bH_2O + cSO_2 + dO_2 + eN_2 \qquad \text{(B.1)}$$

where A = 0.0234, B = 3.785, $a = \frac{(1+h/4+s-o/2)}{\phi}$, $b = \left(\frac{h}{2} + A\frac{(1+h/4+s-o/2)}{\phi}\right)$, $c = s$, $d = \left(1+\frac{h}{4}+s-\frac{o}{2}\right)\left(\frac{1}{\phi}-1\right)$, and $e = \left(\frac{B}{\phi}\left(1+\frac{h}{4}+s-\frac{o}{2}\right)+\frac{n}{2}\right)$.

The mole flow rates in the primary and reburn zones on a dry basis are obtained as

$$\dot{N}_{dry,PRZ} = \dot{N}_{PRZ} \times (1 + c + d + e) \qquad \text{(B.2)}$$

$$\dot{N}_{dry,RBZ} = \dot{N}_{RBZ} \times (1 \times \eta_{comb} + c + d + e) \qquad \text{(B.3)}$$

where $\dot{N}_{PRZ}$ is a mole flow rate in the primary zone, $\dot{N}_{dry,PRZ}$ is a mole flow rate in the primary zone on a dry basis, $\dot{N}_{RBZ}$ is a mole flow rate of the reburn zone, and $\dot{N}_{dry,PRZ}$ is a mole flow rate of the reburn zone on a dry basis. The combustion efficiency, η_{comb}, should be considered for reburn combustion. The mole flow rates at the furnace exit is

$$\dot{N}_{dry,exit} = \dot{N}_{dry,PRZ} + \dot{N}_{dry,RBZ} \tag{B.4}$$

The amounts of NO reduced by the reburn combustion is

$$\dot{N}_{NOx,reduced} = \dot{N}_{dry,PRZ} \times x_{NOx,PRZ} - \dot{N}_{dry,exit} \times x_{NOx,exit} \tag{B.5}$$

where $x_{NOx,PRZ}$ is an initial mole fraction of NO_x produced by the primary fuel, and $x_{NOx,exit}$ is a final mole fraction of NO_x at the furnace exit. The amounts of NH_3 used by the reburn combustion is calculated based on the chemical reaction (B.6)

$$NH_3 + 1.5NO \rightarrow 1.25N_2 + 1.5H_2O \tag{B.6}$$

$$\dot{N}_{NH_3,required} : \dot{N}_{NO,reduced} = 1 : 1.5 \tag{B.7}$$

The reburn fuels contain X% nitrogen, Y% moisture and Z% ash on a mass basis. The mole flow rate of the fuel-nitrogen in the reburn zone is

$$\dot{N}_{DAF,X\%N} = \dot{N}_{NH_3,used} / k \tag{B.8}$$

where $\dot{N}_{DAF,X\%N}$ is the mole flow rate of X% fuel-nitrogen in the reburn zone on a dry ash free (DAF) basis, $\dot{N}_{NH_3,used}$ is the mole flow rate used for 90% NO_x reduction, and k is the amounts (%) of NH_3 converted from the fuel-nitrogen.

$$\dot{N}_{X\%N} = \frac{\dot{N}_{DAF,x\%N}}{(1-Y-Z)} \tag{B.9}$$

$$\dot{N}_{RBZ} = \frac{\dot{N}_{X\%N}}{X} \tag{B.10}$$

where $\dot{N}_{X\%N}$ is the mole flow rate of the fuel-nitrogen in the reburn fuel on an 'as received' basis, and $\dot{N}_{RBZ}$ is the mole flow rate of the reburn fuel on an 'as received' basis. Finally, the amounts of the reburn fuels required for 90% reduction of the NO emission can be obtained by Eq. (B.10) depending on amounts of the fuel-nitrogen, amounts of NH_3 conversion from the fuel-nitrogen and other fuel properties.

Table B.1. Operating conditions for biomass reburning.

Heat Input by Primary Fuel	70% (21 kW or 70,000 BTU/h)
Primary Equivalence Ratio (ER_{PRZ})	0.95
Flow Rate of Primary Fuel (NG)	30.1 SLPM (63.9 SCFH)
Flow Rate of Primary Air	320.3 SLPM (678.7 SCFH)
Flow Rate of Ammonia (NH_3)	0.12 SLPM (0.265 SCFH)
Heat Input by Reburn Fuel	30% (9 kW or 30,000 BTU/h)
RBZ Equivalence Ratio (ER_{RBZ})	1.10

The operation conditions for reburn experiments are listed in Table B.1. It was essentially assumed (1) All amounts of fuel-nitrogen in biomass convert to 60% NH_3, 30% HCN and 10% N_2 on a mass basis, and (2) All amounts of fuel-nitrogen in coals convert to 30% NH_3, 60% HCN and 10% N_2 on a mass basis.

The results of minimum amounts of the reburn fuels required to achieve 90% NO_x reduction are presented in figure B.1. The amounts of LASSD and LAPCFB were typically required three or four time less than those of coals while LAPCFB needed similar amounts to coals due to its high ash contents. Ratios between amounts of required and supplied reburn fuels are presented in figure B.2. In order to achieve 90% NO_x reduction, about 10 to 20% more fuel was required for coals while about 20 to 30% of the supplied fuels was required for biomass. Comparing to the experimental results, the conversion proportions from fuel-nitrogen to NH_3, HCN and N_2 were found to be overestimated to predict the proper fuel consumptions. The conversions of fuel-nitrogen to both NH_3 and HCN were reported 15% and 11% for chicken litter and 11% and 6% for coals using a heating rate of 100ºC/min [16]. Since the heating rate during reburning was approximately 1100ºC/s, the real conversion proportions can be higher than what they were reported. The results using the conversion proportions reported in the literature are presented in figure B.3. The results in figures B.2 and B.3 can provide the range of fuel consumptions.

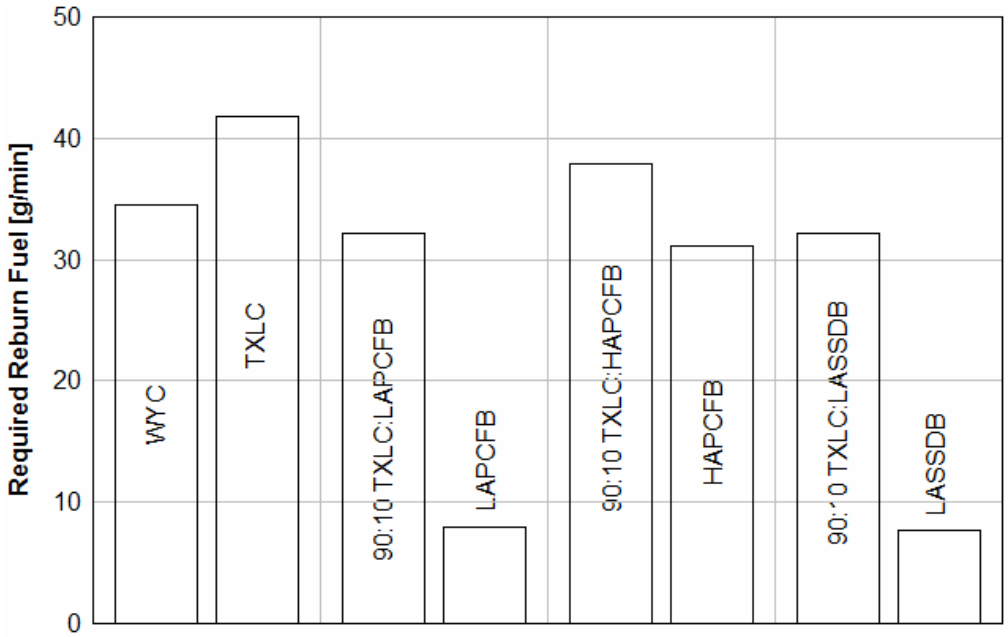

Figure B.1. Minimum amounts of the reburn fuels required to achieve 90% NO_x reduction.

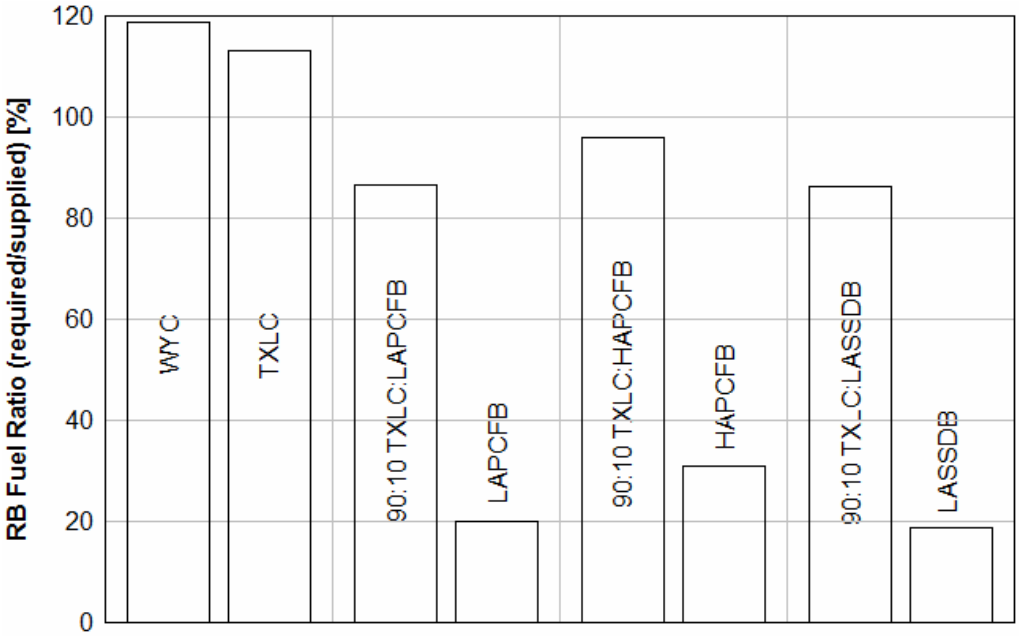

Figure B.2. Ratios between amounts of required and supplied reburn fuels for 90% NO_x reduction by reburning.

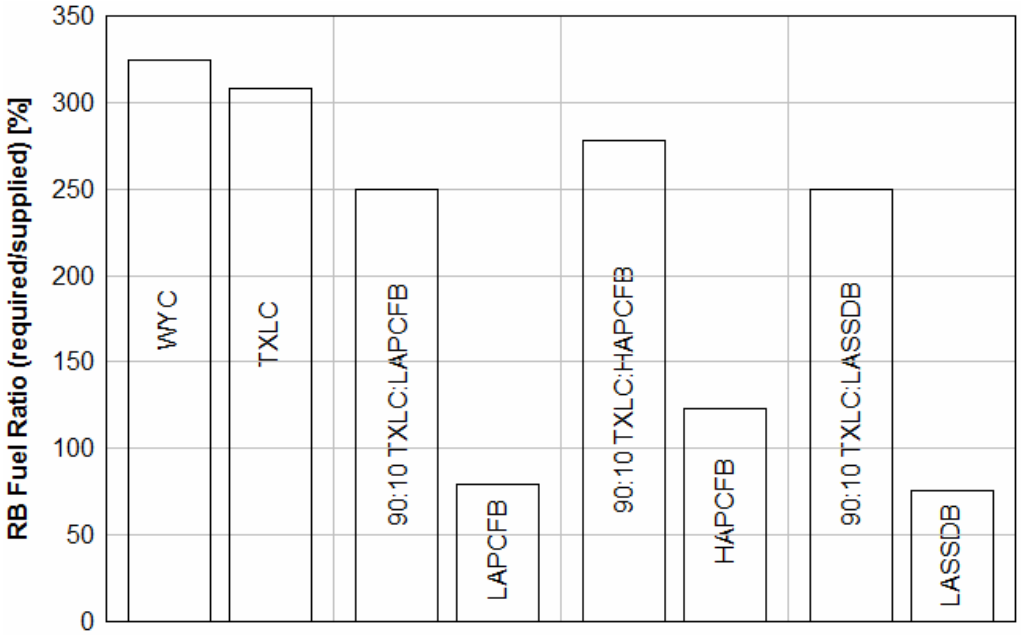

Figure B.3. Reburn fuel ratios using the conversion proportions reported elsewhere [16].

APPENDIX C

ASH FORMATION ANALYSIS

The prediction of the ash concentration [kg/m^3] on the surface of HEXs is briefly discussed in this section. The ash concentration is defined as the amount of ash in the unit volume of the gas stream. The ash fraction, Y_{ash} of the total gas stream is expressed as

$$Y_{ash} = \frac{\dot{m}_{ash}}{\dot{m}_t} = \frac{\dot{m}_{fuel} \times y_{ash,r}}{\dot{m}_t} \tag{C.1}$$

$$\dot{m}_t = \dot{m}_{NG} + \dot{m}_{air,PR} + \dot{m}_{fuel} + \dot{m}_{air,RB} \tag{C.2}$$

where $y_{ash,r}$ is an ash fraction in the dry solid reburn fuels, $\dot{m}_{fuel}$ is a mass flow rate of the reburn fuel, $\dot{m}_t$ is a total mass flow rate of the gas stream in the boiler, $\dot{m}_{NG}$ is a mass flow rate of natural gas, $\dot{m}_{air,PR}$ is a mass flow rate of the primary air, and $\dot{m}_{air,RB}$ is a mass flow rate of the reburn air.

With the assumptions of 1) complete release of ash from fuel and 2) the complete combustion with CO_2, O_2, H_2O, and mainly N_2, the ash concentration, C_{ash} can be expressed as

$$C_{ash} = \frac{\dot{m}_{ash}}{\dot{V}_{gas}} = \frac{\dot{m}_{Fuel} Y_{ash,Fuel}}{\dot{V}_{gas}} \tag{C.3}$$

where $\dot{m}_{ash}$ is a mass flow rate of the ash in the gas stream and $\dot{V}_{gas}$ is the volume flow rate of the gas in the gas stream.

APPENDIX D

MIXING TIME ESTIMATION

Mixing time and residence time of the hot flue gas in the reactor was estimated for the 0° injection using CO_2 and air. This test was performed after the primary fuel shut off. Air was only injected from the primary port when the reactor was still hot. The flow rate of air from the primary port was increased to maintain the total flow rate from the primary burner. Not all amount of the reburn gas was replaced by CO_2 because of the flow limit of the mass flow controller. See Table D.1 for detailed conditions.

Table D.1. Test conditions for the mixing time estimation.

Gas Type	Flow Rate
Air from the primary burner	350 SLPM
Air from the reburn nozzles	33 SLPM
CO_2 from the reburn nozzles	94 SLPM
Total flow	477 SLPM

The concentration of CO_2 was measured at three locations which were 6, 12 and 18 in below the reburn nozzles. The residence times at those three locations were estimated as 350, 700 and 1050 ms, respectively. The results showed the CO_2 concentrations were similar for all cases though a little increase was observed as a function of distance. The complete mixing was not observed at those locations; however, it can be concluded the major mixing took place less than 350 ms. As the fuel particles are injected into the reactor, the mixing time can be longer than 350 ms because the fuel particles are heavier than the CO_2 particles.

VITA

Hyuk Jin Oh received his Bachelor of Science degree in precision mechanical engineering from Chonbuk National University at Jeonju, Republic of Korea (ROK) in 2001. Before graduating, he had served in the Korean Airborne Force. He had received honor scholarships every semester until the graduation. He started studying in thermodynamics and combustion research for his Master's Degree at Texas A&M University in September, 2001. He received his Master of Science degree in mechanical engineering from Texas A&M University at College Station, TX in 2004. His research interests include not only thermodynamics and combustion but also heat transfer and fluid mechanics. He received a Ph.D. in mechanical engineering, and after graduation he now works in the field of combustion research.

Mr. Oh may be reached at Texas A&M University, Department of Mechanical Engineering, 3123 TAMU, College Station, TX 77843. His email is hyukjinoh@hotmail.com.